Architectures de Puissance et Commande associées pour la gestion des ombres dans des installations photovoltaïques

Luiz Fernando Lavado Villa

UNIVERSITÉ DE GRENOBLE

THÈSE

Pour obtenir le grade de

DOCTEUR DE L'UNIVERSITÉ DE GRENOBLE

Spécialité : **Génie Electrique**

Arrêté ministériel : 7 août 2006

Présentée par

« Luiz Fernando LAVADO VILLA »

Thèse dirigée par **« Bertrand RAISON »** et
codirigée par **« Jean-Christophe CREBIER »**

préparée au sein du **Laboratoire de Génie Electrique de Grenoble** dans **l'École Doctorale Electronique, Electrotechnique, Automatique et Traitement du signal**

Architectures de Puissance et Commande associées pour la gestion des ombres dans des installations photovoltaïques

Thèse soutenue publiquement le **«30 Octobre 2013 »**,
devant le jury composé de :

M. Bruno FRANCOIS – Président du Jury
Professeur à l'Ecole Centrale de Lille, France, Rapporteur
M. Felix Alberto FARRET
Professeur à l'Université Fédérale de Santa Maria, Brésil, Rapporteur
M. Bruno ESTIBALS
Professeur à Université Paul Sabatier, France, Rapporteur
M. Ambroise SCHELLMANNS
Maître de conférences à l'Université de Tours, Membre
M. Bertrand RAISON
Professeur à l'Université de Grenoble, France, Directeur de thèse
M. Jean-Christophe CREBIER
Directeur de recherche au CNRS, France, Co-encadrant

UNIVERSITÉ DE GRENOBLE

PhD THESIS

To acquire the degree of

DOCTOR AT THE UNIVERSITY OF GRENOBLE

Especialty : **Electrical Engineering**

Ministerial law from : August 7th 2006

Presented by

« Luiz Fernando LAVADO VILLA »

Thesis supervised by **« Bertrand RAISON »** and
co-supervised by **« Jean-Christophe CREBIER »**

prepared at **Grenoble Electrical Engineering Laboratory** under the **Doctoral School of Electronics, Electrical Engineering, Automatics and Signal Treatment**

Power Architectures and Control Systems Associated for the Management of Shadows in Photovoltaic Plants

Thesis defended publicly **« October, 30th 2013 »**, before the jury composed by :

M. Bruno FRANCOIS – President of the Jury
Professor at the Lille Central School, France, Reviewer
M. Felix Alberto FARRET
Professor at the Federal University of Santa Maria, Brazil, Reviewer
M. Bruno ESTIBALS
Professor at the Paul Sabatier University, France, Reviewer
M. Ambroise SCHELLMANNS
Associate Professor at the University of Tours, Member
M. Bertrand RAISON
Professor at the University of Grenoble, France, Supervisor
M. Jean-Christophe CREBIER
Research director at CNRS, France, Co-Supervisor

Abstract

Photovoltaic energy rates among the most mature renewable sources currently available in the market. However, its growing use in urban environment has met with an important obstacle: shadows. Their study present a two-fold challenge: understanding what they are and how they can be mitigated. While many authors have proposed different solutions for this problem, very few have tried to understand the shadow in its complexity. This thesis seeks, at the same time, a comprehensive view on the shadow itself while proposing a new solution to mitigate it.

The comprehensive view of the shadow is proposed through an intermittency theory, where its optical properties and electrical consequences are taken into account. This theory provides the elements to review the current literature into a new perspective. The available solutions are, then, divided into two families: series and parallel. Series solutions employ several structures, each extracting the power of a reduced number of photovoltaic cells. As a consequence the impact of the shadow is restricted. Parallel solutions use few structures to redistribute the current between shaded and unshaded photovoltaic cells, thus sharing the impact of the shadow.

The new solution proposed to mitigate the shadow is a parallel system called PV Equalizer. Inspired from its battery equivalent, it has a different topology with a high integration potential, easily scalable but seemingly difficult to control. To prove its concept, a study is conducted to determine its functions. It is found to be capable of not only mitigating but also detecting the shadow. These functions are characterized and their results used to conceive a control algorithm. Finally, this algorithm is tested and validated in a prototype under real operating conditions. The system detected the presence of the shadow, chose the best way to mitigate it and raised the power output by roughly 40 %.

Résumé

L'énergie photovoltaïque est à nos jours l'une des sources intermittentes les plus développée. Plusieurs années de recherche confèrent une importante maturité à la fois aux modules et aux systèmes de extraction et traitement de son électricité. Cependant, il lui reste encore un important obstacle à franchir avant son utilisation à large échelle : la présence des ombres. Alors que plusieurs solutions ont été déjà proposées pour ce problème, la recherche sur l'ombre en tel que phénomène complexe reste embryonnaire. Cette thèse a pour but de combler ce besoin à la fois en étudiant la présence d l'ombre et en y proposant une nouvelle réponse.

L'étude de l'ombre comprend la proposition d'une théorie sur l'intermittence qui prend en compte des aspect à la fois électriques et optiques. A travers de cette théorie, une relecture de la littérature est aussi proposée et donne lieu à une classification des solutions existantes en séries ou parallèles. Les solutions séries utilisent plusieurs structures d'électronique de puissance pour extraire l'énergie d'un nombre plus restreint des cellules photovoltaïques et par conséquent y confinent l'impact de l'ombre. En contre partie, les solutions parallèles utilisent des structures spéciales pour redistribuer le courant parmi les cellules ombrées et illuminées, ce qui amène à lŠeffacement de l'ombre.

La nouvelle réponse à l'ombre proposée dans ce travail s'agit d'une structure parallèle à forte potentiel d'intégration monolithique. Inspirée de son équivalent pour les batteries, cette nouvelle topologie est applicable à plusieurs échelles mais sa commande reste un aspect à maîtriser. Son concept de base est validé au niveau d'un seul module photovoltaïque par la création d'un prototype et une validation expérimentale. Sa commande y est ensuite développée, testée et validée. Le système est capable de détecter la présence de l'ombre, choisir la meilleure stratégie pour la mitiger et l'implémenter en toute autonomie. Le résultat final est une augmentation de la puissance de sortie d'environ 40% dans certains cas.

Acknowledgements

When I finished my PhD defense and finally received the degree of doctor from the University of Grenoble, a rare phenomenon took place. I was speechless. It did not matter that I had stood the previous night rehearsing my speech, or that I have done the same many nights in the previous years. When it came down to that moment, I could not utter a sound. I suppose, in many ways, that silence bore all the power of the gratitude I felt towards all the people with whom I had shared this amazing experience. Now, a few weeks afterwards and in the comfort of my study I can finally turn silence into words while remaining speechless.

There are two important elements in acknowledgements: order and singularity. People like to be remembered first and alone, the rest can come later and together. We all abhor being part of and confounded with a great mass. However, it is the mass and its interactions that hold our memory true to its powerful feelings. So I have chosen to thank people in groups, trying my best to be exhaustive in their names and roles. I'll keep the first and the last spot to those special privileged who have earned the pole.

The first group I wish to thank is my supervisors. Both Bertrand and Jean-Christophe were simply amazing in the task, never failing to inspire me to be a better researcher. Our meetings and discussions have ranged from extremely specific subjects of the thesis to powerful personal insights. They have tough me to constantly challenge myself, my work and my dreams. If I ever become someone great, it will be no little to their influence and example. If I don't, they have sure tried.

But we could not work without an environment, which leads me to the second group: the G2ELab. There are, literally, hundreds of people that I know in this amazing laboratory. I had the great pleasure of having most of them at my thesis defense and thanking them in person for their great support. But there are always a few who get to contribute in a special way. My good friends from the Master degree helped me keep my sanity in great moments of doubt: Lyubo, Myriam, Sellé, Julian, Mihn and Hoaghang, thank you. But also the new friends that came along for the ride, who I had the pleasure to supervise (exploit?) like Phu, Xavier, Farshid, Viky, Joris and Bénédicte. The technicians Cédric and Antoine had also an important role in putting together the final prototype or keeping me alive while climbing. Without your work and help, I would never have come so far.

In Grenoble, another institution had a decisive role in forging the prototype used in this work: Freemens S.A. This start-up is composed by a handful of very interesting and dedicated people who have never failed to rescue me from my ignorance. A special thanks to Boris Fanitch for his dedication and professionalism in developing the communication protocol used to transfer information from the PV Equalizer to my computer. A great thanks for Alexander Collet and Fabien Mestralet also helped by shining those heaven sent insights on my ideas in my darkest control-conception moments. Of course, all of them have also provided me with an important degree of companionship which kept me going during these past three years. A bond to which I am also deeply thankful.

Another institution has also helped me to greatly advance my thesis. I can basically say that most of the ideas that I explored came from the three months I spend in the National Informatics Institute in Tokyo, Japan. This powerful moment of my life was only possible due to the help and support from Professor Shinichi Honiden and Doktor Benjamin Klöpper. Your ideas and discussions at the 15^{th} floor of the NII with a breathtaking view of the Skytree will remain carved in my memory for the rest of my existence. Along with, of course, the sunrise from the top of the Mount Fuji. Thank you for believing in my work.

All this help, however, would suit no purpose if there were not people to evaluate and criticize it. Thus, my reviewers and jury are an important piece in this puzzle. Either through their returns or new ideas, their contribution has greatly enhanced the final version of this document. Together we made science advance another step and I could not think of a better jury to share that contribution with. A special thanks goes to Professor Felix Farret whose book has inspired me to take the road of renewable energies to save the world.

In the turmoil of my work, there were times where I would relieve myself through the art of teaching. These very interesting and character building moments were shared with Delphine Riu, Nico Laverdure and Thierry Creuzet, with whom I had many opportunities to discuss about our roles in society and in the classroom. I definitely have to thank the DFI of the University of Grenoble for teaching me how to teach and question my own representation of learning. To my students during my PhD: thank you and sorry. You gave me much more than I could possibly return, a debt I intend to pay forward to the next generations that will come into my classrooms.

To the innumerable friends with whom I have shared important moments of philosophical truth and wisdom during these past few years, my anonymous and eternal thank you. Among them, a special hug to Ando Raminosoa for Merindol and Gwen Maillet for giving me a roof under which I could pile up my stuff. You can now smile as you read these lines.

Finally, there are three important acknowledgements missing in this text. First of the last is Professor Seddik Bacha, whose "yes" over the telephone 5 years ago has changed my life forever. It is impossible to tell what would have happened to me if I had called someone else, but I guess a good part of life is made of luck and another of the good people we meet. I was lucky to meet a great person then and glad for being his friend now.

Before the end, as always, we remember the people we whom we share natural bonds of love. These people help us form ourselves, our qualities and our limitations. Their choices impact us to the very last day of our lives and lives on through our choices onto the life of others. To my both grandmothers who have crossed long oceans, one of water and another of tears, in the name of the love for their families, my eternal love. To my both parents who have found in them the courage to believe in their own education, invest their time and patience into it, to finally share this important gift with me, my deepest thanks. You are all extremely important role-models, even if I never follow what you tell me to do.

And last, because the last are always the first from the beginning, Cecilia. To you, gatinha, no words are necessary. Or enough.

To All

Research is what I'm doing
when I don't know what I'm doing.
Wernher von Braun

Contents

List of Figures

List of Tables

Résumé de la thèse

Une grande portion du potentiel photovoltaïque installé dans le monde se trouve en zones urbaines ou suburbaines. Leur proximité de la charge est un atout important à leur emplacement, avantage réduit par la présence des ombres. Celles-ci peuvent être issues de la présence d'arbres, de cheminées ou d'autres obstacles situés aux alentours des installations photovoltaïques.

Les ombres et leur impact sur la production photovoltaïque ont fait l'objet de plusieurs études. Cependant, il manque encore une vision globale qui permet à la fois de comprendre le phénomène d'ombrage et d'évaluer les solutions jusqu'à présent proposées. Sans cette méthode d'analyse, la question de l'intermittence demeure simplement une motivation à l'introduction des nouvelles topologies d'électronique de puissance ou algorithmes de commande.

Dans ce contexte, les travaux de thèse décrits dans ce document ont deux objectifs complémentaires. D'une part, ils proposent une théorie capable de décrire la totalité des solutions actuellement disponibles dans la littérature scientifique et d'autre part, il s'en sert pour proposer une nouvelle solution. Par conséquent, ses contributions sont aussi divisées en deux parties.

Dans un premier temps, une étude générale des systèmes photovoltaïques et de leur intermittence sera conduite. Elle propose un modèle d'ombre original qui est capable de réunir, à la fois la géométrie de l'ombre et les interconnections électriques du module photovoltaïque. Ce modèle est utilisé pour proposer une théorie sur l'intermittence photovoltaïque, aussi originale dans le domaine. Ces deux sont réunis pour faire une lecture des différentes solutions qui figurent dans la littérature au moment de l'écriture de ce document, classifiés par la suite en solutions du type séries et parallèles. Suite à une mise en évidence de leurs points forts et de leurs limitations, le choix a été fait de contribuer à l'amélioration des solutions de type parallèle. Cette première partie correspond à la première section de ce résumé ou le chapitre 2 du manuscrit.

Dans un deuxième temps, une étude approfondie d'une solution parallèle innovante appelée l'Equilibreur PV sera proposée. Le principe de fonctionnement de l'Equilibreur PV repose sur l'équilibrage de la disparité des courants au sein d'un module photovoltaïque ombré. Sa topologie d'électronique de puissance est présentée et étudiée en détails permettant la description de ses différentes fonctions. Chacune d'entre elles est analysée séparément et leurs résultats sont réunis pour la création d'un système de commande pour l'Equilibreur PV. Cette partie est composée par les reste de ce résumé ou les chapitres 3 à 6 du manuscrit.

Finalement, la conclusion propose une comparaison entre l'Equilibreur PV et les autres solutions et des perspectives de recherche future.

Chapitre 2 : Les systèmes photovoltaïques

Cette section porte sur l'étude générale des systèmes photovoltaïques (PV) et ses problèmes d'intermittence. A leur intersection se trouvent plusieurs travaux disponibles dans la littérature, qui seront aussi étudiés. Les conclusions sont d'autant plus importantes qu'elles seront utilisées pour justifier les contributions proposées dans les prochaines sections de ce résumé.

Les principes du PV

Les applications PV convertissent la lumière en électricité par le phénomène appelé effet photovoltaïque. Son expression, détaillée dans l'équation 1, relie le courant, la tension, la température et la lumière.

$$i = i_{ph} - i_0 \left(\exp \left[\frac{(V + i \cdot R_s)}{V_t} \right] - 1 \right) - \frac{V + i \cdot R_s}{R_p} \tag{1}$$

i_{ph} représente le photo-courant, R_p et R_s respectivement la résistance parallèle et série, i_0 le courant de saturation inverse, i et V le courant et la tension de sortie. La variable V_t symbolise la tension thermique et est décrite par l'équation 2.

$$V_t = \frac{A \cdot k \cdot T_c}{q} \tag{2}$$

La variable A est le facteur d'idéalité, k constante de Boltzman, T_c la température d'opération et q la charge électronique. L'énergie dégagée par une source de lumière est appelée *irradiance* et mesurée en watt par mètre carré ($\frac{W}{m^2}$).

Pour des questions de simplicité, la production PV est décrite par des courbes caractéristiques. A titre d'exemple, deux courbes génériques sont montrées dans la figure 2.3, à savoir la courbe qui montre la variation du courant en fonction de la tension (I-V) et celle qui montre la variation de la puissance avec la tension (P-V).

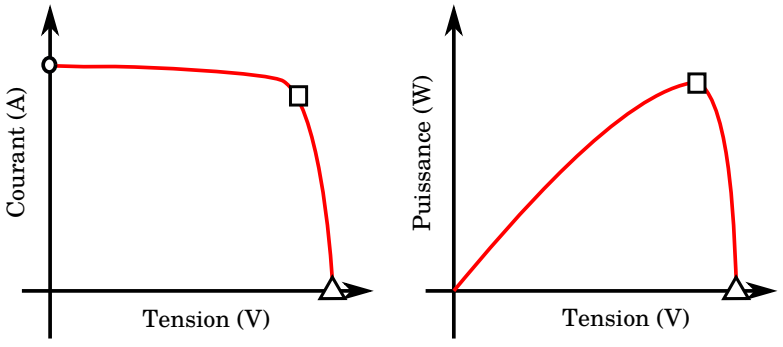

(a) La courbe I-V (b) La courbe P-V

Figure 1: Deux courbes caractéristiques génériques

Il est possible de distinguer trois points communs aux deux courbes ci-dessus. Il s'agit du *courant de court-circuit* (i_{SC}) représentée par un cercle, de la *tension de circuit ouvert* (V_{OC}) représentée par un triangle et le *point de puissance maximale* (MPP) représenté par un carré. Ce dernier représente la tension ou le courant qui maximise la production d'énergie.

Le MPP d'une application PV peut éprouver des changement selon les conditions de température et de lumière. Il est, donc, impératif de l'asservir à l'aide des structures d'électronique de puissance.

Les systèmes PV

L'objectif des systèmes PV est d'extraire l'énergie produite par les modules photovoltaïques et de l'acheminer jusqu'à une charge ou le réseau électrique. La figure 2 montre une vue simplifiée du système dans sa totalité.

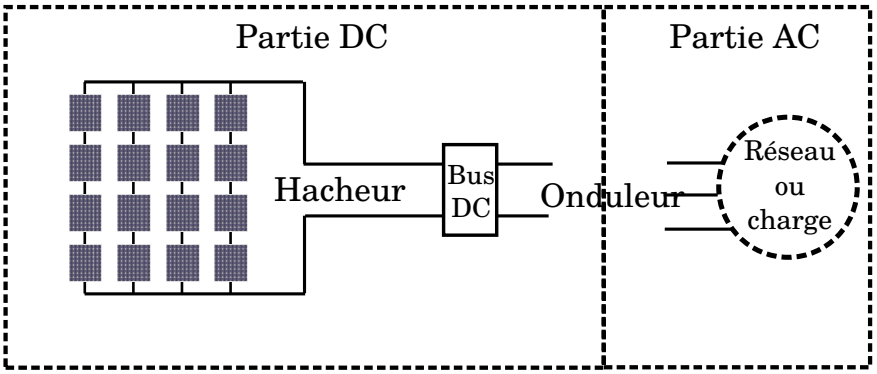

Figure 2: Le système PV complet

Deux parties sont mises en évidence dans la figure ci-dessus: à gauche la partie DC et à droite la partie AC. La première est composée par l'application PV, le hacheur DC, le bus continu et l'entrée de l'onduleur. La deuxième est composée par la sortie de l'onduleur et le réseau ou la charge. Ce document considère que l'effet de l'ombre est limité à la partie DC et que la tension du bus continu est fixe.

Pour des contraintes techniques, les études de cette thèse ont été menées à l'échelle d'un seul module PV, dit module de référence. Ceci est composé par 72 cellules connectées en série regroupées par groupe de 18 cellules. Dans ce texte, ces groupes PV seront appelés PV_I, PV_{II}, PV_{III} et PV_{IV}. Leurs symboles figurant dans les schémas électriques sont montrés dans la figure 3. Les caractéristiques complètes du module sont disponibles dans l'Annexe B.

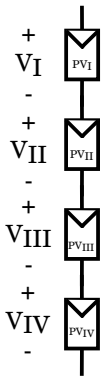

Figure 3: Symbole électrique du module PV de référence

Du fait de l'intermittence, le MPP du module PV est susceptible de varier au cours du temps. Cette forte contrainte fait appel à une loi de commande spéciale pour piloter le hacheur DC-DC connecté en série au module PV appelée *Maximum Power Point Tracking (MPPT)*. Elle repose sur le format de la courbe P-V du module montrée à la figure 2.11.

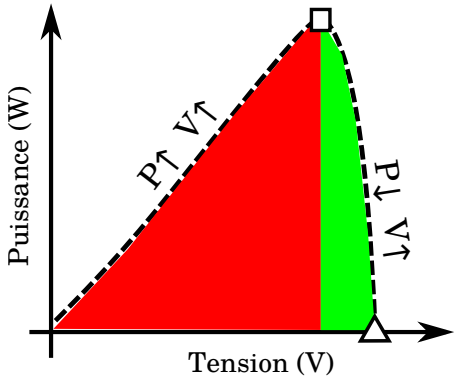

Figure 4: Les deux zones de la courbe P-V

La partie rouge de la figure ci-dessus constitue une zone dans laquelle une augmentation de la tension conduit à une augmentation de la puissance produite par le module. A contrario, dans la zone verte une diminution de la tension mène à une augmentation de la puissance. Le MPPT appliquera des légères variations de tension et observera la réaction de la puissance de sortie. Si celle-ci monte, le sens de la variation reste inchangé, alors que si elle baisse, le sens est inversé.

Compte tenu du fait que le module PV peut être vu comme une source de courant, le système PV total est remplacé par une source de courant variable, comme montre la figure 5.

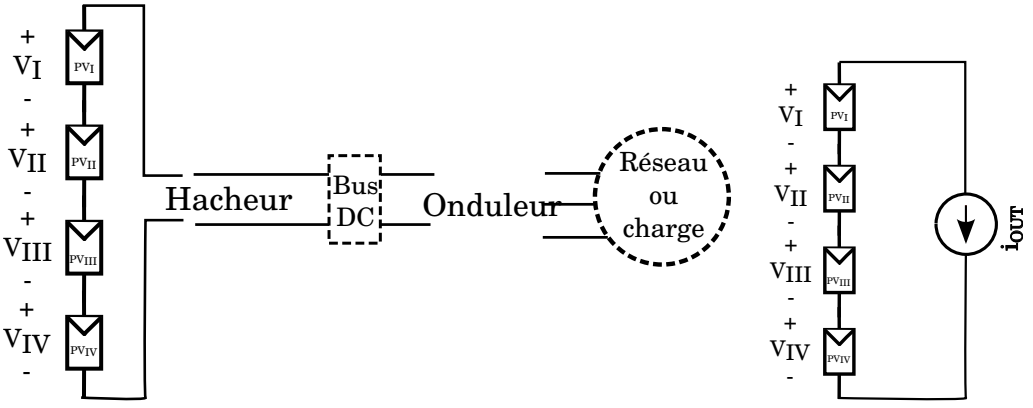

(a) Le système PV complet

(b) Le système PV simplifié

Figure 5: L'équivalence du système PV

Après l'introduction des simplifications et des principes de la production PV, ses imperfections peuvent maintenant être présentées.

Les imperfections de la production PV

Dans ce travail, les imperfections des systèmes PV sont classifiées comme internes et externes.

Les imperfections internes ont leurs origine à l'intérieur des modules PV. Par exemple elle, peuvent être dues aux mauvaises soudures, au vieillissement des cellules, aux impuretés dans les cristaux de silicium ou à la variabilité de la production des modules. Ils affectent principalement la résistance série (R_s), la résistance parallèle (R_p) et le courant

de saturation inverse (i_0) [van Dyk and Meyer, 2004, Bun, 2012]. Plusieurs auteurs ont déjà travaillé sur cette problématique [Appelbaum et al., 1995, Junior, 1979, Chamberlin et al., 1995, Picault et al., 2010b,a, Kaushika and Rai, 2007, Kaplanis and Kaplani, 2011, Ye et al., 2013]. Quelques techniques pour combattre ce type d'imperfection peuvent être trouvées dans [Appelbaum et al., 1995, Chamberlin et al., 1995].

Les imperfections externes sont liées aux changement du photo-courant (i_{ph}) ou de la tension thermique (V_{th}) du module PV. Celles-là peuvent être causées par des fissures dans les cellules PV suite à un stress mécanique ou thermique [Ramli and Salam, 2011, Arnett, 1981, Alonso-Garcia et al., 2006] ou par la connexion en série des cellules PV avec des irradiances différentes [Abdalla et al., 2013, Ramli and Salam, 2011, Wang et al., 2012, Bidram et al., 2012, Villa et al., 2013]. Dans ce travail, une attention particulière a été portée sur ses dernières, appelées *ombrages partiels*.

Lorsqu'un module PV se trouve sous des conditions d'ombrage partiel, une ombre se trouve sur un ou plusieurs de ses groupes de cellules. Par conséquent, les groupes ombrés produiront un courant plus faible que les groupes illuminés. Ce fait conduit à une limitation du courant des groupes illuminés dans le meilleur des cas. Dans le pire cas, le courant le plus élevé est imposé sur les groupes ombrés qui finissent par être détruits [Kawamura et al., 2003]. Pendant le reste de ce travail, le MPPT est considéré comme capable d'éviter le deuxième cas, mais pas le premier.

L'ombre étant un élément clé de ce travail, un effort de modélisation particulier lui a été dédié par la suite.

Le modèle de l'ombre

Une ombre est considérée dans ce travail comme une projection à deux dimensions d'un objet à trois dimensions. Elle compte une longueur et une largeur, selon l'objet qui la projette.

Une autre « dimension » intervient aussi dans le cas des ombres pour le photovoltaïque: l'opacité. Plus l'ombre est opaque, plus faible est le courant des cellules PV ombrées.

L'opacité est appelée *taux d'ombrage (TO)* dans ce document et elle est représentée par un chiffre entre 0 et 1. Un TO de 0 signifie absence de l'ombre, alors qu'un TO de 1 dénote un filtrage total de l'irradiance par l'ombre. Les dimensions géométriques de l'ombre et son TO sont représentés dans la figure 6.

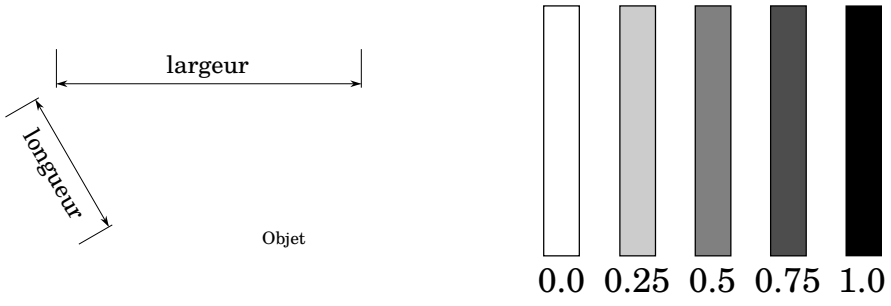

(a) La largeur et longueur d'une ombre (b) Le taux d'ombrage

Figure 6: La description de l'ombre

Une quatrième dimension peut être aussi intégrée à l'ombre: le temps. Compte tenu de l'existence de plusieurs groupes de cellules à l'intérieur du module PV, l'ombre et son évolution dans le temps seront représentés par des *états*. Un état est composé par un

vecteur à quatre chiffres, dont chacun décrit le taux d'ombrage d'un groupe de cellules. La figure 7 montre l'équivalence entre le module PV de référence et son modèle à états.

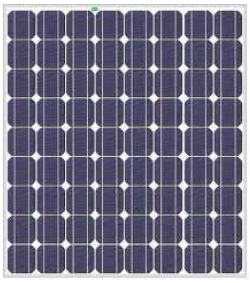

(a) Le module PV de référence

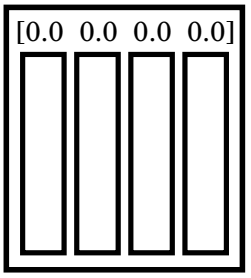

(b) Le modèle à états

Figure 7: Le module PV de référence et le modèle à états

Pour simplifier la représentation des états d'ombre, un modèle binaire est aussi utilisé. Il consiste à utiliser un seuil de référence sur TO et le comparer avec les TO de chaque groupe PV. Les groupes dont la valeur du TO dépasse celle de référence seront considérés comme ombrés (1) et ceux dont la valeur du TO se trouve en dessous seront considérés comme non-ombrés (0).

En guise d'exemple, la figure 8 montre l'application du modèle à états et sa simplification en modèle binaire avec un TO de référence de 0.3.

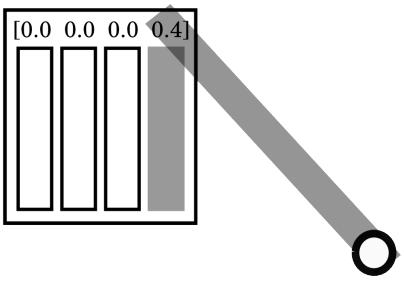

(a) Le modèle à états et son vecteur d'ombre

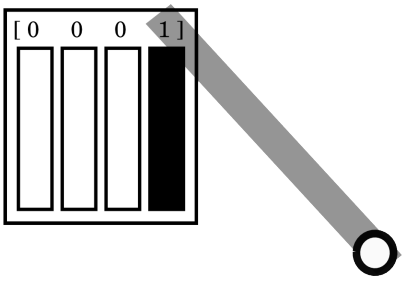

(b) Le modèle binaire et son vecteur équivalent

Figure 8: La simplification du modèle à états en modèle binaire

Dans certains schémas électriques, le modèle à états est utilisé pour faciliter leur lisibilité. La figure 9 montre l'équivalence entre celui-ci et le symbole électrique du module PV. La valeur précise du TO est donnée pour le circuit où figure l'ombre.

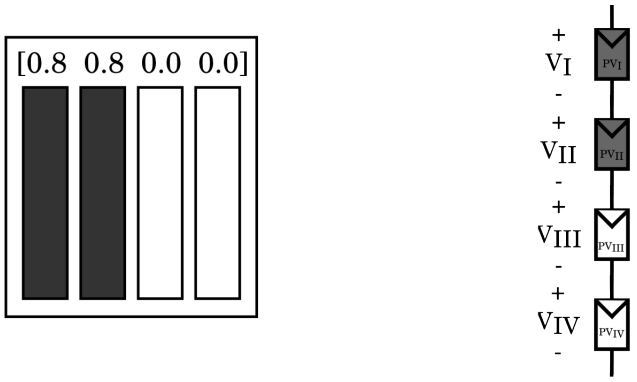

(a) Un exemple d'ombre décrite par le modèle à états (b) Son circuit électrique équivalent

Figure 9: L'équivalence entre le module à état et le symbole électrique du module PV

Les modèles ci-dessus impliquent un lien entre l'ombre et les connectiques électriques internes du système PV. Ce principe est à la base de la théorie d'intermittence proposée ci-dessous.

Une théorie sur l'intermittence PV

La théorie proposée dans cette thèse affirme que *l'intermittence PV est composée de deux parties: optique et électrique.*

L'intermittence optique vient limiter la quantité d'*énergie reçue* par les cellules PV. Elle ne peut être résolue que par l'utilisation des solutions externes à l'application PV. Ces solutions doivent apporter l'énergie perdue, pouvant être composées par du stockage électrique ou d'autres centrales de production d'électricité. Les applications PV capables de produire régulièrement de l'énergie en présence des ombrages partiels peuvent être considérées comme **stables**. Plus une application PV est stable, moins elle fera recours à de l'aide externe.

L'intermittence électrique affecte la quantité d'*énergie délivrée* par les cellules PV. Elle ne peut être adressée que par des solutions internes à l'application PV. Ces solutions doivent garantir une extraction maximale de l'énergie PV en présence d'ombre. Les applications PV capables de produire plus d'énergie lors que la présence des ombrages partiels sont considérées comme **robustes**. Plus une application PV est robuste, moins elle a besoin de modules supplémentaires pour délivrer une même quantité d'énergie.

Les concepts de stabilité et robustesse d'une centrale PV mènent à trois corollaires de cette théorie. Le premier corollaire affirme qu'*une centrale robuste a besoin de moins d'aide externe pour être stable.* Le second corollaire pose qu'*il existe une limite pour la robustesse mais aucune pour la stabilité.* Le troisième corollaire défend qu'*il n'existe que quatre méthodes pour augmenter la robustesse d'une centrale photovoltaïque.*

Les méthodes citées dans le troisième corollaire consistent à surdimensionner l'application PV, diminuer le nombre de cellules par groupe, redistribuer le courant entre les groupes de cellules et court-circuiter les cellules ombrées. Elles regroupent toute la littérature existante concernant la résolution du problème d'ombrage partiel dans les applications PV. Dans ce travail, elles seront appelées PRobES (de l'anglais Photovoltaic Robustness Enhancing Solutions).

Photovoltaic Robustness Enhancing Solutions - PRobES

La **PRobES de référence**, largement employée par l'industrie, est la diode de bypass. Elle devient naturellement passante dans le pire cas d'ombrage naturel, où les cellules illuminées imposent leur courant sur celles qui sont ombrées. Les cellules ombrées deviennent à leur tour court-circuitées et leur puissance est perdue. Par conséquent, les courbes P-V sont déformées, rajoutant un nouveau challenge au MPPT. Plusieurs chercheurs concentrent leurs efforts sur la conception d'algorithmes performants et capables de trouver le MPP sous n'importe quelle condition d'ombrage [Ramos-Paja et al., 2010, Ishaque, 2012, Nguyen and Low, 2010].

Après les diodes de bypass, il existe deux grandes familles de PRobES dans la littérature: séries et parallèles.

Les **PRobES séries** reposent sur l'utilisation d'un grand nombre de convertisseurs d'électronique de puissance au sein de l'application PV. Cela permet une diminution du nombre de cellules asservies par chaque convertisseur et une restriction de l'effet de l'ombre. Leur défi technologique est concentré sur l'efficacité des convertisseurs à basse puissance. [Ishaque, 2012, Safari and Mekhilef, 2011, Ramos-Paja et al., 2010, Giral et al., 2011, Nguyen and Low, 2010, Woyte et al., 2003]

Les **PRobES parallèles** cherchent à redistribuer le courant entre les cellules ombrées et non-ombrées, son principe est illustré par la figure 10.

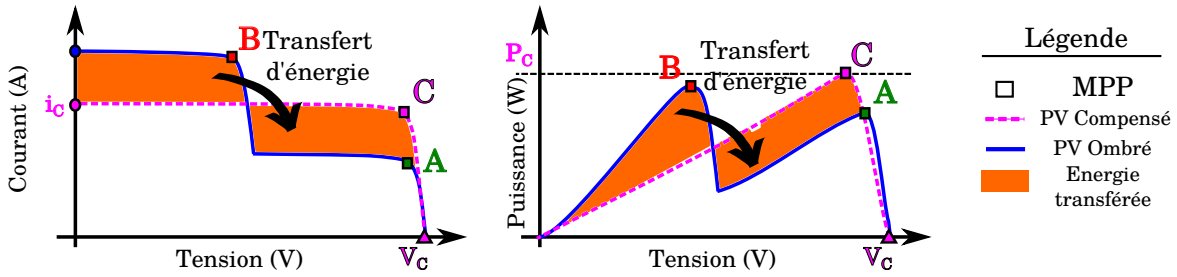

(a) Leur effet sur la courbe I-V (b) Leur effet sur la courbe P-V curve (c) Légende

Figure 10: Le principe des PRobES parallèles

La redistribution du courant consiste à répartir l'effet de l'ombre de façon équivalente entre les cellules PV. Par conséquent, l'énergie disponible dans les cellules ombrées n'est pas perdue. Cependant, les PRobES parallèles ont deux contraintes technologiques fortes: la complexité de leurs inductances et de leurs commandes [Kadri et al., 2011, Walker et al., 2003, Nimni and Shmilovitz, 2010, Shimizu et al., 2001, 2003]. Ces deux verrous les empêchent d'être utilisées par l'industrie.

Inspiré de ces challenges, la contribution majeure de cette thèse porte sur une PRobES parallèle, sa topologie innovante et sa commande associée.

Chapitre 3 : L'équilibreur photovoltaïque

L'innovation majeure proposée dans ce document est une PRobES appelée « Equilibreur PV ». Elle est inspirée d'une topologie appliquée au stockage électrique [Park et al., 2009], qui est présentée dans cette section avec ses fonctions et caractéristiques.

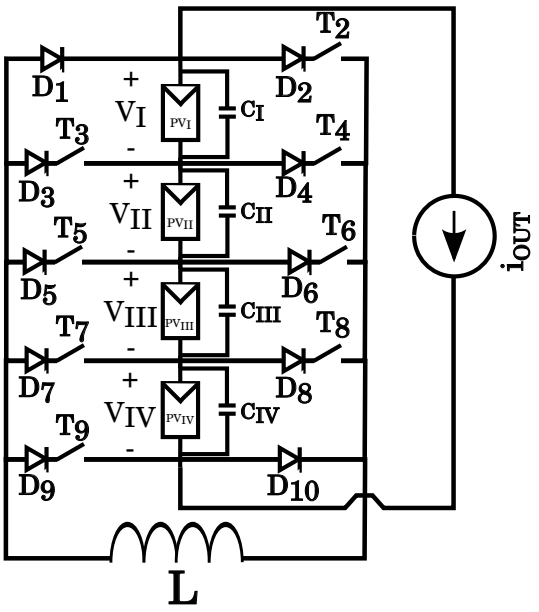

Figure 11: La topologie de l'Equilibreur PV

La topologie proposée

La figure 11 présentée la topologie de l'Equilibreur PV. Elle est composée de 8 transistors (T_2 - T_9), 10 diodes (D_1 - D_{10}), 4 condensateurs (C_I - C_{IV}) et une seule inductance (L).

Le réseau de transistors autour des cellules PV permet le transférer du courant entre elles à travers de la seule inductance. Les condensateurs C_I à C_{IV} ont pour rôle de filtrer les variations de courant et de tension dans les cellules PV lors des commutations des transistors. Les diodes D_1 et D_{10} constituent une fonction de sécurité supplémentaire qui se déclenche automatiquement si la tension du module PV devient négative.

Les fonctions de l'Equilibreur PV

L'Equilibreur PV peut compenser ou détecter la présence de l'ombre. La compensation est assurée par la fonction d'équilibrage et de bypass, alors que la détection se sert de la fonction de scrutation. Ces trois fonctions sont introduites dans cette section et étudiées en détail dans les sections suivantes.

La fonction d'équilibrage

La fonction d'équilibrage utilise une stratégie de commutation et un rapport cyclique pour faire le transfert d'énergie entre les groupes de cellules PV.

Une stratégie de commutation est composée par une seule charge et décharge de l'inductance. Elle est appelée **BSS**, de l'anglais basic switching strategy. Tous les BSS sont représentés par une notation spéciale présentée par les circuits dans la figure 12. Dans ces trois cas, l'ombre se trouve sur le groupe de cellules PV_{III}.

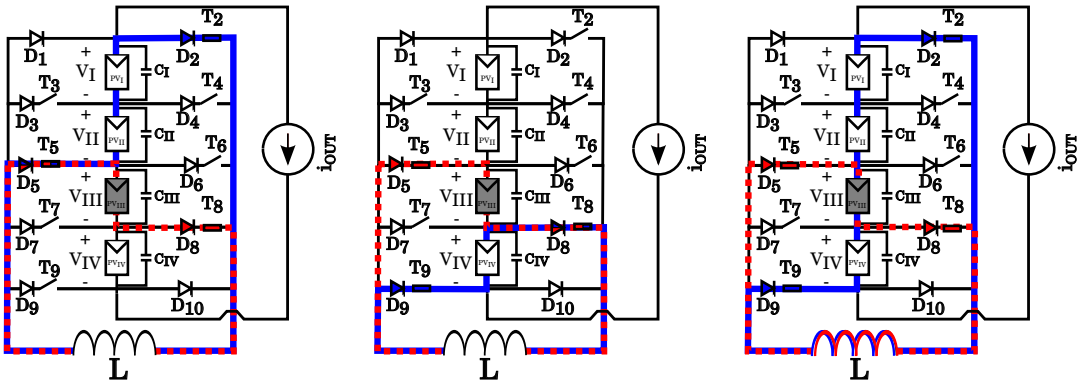

(a) $I.II \rightarrow III$ (b) $IV \rightarrow III$ (c) $All \rightarrow III$

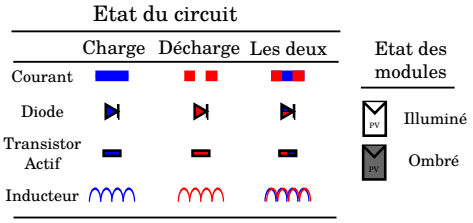

(d) Légende

Figure 12: La notation des stratégies de commutation

Dans le circuit de la figure 12(a), les groupes PV_I et PV_{II} sont utilisés pour charger l'inductance. Lors de la phase de décharge, celle-ci est connectée en parallèle au groupe PV_{III}. Cette BSS est représentée par $I.II \rightarrow III$, la flèche donnant le sens du transfert d'énergie. Les groupes qui donnent de l'énergie figurent à gauche et celui qui en reçoit se trouve à droite. La même convention est utilisée pour l'exemple de la figure 12(b), ce qui donne $IV \rightarrow III$. La stratégie résultante de l'utilisation consécutive des 2 BSS des figures 12(a) et 12(b) est appelée **CSS** de l'anglais Complex Switching Strategy

Afin d'éviter l'utilisation des CSS, un autre type de stratégie de commutation est proposé par la figure 12(c). Cette stratégie, dite **Universelle**, est représentée par $All \rightarrow III$ où All fait référence à toutes les groupes de cellules PV.

Le rapport cyclique est calculé selon l'équation 3, où n_{CH} correspond au nombre des groupes utilisés pour charger l'inductance et n_{SH} au nombre des ceux qui la déchargent.

$$D = \frac{n_{DCH}}{n_{CH} + n_{DCH}} \tag{3}$$

Les BSS sont considérées comme indépendantes et lorsqu'elles composent une CSS leur rapport cyclique est calculé séparément.

La fonction de bypass

La fonction de bypass a pour rôle de court-circuiter les groupes de cellules PV ombrés. Cela permet au MPPT de chercher le MPP le plus haut, comme dans le cas des diodes de bypass. Pour ce faire, l'Equilibreur PV doit simplement fermer les transistors de décharge autour des groupes de cellules ombrées. Lorsque le MPPT impose un courant plus élevé que l'i_{SC} des cellules ombrées, leurs tensions deviennent négatives et un courant circule à travers de l'inductance. Ce principe est illustré par la figure 13.

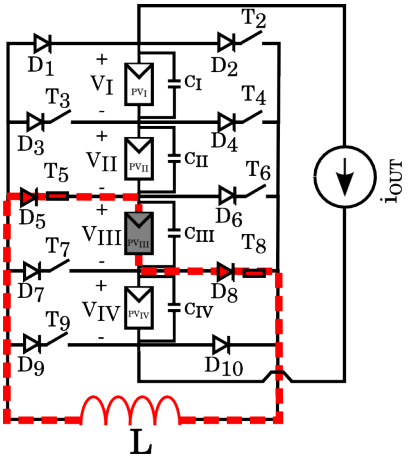

Figure 13: Le principe de la fonction bypass

La fonction de scrutation

Le principe de la fonction de scrutation consiste d'échantillonner l'énergie de chaque groupe de cellules PV pour en déduire l'emplacement de l'ombre. Cela est fait au travers de lectures de courant prélevées suite à des charges très courtes de l'inductance par un seul groupe. Leurs résultats sont comparés entre eux une fois la scrutation finie. La figure 14 illustre ce principe par un exemple où l'ombre est située sur PV_I.

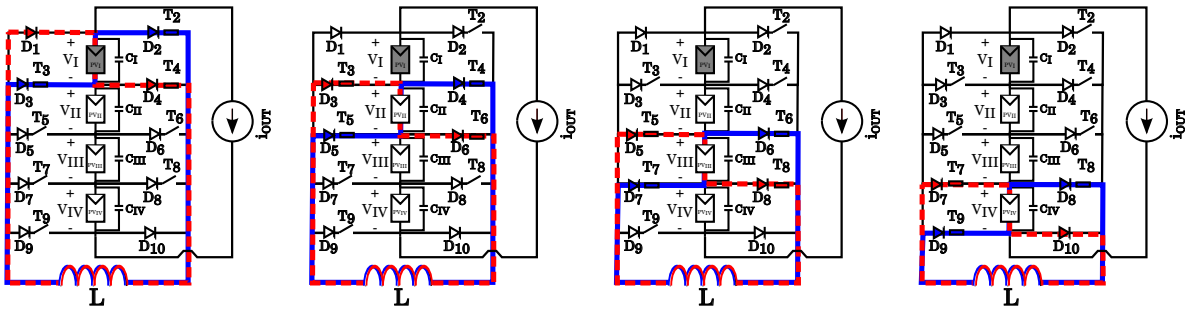

(a) Scrutation sur PV_I (b) Scrutation sur PV_{II} (c) Scrutation sur PV_{III} (d) Scrutation sur PV_{IV}

Figure 14: Le principe de la fonction de scrutation

L'évolution dans le temps de la tension et du courant dans l'inductance est illustrés par la figure 15, où le pic plus bas indique la présence de l'ombre.

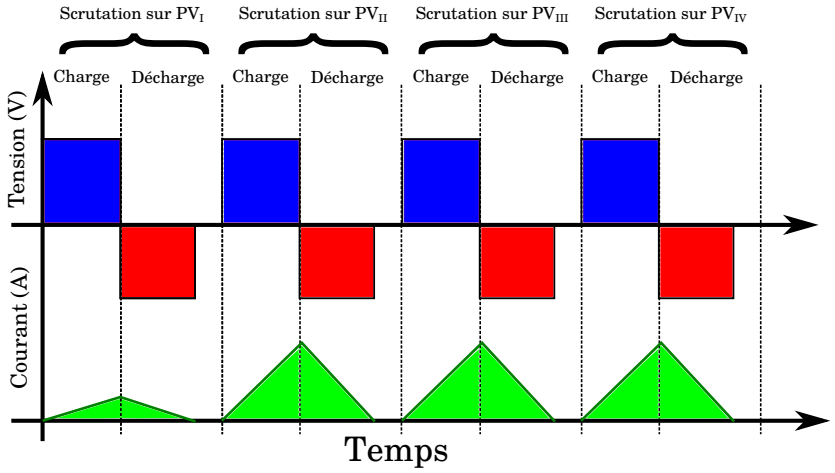

Figure 15: La tension et le courant dans l'inductance pendant la scrutation

Il est important de remarquer que l'utilisation de la fonction de scrutation cause l'interruption de la production d'énergie. Même si celle-ci dure seulement quelques microsecondes, son coût énergétique est non nul. Par conséquent, elle doit être utilisée avec parcimonie.

Validation pratique

Pour valider l'Equilibreur PV, deux séries de mesures ont été réalisées à l'aide du prototype développé dans ce travail et décrit dans l'annexe B. Leur objectif est de estimer les gains énergétiques pour différents taux d'ombrage. Chaque série est composée de quatre mesures, toutes faites avec les mêmes BSS et rapport cycliques. Le tableau 1 en décrit les détails.

Table 1: Les détails des mesures réalisées

Stratégie de Commutation	*irr* ($\frac{W}{m^2}$)	T_A (℃)	T_M (℃)	*Taux d'ombrage* PV_I	PV_{II}	PV_{III}	PV_{IV}
$II.III.IV \rightarrow I$	798	34.2	51.4	0.21	0	0	0
	773	33.9	51.4	0.36	0	0	0
	755	33.9	51.2	0.47	0	0	0
	735	33.4	51.3	0.56	0	0	0
$III.IV \rightarrow I.II$	851	29.2	47.2	0.21	0.21	0	0
	852	29.3	47.2	0.36	0.36	0	0
	833	30.6	49.3	0.47	0.47	0	0
	834	30.8	49.1	0.56	0.56	0	0

La figure 16 montre la variation de la puissance de sortie en fonction du taux d'ombrage. Les points représentent les mesures et les lignes leurs projections linéaires.

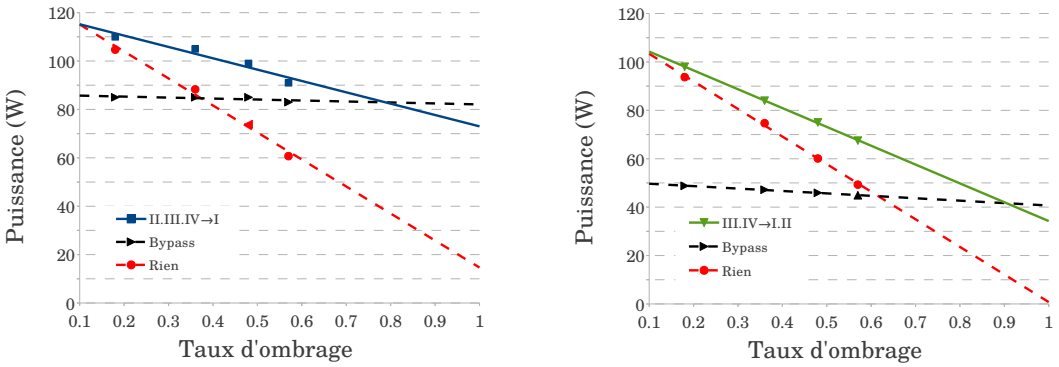

(a) $II.III.IV \rightarrow I$ (b) $III.IV \rightarrow I.II$

Figure 16: L'impact du taux d'ombrage sur la puissance du module de référence

Dans les deux cas, l'utilisation de l'Equilibreur PV augmente la puissance de sortie. Sur la figure 16(a), le gain maximal est de l'ordre de 15 W ce qui représente environ 18%. Ce gain est encore plus important pour la figure 16(b) qui compte avec un gain de 18 W soit 36%. A la vue de ces résultats très encourageants, le potentiel de cette solution est considéré comme validé. Plus des détails sur la caractérisation des pertes sont disponibles dans le chapitre 3 Cependant, son utilisation est conditionnée au développement de sa commande, sujet auquel les prochaines sections sont dédiées.

Chapitre 4 : La compensation de l'ombre

La commande de l'Equilibreur PV doit être capable de localiser l'emplacement de l'ombre sur l'ensemble des cellules et de choisir la stratégie capable de maximiser la puissance produite. Cette section présente le premier pas vers son développement par la caractérisation des fonctions de compensation de l'ombre. Elle est divisée en deux parties: la première sur le choix de la stratégie de commutation et la deuxième sur le choix du rapport cyclique.

Choix de la stratégie de commutation

La stratégie de commutation a fait l'objet d'une étude quasi-exhaustive qui comprend 20 cas d'ombre et 178 stratégies différentes. Compte tenu de sa complexité, les détails ne sont pas traités dans ce résumé. A la place, les principaux résultats sont expliqués par l'intermédiaire de l'algorithme montré dans la figure 17.

Les différents états d'ombre ont été divisés en trois types, à savoir les ombrages contigus, les non contigus et les modérés. Le choix des stratégies repose sur la comparaison du nombre de groupes ombrés (N_{SH}) et illuminés (N_{USH}).

Une seule stratégie n'est pas capable de compenser toutes les types d'ombres. En effet, chaque cas d'ombre exige une stratégie différente selon son état. Il est donc très important de détecter la présence de l'ombre correctement.

Après le choix de la stratégie de commutation, son rapport cyclique doit être estimé.

Choix du rapport cyclique

L'impact du rapport cyclique dans la puissance de sortie du module PV est étudié en théorie, simulation et pratique.

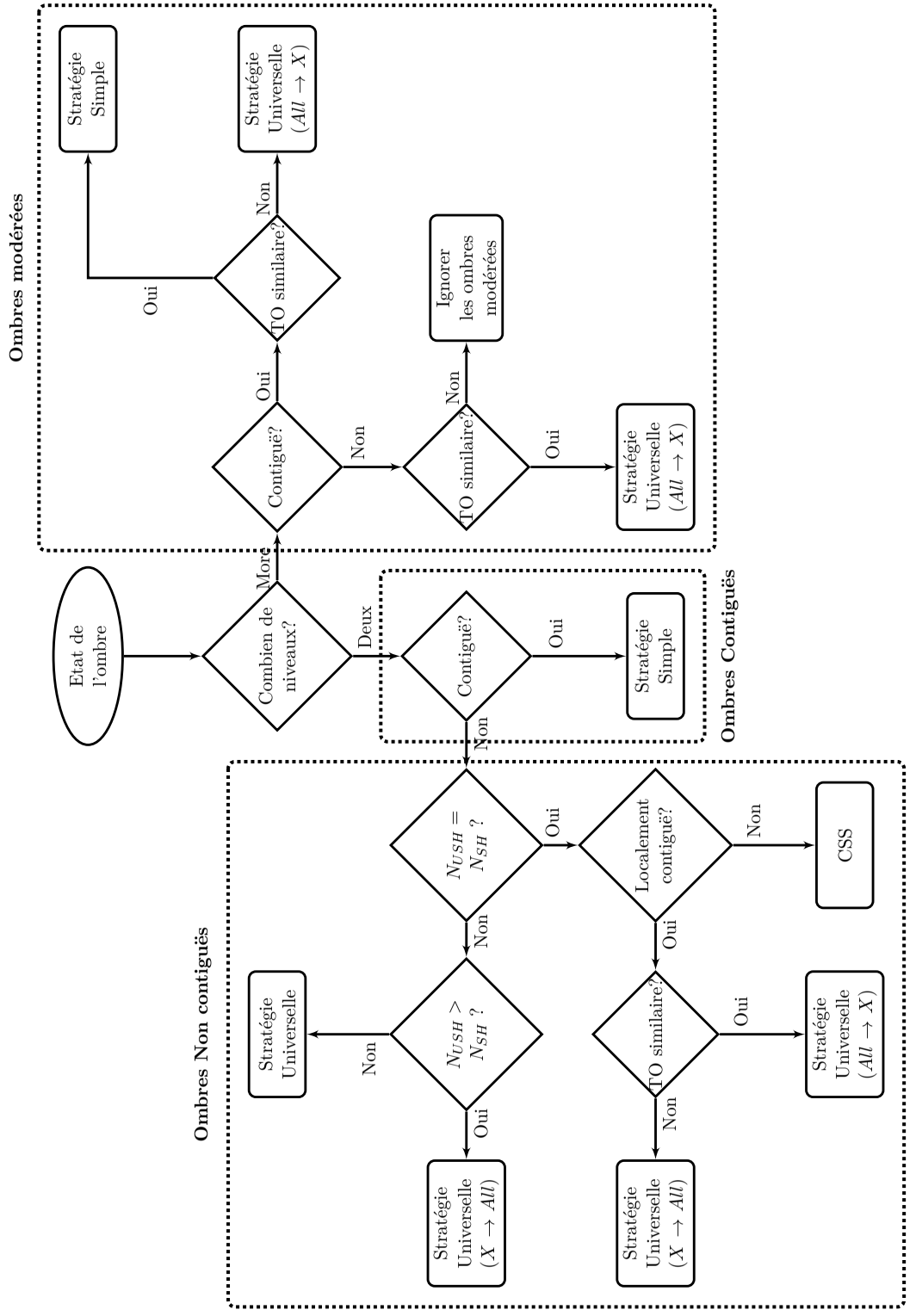

Figure 17: Algorithme utilisé pour choisir la stratégie optimale

L'étude théorique du rapport cyclique repose sur une expression mathématique qui relie celui-ci à la puissance de sortie. La figure 18 montre son résultat pour le BSS $I.II \rightarrow III.IV$.

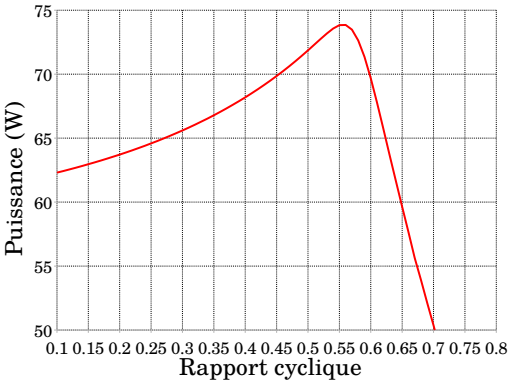

Figure 18: La puissance de sortie en fonction du rapport cyclique

La puissance de sortie pendant l'équilibrage est maximale pour un seul rapport cyclique. Pour expliquer ce phénomène, une étude par simulation a été conduite et validée en pratique.

Les conditions lors des mesures sont détaillées dans le tableau 2.

Table 2: Détails des mesures effectuées pour l'étude du rapport cyclique

Case	*Duty Cycle*	*Irr* $(\frac{W}{m^2})$	T_A ℃	T_M ℃	*SF*
$I.II \rightarrow III.IV$	0.20	757	34.1	53.9	[0 0 0.76 0.76]
	0.24	752			
	0.28	751			
	0.30	748			
	0.40	745			

La figure 19 montre l'impact du rapport cyclique sur la courbe P-V du module de référence.

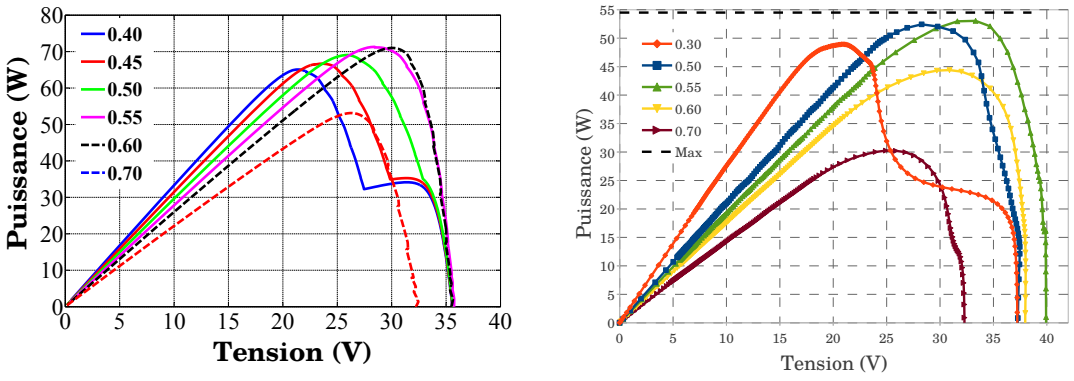

(a) Résultats de simulation (b) Résultats expérimentaux

Figure 19: Effet du rapport cyclique dans la courbe P-V

L'augmentation du rapport cyclique fait disparaître les deux MPP figurant dans la courbe P-V. Ils donnent lieu à un seul MPP, qui est maximale lorsque la valeur optimale est atteinte. Au-delà de celle-ci, la puissance diminue à cause des diodes de l'Equilibreur PV. Ces résultats montrent qu'un algorithme du type Disturb & Observe peut être utilisé pour optimiser le rapport cyclique pour n'importe quelle stratégie de commutation. Il est appelé **ODCT**, de l'anglais Optimal Duty Cycle Tracker.

L'algorithme décrit dans la figure 17 et l'ODCT donnent à l'Equilibreur PV la capacité de réagir à tous les états d'ombres possibles. Il lui reste maintenant à les trouver.

Chapitre 5 : La détection de l'ombre

La détection de l'ombre peut être faite par les méthodes directe, semi-directe et indirecte. Chacune fait l'objet d'études approfondies dont seuls les résultats sont expliqués dans cette section.

La méthode directe

La méthode directe repose sur l'utilisation récurrente de la fonction de scrutation et l'analyse de ses lectures de courant. Celles-ci représentent les écarts de tension entre les différent groupes de cellules. Cet écart peut changer si l'Equilibreur PV est actif ou pas.

Dans le cas où l'Equilibreur PV n'est pas actif, l'interprétation des lectures porte sur leurs écarts. Les valeurs maximale et minimale sont utilisées pour calculer un seuil d'ombre. Tout groupe de cellules dont la lecture s'en trouve au-delà est considéré comme non-ombré, alors que celui qui se trouve en deçà est considéré comme ombré. Cette approche est illustrée par la figure 20.

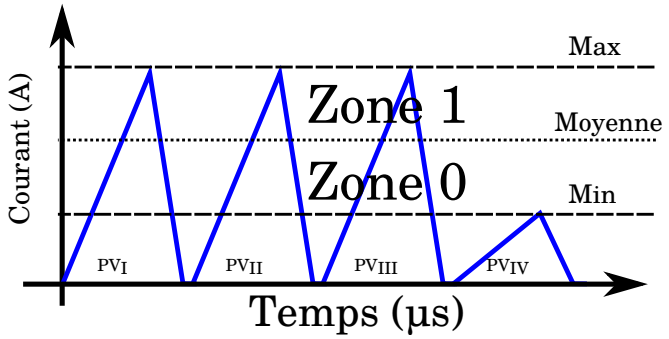

Figure 20: Interprétation des pics lorsque l'Equilibreur PV est à l'arrêt

Si l'Equilibreur PV et la fonction d'équilibrage sont actifs, l'interprétation des lectures est fortement influencée par la stratégie de commutation et l'état de l'ombre. Deux points de référence peuvent être pris pour évaluer les lectures.

Le premier point la plus haute valeur issue des groupes de cellules considérés comme illuminés. Une zone d'incertitude est établie autour d'eux, car lorsque l'équilibrage est réussit, les tensions des groupes de cellules se rapprochent et aucune information peut en être retirée. Les groupes illuminés dont la valeur des lectures se trouve en deçà de la zone d'incertitude ont leur état changé vers ombré ($0 \rightarrow 1$), alors que les groupes ombrés dont les lectures se trouvent au-delà deviennent illuminés ($1 \rightarrow 0$).

Le deuxième point de référence utilise la valeur la plus faible issue des groupes de cellules considérés comme ombrés. Le principe de la zone d'incertitude reste inchangé,

aussi bien que l'interprétation des pics. Un exemple de deux références est disponible dans la figure 21.

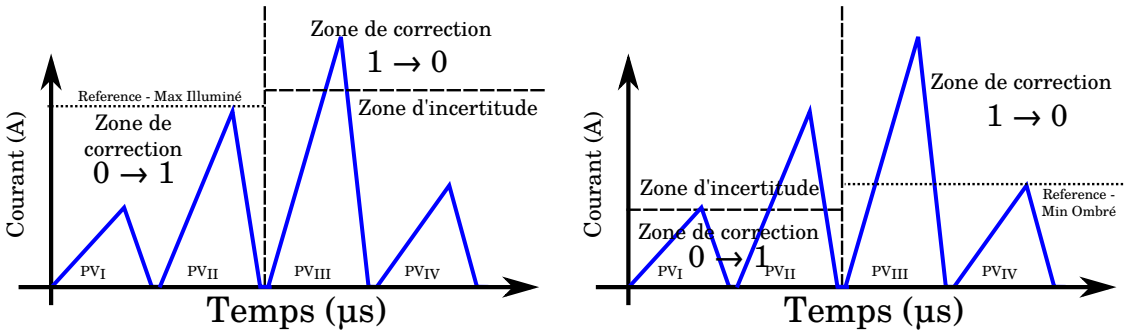

(a) Interprétation avec le premier point de référence

(b) Interprétation avec le deuxième point de référence

Figure 21: Interprétation des lectures lors de l'équilibrage

L'utilisation systématique et récurrente de la fonction de scrutation rend la méthode directe stable mais énergétiquement chère. Ce problème est traité par la méthode semi-directe.

La méthode semi-directe

Le but de la méthode semi-directe est de trouver une ou plusieurs variables dont le comportement peut être observé et lié au mouvement de l'ombre. Cela permet de déclencher la scrutation seulement si nécessaire. Les variations des valeurs moyennes du courant dans l'inductance et du courant de sortie portent l'information voulue. Le tableau 3 montre leur relation avec l'ombre.

Table 3: Les relations entre les changements dans l'ombre et les courants observés

	$\Delta\overline{i_L} > 0$	$\Delta\overline{i_L} < 0$
$\Delta\overline{i_{OUT}} > 0$	L'ombre se contracte et son TO est constant.	L'ombre ne se déplace pas et son TO diminue.
$\Delta\overline{i_{OUT}} < 0$	L'ombre ne se déplace pas et son TO augmente.	L'ombre est en expansion et son TO est constant.

La détection des mouvements liés à la forme de l'ombre doit être prioritaire car ils doivent être suivis d'un changement de la stratégie de commutation. Par conséquent, lorsque des changements avec le même signe sont observés pour les valeurs moyennes des courants, une scrutation doit être déclenchée. Le taux d'ombrage peut être corrigé par des changements dans le rapport cyclique, ce qui est fait automatiquement par l'ODCT.

Les méthodes directe et semi-directe partent de l'hypothèse que l'ombre est un phénomène complètement aléatoire. La méthode suivante cherche à réviser cette idée et à proposer un modèle qui peut être utilisé par l'Equilibreur PV pour « anticiper » les mouvements de l'ombre.

La méthode indirecte

La méthode indirecte cherche à créer un modèle qui lie les états d'ombres entre eux à travers des probabilités de transitions. Un certain nombre d'ombres et de trajectoires théoriques sont confrontés au modèle d'état du module PV, ce qui a abouti à la chaîne de Markov de la figure 22.

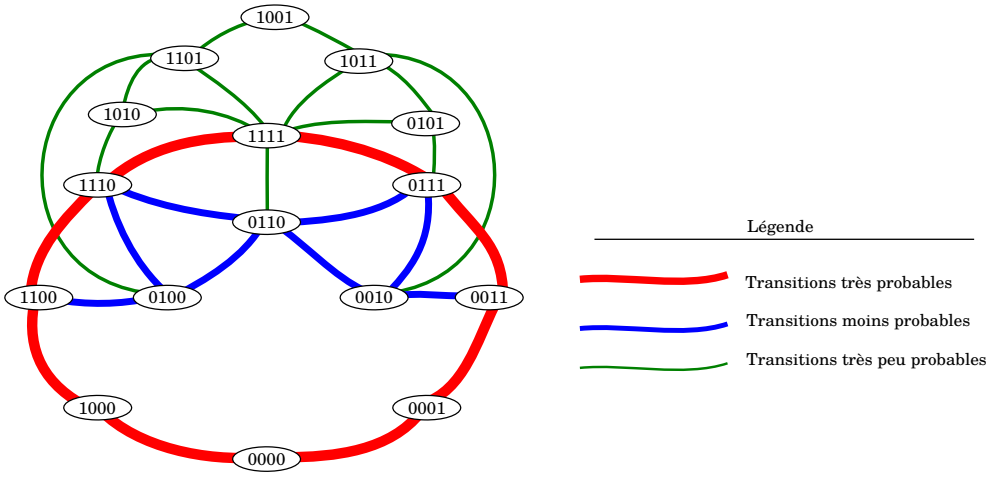

(a) Le modèle de Markov de l'ombre pour le module de référence

(b) Légende

Figure 22: Les résultats de l'étude théorique sur l'ombre

Les traits rouges marquent des transitions avec une probabilité plus forte, suivis par les traits bleus et verts pour des probabilités de plus en plus faibles.

L'actualisation des liens entre les états peut être faite automatiquement par l'Equilibreur PV suite à leur détection. Avec le temps, au lieu de déclencher une scrutation celui-ci pourra tout simplement consulter un tableau de probabilités, changer d'état et choisir la stratégie correspondante.

La détection est maintenant considérée comme résolue et le prochain pas consiste à l'intégrer avec les méthodes de compensation d'ombres dans un seul algorithme de commande.

Chapitre 6 : Le système de commande

Le système de commande de l'Equilibreur PV repose sur les résultats des études sur la compensation et la détection de l'ombre. La figure 23 présente l'algorithme développé. Il est composé de quatre blocs, à savoir initialisation, attente, détection et exécution.

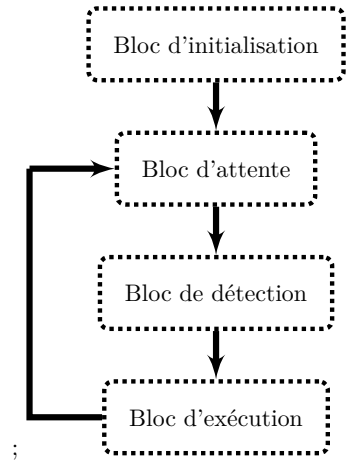

Figure 23: L'algorithme de commande

Le bloc d'initialisation lance les routines de configurations propres au microcontrôleur sur lequel est embarqué le code développé. Il est aussi responsable de la calibration des lectures de courant et de la validation de leur résistance au bruit. Le bloc d'attente gère la recherche du rapport cyclique optimal et observe l'évolution des valeurs moyennes des courants dans l'inducteur et de sortie. Le bloc de détection fait l'acquisition des lectures de chaque groupe de cellules PV, interprète les résultats, met à jour l'état de l'ombre et choisit la stratégie de commutation. Le bloc d'exécution calcule la valeur initiale du rapport cyclique et reprogramme les routines qui envoient directement les impulsions à la commande rapprochée des transistors.

Cet algorithme est validé par une série de mesures.

Validation expérimentale

Du fait de contraintes de temps, la validation expérimentale de la commande développée a été limitée aux méthodes directe et semi-directe. L'ombre est placée sur le groupe PV_{IV} et les conditions pendant les expériences sont décrites dans le tableau 4.

Table 4: Les détails des mesures réalisées

Variable	*Méthode utilisée*	
	Direct	*Semi-direct*
Durée	6'07"	5'32"
Apparition de l'ombre	0'47"	0'43"
Disparition de l'ombre	4'40"	4'38"
TO	0.52	0.52
Etat de l'ombre	[0001]	[0001]
Irradiance	939	950
T_A *(℃)*	38	35
T_M *(℃)*	57	59

Le résultats pour les deux méthodes de commande sont montrés sur la figure 24.

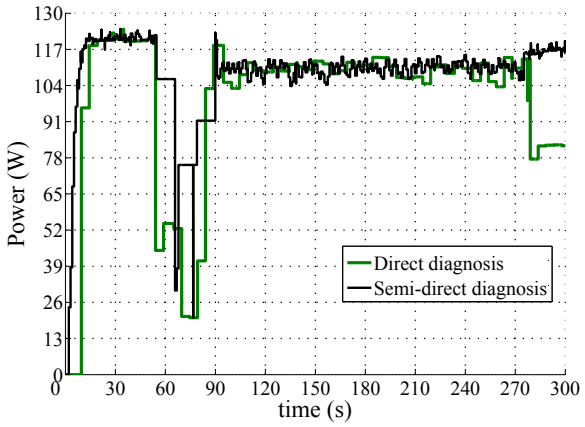

Figure 24: Comparaison entre les méthodes

Les deux méthodes ont des résultats équivalents. Elles sont capables de trouver l'ombre et maximiser la puissance produite par le module PV. Cependant, aucune des deux n'a réussi à arrêter l'équilibrage à cause de la zone d'incertitude autour des lectures.

Chapitre 7 : Conclusions et perspectives

Cette thèse a apporté deux contributions majeures sur l'intermittence de l'énergie photovoltaïque.

La première contribution a été la théorie de l'intermittence photovoltaïque qui réunit toute l'activité de la littérature scientifique en une seule équation. La deuxième a été la proposition d'une structure d'électronique puissance innovante appelée l'Equilibreur PV.

Les différents tests et études effectuées peuvent maintenant être utilisés pour comparer l'Equilibreur PV avec d'autres PRobES. Les détails sont disponibles dans le tableau 5.

Table 5: Les conditions équivalentes entre l'Equilibreur PV et d'autres solutions

PRobES	*TO*	*BSS équivalent*
DMPPT 1 [Ramos-Paja et al., 2010]	0.36	$I.II.III \rightarrow IV$
DMPPT 2 [Giral et al., 2011]	0.57	$I.II \rightarrow III.IV$
DMPPT 3 [Nguyen and Low, 2010]	0.48	$I.II.III \rightarrow IV$
GCC 1 [Shimizu et al., 2003]	0.37	$I.II.III \rightarrow IV$
GCC 2 [Shimizu et al., 2001]	0.60	$I.II \rightarrow III.IV$
REA 1 [Nimni and Shmilovitz, 2010]	0.50	$I.II \rightarrow III.IV$

Les résultats se trouvent dans la figure 25.

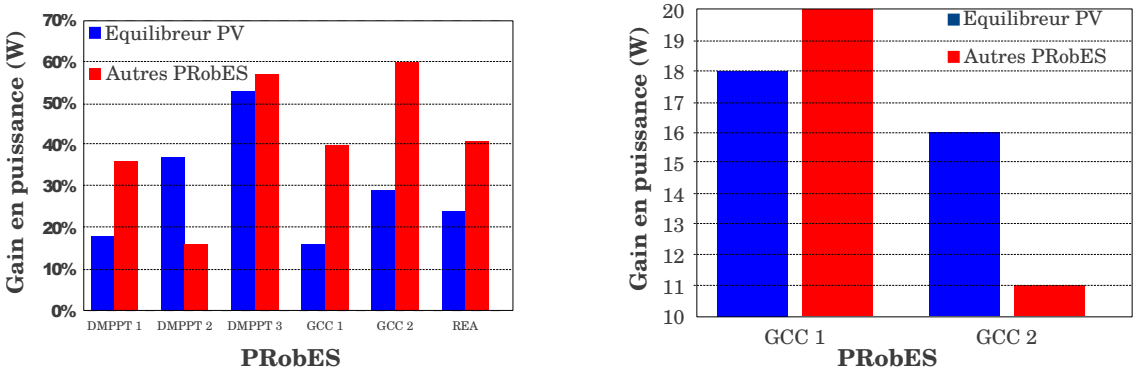

(a) Gains relatifs

(b) Gains absolus entre l'Equilibreur PV et le GCC

Figure 25: La comparaison entre les gains de puissance

Pour plusieurs cas, le gain de puissance de l'Equilibreur PV est inférieur à celui des autres structures. Cela s'explique parce que les données pour l'Equilibreur PV sont issues des mesures alors que celles des autres solutions proviennent des simulations qui ne prennent pas en compte les pertes. Les seules deux exceptions sont pour le GCC1 et GCC2 dont les données sont aussi expérimentales. Cependant, leur gain absolu est plus faible et leur module n'est pas exposé à des conditions environnementales naturelles.

L'amélioration de ces résultats font l'objet d'un certain nombre des perspectives de recherche. D'abord le remplacement des diodes par des transistors amènera une diminution significative des pertes de conduction. L'intégration monolithique de cette structure est, sans doute, la meilleure voie pour augmenter la fiabilité de la topologie proposée. Elle doit être le prochaine étape dans la recherche de l'Equilibreur PV. La validation de la méthode indirecte ou la création d'une centrale PV ultra-robuste à partir de l'utilisation des concepts introduits dans cette thèse constituent des perspectives à plus long terme.

Chapter 1

Introduction

The world is at an important crossroad: decarbonating its economy or facing the uncertainty of global warming. This complicated choice has important consequences in the very fabric of society, from the most complex financial transactions to the simplest choices of everyday life. Aware of these implications, some countries have made efforts in many different fronts. These go from raising efficiency standards for their respective industries to launch an overall effort to completely change their electricity production.

In the wake of these changes, renewable energies have moved from mild contributors to major players in the world energy mix. Among them a special attention can be brought to photovoltaic energy. Rating among the most mature renewable energies currently available in commercial scale, photovoltaic energy has the potential of effectively helping answering the problems of energy production in the world. It could be, ideally, installed directly on rooftops in order to tackle the immense amount of energy shinning over cities all over the world everyday. This proximity with the load, could reduce losses and create a new offer of abundant energy. And, as of this moment, one thing stands on its way: shadows.

Urban and suburban environments are ridden with all sorts of obstacles to light: tree, chimneys, details in the facades of the buildings. This issue has been studied by researchers in the field of photovoltaics for the past few decades, yielding many interesting results. However, there is no consensus in the current literature as to what intermittency really is or how all the different approaches developed so far are related to each other.

In this context, this work proposes contributions in both theoretical and practical aspects of partial shading mitigation.

The theoretical aspect is addressed in **chapter 2**, by introducing the problem of shading through an unique perspective. Allying the effect of the shadow on PV systems with its physical properties, an new shadow model is proposed. Along with it, a theory on the PV intermittency is also proposed, putting it into a different perspective from the current literature. Finally, a qualitative method for evaluating solutions to the partial shading phenomena is also developed and applied on the current literature. From its overall conclusions, the needs of innovation are identified and used to propose a practical contribution which will be explored during this work.

This contribution is called *PV Equalizer* , being an adaptation of its battery equivalent. This solution is capable of accessing any group of PV cells within a given PV module and redistribute their current. In the presence of shadow, the PV Equalizer brings the values of these currents very close to one another, effectively equalizing them. Its power electronics structure is described into detail in **chapter 3**, along with its principle of operation. This principle is expanded into several functions, which are used as a basis for assessing the current and voltage constraints of the system.

There are two types of functions: shadow mitigation and diagnosis. The first intervene in the PV module in order to reroute the current among the cell groups and raise power production. The second are used to find the shadow and estimate its characteristics. They provide the data for calculating PV Equalizer losses, giving way to a discussion of its limitations.

The shadow mitigation functions are the focus of **chapter 4**. They are characterized through the study of several switchings conditions under many different shadow scenarios. They yield an algorithm for finding the optimal response to a given shadow.

Chapter 5 studies the shadow diagnosis functions. Three diagnosis methods are proposed: direct, semi-direct and indirect. The first uses the recurrent observation of current peaks acquired by using the PV Equalizer. The second uses the observation of certain specific electric variables to determine the best moment to acquire the current peaks. The third is based on the prediction of the shadow state through the use of natural shadow observations. All these methods provide a wealth of data and insight that, together with the correction functions, are put together into a single control algorithm.

The control algorithm of the PV Equalizer is developed in **chapter 6**. It is based on the three diagnosis methods and the two mitigation functions. They are validated through measurements and a discussion concerning their limitations follows, putting the PV Equalizer and its concept in perspective.

Finally, a conclusion based on all the provided data is given in **chapter 7**. It summarizes the characteristics of the PV Equalizer and compares it to other solutions, proposing perspectives and ideas for future work.

Chapter 2

PV Systems and Intermittency

This chapter is dedicated to introduce the main concepts of the photovoltaic systems, explain the current visions and evaluate the work of the scientific community on the PV intermittency issue.

The first aspect to be treated is the PV system itself and its principles of operation.

This is followed by the proposition of a new shadow model. Most authors are quick to attach the shadow with a simple model, usually linked to how much light it filters. They are, thus, free to focus their work on the exquisite solutions to mitigate its effects. The model proposed in this work is issued from a cross comparison of the shadow and the electric connections of a PV module. Generic but simple, this model portraits the shadow on a new perspective fusing it with the PV module itself. It yields a numeric representation that can be easily called upon for later studies and developments.

After addressing the shadow, the intermittency itself is studied. There is a vast wealth of work on it, but no overall consensus. Thus, a theory linking the shadow and the power production capabilities of the PV system is proposed, translating this bond into the concept of robustness.

The current literature is then reviewed under the light of this theory and a method for comparing its different contributions is proposed. Based on this comparison, a potentially interesting research theme is unveiled, being explored further in the next chapters.

Contents of this chapter

2.1 Overview of PV systems

The systems needed to harvest and convert sunlight into electricity are composed of many elements. This section introduces them, their terminologies and characteristics. They will be used later as a basis for understanding the phenomena of intermittency.

2.1.1 The PV physics

The photovoltaic effect, which drives the power production of PV plants, can be modeled by the known expression shown in equation 2.1 [Picault et al., 2010b] .

$$i = i_{ph} - I_0 \left(\exp \left[\frac{(V + I \cdot R_s)}{V_t} \right] - 1 \right) - \frac{V + I \cdot R_s}{R_p} \tag{2.1}$$

The I_{ph} stands for the photo-current, R_p for the parallel resistance and R_s for the series resistance. The i is the output current, V is the output voltage and I_0 is the reverse saturation current. The variable V_t, or thermal voltage, is defined by equation 2.2:

$$V_t = \frac{A \cdot k \cdot T_c}{q} \tag{2.2}$$

The variable A stands for the ideality factor, k is the Boltzman's constant, T_c is the operating temperature of the PV module and q is the electronic charge.

These parameters vary with the materials used to manufacture the PV system [Tyagi et al., 2013]. They also change with time due to diverse factors such as aging [Kaplanis and Kaplani, 2011] or degradation due to exposure to light [Kuznicki et al., 1999]. These imperfections will be explored in more detail further below.

These equations can be converted into a circuit representation, which is more suitable for simulations or for studying complex PV applications.

Equivalent Circuit model

The equivalent circuit model of equation 2.1 is represented in figure 2.1. This is called the one-diode model and will be used throughout this work.

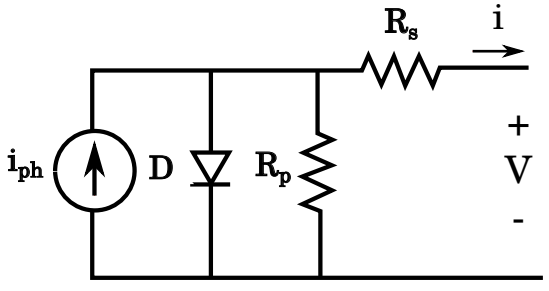

Figure 2.1: The one-diode model

The diode in the circuit models the non-linear behavior of the output current and voltage. The series and parallel resistances model imperfections of the PV model, such as solder bonds or crystalline impurities. The current source represents the photo-current [Karatepe et al., 2007, Ikegami et al., 2001].

For applications in electrical engineering, a more simplified and intuitive representation is proposed through a set of characteristic curves.

PV characteristic curves

The photovoltaic effect described by equation 2.1 defines a non-linear dependency between current and voltage. In the PV domain this dependency is expressed by the current versus voltage curve, as showed in figure 2.2 .

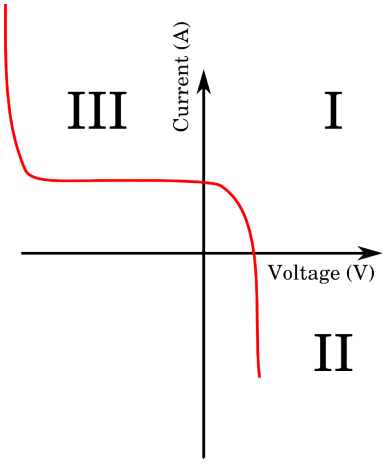

Figure 2.2: A generic I-V curve

This curve extends itself over three different quadrants. Quadrant I represents the positive power section of the curve, where voltage and current are both positive. Most of the analysis proposed in this work will concentrate itself in this quadrant.

The other two represent the negative power sections of the curve. Either the current or the voltage are negative. The conditions for a PV application to operate into quadrants II or III are explained further below.

Commercial PV applications use the curve drawn in quadrant I along with another typical curve representing the power versus voltage evolution of the module. Both curves are drawn in figure 2.3

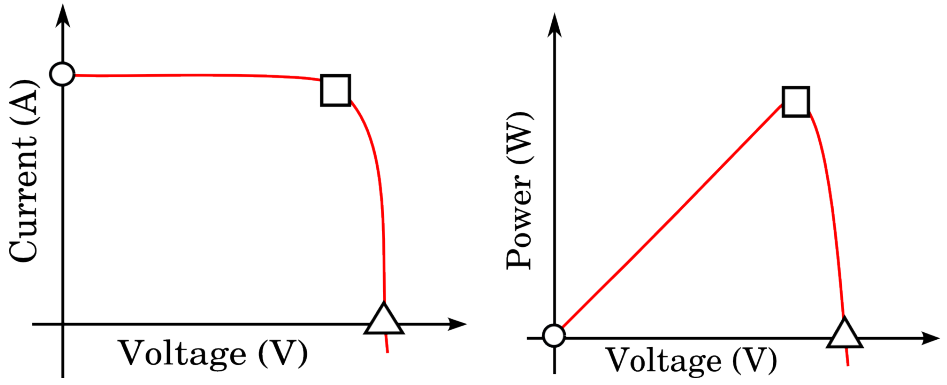

(a) The I-V curve (b) The P-V curve

Figure 2.3: The characteristic PV curves

Three important points can be identified in both curves. First, at zero voltage, is the **short circuit current** (i_{SC}), represented by a circle. Second, at zero current, is the

open circuit voltage (V_{OC}), represented by a triangle. Finally, between them is the **maximum power point** (MPP), represented by a square.

As its name states, at MPP the power production of the PV module is maximized [Farret and SimÃţes, 2006]. However, it is by no means constant, changing with the external conditions of the PV module. Two variables have a very important influence over the MPP: light and temperature.

The influence of light and temperature

The amount of power delivered by a light source is called **irradiance** and can be expressed in watts per square meter($\frac{W}{m^2}$). The inclination and orientation of the PV module have a direct influence over the irradiance it receives. Ideally, the module should be oriented towards the equator, its inclination rising with the latitude [Farret and SimÃţes, 2006]. As irradiance varies, so does the photo-current in equation 2.1. As a consequence, the I_{SC} is directly affected by variations in the irradiance. Figure 2.4 illustrates the influence of the irradiance over the characteristic curves of the PV module.

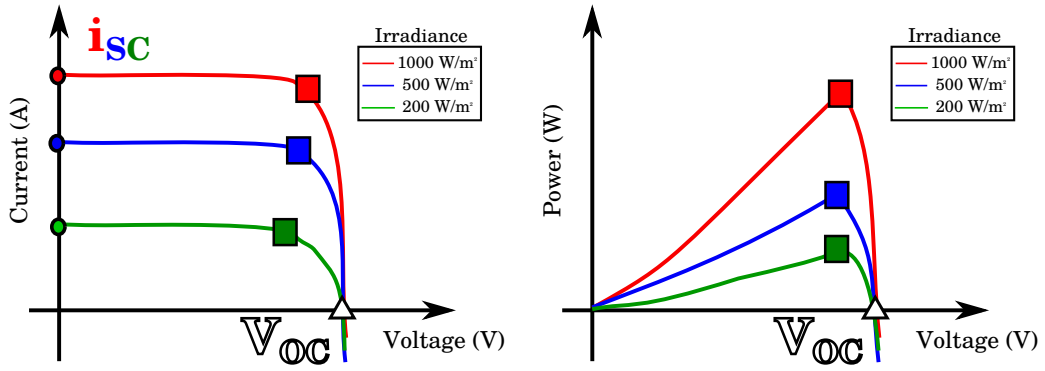

(a) Changes on the I-V curve (b) Changes on the P-V curve

Figure 2.4: Influence of the irradiance over the PV module

Temperature has a direct influence over the thermal voltage, in equation 2.2. making the V_{OC} the variable mainly sensitive to variations in temperature [Ichida et al., 2009]. As the PV module heats up, its voltage falls along with its power production. This effect is represented in figure 2.5.

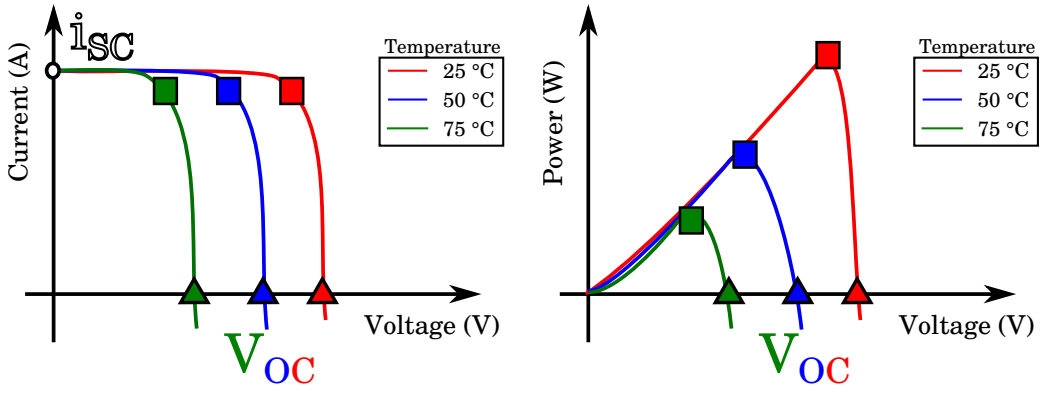

(a) Changes on the I-V curve (b) Changes on the P-V curve

Figure 2.5: Influence of temperature over the PV module

Ideally, a PV module should operate at cool temperatures and high irradiance. However, the losses in voltage due to first are largely offset by the gain in current due to the second [Ye et al., 2013]. Thus, sunny locations while hot are still preferable for the installation of PV modules.

This analysis gives a first hint to the influence of shadows in PV applications. Their inherited sensitivity to light variations make them particularly vulnerable to shadows. This weakness will be explored into further detail in section 2.1.3.

2.1.2 PV power harvesting

The model and curves introduced above show that a PV application is a light-dependent and voltage-controlled current source. Thus, its power output is totally dependent, at the same time, on its irradiance, temperature and load. The first two have an influence over what is called, in this work, *PV power production*. The load influences another aspect called *PV energy conditioning*. Together they harvest the power from the light and carry it to the end-user. Their description is necessary to fully understand the influence of intermittency in photovoltaic power production.

PV power production

In order to produce a certain power a PV system must attain a certain voltage and current. These, in turn, require a certain surface. Since semiconductor wafers have a limited section, the entire power production unit must be composed of many little contributions from many small cells.

The smallest part of the PV system is the cell. Its area depends on the technology used to produce it. The material composing it also varies, having a direct impact over its series and parallel resistances. Both have, direct or indirectly, an influence in the output current of the PV cell [Bun, 2012].

When cells are put together, the overall I-V curve changes. Connecting them in series raises the V_{OC}, while connecting them in parallel raises the i_{SC}. The I-V curves for such connection schemes between two identical PV cells under the same irradiance are shown in figure 2.6 (a) and (b).

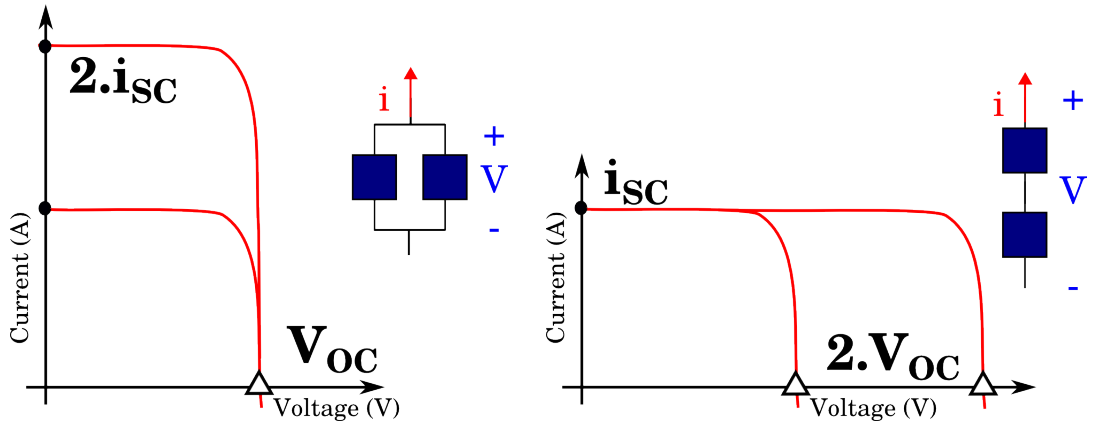

(a) Parallel connection (b) Series connection

Figure 2.6: Types of connections among PV cells and their respective I-V curves

When connected in series to attain a certain voltage, the PV cells form a module. The number of cells within a single module depends on the manufacturer. Some modules give

the user the flexibility of changing the output current or voltage by allowing access to groups of cells.

During this work, a polycrystalline PV module was used in simulations and measurements. Its picture and I-V curves are drawn in figure 2.7

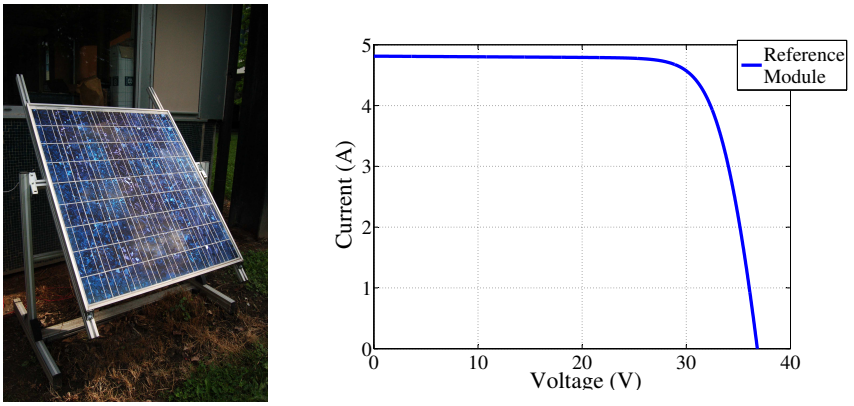

(a) A picture of the reference module

(b) Its characteristic I-V curve

Figure 2.7: The PV module used in this work

To build a PV plant, several modules are connected in series to reach a certain voltage, composing strings. Strings are then connected in parallel to reach a certain current, according to desired power output. This power output, however, will change according to the temperature and irradiance of the PV central. Thus, it is essential to conceive applications capable of adapting themselves to these changes and always draw the maximum power available at the PV plant. Once the PV power plant is installed and operational, a conditioning system will connect it to a load.

PV energy conditioning

Consider that a PV plant is connected directly to a certain load. What would be its output current, voltage and power?

To answer this question, figure 2.8 shows the PV module connected directly to three types of load along with their impact over the I-V curve. The PV module is represented by the element to the left that looks like an envelope. The circles, triangles and squares still represent the i_{SC}, V_{OC} and MPP, respectively. The X represent the point where the PV module is operating. The three different loads impose different operation conditions to the PV module.

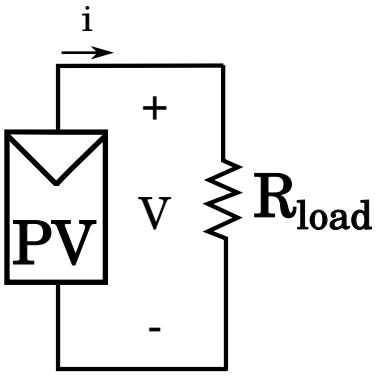

(a) PV module connected to a resistive load

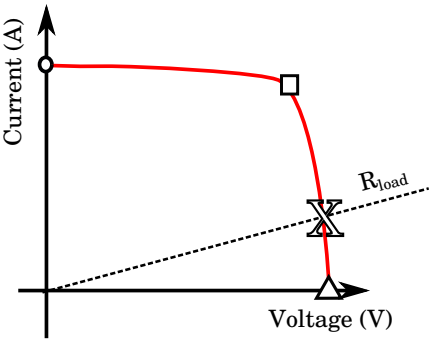

(b) Effect of the resistive load on the I-V curve

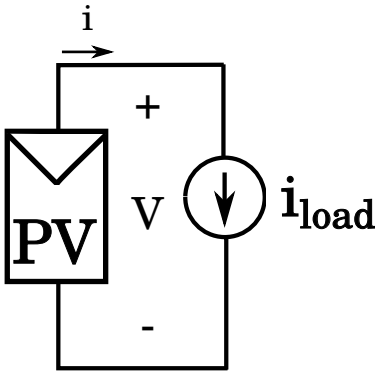

(c) PV module connected to an inductive load

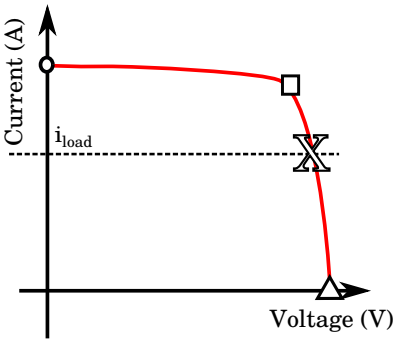

(d) Effect of the inductive load on the I-V curve

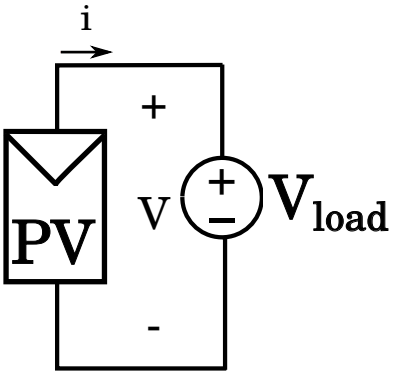

(e) PV module connected to a capacitive load

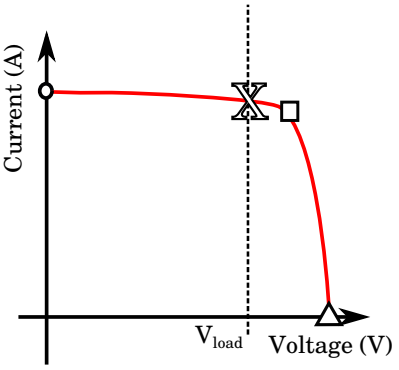

(f) Effect of the capacitive load on the I-V curve

Figure 2.8: Operation conditions for different loads

Figure 2.8(a) shows the PV module connected directly to a resistive load. This resistive load will impose a fixed relation, yield a single voltage and current pair. It imposes a non-optimal power point, as shown in figure 2.8(b).

The inductive load is represented by a fixed current source, as shown in figure 2.8(c). It imposes a fixed current (i_{load}), as shown in figure 2.8(d).

The capacitive load is represented by a fixed voltage source, as shown in figure 2.8(e). It imposes the fixed voltage (V_{load}),as shown in figure 2.8(f).

In all of these three cases, there is a weak chance for the X to cross the square. In other words, it is difficult to maximize power output with a fixed load. This is due to

the fact that the **PV module is a power source that always adapts its operation conditions to its load**.

Now, imagine that the resistive load is fixed in order to draws the maximum power from the PV module. What happens if the light changes? Figure 2.9 shows this effect for different irradiances.

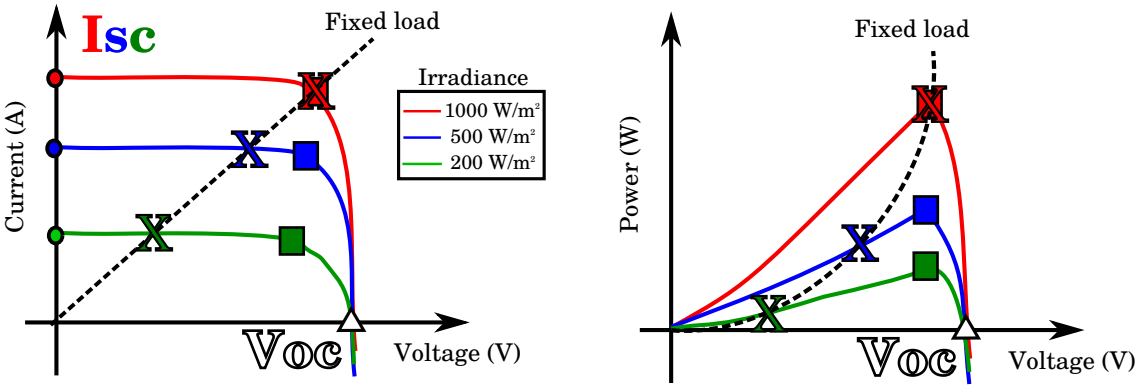

(a) I-V curve (b) P-V curve

Figure 2.9: The influence of light variation on a fixed load

The load is only optimal for the irradiance of 1000 $\frac{W}{m^2}$. In order to understand what this represents in terms of energy, consider that the optimal irradiance is only available at noon. Thus, the fixed load is non-optimal during the morning and the afternoon. Figure 2.10 shows the daily power production of the PV module used in this work. It is superposed with the power that would be harvested by the direct connection of a fixed load.

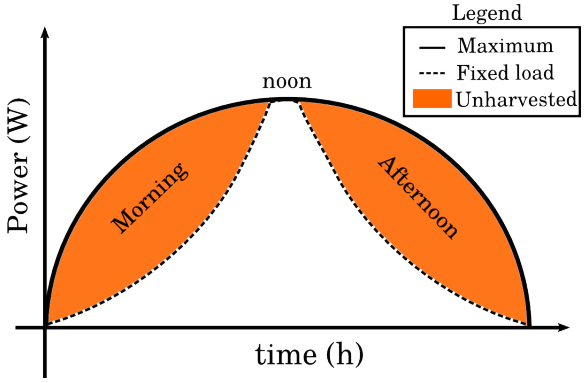

Figure 2.10: Comparison of daily power productions

The full line represents the maximum power output, which follows a similar pattern to the movement of the Sun. On the left side is the energy available in the morning, on the top is the energy at noon and on the right side is the energy during the afternoon.

The dashed line represents the power output of the fixed load shown in figure 2.9. Since the load is fixed, the actual power production of the PV plant does not follow the solid line and it is not optimal during the day. Only at noon and during a brief period of time do these meet. As a consequence, an important amount of energy remains unharvested, as shown by the orange zones.

Theoretically, the best solution would be to have a load constantly changing and optimal. Such a solution is unfeasible in reality. However, a power electronics converter can be connected between the load and the PV module in order to constantly adapt one to the other. Such power electronics converter can provide the necessary flexibility to constantly keep the operation point of the PV module near to its MPP.

This solution is called a MPPT, having many different topologies and algorithms [Ishaque, 2012]. It can be considered, from the PV plant point of view, as an external current source which constantly maximizes the power production. Its algorithm is based on the particular shape of the P-V curve, as shown in figure 2.11.

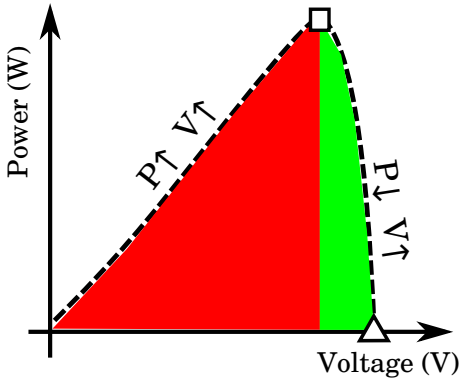

Figure 2.11: The two zones of the P-V curve

On the red part of figure 2.11, the power rises with the voltage. On the green part, the power drops as the voltage increases. Thus, if the voltage is raised by a small step and the power also raises, then the voltage should keep rising. If, on the contrary, the voltage is raised by a small step and the power lowers, then the voltage should be stop rising and start being reduced. This algorithm is called disturb and observe, since it advances by creating small disturbances in the system and observing its behavior.

The output of the MPPT chopper is directly connected to a DC bus. It serves as an interface between the PV and other direct current type sources of energy or batteries. Its voltage is stable and controlled by one of the elements of the entire system.

In alternative current (AC) applications, the DC bus is controlled by an inverter. It injects the power output of the PV system into the grid or an alternative load, generating active power, reactive power or even both. The inverter may come in many different shapes, sizes, nominal power and efficiencies [Cacciato et al., 2010, Picault, 2010, de Cardona and LÃşpez, 1998].

Finally, a complete PV system is shown in figure 2.12.

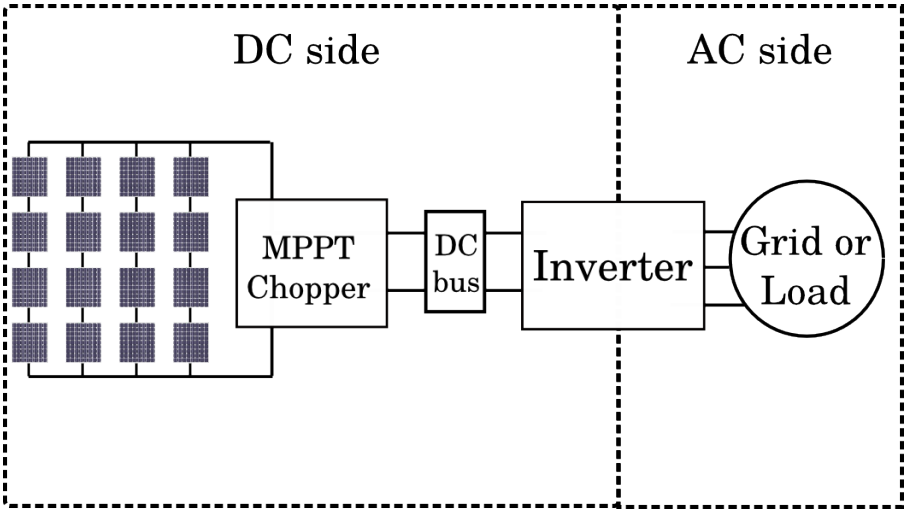

Figure 2.12: A complete PV system

On the DC side is the PV plant is the PV module or plant. The MPPT, DC bus and the input of the inverter follow suit. On the AC side is the three phased output of the inverter and the AC grid or load.

The DC bus decouples both sides, making their behavior quasi-independent. The AC side of the PV system is mostly affected by changes in the grid or the load. The DC side is affected by changes in the energy source. These changes are first explained locally and then generalized through the shadow model.

2.1.3 The imperfections of PV power production

The ideal power production situation is to have every single cell of the entire PV plant to be identical and constantly working at their own MPP. In reality each cell is slightly different from one another and may receive different irradiances.

As different parts of the entire plant react differently to the light received, they can cause power oscillations and lower power production. These operating irregularities are sometimes called **PV mismatch** in the literature, but there is currently no consensus about it.

The PV mismatch is the key to explaining how the intermittency affects PV production. Its definition proposed in this work is **the difference between expected and actual power outputs of a PV system**. It can classified as internal or external, according to its origin.

Internal mismatch - Cell mismatch

Imperfections within PV modules or cells, induced by aging, poor solder bonds, impurities in the silicon crystal or variability in production result in different performances of the modules connected in series. The parameters from the model 2.1 affected are the series resistance (R_s), parallel resistance (R_p) and the reverse saturation current (i_0) [van Dyk and Meyer, 2004, Bun, 2012].

Since their origin are more linked to production processes, the internal PV mismatch has been widely analyzed in the literature [Appelbaum et al., 1995, Junior, 1979, Chamberlin et al., 1995, Picault et al., 2010b,a, Kaushika and Rai, 2007, Kaplanis and Kaplani, 2011, Ye et al., 2013] . Some techniques to mitigate it can be found in [Appelbaum et al., 1995, Chamberlin et al., 1995]. It is considered to be responsible for nearly 2% of the

overall losses in the PV systems and most precautions needed to avoid it must be taken during cell production.

External mismatch - Source mismatch

All conditions leading to a change in the photocurrent (i_{ph}) or thermal voltage (V_{th}) of a part or the whole PV plant are considered as external mismatch. They can be affected by several sources.

Mechanical or thermal stresses, may lead to cell cracking [Ramli and Salam, 2011, Arnett, 1981, Alonso-Garcia et al., 2006]. Poor efficiency of the MPPT associated topology or program may lead to extra losses [Ishaque, 2012, Ramos-Paja et al., 2010, Safari and Mekhilef, 2011]. These two can be mitigated by a careful planning and care during the sizing and deployment of the PV plant [Picault, 2010, Villa et al., 2012].

Inhomogeneous irradiances on cells connected in series may create partial shading conditions and hot-spots [Abdalla et al., 2013, Ramli and Salam, 2011, Wang et al., 2012, Bidram et al., 2012, Villa et al., 2013]. While careful site study is still an important method to avoid partial shading, it is still an unresolved issue which with a non-negligible destructive potential.

A PV module is partially shaded when the light cast upon some of its cells is obstructed by some object, creating a shadow. The shaded PV cells will produce less current than the others, which leads to several different problems [Kawamura et al., 2003]. Figure 2.13 shows the I-V curves of two PV cells connected in series before and during partial shading.

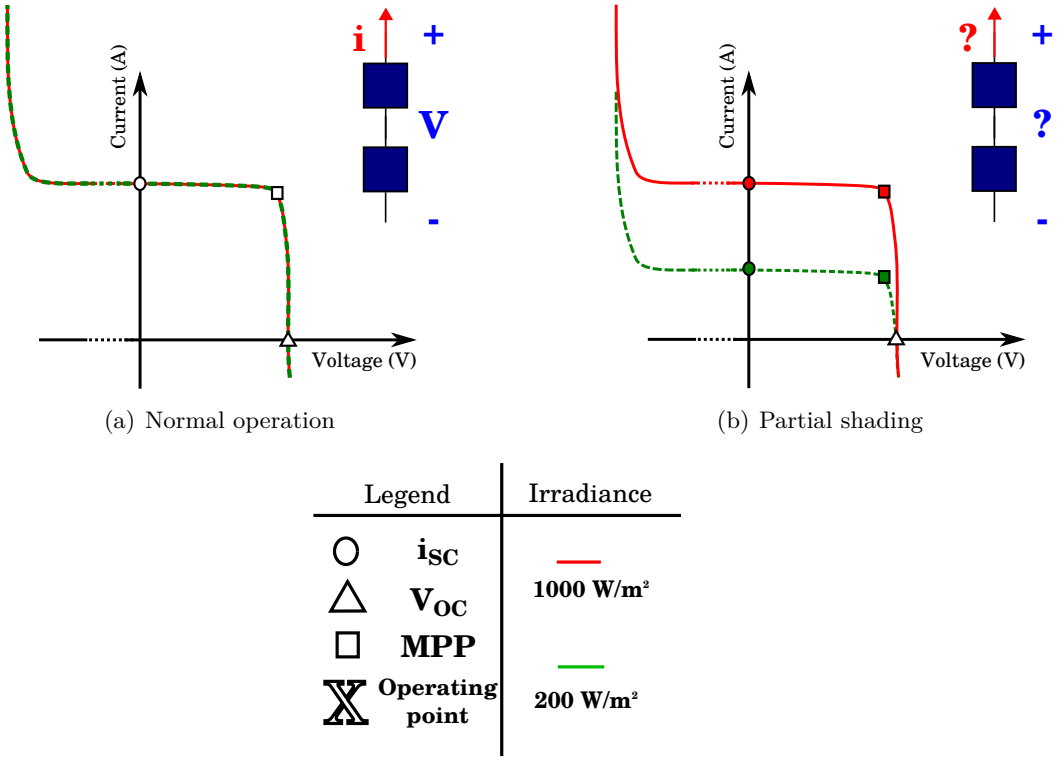

(a) Normal operation

(b) Partial shading

(c) Legend

Figure 2.13: I-V curves of a PV system under different conditions

The dotted part of the graphs represent the great voltage distance between V_{OC} and the avalanche voltage. Considering that the system is connected to a MPPT, the operation of two PV cells in series may only lead to one of the two scenarios represented in figure 2.14. Where the output current is represented by i_{OUT}.

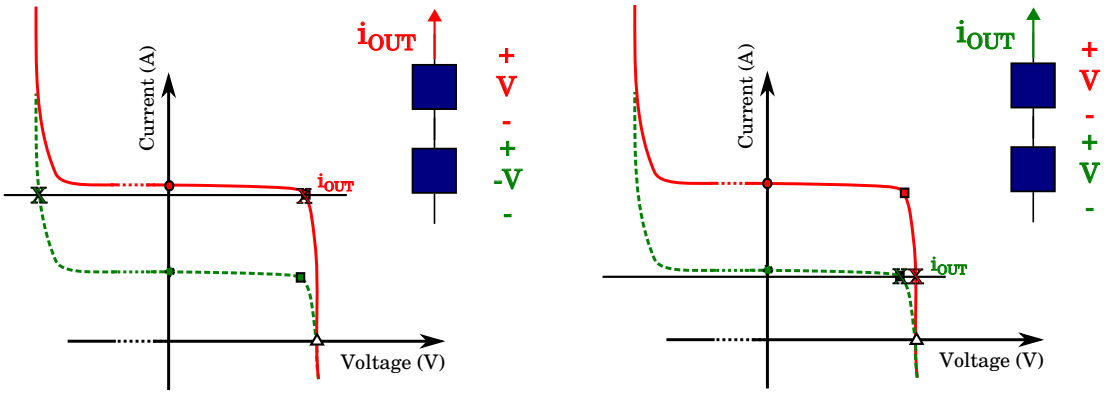

(a) High current (b) Low current

Figure 2.14: Two possible scenarios for the mismatch

In figure 2.14(a), the MPPT tracks the unshaded cells MPP, imposing its higher current and making the unshaded cell work under a highly negative voltage. It starts dissipating power and risk being destroyed by heat or hot-spots[Appelbaum et al., 1995, Junior, 1979, Arnett, 1981]. This is usually a transitory situation, since the MPPT will not remain at an operation point which greatly limits power production.

In figure 2.14(b), the MPPT tracks the MPP of the shaded cell, imposing its lower current. The unshaded cell in then forced to produce less energy. In this situation there is no risk of destruction and the MPPT will tend remain in it while the shadow is cast over the PV module [Ubisse and Sebitosi, 2009, Picault et al., 2010b].

Now that the effects of the shadow have been introduced, this chapter takes a closer look at what shadow is and how it can be modeled from a PV perspective.

2.2 The Shadow Model

The development of the shadow model suits many different purposes for this work.

First, having a coherent and simple shadow model allow the analysis of the intermittency as a general phenomenon. It provides the basis for evaluating the trends in the current literature and discerning interesting lines of research.

Second, a model can transform a physical phenomenon into a mathematical expression. They can be translated into information that can be manipulated by a microcontroller, thus aiding in the development of new solutions. They are also useful for organizing studies about how the shadow impacts power production.

Third, there is no consensus in the literature. Some authors only take the geometry of the shadow into consideration [Picault, 2010, Wang and Hsu, 2009, Ubisse and Sebitosi, 2009, Drif et al., 2008, Fujisawa and Ohya, 2003, Kovach and Schmid, 1996]. While others focus themselves on the opacity of the shadow [Alonso-Garcia et al., 2006, Safari and Mekhilef, 2011, Ramos-Paja et al., 2010]. Just a few authors have tried to integrate both aspects in their shadow models [Lin et al., 2012, Patnaik et al., 2011] and usually without

any clear regard to the propagation of the shadow. In any case, there is no general shadow model.

This section will propose a shadow model which will be used throughout this work.

First, a general shadow concept will be presented. It takes into account the length, width and depth of the shadow, along with their variation over time. All these aspects make this first view of the shadow complex but complete.

The interaction between the PV module and this general shadow is then brought to focus. As the details from the PV systems are included in the analysis, the shadow model comes to being, revealing a simpler yet complete model. Its potential is discussed in a final summary.

2.2.1 General shadow concept

In this work, the shadow is considered as *the obstruction of a light source by any given object*. An example of such objects can be filters, which partially obstruct light or polarize it, depending on how it is designed. The objects commonly surrounding a photovoltaic application and susceptible of casting their shadow over it tend to be opaque, such as chimneys or buildings.

Casting a shadow implies in the 2-D projection of a 3-D object. Thus, the shadow has a shape, which can be roughly simplified by two dimensions: length and width. This idea is represented in figure 2.15

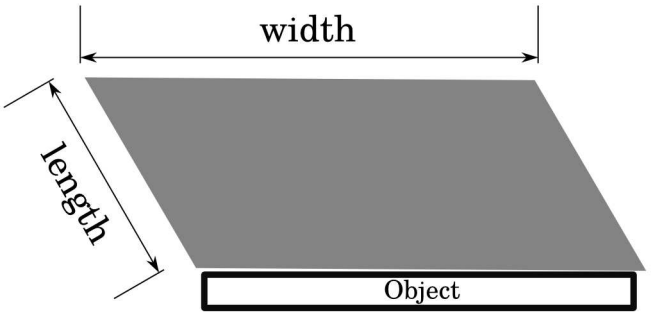

Figure 2.15: The projection of a shadow, showing its length and width.

A shadow also has a depth or opacity, called *shading factor (SF)*. The more opaque the shadow, the less light passes trough it. Thus, a higher shading factor mean less irradiance for the shadow, giving equation 2.3.

$$Irradiance_{shadow} = Irradiance_{total} \cdot (1 - SF) \tag{2.3}$$

The shading factor is considered as linear, ranging from zero to one. When zero, there is no obstruction. When one, all light is blocked by the object projecting the shadow. This is represented by figure 2.16.

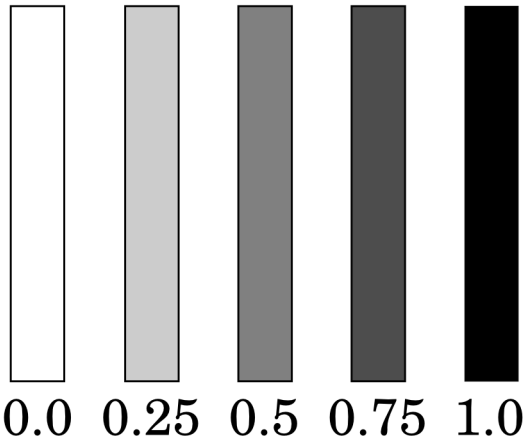

Figure 2.16: The shading factor

The shadow also has a fourth dimension: time.

The dynamics of optical shading depend on the movements of both the light source and the object obstructing it. The light source in this work is the Sun and its movement is well known and studied. A static object obstructing sunlight will have a shadow that varies over time according to its shape and the position of the Sun. Figure 2.17 illustrates their influence.

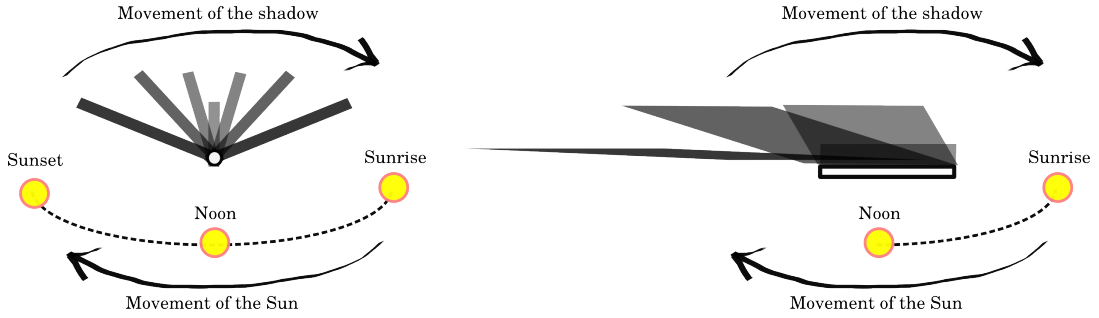

(a) Cylindrical object (b) Rectangular object (Partial movement)

Figure 2.17: Example of a shadow from an static object

In figure 2.17(a), both the shading factor and the length of the shadow have changed with the position of the Sun. However, its width remained constant. This is not the case of the shadow in figure 2.17(b), where the rectangular shape of the object has an important impact over the shape of its shadow. The shadow is shown only from sunrise to noon to ease its analysis.

As the Sun moves with the seasons, its arc will change and so will the shadows it projects, as shown in figure 2.18.

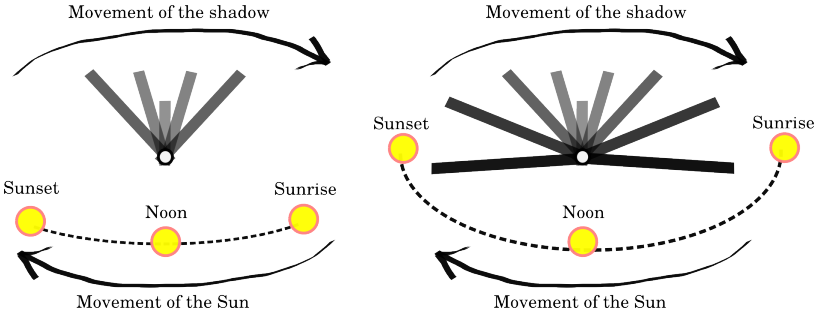

(a) Winter shadow trajectory (b) Summer shadow trajectory

Figure 2.18: Example of season influence over the shadow

The impact these changes will have over a PV module will depend on its location relative to the object and their orientation relative to the Sun. This is usually taken into account when installing a PV plant, but there are cases in which unsuspecting objects have cast shadows over PV plants, having devastating effects on their power production.

As for moving objects, these must fly. This restrains the possibilities to either clouds or birds, both of them moving much faster than the Sun. In these cases, it is the Sun that is considered as fixed. Clouds will slowly cover the totality of the PV central, while the shadow of the birds will most probably have no measurable impact in power production.

Static shadows are considered resting directly over the glass that covers the PV module, such as dirt, snow or bird droppings. In their case, time is not an issue and they are represented only by its length, width and shading factor.

All these characteristics compose a general shadow model which is a moving 2-D projection with varying shading factor. Putting all of them together makes the description of shading phenomenon seem, at first, to have a deterministic and well defined approach. It suffices to know the latitude and longitude of the site, the date of the year, time of day, the position of the objects around the site, their shape, the position of the clouds in the sky, the wind speed and its direction.

However precise, this exhaustive approach does require a large set of data which is not always (or even never) available, especially at the scale of a single PV module. Thus, a paradigm shift is necessary to further simplify this general model. Instead of taking the shadow as a reference, the model should describe it from the PV plant perspective.

2.2.2 Geometric shadow

Geometrically speaking, the PV plant is a group of flat plates, each of seemingly square shape. Within them, many cells are arranged to occupy as much of the surface as possible. The geometric representation of a single PV plant can, thus, go from several modules down to each cell.

During this thesis, a technological choice was made to work on the PV module scale. This choice leads to the adoption of the geometric model shown in figure 2.19.

(a) The reference PV module (b) The geometric PV module

Figure 2.19: The PV module and its geometric equivalent

When a shadow is cast upon the PV module, it covers the cells in some particular geometrical shape and with a particular shading factor. To understand how this impacts the PV module, the general shadow model will be cross-compared with the geometric PV module. The shadow that will be used to make this comparison is shown in figure 2.20.

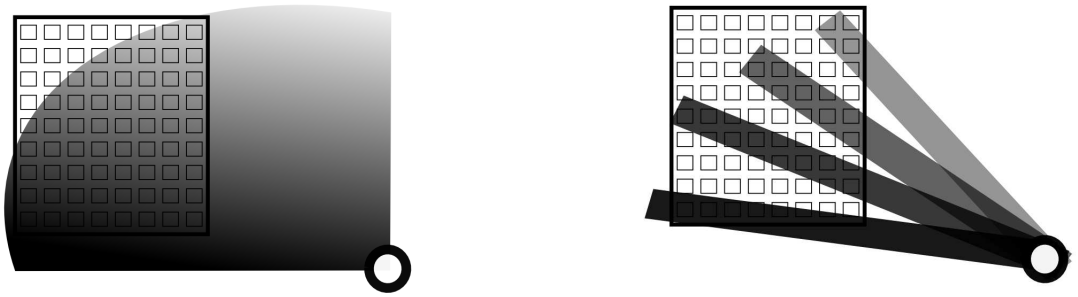

(a) Time-continuous shadow (b) Time-discrete shadow

Figure 2.20: Example of a shadow projection over the geometric model of the PV module

The object used to cast the shadow in figure 2.20 is cylindrical, represented by the white circle. Its shadow is a continuous variation of length, width and shading factor over time, shown in figure 2.20(a). Since the power conditioning system consist of electronics sensors which acquire data on a discrete basis, the shadow will be considered a succession of states. Its discrete representation is composed of four states, shown in figure 2.20(b). It moves from left to right, starting at the low, long and dark projection and finishing at the higher, shorter and lighter one.

Each state of the shadow is shown in detail in figure 2.21.

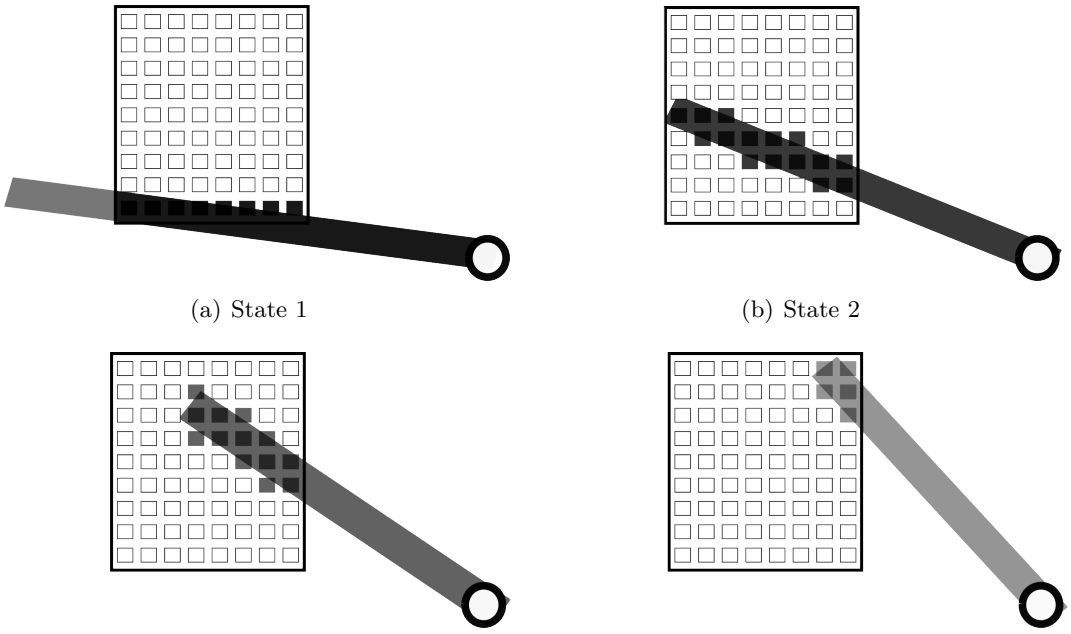

(a) State 1 (b) State 2

(c) State 3 (d) State 4

Figure 2.21: Decomposition of the dynamic shadow over time

The impact of the length and width of the shadow will depend on its position relative to the PV module. In the case of state 1, the shadow seen by the PV module has a width of 8 cells and a length of 1 cell. They change to 8 by 2, 5 by 3 and 2 by 3 for states 2, 3 and 4, respectively.

The point of origin for the length and the width of the shadow is considered to be the lower left corner of the PV module. The shadow can then be represented by a Cartesian projection with width on the x axis and length on the y axis. Thus, a shadow covering several cells in the x axis can be seen as *wide*, while those covering several cells in the y axis can be seen as *long*.

In terms of shading factor, its impact changes as the shadow moves over the module. In this example, the SF decreases as the shadow moves, which is seen by the cells as a change in their individual shading factor.

The trajectory of the shadow is linked to the distance of the object and the succession of states. While its speed does not show directly on the example. Of course, faster shadows mean less energy loss but they can be expressed by the same four states shown above.

This geometric cross-over gives the SF of each cell composing the PV module. In practice, their electrical connections also play an important role in determining the impact of shadows.

2.2.3 Electrical shadow

If each cell were independent, their current production would react according to their own shading factor. In reality, several cells are connected in series to reach a certain voltage output. However, depending on how the connections are oriented, the impact of the shadow changes. Two different and yet simple electrical connection schemes are presented in figure 2.22.

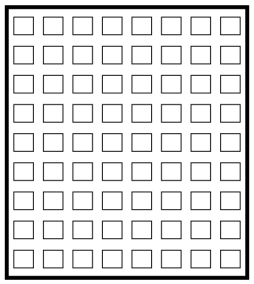

(a) The geometric PV module

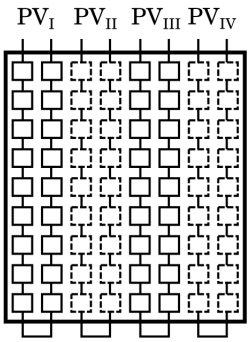

(b) First electrical PV module

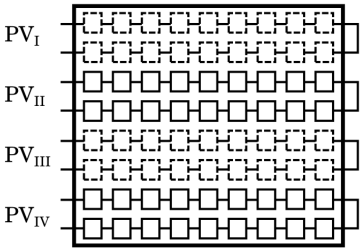

(c) Second electrical PV module

Figure 2.22: The geometric PV module and two electrical equivalents, with the cell groups indicated.

The reference PV module, shown in figure 2.22(a), has 72 cells disposed in 8 lines and 9 columns. These cells are connected to each other vertically, forming columns. Each column pair constitutes a cell group, from PV_I to PV_{IV} as seen in figure 2.22(b). Within these cell groups, all cells share the same current and the most shaded cell imposes its low current over all the others. The groups, however, are considered as independent among themselves.

This module is then pivoted by 90° in figure 2.22(c). Because of different orientations, a same shadow will not have the same impact over both connection schemes.

Figure 2.23 projects the shadow example over the first electrical connection scheme.

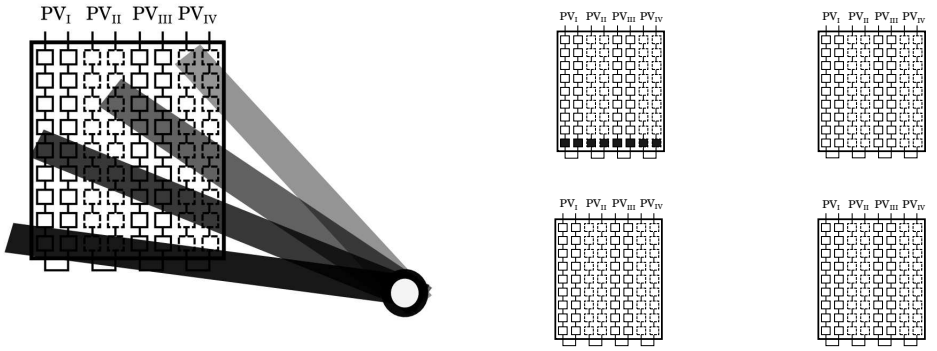

(a) A shadow cast over the first electric scheme (b) The four states decomposition

Figure 2.23: Impact of a shadow over the first electric scheme

The width of the PV module is no longer the same, changing the impact of the shadow over it. In the first and second states the shadow touches all the cell groups, imposing their shading factor over the totality of the PV module. In the third state, groups PV_{II}, PV_{III}, and PV_{IV} are all affected by the shadow. Even if only the fourth column is touched by the shadow, the totality of group PV_{II} has its current production blocked. The fourth state shows that the shadow is now cast only over cell group PV_{IV}. From its 18 cells, 5 are shaded and the other 13 blocked.

Pivoted the PV module by 90° changes the effect of the shadow, as shown in figure 2.24

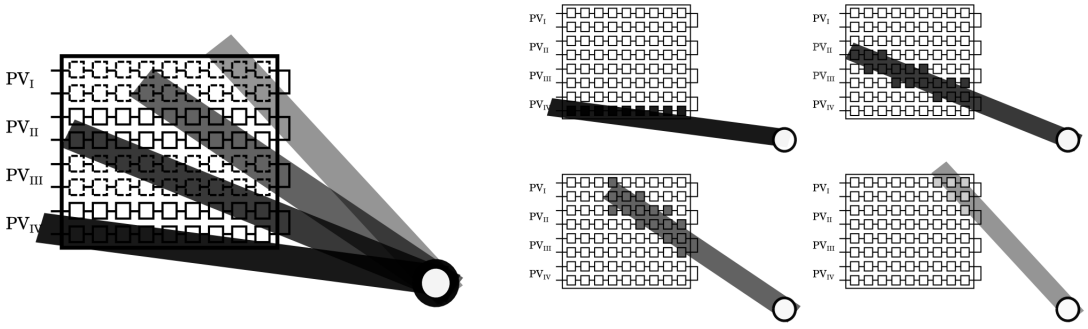

(a) A shadow cast over the first electric scheme (b) The four states decomposition

Figure 2.24: Impact of a shadow over the second electric scheme

In figure 2.24, it is the width of the PV module that is no longer the same. In the first state, only half of group PV_{IV} is shaded, meaning that the current of all cells are limited to the same SF. The second state shows groups PV_I, PV_{II} and PV_{III} touched by the shadow. The third state has a similar situation, but it is only PV_{IV} that remains unshaded. Finally, even though the shadow is cast over a reduced number of cells, groups PV_I and PV_{II} have their currents limited by it.

Despite their differences, both connection schemes share a common characteristic: their shadows loose a dimension due to the electric connections among the PV cells. The length

for the first and the width for the second. Furthermore, their remaining dimension was reduced from 8 lines/columns to 4 cell groups. Hence, the electrical interconnection of the PV cells has a direct impact in the shadow model.

The connection scheme used in this work is the one in figure 2.23. It can be used to express a mathematical shadow model, as shown below.

2.2.4 Numeric and digital shadow

In mathematical terms, the electrical shadow can be represented by a numeric vector, where each element represents the shading factor of a different cell group. An example of such vector is proposed in figure 2.25.

(a) The PV module electric connection scheme (b) The numerical shadow model

Figure 2.25: The electrical PV module and its numerical equivalent

The elements in the vector seen in figure 2.25(b) represent the shading factor of the rectangles directly below them. Each represents a cell group of the PV module. Their values can range continuously from 0 to 1, giving infinite combinations of shadows.

The impact of the shadow over the numeric shadow model is shown in figure 2.26. Its states are decomposed for a better representation. Since each cell group has the SF of its most shaded cell, their rectangles are painted in uniform shades of gray according to their SF.

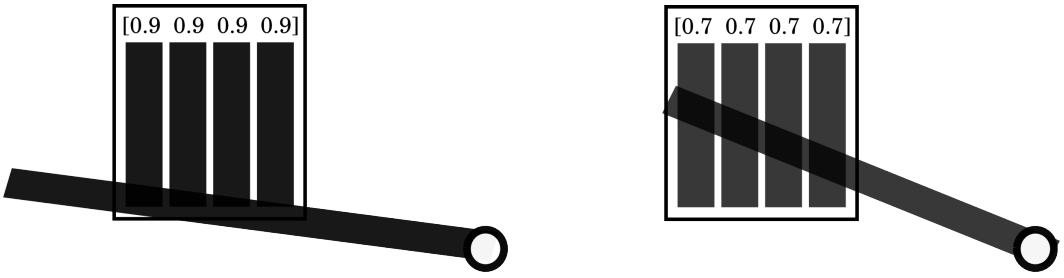

(a) First state (b) Second state

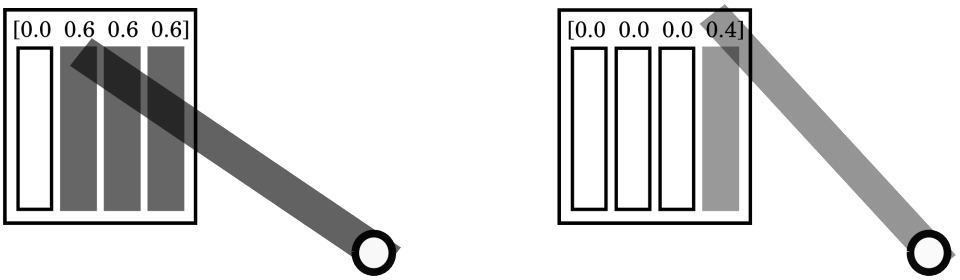

(c) Third state (d) Fourth state

Figure 2.26: Impact of the dynamic shadow over the numeric model

The movement of the shadow is translated into a variation in the value of the elements composing the vector. Between the first and second states, figures 2.26(a) and 2.26(b), the only visible variation is the shading factor. In both cases the width of the shadow remains the same. In figure 2.26(c) the first cell group is unshaded, represented by its zero SF. The same trend continues as three groups are shown unshaded in 2.26(d).

Due to its many possible scenarios, a simplification of the numeric shadow model will be used in many occasions throughout this work. It consists of converting the elements of the numeric vector from a continuous representation to binary. It reduces the number of possibilities to only 16: [0 0 0 0] to [1 1 1 1]. This simplification can be achieved by comparing the original vector with an arbitrary threshold, labeling 0 the values below and 1 those above it. As an example, the numeric shadows shown in figure 2.26 are simplified to binary equivalents in figure 2.27.

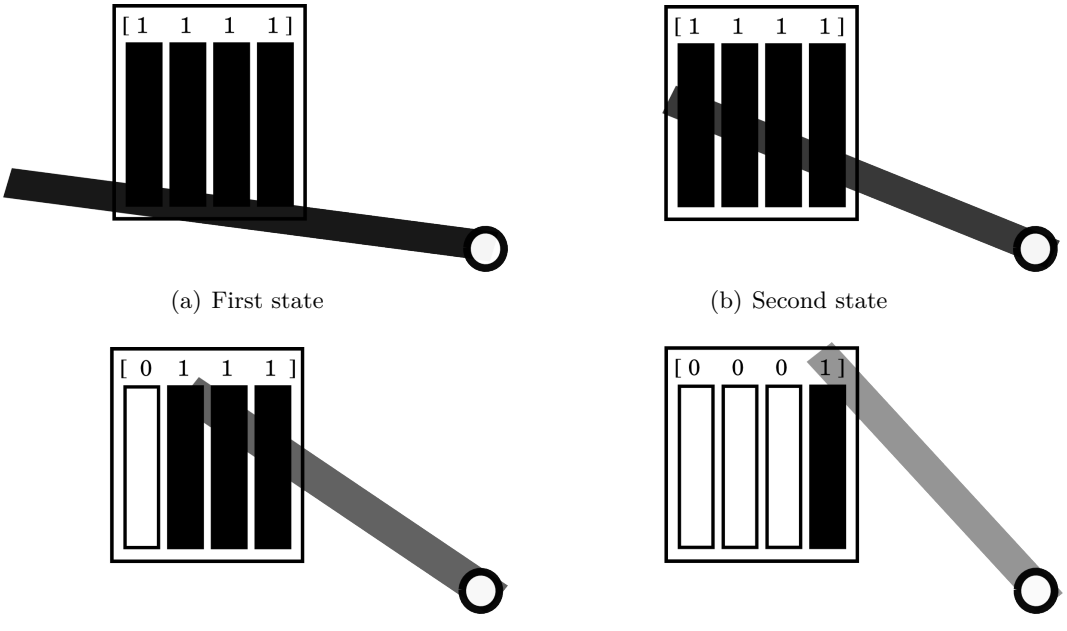

(a) First state (b) Second state

(c) Third state (d) Fourth state

Figure 2.27: Impact of the dynamic shadow as seen by the binary model

The thresholds used in the figures 2.27(a), 2.27(b), 2.27(c) and 2.27(d) are 0.8, 0.6, 0.5 and 0.3, respectively. They were chosen according to their respective SF.

The binary representation concentrates itself on the evolution of the shadow shape rather than the shading factor. This represents a further simplification of the shadow

model, which can now be seen as having a more limited influence of the shading factor. It will be used extensively in chapters 3, 4 and 5.

2.2.5 Summary of the shadow model

The shadow model of this work is a cross-analysis of an optical model of the shadow, the geometry of the PV module and its electric connections. By taking these into consideration, the shadow can be simplified from a continuous, space and time variant phenomenon to a discrete succession of states. They are represented by vectors of data, whose elements represent the shading factor of the cell groups composing the PV module.

Each vector represents the shadow in a certain moment in time, as the shadow moves the vector changes accordingly. Its elements are considered to vary continuously from 0.0 to 1.0, yielding a great number of possible states. They can be simplified by using thresholds to convert them to any n-nary representation deemed interesting. In this work, the choice was made to use a binary representation, restricting the number of possible states to 16, from [0 0 0 0] to [1 1 1 1].

Finally, figure 2.28 illustrates the numeric and binary shadow models proposed in this work.

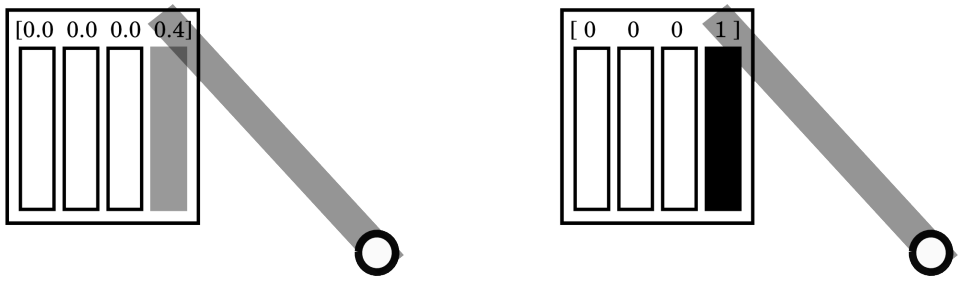

(a) The numeric shadow model (b) The binary shadow model

Figure 2.28: The shadow model

Even if this shadow model was developed at the scale of a PV module, it can be expanded to engulf the totality of a PV plant. It is used in the next section to propose a general theory on PV intermittency.

2.3 A theory of PV intermittency

One of the greatest difficulties surrounding the study of intermittency is the lack of a comprehensive theory regarding its effect on PV systems. Some authors in the scientific community see it as a *power source mismatch*, meaning that its origin is the uneven distribution of light among the cell groups[Patnaik et al., 2011, Ramli and Salam, 2011, Sun and Yang, 2010, Deline, 2009]. Others see it as a *power production problem*, mainly an inefficient MPPT algorithm, incapable of finding the optimal power production [Abdalla et al., 2013, Wang and Hsu, 2009, Eltawil and Zhao, 2010, Ramos-Paja et al., 2010]. Both visions are still lacking an overall comprehension of the phenomenon, which the intermittency theory proposed in this work seeks to provide.

The theory proposed in this work is that **PV intermittency is a two-fold issue: optical and electrical**.

Optical intermittency limits the amount of energy *received* by the PV cells. It can only be addressed through means outside of the PV plant, such as energy storage. PV plants

which are capable of yielding extra power during partial shading conditions are considered to be **stable**. Stable PV plants are reliable sources of energy, producing its nominal power more often.

Electrical intermittency limits the amount of energy *delivered* by the PV cell. It is intimately linked to how the PV cells composing the plant are connected among themselves. Plants whose connections allow a maximum harvest of the available energy under partial shading conditions are called **robust**. Robust PV plants are efficient sources of energy, harvesting more power per square meter.

A **first corollary** of this theory is that: *a robust PV plant requires less storage to be stable*. If the same number of cells can produce more power and more often, less storage is needed to stabilize them.

A **second corollary** of this theory is that: *there is a limit to robustness and none to stability*. While more storage can always be added to a PV plant, the plant itself cannot produce more power than what is shinning over its cells. Thus, robustness is intimately linked to structure of the plant itself.

An example, composed of a PV plant and a shadow, is proposed to illustrate this theory.

The PV plant is made of 4 PV modules similar to the one used throughout this work. Each is composed of 72 cells disposed in 9 lines by 8 columns. They are placed side by side as shown in figure 2.29(a).

The shadow will be consider to propagate itself from the bottom left to the upper right corner of the PV plant. It will move one cell at a time on the Y axis until filling up a column, as shown in figure 2.29(b). Once the column is full, it will start propagating from the bottom of the next column, as shown in figure 2.29(c). Its shading factor is fixed at 0.5.

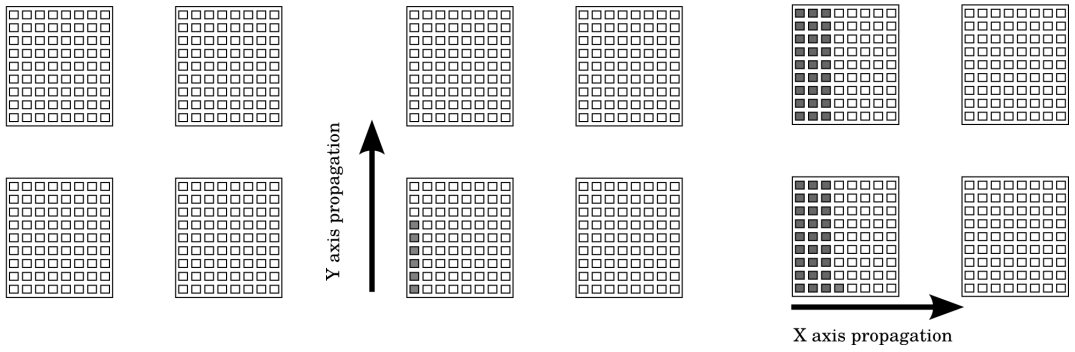

(a) The PV plant unshaded

(b) The shadow propagating in the y axis

(c) The shadow propagating in the x axis

Figure 2.29: The propagation of the shadow in the example (SF of 0.5)

The cells of the PV plant will be considered, at first, as not connected among themselves. As the shadow spreads itself over the PV plant, the number of shaded cells rises and the total power available falls as shown in figure 2.30(b). The grey region represents the power produced by the shaded cells. The green region represents the power that must be supplied by outside means, such as storage.

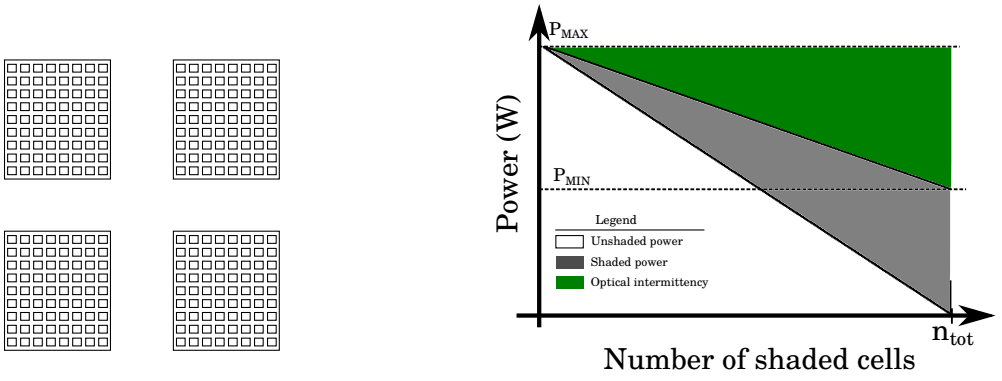

(a) The cells of the PV plant

(b) Power production variation with the shadow (SF 0.5)

Figure 2.30: A PV plant, its cells and variations of power production

The total number of cells is represented by n_{tot}. The P_{MAX} represents the power available with no shadow and P_{MIN} represents the power if all cells are shaded. Their expressions are given by equations 2.4 and 2.5, respectively.

$$P_{MAX} = P_{USH} \cdot n_{tot} \tag{2.4}$$

$$P_{MIN} = P_{SH} \cdot n_{tot} \tag{2.5}$$

The variable P_{USH} represents the power available at the unshaded cell groups and P_{SH} is given by equation 2.6.

$$P_{SH} = (1 - SF) \cdot P_{USH} \tag{2.6}$$

The sum of the white and grey areas in figure 2.30(b) represents the maximum amount of power per cell available. It is considered as its highest robustness possible and its expression is given by equation 2.7.

$$Rob_{MAX} = n_{tot}^2 \cdot \frac{(P_{USH} + P_{SH})}{2} \tag{2.7}$$

The cells of the plant are connected together to reach a certain voltage, forming groups. As a consequence, the overall robustness falters. Since all cells within a group share the same current, if the shadow touches one, its SF will limit the current of all the others. As the groups are connected further together, this effect aggravates itself, as shown in figure 2.31.

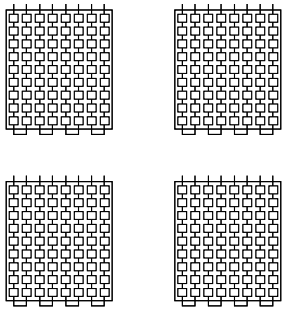

(a) The cell groups of the PV plant

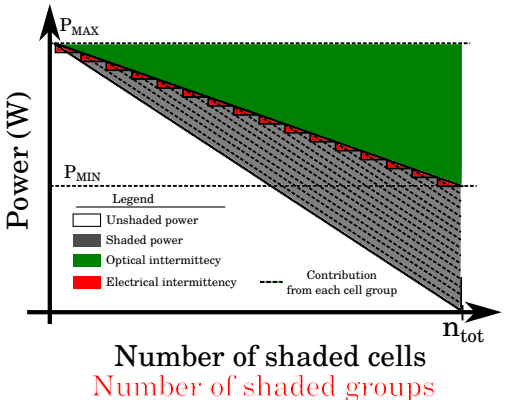

(b) Power production variation with the shadow

Figure 2.31: A PV plant and its cell groups

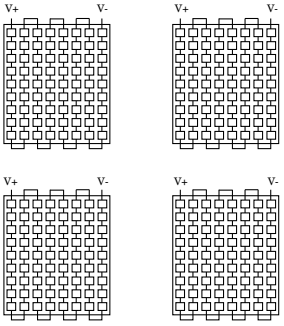

(a) The modules of the PV plant

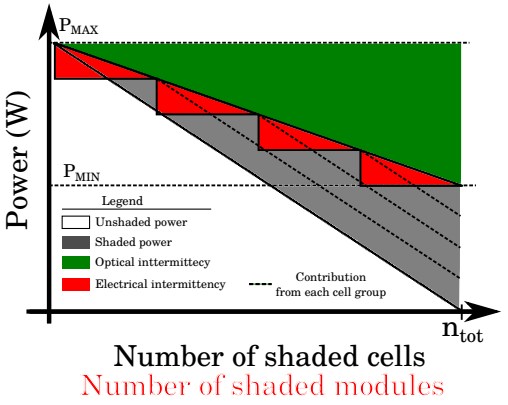

(b) Power production variation with the shadow

Figure 2.32: A PV plant and its modules

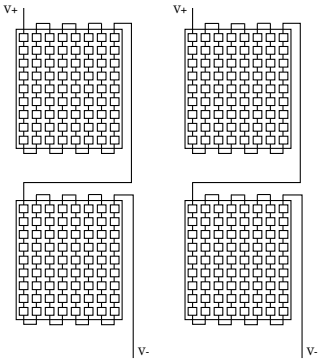

(a) The strings of the PV plant

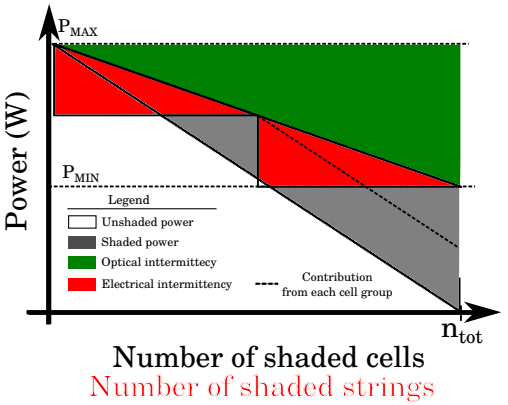

(b) Power production variation with the shadow

Figure 2.33: A PV plant and its strings

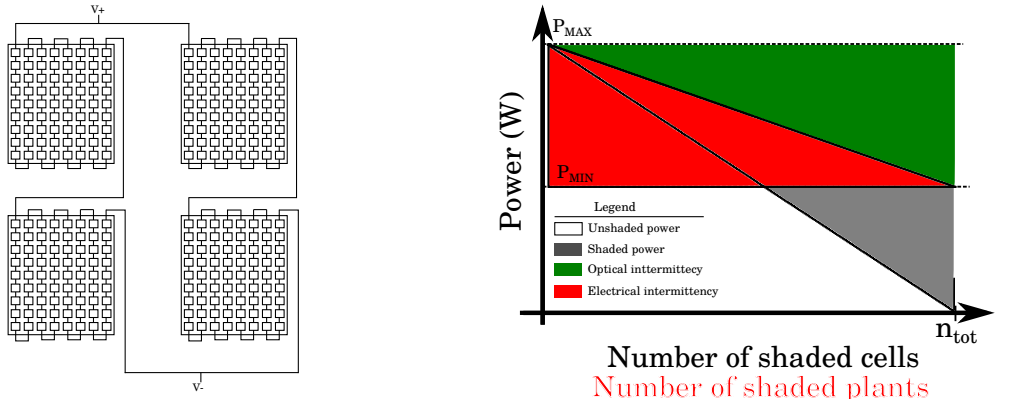

(a) The PV plant

(b) Power production variation with the shadow

Figure 2.34: A totally interconnected PV plant

Figures 2.31(a), 2.32(a), 2.33(a) and 2.34(a) show the composition of a PV plant by connecting its cells together in groups, modules, strings and plant, respectively. Their impact over the robustness is represented by the red triangles in figure 2.31(b), 2.32(b), 2.33(b) and 2.34(b). The dashed lines represent the power of the groups which are completely shaded.

The area of a red triangle can be calculated as seen in figure 2.35.

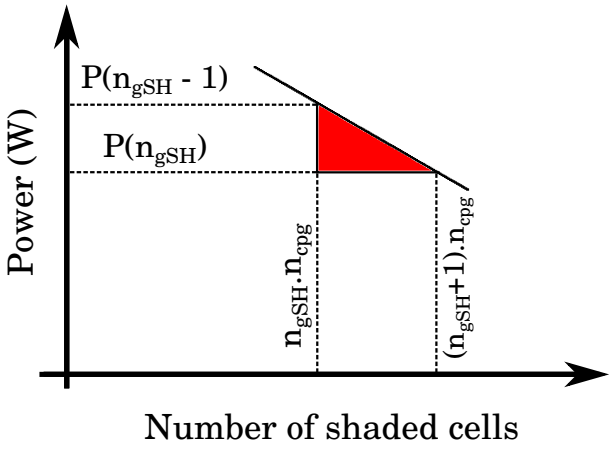

Figure 2.35: The details of the triangle representing robustness losses

Its basis is the number of cells per group (n_{cpg}) and its height is the difference between the power before and after the shadow reaches the group. The number of shaded groups is given by n_{gSH}. The power for a given number of shaded cell groups is given by equation 2.8.

$$P(n_{gSH}) = n_{cpg} \cdot [n_{gtot} \cdot P_{USH} + n_{gSH} \cdot (P_{SH} - P_{USH})] \tag{2.8}$$

The variable n_{gtot} represents the total number of cell groups. Calculating the area lost by all the triangles, adding them to equation 2.7 and dividing the whole by Rob_{MAX}, gives equation 2.9. More details are given in appendix D.

$$Rob = 1 - \left(\frac{n_{cpg}}{n_{tot}} \cdot \frac{P_{USH} - P_{SH}}{P_{USH} + P_{SH}} \right) \tag{2.9}$$

An analysis of equation 2.9 gives the third corollary of the PV intermittency theory. **There are only four methods to raise the robustness of a PV plant.** The first is to raise the number of cells within the PV plant, thus oversizing the plant. The second is to minimize the number of cells per group, thus confining the effect of the shadow. The third is to redistribute the power between the shaded and unshaded cells, thus erasing the presence of the shadow. The fourth is to drive the power of the shaded cell groups to zero, thus ignoring their presence.

This work claims that the second, third and fourth methods drive the overall research on robustness enhancement in the current literature.

2.4 Photovoltaic Robustness Enhancing Solutions - PRobES

The intermittency theory has shown that there are four possible ways to raise the robustness of a photovoltaic power plant. Three of them regroup the overall work of the literature: reducing the number of cells per group, redistributing their available power or ignoring shaded cell groups. The first two provide the basis for two families of PV robustness enhancing solutions or PRobES, namely, series and parallel. The last one is the idea behind bypass diodes.

Series PRobES seek to raise the number of power electronics structures within the a single PV plant. Each would be able to track the local MPP, no matter the shadow, thus harvesting more power per cell. However, less number of cells per group means less power. Their challenge is, thus, making power electronics converters more efficient at low power applications. [Ishaque, 2012, Safari and Mekhilef, 2011, Ramos-Paja et al., 2010, Giral et al., 2011, Nguyen and Low, 2010, Woyte et al., 2003]

Parallel PRobES aim at redistribute the available power of the system. They reroute the current distribution among the cells, reducing the difference of power between those shaded and unshaded. Their challenge is the optimization of the topologies capable of such current distribution[Kadri et al., 2011, Walker et al., 2003, Nimni and Shmilovitz, 2010, Shimizu et al., 2001, 2003].

Bypass diodes have been used, for the past decades, as the *de facto* PRobES by the industry. It becomes naturally biased when the voltage of the shaded cell group becomes negative, short-circuiting them and ignoring their power [Woyte et al., 2003, Acciari et al., 2011]. They will be used as the reference solution in this work.

A method to compare the solutions from the two families is currently inexistent in the literature. Thus, this work proposes one based on their similar challenges. Its objective is to assess possible room for improvement which can yield new research themes.

2.4.1 Analysis method and criteria

The analysis below is based on the challenges common to all the existing PRobES. Some of its criteria are more quantitative while others are grant a more qualitative view. They are, namely, granularity, efficiency, power gain, reliability, integration potential and control complexity.

Granularity is the number of cells operating independently. More granular systems have less cells per group, tend to harvest more energy per cell and are more robust to shadows.

Passive components describes the number and complexity of passive components in the solution. They lead to more volume, cost, losses and reduce the integration potential of the system.

Efficiency is the relation between power input and output during the PRobES operation. Since PV modules do not have a high efficiency themselves it is paramount that their PRobES do.

Power gain is the surplus power actually collected by the solution in comparison with a reference. The common reference used to compare all PRobES is presented below.

Reliability is the capacity of the system to remain functional in the case one or more element faults. More complicated solutions tend to require more maintenance, cost more and break more often, undermining their robustness.

Integration potential evaluates how feasible it is to integrate the active and passive elements of the system within a chip. Integration means less volume, better efficiency, less cost and more reliability.

Control simplicity evaluates the cost in energy, sensors and time that the system actually requires to perform its functions. Complex solutions may require dedicated and often complicated algorithms to operate. On top of that, their control system may need many sensor which lower the overall reliability.

The use of these criteria require a precise and well defined evaluation scale. The one used in this work is detailed in table 2.1.

Table 2.1: The evaluation scale

Analysis criteria	*Very Low (1)*	*Very High (4)*
Granularity	Several modules	One single cell
Passive components	Many and complex	Single and simple
Efficiency	Lower than 80%	Higher than 90%
Power gain	0% over reference	Higher than 90% over reference
Reliability	A fault in an active element stops the system	A fault in 4 or more active elements stops the system
Integration potential	No element can be integrated	All elements can be integrated
Control simplicity	Several sensors and a complex algorithm required	No control required

After a review of the PRobES state-of-the-art, a graph will be traced to compare their performances.

2.4.2 The reference PRobES- Bypass and blocking diodes

The PRobES used as a reference in this work is the *de facto* solution used by the industry: bypass diodes. They are installed in PV modules to protect the shaded cells from being destroyed and to minimize losses in power production Ho [2013]. They prevent the shaded cells from working under reverse bias by short-circuiting them. This effect is illustrated by the example in figure 2.36.

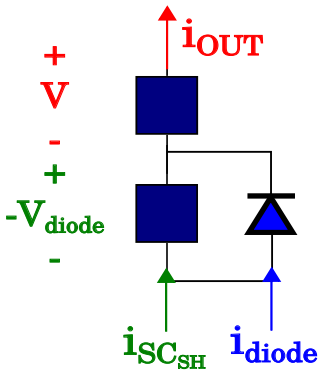

(a) The bypass diode protecting the shaded cells

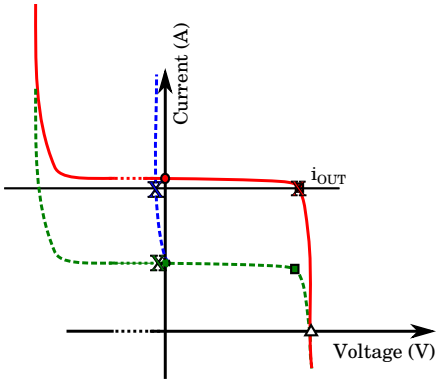

(b) The effect on the I-V curve

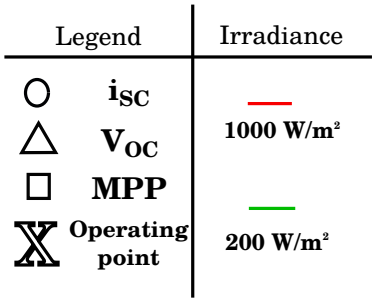

(c) Legend

Figure 2.36: The working principle of the bypass diode

The output current, i_{OUT}, is represented in red. Due to the presence of the bypass diodes, it is divided between the shaded cells in green and the bypass diodes in blue. They are represented by i_{SH} and i_{bypass} respectively.

The scenario shown in figure 2.36 shows a high current being imposed over the two cells by the MPPT. The unshaded cell have no problem supplying such a current, but the one shaded is forced in reverse bias. Its voltage becomes negative, naturally activating the bypass diode. Once short-circuited, the shaded cells supplies its i_{SC}, while the excess current flows through the diode. Some authors work on replacing them with active switches to reduce losses [Acciari et al., 2011].

The consequence of this approach is that the effect of the shadow is confined to the shaded cell, creating a control challenge. The activation of bypass diodes deforms the I-V and P-V curves of a PV plant. By doing so, they change the specific shape of the P-V curve upon which the MPPT algorithm is based. As the shadow propagates itself, the maximum power point of the system changes, making it virtually impossible for a simple disturb and observe algorithm to track it. Thus, other methods are required, yielding a vast range of contributions from the literature [Woyte et al., 2003]. The challenge of the authors working with bypass diodes is to always find the highest available power, no matter the shadow shape or shading factor [Ramos-Paja et al., 2010, Ishaque, 2012, Nguyen and Low, 2010].

To illustrate this situation, figure 2.37 shows two examples of shadows cast over the reference plant used in the previous section. The plant is now equipped with bypass diodes.

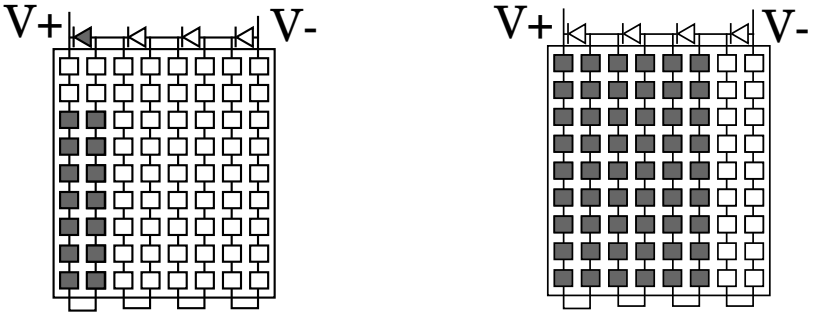

(a) Shadow 1 (b) Shadow 2

Figure 2.37: Two examples of shadow over the PV plant

The influences of these shadows in the I-V and P-V curves of the PV plant are shown in figure 2.38.

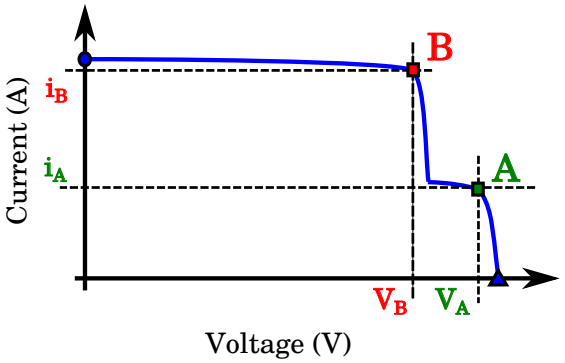

(a) I-V curve of the PV plant under shadow 1

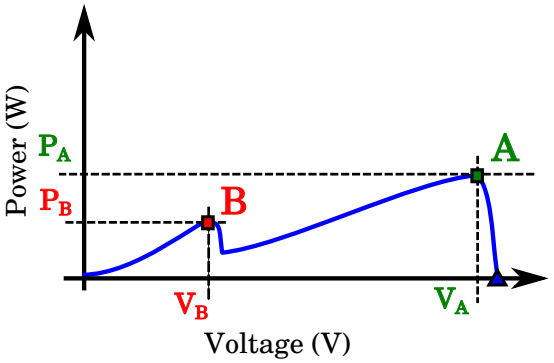

(b) P-V curve of the PV plant under shadow 1

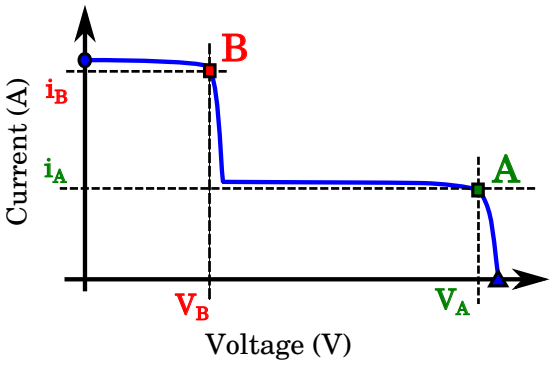

(c) I-V curve of the PV plant under shadow 2

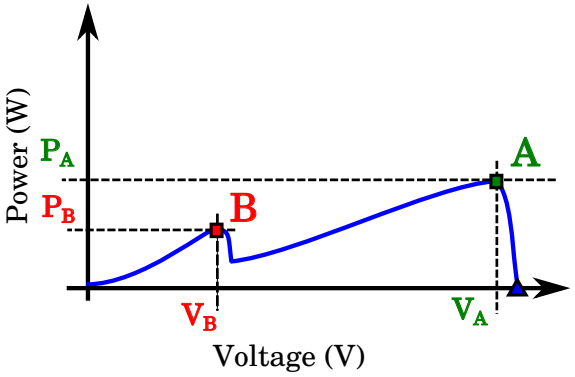

(d) P-V curve of the PV plant under shadow 2

Figure 2.38: Impact of the shadows on the characteristic curves of the PV plant

Two operating points are distinguishable in both I-V curves in figure 2.38.

At point A the output current of the entire module is limited by the shaded cells. This is usually the point found by a simple disturb and observe algorithm, which becomes blocked and cannot go further. In figure 2.38(a), where the highest power point is B, staying at A represents a loss of power. The opposite is true for figure 2.38(c).

When the plant is operating **at point B**, its bypass diodes become active. The shaded cells are short circuited and the output current is equal to that of the unshaded cells. In

figure 2.38(a), this represents a gain in power. However, point B is not recommended in the case shown in figure 2.38(c).

From a robustness point of view, bypass diodes give the PV plant the possibility of ignoring the shaded cells, reducing their power to zero. However, with the shaded cells short-circuited their number is constantly zero, reducing the total number of cells. Thus, there is a gain in robustness by using bypass diodes but it is limited by how many cells are short-circuited. The robustness diagram of the plant used in figure 2.37 is shown in figure 2.39.

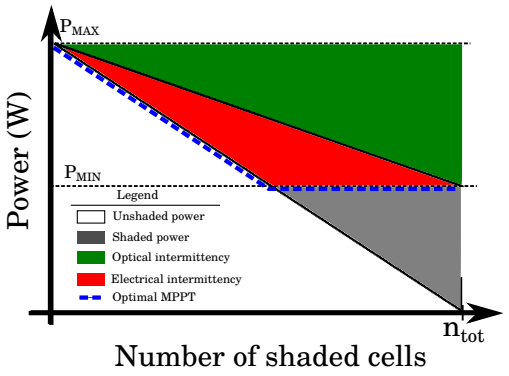

Figure 2.39: The robustness diagram of a PV plant equipped with bypass diodes

There is an inherent loss of robustness due to the electrical connections withing the PV plant, shown in red. The blue line shows the challenge faced by the researchers that propose new algorithms for tracking the MPPT under partial shading conditions. It uses the bypass diodes to automatically ignore the shaded cells, following the unshaded slope on the left side of the figure, represented by point B on figure 2.38(a). As the shadow expands, the algorithm will eventually start tracking point A on figure 2.38(c), always staying at the maximum power available.

The use of bypass diodes, however, leads to another problem: return currents. It happens when an unshaded PV string is connected in parallel with another one having a shaded and bypassed cell group or module. Since the shaded cells were short-circuited, bringing their voltage to zero, the string containing it will have a lower voltage. Thus, a current will start flowing between the two strings due to their voltage differences Bun [2012]. This effect is shown in figure 2.40.

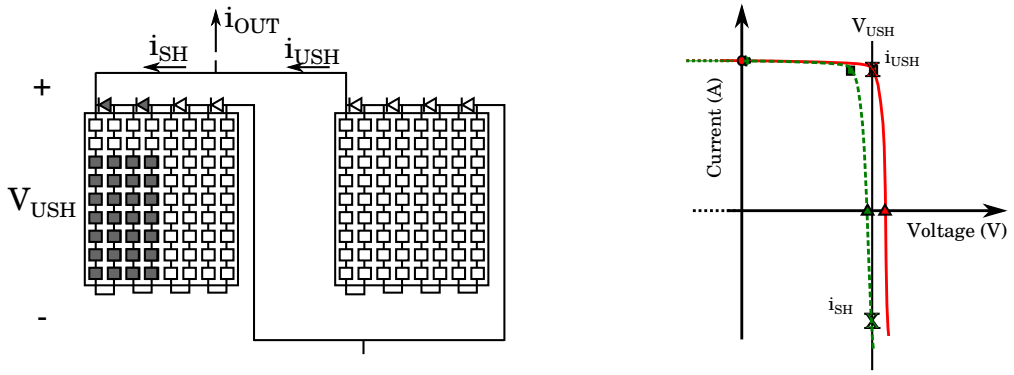

(a) The reverse currents

(b) The effect on the I-V curve

Figure 2.40: An example of the effect of reverse currents and blocking diodes

The I-V effect of these return currents is shown in figure 2.40(b). The shaded string may be forced to work at a higher voltage, reaching into Quadrant II, where its current is negative. In this situation, the PV module will consume power not due to a reverse bias, but rather due to negative current and positive voltage Bun [2012].

The answer to avoid this problem: more diodes! Figure 2.41 shows the use of blocking diodes in series with the shaded module to avoid the reverse currents. The great disadvantage of this effect is that a shadow over a single cell may finally completely jeopardize the power production of an entire string.

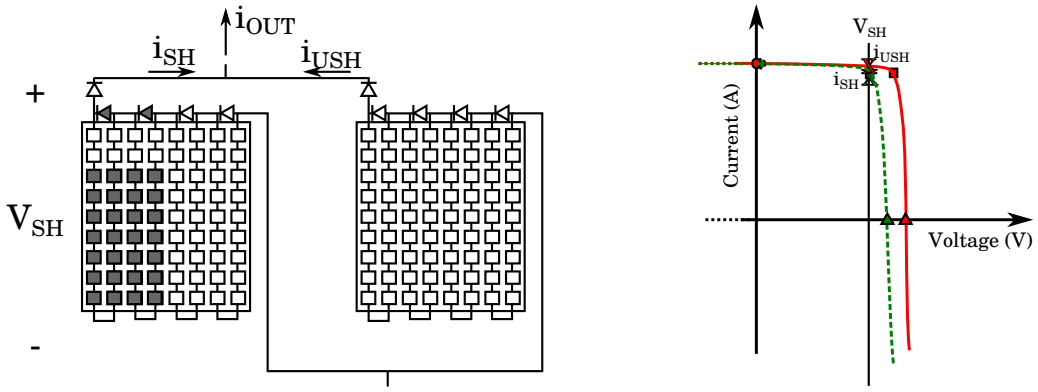

(a) The blocking diodes

(b) The effect on the I-V curve

Figure 2.41: An example of the effect of reverse currents and blocking diodes

In terms of robustness, blocking diodes reduce the unshaded power available over the cells.

Finally, the robustness diagram of a PV plant equipped with bypass and blocking diodes along with a single MPPT chopper is shown in figure 2.42. It will be considered, in this work, as the reference to evaluate all other PRobES.

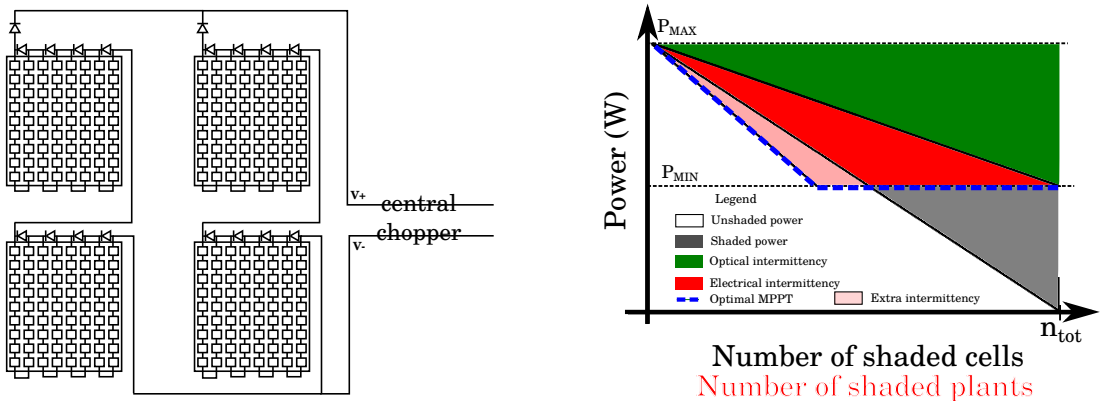

(a) The reference PRobES

(b) Its robustness diagram

Figure 2.42: The reference PRobES and its robustness diagram

The PRobES shown in figure 2.42(b) will be used as a reference and called central inverter. It is the cheapest and simplest solution available as of the moment this work was

written. Since it is a single chopper, it can easily achieve 96% to 98% efficiency Woyte et al. [2003], being the most efficient alternative. It also gets a high score for its passive component, since it has only one chopper. Its control is somewhat simple, requiring some special algorithm to always find the highest MPP. It has a very low integration potential due to its high power. Its reliability is also low since if the chopper fails, the entire power production stops.

Using this reference, the other PRobES can now be presented.

2.4.3 Series PRobES

Series PRobES use power electronics topologies connected to as few cells as possible within the PV plant. They track the MPP locally, either converting the output DC current directly to AC or converting it to another DC level, which is then sent to the DC bus. They are often called distributed MPPT (DMPPT) or micro-converters in the current literature Bidram et al. [2012].

This work considers that there are three types of series PRobES: multi-string, module embedded and micro-converters. They are all based on the same principle: reducing the number of cells per group. Figures 2.43, 2.44 and 2.45 illustrate their application over the reference PV plant.

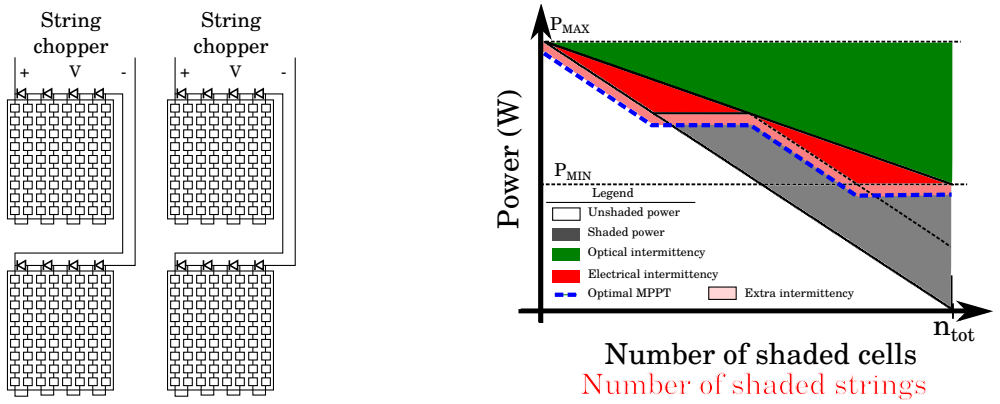

(a) PV plant equipped with multi-string series PRobES and bypass diodes

(b) Multi-string series PRobES robustness diagram

Figure 2.43: Multi-string series PRobES and their robustness diagrams

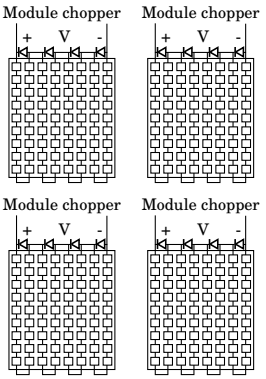

(a) PV plant equipped with module series PRobES and bypass diodes

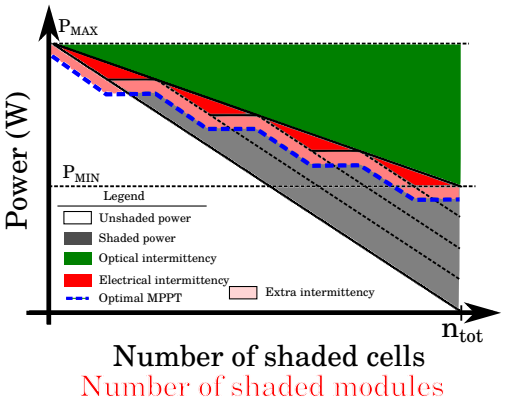

(b) Module series PRobES robustness diagram

Figure 2.44: Module series PRobES and their robustness diagrams

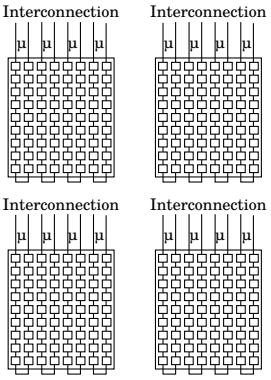

(a) PV plant equipped with micro-converters series PRobES and no bypass diodes

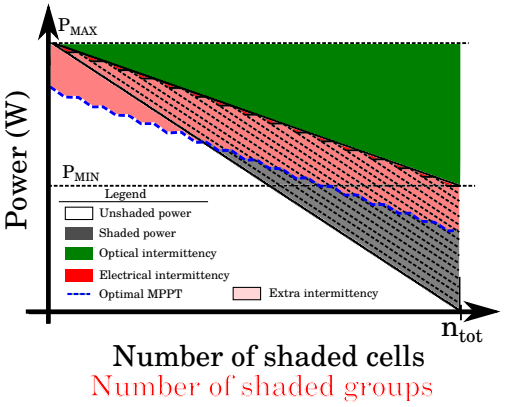

(b) Micro-converters series PRobES robustness diagram

Figure 2.45: Micro-converter series PRobES and their robustness diagrams

As the series PRobES approach the cell, their granularity raises. By handling smaller groups of cell, their control system can use less complex algorithms. Smaller groups mean for smaller choppers. These have a higher integration potential, driving up their reliability.

On the opposite sense, smaller chopper have lower efficiency rates. As their efficiency falters, it reduces their power gains. This is illustrated by the pink zones in figures 2.43(b), 2.44(b) and 2.45(b).

Finally, with the multiplication of choppers, the number of passive components also increases and, along with them, the losses.

Figure 2.46 shows a diagram that superposes the evaluation of these series PRobES and the reference.

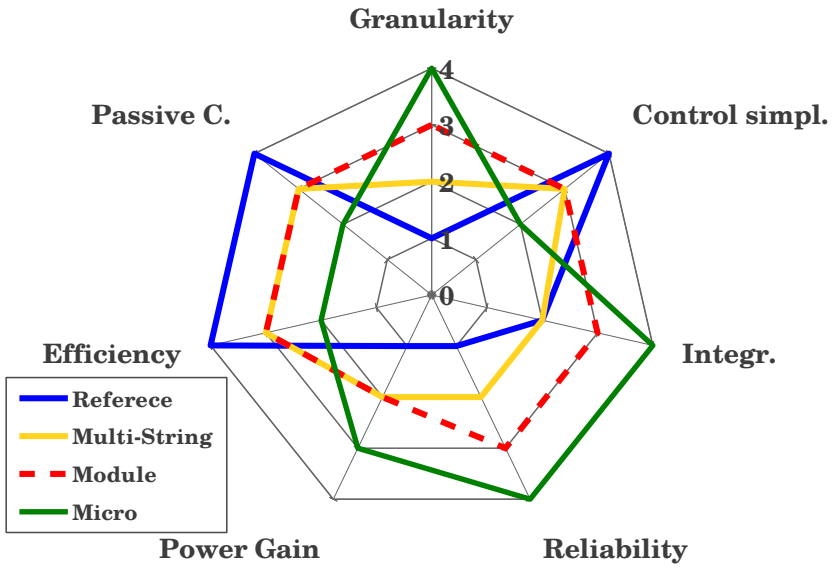

Figure 2.46: Comparison of the different series solutions

The great challenge remaining to the scientific community in this area is to **raise the efficiency of micro-converters**.

2.4.4 Parallel PRobES

Parallel applications use inductors to share the energy among PV cell groups. They eliminate local MPP created by the shadow, replacing them with one global MPP. This principle is shown in figure 2.47. The new MPP, represented by point C, maximizes the output power for all cells but a series PRobES must be used to track it.

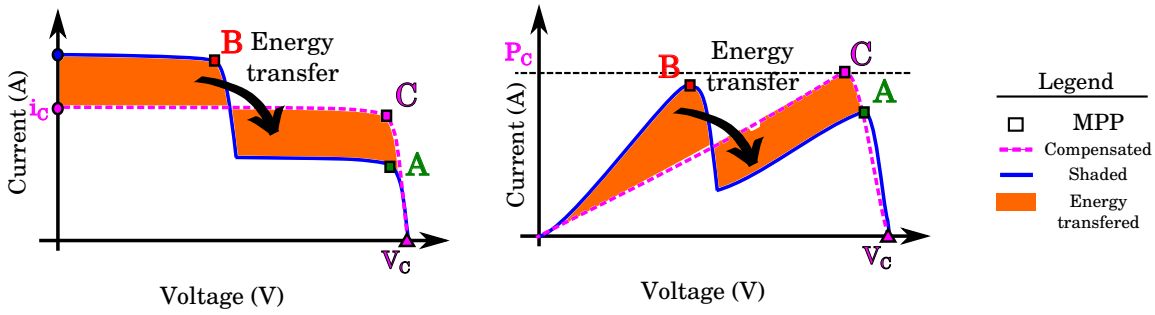

(a) Their effect on the I-V curve (b) Their effect on the P-V curve (c) Legend

Figure 2.47: The principle of parallel PRobES

In terms of robustness, parallel PRobES seeks to make P_{USH} as close to P_{SH} as possible. Its effect over the reference PV plant is shown in figure 2.48.

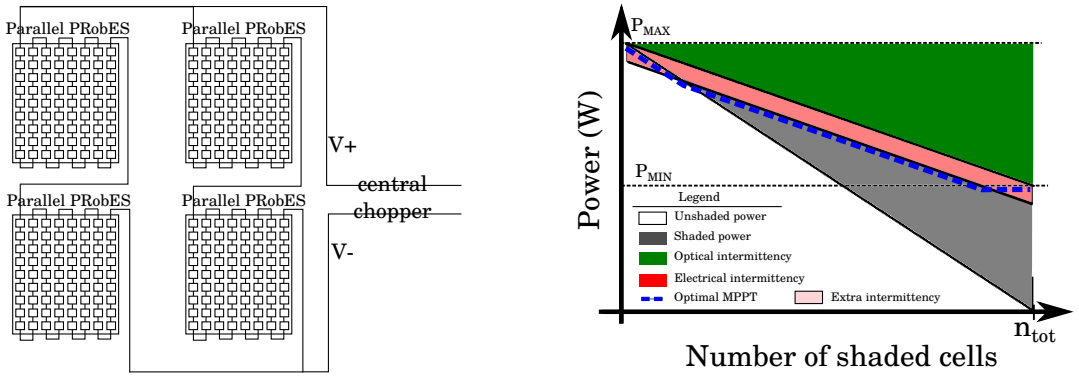

(a) A PV plant equipped with parallel PRobES

(b) Its robustness diagram

Figure 2.48: The impact of parallel PRobES over the robustness

By replacing the bypass diodes with parallel PRobES, the PV plant can dramatically raise its robustness without even replacing its central chopper. This is represented by the pink zone in figure 2.48(b). The robustness of such PV plant would only depend on the efficiency and reliability of the parallel PRobES. Thus, the efficiency of large series PRobES can be combined with the granularity of parallel PRobES to yield a more robust PV plant.

In the literature, parallel PRobES do not have a common denomination, with authors calling their own approaches differently. The main contributions as of the moment of this work are either based on two power electronics topologies. The first is the Cùk converter, its applications are called Generation Control Circuit (type B), Active bypass or Non Dissipative String Current Inverters [Shimizu et al., 2001, Giral et al., 2011, Kadri et al., 2011]. The second is based on the Flyback converter and its applications are called Generation Control Circuit (type A), PV String Per-module Maximum Power Point Enabling Converter, Return Energy Current Converters or Submodule Integrated Converters [Shimizu et al., 2001, Walker et al., 2003, Nimni and Shmilovitz, 2010, Olalla et al., 2012].

Figure 2.49 shows the topologies of these solutions. In it, the small PV modules represent the cell groups, their voltages are represented by V_{PV} and the current leaving the system is represented by i_{PV}.

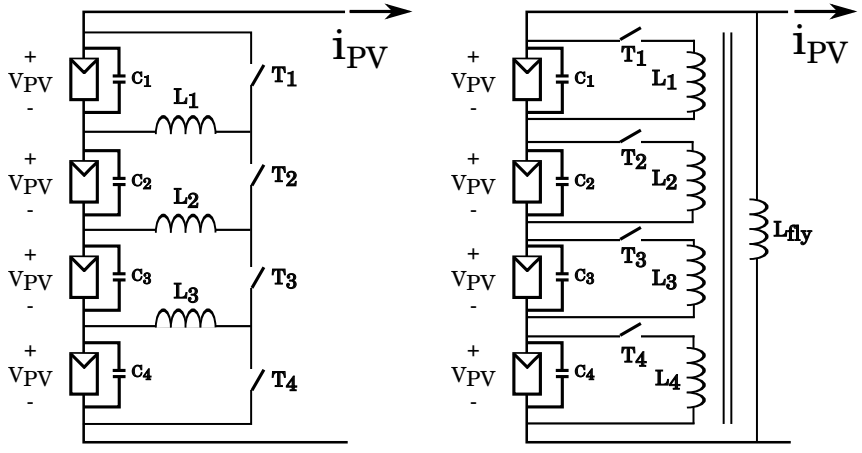

(a) Cùk based concept

(b) Flyback concept

Figure 2.49: Topologies of the typical parallel solutions

The transistors are denoted by T_i, capacitors by C_i and inductors by L_i, where i can go from 1 to 4. In the Flyback based application, the inductor coupled with all the others is called L_{fly}.

The concepts based on the Cùk converter are better crafted to share current among adjacent cell groups. Its control is based on the search of the optimal voltage distribution through the correction of the duty cycle driving all its transistors [Shimizu et al., 2003] They all share a similar efficiency problem: its current must flow through all switches. Furthermore, their integration is limited due to the floating potential between their transistors.

The Flyback-based concept has a too cumbersome inductor to allow integration. Its efficiency, however, is higher since its current flows through fewer switches. Its control system is more complicated and does not provide clues as to how the shadow can be found and which cell group should be chosen to receive current [Nimni and Shmilovitz, 2010].

Their characteristics are compared in figure 2.50.

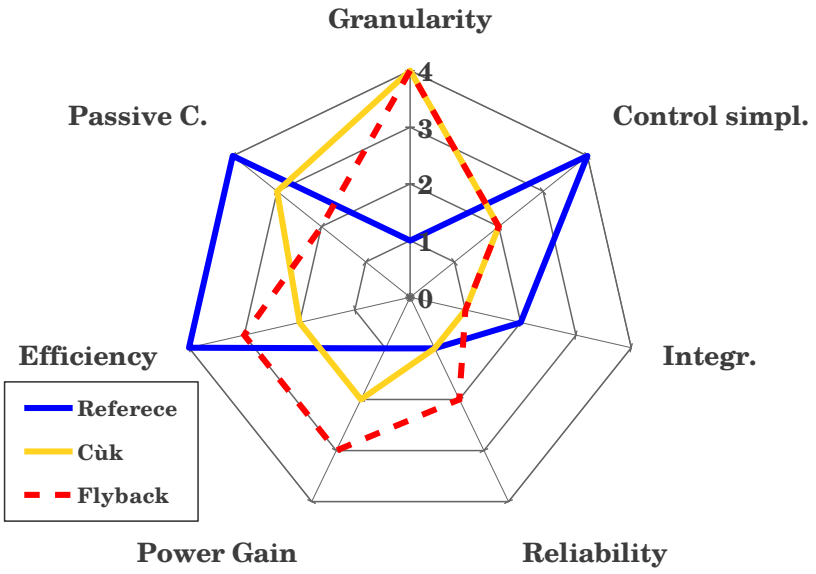

Figure 2.50: Comparison of the different parallel solutions

The lack of integration potential and the complexity of the passive components are the great drawbacks of all these structures. If they are not integrated, their power gain, efficiency and reliability cannot be improved. Without these improvements, these solutions are bound to never make it to the factory floor or deployed in large scale on the existing PV plants.

2.5 Conclusion

This chapter has proposed an overall study of the problem of intermittency in photovoltaic systems. Its objective was to propose a new perspective for understanding the current literature and find themes that need further improvement and research.

An overview of photovoltaic systems was conducted to understand intermittency from the PV plant point of view. Its result is a shadow model, which cross-analyzes the shadow as an optical and electrical phenomenon.

It was followed by an intermittency theory capable of regrouping the overall contributions of the literature under a single and comprehensive point of view. This theory states that the photovoltaic intermittency is a two-fold issue: optical and electric.

Optical intermittency relates to a PV plant stability or how close to its nominal power a PV plant can be under shaded conditions. Stability can only be achieved by acting outside the PV plant, such as using storage or other sources of energy.

The electric intermittency regulates its robustness or how much power per square meter the PV plant is capable of delivering while shaded. Robustness, however, was proven to be only solved within the PV plant and by four possible means: making PV plants bigger, controlling the power of smaller cell groups, redistributing the power among cell groups or ignoring the shaded cell groups. All contributions in the literature are, to some extent, a declination of one of these techniques.

These solutions to the partial shading problem were called Photovoltaic Robustness Enhancement Systems or PRobES. They were classified in two families: series and parallel solutions.

While series PRobES have arrived at a certain stage of maturity, parallel PRobES seem blocked by their design limitations. Contributing to the former implies a further development of integration techniques to tackle the efficiency challenge. Contributions to the latter require a different approach to the conception of the entire system in order to break free from its topological constraints. In this work, the second path was chosen over the first.

This necessary topological breakthrough is proposed in the next chapter.

Chapter 3

The Photovoltaic Equalizer

The previous chapter has proposed a theory for analyzing the intermittency in photovoltaic systems. It was shown that there are few techniques capable of granting a maximal power production under shading conditions. Two of them are the basis for the overwhelming majority of current scientific activity in the literature. One is the reduction of cells per power electronics chopper connected in series, leading to a close-up control of their maximal power point and confinement of the shading problem. The other is to use specialized circuits parallel to the main current production loop to redistribute the power among cells as to erase the effects of shading. These techniques were called Photovoltaic Robustness Enhancement Solutions or PRobES.

PRobES were found to be divided into two families: series and parallel. Their state-of-the-art was described and discussed, showing the general challenges of each. Parallel PRobES are those who have caught the interest of this work for they require a paradigm breakthrough in terms of topology and control techniques.

This chapter proposes a topological breakthrough for the parallel PRobES called **Photovoltaic Equalizer**. This chapter is dedicated to explain its topology and its advances in comparison with the literature.

To do so, the topology in itself will be introduced along with its switching rules. From these will be deduced a series of potentially interesting functions. These functions will be, in turn, used in an extensive study of the system losses and limitations. Finally, a conclusion will describe its challenges and provide the steps to be taken in the next chapters.

Contents of this chapter

3.1 Circuit representations used in this chapter

Most of the attention in this chapter is dedicated to a new power electronics topology and its inherent functions to deal with partial shading. It is expected, thus, that many circuits will be drawn. To ease their drawing, some circuit representations involving photovoltaic systems will be introduced and explained in this section.

PV module circuit representation

Chapter 2 has shown that a PV module is constituted of a certain number of cells connected in series to attain a certain voltage under the nominal cell current. It was also shown that in order to protect the cells and raise PV robustness, manufacturers equip their PV modules with bypass diodes. To reduce costs, however, commercial PV modules are equipped with only a few diodes, changing their granularity from PV cells to **PV cell groups**. The number of PV cells per PV cell group varies with the model and manufacturer of the PV module.

The reference PV module adopted in this work has 72 cells connected in series. They are bundled into 4 cell groups, which will be labeled as PV_I, PV_{II}, PV_{III} and PV_{IV} in Roman numerals. Figure 3.1 shows the circuit representation of the reference module.

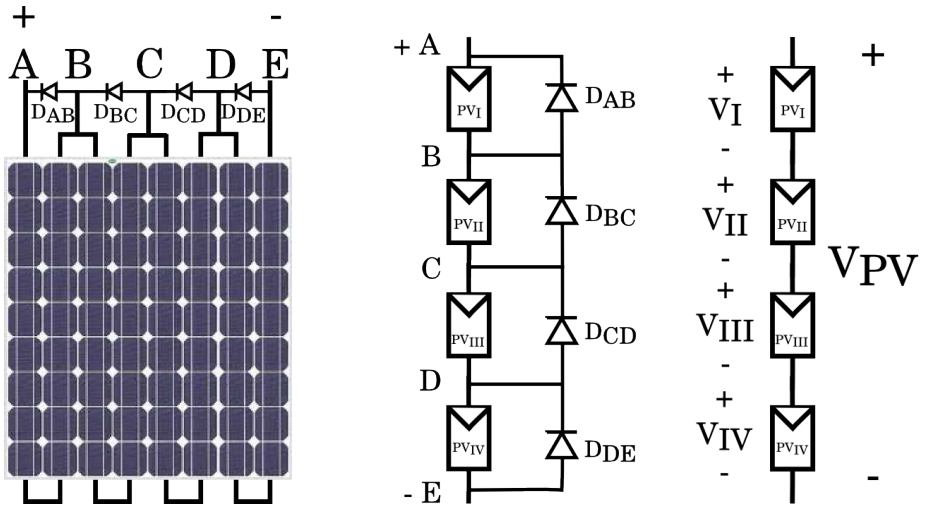

(a) PV module connection points with bypass diodes

(b) Circuit representation with bypass diodes

(c) Circuit representation without bypass diodes

Figure 3.1: Equivalence between the real PV module and its circuit representation

The real PV module, its electrical connections and bypass diodes are shown in figure 3.1(a). The points A through E represent the connections available at the rear of the PV module. Thus, the positive (+) extreme terminal is shown over point A, while the negative (-) one is shown over point E. The four bypass diodes are labeled D_{AB}, D_{BC}, D_{CD} and D_{DE} according to the points they are connected to.

The circuit representation of its four cell groups are the four mini PV modules connected in series and shown in figure 3.1(b). The points A through E in both figures 3.1(a) 3.1(b) are the same, just as their respective bypass diodes.

Finally, the circuit shown in figure 3.1(c) is used in this chapter. It has no bypass diodes and the PV Equalizer will be connected to its available connection points. The voltage of each cell group is represented by V_I to V_{IV}, respectively. The total voltage of

the system is represented by V_{PV}. A complete set of characteristics, including various I-V curves, of this PV module are available in Appendix B.

Shadow circuit representation

The shadow was introduced in the previous chapter through an extended cross-analysis between optical shadow and its effects on the reference PV module. This analysis issued a shadow model consisting of a numeric vector whose elements represent the shading factor of each cell group. A similar representation will be used throughout this chapter, but on a circuit version, as shown in figure 3.2.

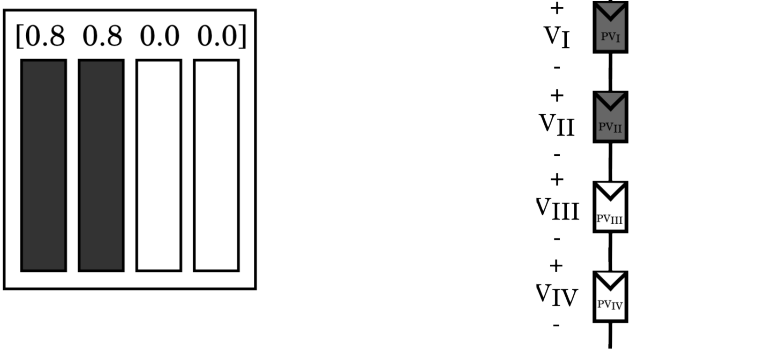

(a) A numeric shadow example

(b) Its electric circuit representation

Figure 3.2: Examples of the shadow shape

The grey mini PV modules represent the location of the shadow, while their contrast represents the shading factor. The precise SF value will be given separately, according to the example.

Simplified circuit representation of the PV power conditioning system

The whole PV system includes the MPPT chopper, the DC bus, the inverter and the grid. While complete, such an extensive representation is considered unnecessary, in this work, to study the partial shading phenomena.

Considering that the DC bus is fixed and controlled by the inverter allows the DC chopper to focus its MPPT control on its own duty cycle. Variations in the DC chopper duty cycle imply in changes in the current and voltage of the PV module. As a consequence, the equivalent load seen by the PV module can be represented by either a voltage or a current source.

Since the shadow has a direct effect on the current production of the PV system, it is more convenient to analyze it from the current perspective. Thus, a current source representation of the power conditioning system was chosen in this work. Their equivalence is shown in figure 3.3(b).

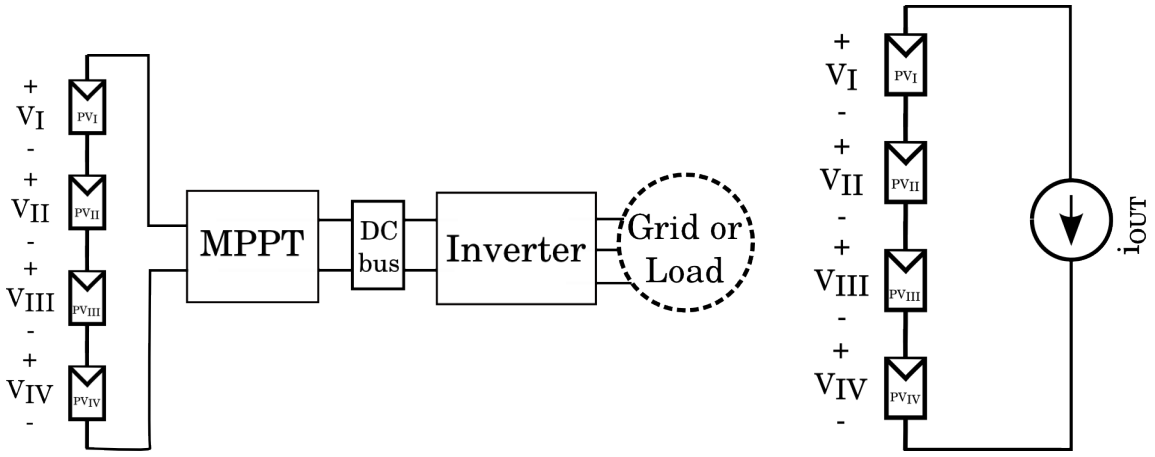

(a) Complete PV system (b) Simplified PV system

Figure 3.3: PV system equivalence

Now that these circuit representations are set, the PV Equalizer can be introduced.

3.2 The PV Equalizer

The parallel PRobES studied in this work is called **PV Equalizer** , inspired from its equivalent battery equalizer Park et al. [2009]. As its name suggests, this structure equalizes the uneven current distribution among the shaded and unshaded cell groups of a PV module. This redistribution is achieved by surrounding the PV cell groups with transistors, all connected to a single inductor. This creates a modular and elementary PV Equalizer, as shown in figure 3.4. This elementary PV Equalizer can be connected to as many cell groups as needed, giving it an important modular feature.

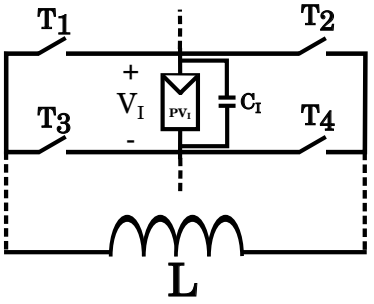

Figure 3.4: The elementary PV Equalizer

To explain the switching rules of the PV Equalizer, an example with only two cell groups is shown in figure 3.7. Cell group PV_{II} is shaded while cell group PV_I is unshaded. There are two possible states according to the energy flow within the inductor: charge or discharge.

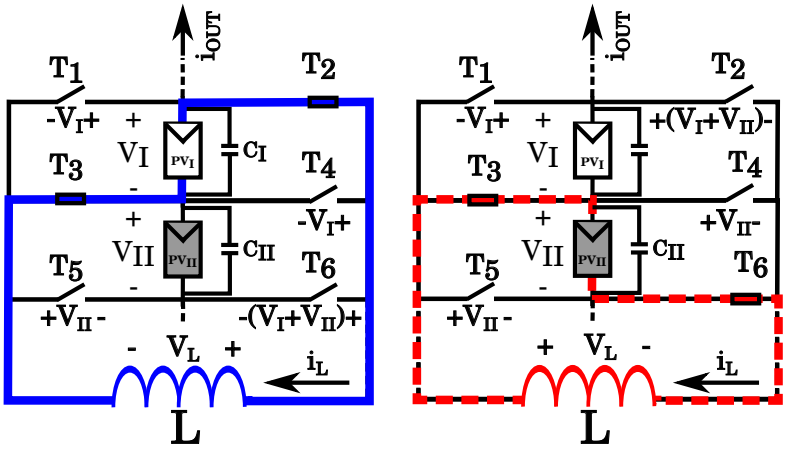

(a) State 1: inductor charging (b) State 2: inductor discharging

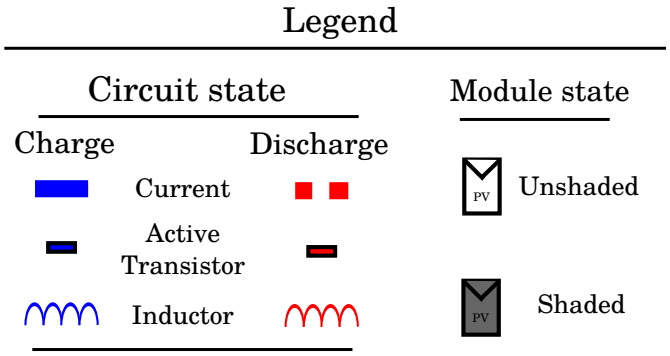

(c) Circuit legend

Figure 3.5: The two possible states of the inductor current paths

Figure 3.6 shows how each state affects the voltage and current in the inductor.

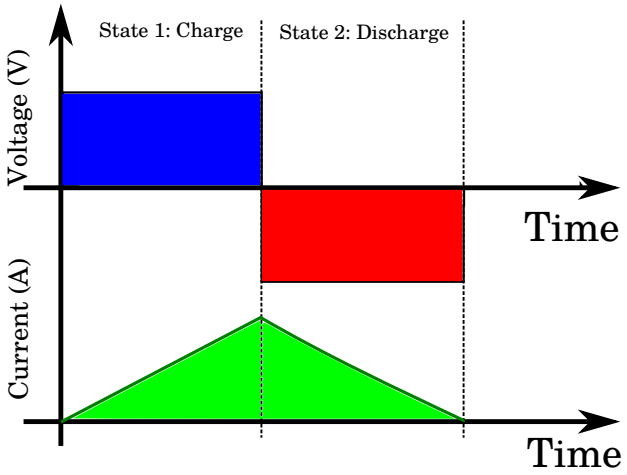

Figure 3.6: Qualitative effect each state over the inductor voltage and current

When in *Charge*, a positive voltage is applied to the inductor. Current starts flowing through the provided loop, accumulating energy. This charge is only possible by activating even transistors connected to the positive voltage of the PV cell group and odd transistors connected to its negative voltage, as shown in figure 3.5(a).

When in *Discharge*, a negative voltage is applied to the inductor. The loop now allows the inductor current to flow while liberating energy. This discharge is only possible by activating even transistors connected to the negative voltage of the PV cell group and odd transistors connected to its positive voltage, as shown in figure 3.5(b).

In both cases the current across the transistors remains unidirectional, while the voltage may inverse itself as in the case of T_4. Moreover, the presence of the shadow can briefly inverse the voltage of the shaded cell groups also inversing the voltage across the transistors. It this happens, current may flow across the body diodes within the transistors, creating undesired short-circuits. The answer to this problem is to force the switching legs to be voltage-bidirectional but current-unidirectional. This is achieved in this through the use of a diode in series with the transistor, as shown in figure 3.7.

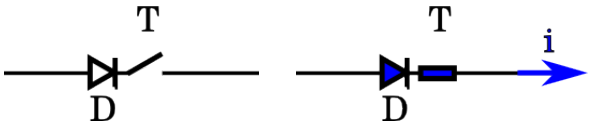

(a) Switching leg open (b) Switching leg conducting

Figure 3.7: A generic voltage-bidirectional but current-unidirectional switching leg

Applying the elementary PV Equalizer to the reference PV module gives the final topology used in this work. It is shown in figure 3.8.

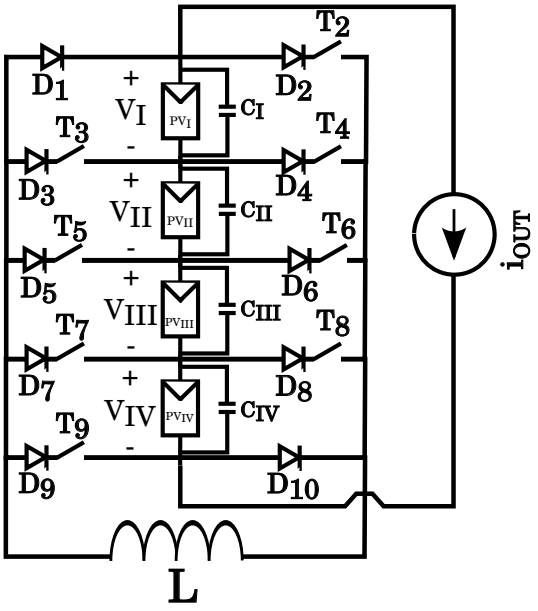

Figure 3.8: PV equalizer topology

The PV Equalizer used in this work has 8 transistors (T_2 - T_9), 10 diodes (D_1 - D_{10}), 4 capacitors (C_I - C_{IV}) and a single inductor (L).

The use of diodes D_1 and D_{10} grant a security feature, acting as a global *discharge*. In the case of a control failure and no path is offered to the inductor current, then these diodes will automatically discharge it over the entire PV module.

While the structure is active, the high switching frequency imposes rapid variations in current to the cell groups. Acting as filters, capacitors are connected in parallel to each

cell group, represented respectively by C_I to C_{IV}. They interact closely with the inductor, transferring instantaneous power to and from it.

The single inductor is capable of accessing any number of cell groups due to the transistor network. It can be used to transfer energy to and from any of the four PV cell groups. Thus, not only the PV Equalizer is modular, but also it is flexible.

The description of the equations associated to the PV Equalizer will be done through the analysis of a working example.

3.2.1 Working example

Figure 3.9 shows an example where only cell group PV_{IV} is shaded by a certain shading factor (SF). Its current is reduced according to equation 3.1.

$$i_{SH} = (1 - SF) \cdot i_{USH} \tag{3.1}$$

Where i_{USH} represents the current of any unshaded PV cell group and i_{SH} of those shaded.

In this example, groups PV_I, PV_{II} and PV_{III} are used to charge the inductor while PV_{IV} is used to discharge it. The current flow during charge and discharge of the inductor are shown in figures 3.9(a) and 3.9(b), respectively.

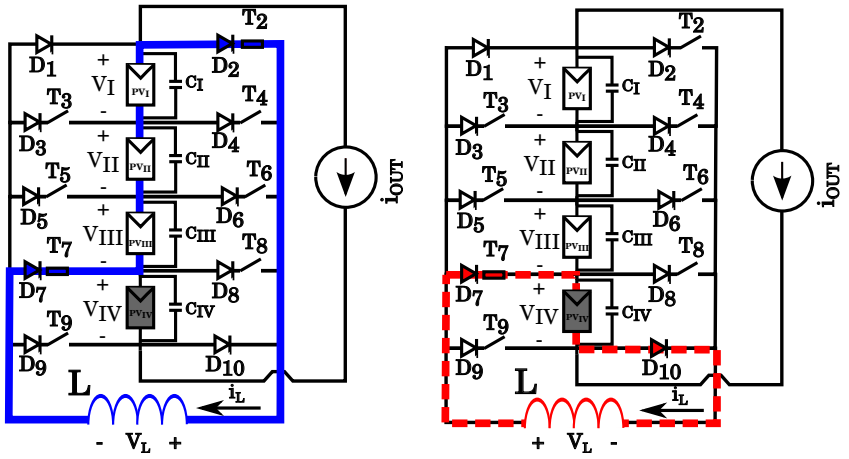

(a) Charge period

(b) Discharge period

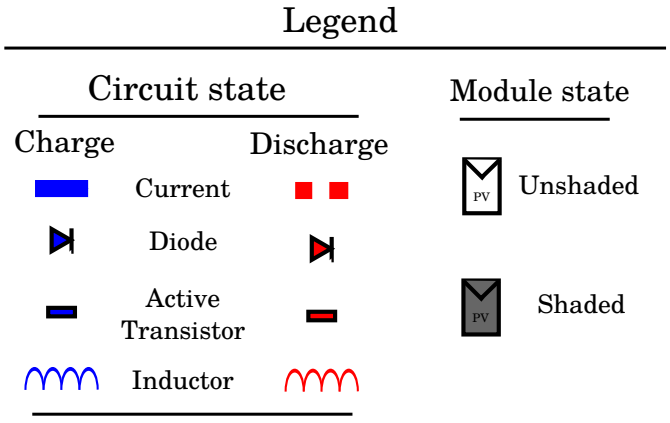

(c) Circuit legend

Figure 3.9: Working example of the equalizer topology switching

The current and voltage in the inductor in steady-state are shown in figure 3.10. In it, D represents the duty cycle of the system and T its period. The time scale is not specified for this example.

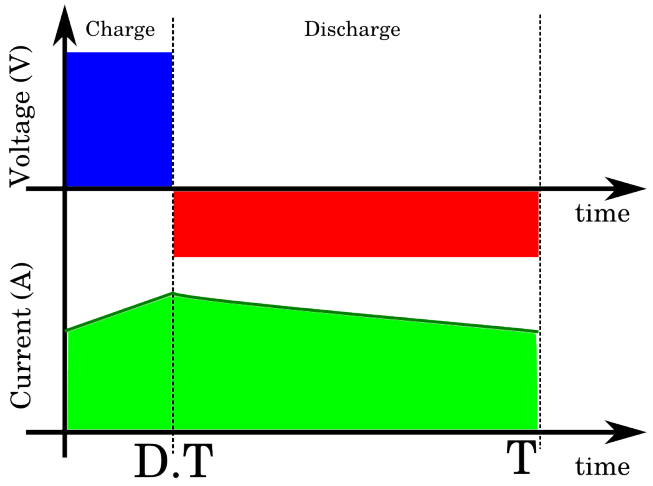

Figure 3.10: Steady-state voltage and current in the inductor during a switching period

The circuit equations of the charge and discharge periods from figure 3.10 are given in table 3.1.

Table 3.1: Circuit equations

Charge Phase		*Discharge Phase*	
$V_{L_{CH}} = V_{I_{CH}} + V_{II_{CH}} + V_{III_{CH}}$	(3.2)	$V_{L_{DCH}} = V_{IV_{DCH}}$	(3.3)
$i_{OUT} + i_L = i_{USH} + i_{CUSH_{CH}}$	(3.4)	$i_{OUT} = i_{USH} - i_{CUSH_{DCH}}$	(3.5)
$i_{OUT} = i_{SH} + i_{CSH_{CH}}$	(3.6)	$i_{OUT} - i_L = i_{SH} - i_{CSH_{DCH}}$	(3.7)

The indexes used in these equations are listed below.

- $_{CH}$ and $_{DCH}$ represent a variable during charge and discharge phase, respectively
- $_{USH}$ and $_{SH}$ represent variables related to the unshaded and shaded cell groups, respectively
- i_{OUT} is the current imposed by the external MPPT
- V_L and i_L are the voltage and current of the inductor
- V_C and i_C are the voltage and current of the capacitors
- V_i and i_i represent the voltage and current of the i^{th} cell group

To analyze the equations of the PV Equalizer, a few simplifying hypothesis will be considered.

First, the system will be considered to be operating in steady-state conditions and at its maximum power point. This allows to consider i_{OUT}, i_L, V_i and i_i to be constant during an entire switching period.

Second, the current in all unshaded cell groups (PV_I, PV_{II}, PV_{III}) is considered equal. They will all be represented by i_{USH} in 3.4 and 3.5. Their capacitor currents are also

considered equal and represented by i_{CUSH}. In the case of the shaded cell group PV_{IV} and its capacitor, their currents will be represented by i_{SH} and i_{CSH}, respectively.

Third, the analysis of these equations will consist in defining the duty cycle, mean output current and mean inductor current of the PV Equalizer under ideal conditions. They will be specially useful in sizing the passive components. These will be revised later to include losses and other imperfections.

A summary is given in page 78.

Duty cycle

Ideally, the steady-state duty cycle of the PV Equalizer is calculated based on the inductor average voltage in figure 3.9(c). The average charge and discharge voltages are given by equations 3.8 and 3.9.

$$\overline{V_{L_{CH}}} = V_{L_{CH}} \cdot D \tag{3.8}$$

$$\overline{V_{L_{CH}}} = V_{L_{DCH}} \cdot (1 - D) \tag{3.9}$$

Considering steady-state conditions *the average inductor voltage is zero* and combining the two equations above gives equation 3.10.

$$V_{L_{CH}} \cdot D = V_{L_{DCH}} \cdot (1 - D) \tag{3.10}$$

By replacing equations 3.2 and 3.3 into 3.10 gives the equation for the duty cycle, shown in 3.11.

$$D = \frac{V_{IV_{DCH}}}{V_{I_{CH}} + V_{II_{CH}} + V_{III_{CH}} + V_{IV_{DCH}}} \tag{3.11}$$

If the voltages in each cell group are considered equal, than this equation can be simplified as follows. Its variable n_{DCH} represents the number of cell groups receiving energy from the inductor, while n_{CH} represents the number of cell groups providing energy to it.

$$D = \frac{n_{DCH}}{n_{CH} + n_{DCH}} \tag{3.12}$$

This result means that, ideally, *the duty cycle of the PV Equalizer is independent from the operating conditions of the PV module*. It can be estimated by knowing the number of shaded and unshaded cell groups.

To understand the consequences of this fact, consider the case where the voltages across the cell groups are NOT equal. Theoretically, if the duty cycle is not correctly controlled in these circumstances the inductor average current will be non-zero. This would lead to its indefinite rise, ultimately destroying the inductor. An example of such situation is when the inductor is simply connected to an ideal voltage source.

However, PV modules are NOT ideal voltage sources. As shown by its I-V curves, PV voltage *falls* as its current rises. This means that if the inductor current starts to rise, the voltage of the PV cell group to which it is connected will fall. Thus, the current and voltage outputs of a given PV cell group adapt themselves to the PV Equalizer duty cycle.

The consequence is that **the PV Equalizer can operate at a fixed duty cycle**. Whether the ideal duty cycle maximizes power production or not under real operating conditions is a different issue, which will be explored further in chapter 4.

Average inductor current

The average inductor current can be calculated by analyzing the charging and discharging capacitor currents. The current within a capacitor is given by equation 3.13, where C_i refers to the i^{th} capacitance and t denotes the time.

$$i_{Ci} = C_i \cdot \frac{dV_{Ci}}{dt} \tag{3.13}$$

By using equation 3.13 along with the capacitor currents defined in 3.4 and 3.5 will give current $i_{I_{CH}}$ and $i_{I_{DCH}}$ can be described as follows.

$$C_I \cdot \frac{dV_{CI_{CH}}}{dt} = i_{OUT} - i_{USH} + i_L \tag{3.14}$$

$$C_I \cdot \frac{dV_{CI_{DCH}}}{dt} = -i_{OUT} + i_{USH} \tag{3.15}$$

Considering the system in steady-state, the variations in the capacitor voltage can be described as follows.

$$\Delta V_{CI_{CH}} = \frac{D \cdot T}{C_I} \cdot (\overline{i_{OUT}} - \overline{i_{USH}} + \overline{i_L}) \tag{3.16}$$

$$\Delta V_{CI_{DCH}} = \frac{(1-D) \cdot T}{C_I} \cdot (-\overline{i_{OUT}} + \overline{i_{USH}}) \tag{3.17}$$

Since $\Delta V_{CI_{CH}}$ is equal to $\Delta V_{CI_{DCH}}$, equations 3.16 and 3.17 can be combined to yield equation 3.18.

$$D \cdot \overline{i_L} = \overline{i_{USH}} - \overline{i_{OUT}} \tag{3.18}$$

A similar analysis with equations 3.6 and 3.7 yields equation 3.19.

$$(1-D) \cdot \overline{i_L} = \overline{i_{OUT}} - \overline{i_{SH}} \tag{3.19}$$

Adding up equations 3.18 and 3.19 gives the expression of $\overline{i_L}$.

$$\overline{i_L} = \overline{i_{USH}} - \overline{i_{SH}} \tag{3.20}$$

Which can be simplified by using equation 3.1, giving the mean inductor current.

$$\overline{i_L} = SF \cdot i_{USH} \tag{3.21}$$

Equation 3.21 leads to two important conclusions.

First, the current flowing through the inductor depends on the shading factor. Its influence in the efficiency of the PV Equalizer will be studied in detail later in this chapter.

Second, the inductor current can be used to detect changes in the shading factor. Such detection functions will be studied in chapter 5.

Output current

The next step into understanding how the Equalizer improves power production is to estimate its impact in the output current. It can be deduced from equation 3.18, with the system in steady-state, yielding:

$$\overline{i_{OUT}} = \overline{i_{USH}} - D \cdot \overline{i_L} \tag{3.22}$$

Replacing the mean inductor current by its definition found in equation 3.21 gives:

$$\overline{i_{OUT}} = (1 - SF \cdot D) \cdot \overline{i_{USH}} \tag{3.23}$$

Equation 3.23 shows that the Equalizer has a direct impact on the shading factor perceived by the MPPT, effectively reducing it. Thus, the MPPT becomes capable of tracking a higher current while preserving all cell groups in operation. Under these ideal conditions the currents in the unshaded and shaded cell groups are the same raising the system robustness to one, according to equation 2.9 in page 51.

To understand what happens to the current of each PV cell group, both equations 3.18 and 3.19 will be expanded by using the inductor and output current definitions from 3.21 and 3.23, yielding:

$$\overline{i_{USH}} = (1 - SF \cdot D) \cdot \overline{i_{USH}} + D \cdot SF \cdot \overline{i_{USH}} \tag{3.24}$$

$$\overline{i_{SH}} = (1 - SF \cdot D) \cdot \overline{i_{USH}} - (1 - D) \cdot SF \cdot \overline{i_{USH}} \tag{3.25}$$

Simplifying these equations give the average local current of each cell group.

$$\overline{i_{USH}} = \overline{i_{USH}} \tag{3.26}$$

$$\overline{i_{SH}} = (1 - SF) \cdot \overline{i_{USH}} \tag{3.27}$$

Equations 3.26 and 3.27 shows the cell groups producing at their local maximum current in steady-state. This is further evidence that the PV Equalizer can, theoretically, rise the robustness of the system to one. Its imperfections must be studied to determine how well it can really perform this task.

3.2.2 Passive components

Deducing the equations related to the design of the passive components L and C is a necessary step to create a prototype of the system. They give clues to the choices available for designers to size the PV Equalizer and shed some light on its limitations.

Capacitance

The general capacitance expression was recalled previously in equation 3.13. Replacing it in 3.6 and 3.7 while solving for C gives:

$$C_{USH} = (i_{USH} - i_{OUT}) \cdot \frac{dt}{dV_{CUSH}} \tag{3.28}$$

$$C_{SH} = (i_{OUT} - i_{SH}) \cdot \frac{dt}{dV_{CSH}} \tag{3.29}$$

With the system in steady state, the definitions of $\overline{i_{USH}}$, $\overline{i_{SH}}$ and $\overline{i_{OUT}}$ given by equations 3.26, 3.27 and 3.23 can be used to give:

$$C_{USH} = (1 - D) \cdot D \cdot SF \cdot \frac{i_{USH} \cdot T}{\Delta V_{CUSH}} \tag{3.30}$$

$$C_{SH} = (1 - D) \cdot D \cdot SF \cdot \frac{i_{USH} \cdot T}{\Delta V_{CSH}} \tag{3.31}$$

These equations show some important facts to take into consideration while sizing the capacitors of the PV Equalizer. First, all capacitors are sized by the same rule, no matter if they are charging or discharging. Second, the shading factor and the duty cycle have an influence in the sizing of the capacitors. Thus, bigger capacitors are required for covering a broader range of both. Finally, the choices made during the sizing of the PV Equalizer will have a direct impact over how it improves the robustness of its PV module.

Inductance

The inductor voltage is defined by equation 3.32.

$$V_L = L \cdot \frac{di_L}{dt} \tag{3.32}$$

With the system in steady state, using the definition of the duty cycle given in equation 3.12 and considering the voltages in all cell groups as equal to V_{USH} gives the expression of the inductance.

$$L = (n_{CH} \cdot D) \cdot \frac{V_{USH} \cdot T}{\Delta i_L} \tag{3.33}$$

$$L = (n_{CH} \cdot D) \cdot \frac{V_{USH} \cdot T}{\Delta i_L} \tag{3.34}$$

An important conclusion can be drawn from these equations: **the inductance does not depend on the shading factor**. Rather, it depends on how many cell groups are used during the charge phase and their duty cycle. Again, choices done during the sizing of the system have a direct impact over its control possibilities.

3.2.3 Overview

Based on the ideas above, the following table gives an overview of the important equations and their associated conclusions.

The most important conclusion from this section is that the design of a PV Equalizer depends on how it will be used to compensate the shadow. Passive components are affected by either the presence of the shadow or the strategies chosen to mitigate it. Thus, capacitor or inductor sized for a certain shadow state and switching strategy might be ineffective when either or both change. And since the objective of this work is raising robustness *as a whole*, the PV Equalizer should be designed to be effective against *any* shadow state.

Further studies will correlate the use of the PV Equalizer with its performance.

Table 3.2: Overview of the working variables

Equation	Eq. Number	*Conclusion*
$D = \frac{n_{SH}}{n_{SH} + n_{USH}}$	3.12	The equalizer can work at a fixed duty cycle.
$i_L = SF \cdot i_{USH}$	3.21	Losses in the inductor are directly proportional to the shading factor.
$i_{OUT} = (1 - SF \cdot D) \cdot i_{USH}$	3.23	The output current rises and all the cells are producing at their local maximum.
$C = (1 - D) \cdot D \cdot SF \cdot \frac{i_{USH} \cdot T}{\Delta V_C}$	3.31	Higher SF requires bigger capacitors.
$L = (n_{USH} \cdot D) \cdot \frac{V_{USH}}{\Delta i_L \cdot f}$	3.33	The size of the inductor depends only on the shape of the shadow.

3.3 Circuit functions

The high flexibility of the transistor network within the equalizer allows it to access any PV cell group in any order. The previous section has given the basis for exchanging energy to and from the inductor. The next step is to use these to describe the **functions** through which the circuit mitigates the presence of shadows.

The PV Equalizer can perform three types of functions: shadow correction, shadow diagnosis and idle. The shadow correction functions have the objective of erasing the presence of the shadow. They are marked by the use of a switching strategy and duty cycle, which are chosen according to the shadow state. These functions are, namely, equalize and bypass.

The diagnosis functions have the objective of acquiring information on the shadow and estimating its state. Several techniques may be used to accomplish this, but this chapter will only present the most intrusive one, called the search function.

While idle the PV Equalizer does not use any of its functions. Its transistors are all blocked but ready to perform any needed task.

The bypass and equalize functions will be characterized in specific provided in chapters 4 and 5. Their description in this chapter is introductory and aimed at providing information on how they impact the PV Equalizer losses. The idle function will have an important role during the design of the control system in chapter 6. Its energy requirements are considered as negligible in comparison to other functions, and it will not be presented further in this chapter.

3.3.1 Equalize function

The equalize function handles the transfer of energy from unshaded to shaded cell groups. It is driven by switching strategies whose complexity may vary significantly according to the shadow state. Their fundamental block is called **basic switching strategy or BSS**, which has only one charge and discharge period.

In this work, the BSS will be represented by a specific notation. For example, when cell groups PV_I and PV_{II} are used to charge the inductor while cell groups PV_{III} and PV_{IV} are used to discharge it, their BSS is represented by "$I.II \rightarrow III.IV$". In this notation, the arrow represents the flow of energy, pointing who receives it. The roman numerals

represent their respective cell groups and when these are used together in either charge or discharge they are separated by a point.

Table 3.3 provides other examples of BSS to illustrate the flexibility of the PV Equalizer. They are ranked by the number of cell groups discharging the inductor.

Table 3.3: A few examples of BSS

Cell groups charging	*Cell groups discharging*	*BSS*	Duty Cycle	*Figure*
II, III & IV	I	$II.III.IV \rightarrow I$	0.25	3.11(a)
III & IV	II	$III.IV \rightarrow II$	0.33	3.11(b)
IV	I	$IV \rightarrow I$	0.50	3.11(c)
II & III	I & II	$II.III \rightarrow I.II$	0.50	3.11(d)
IV	II &III	$IV \rightarrow II.III$	0.66	3.11(e)
I	II, III & IV	$I \rightarrow II.III.IV$	0.75	3.11(f)

The circuit representation of all of the examples are shown in figure 3.11.

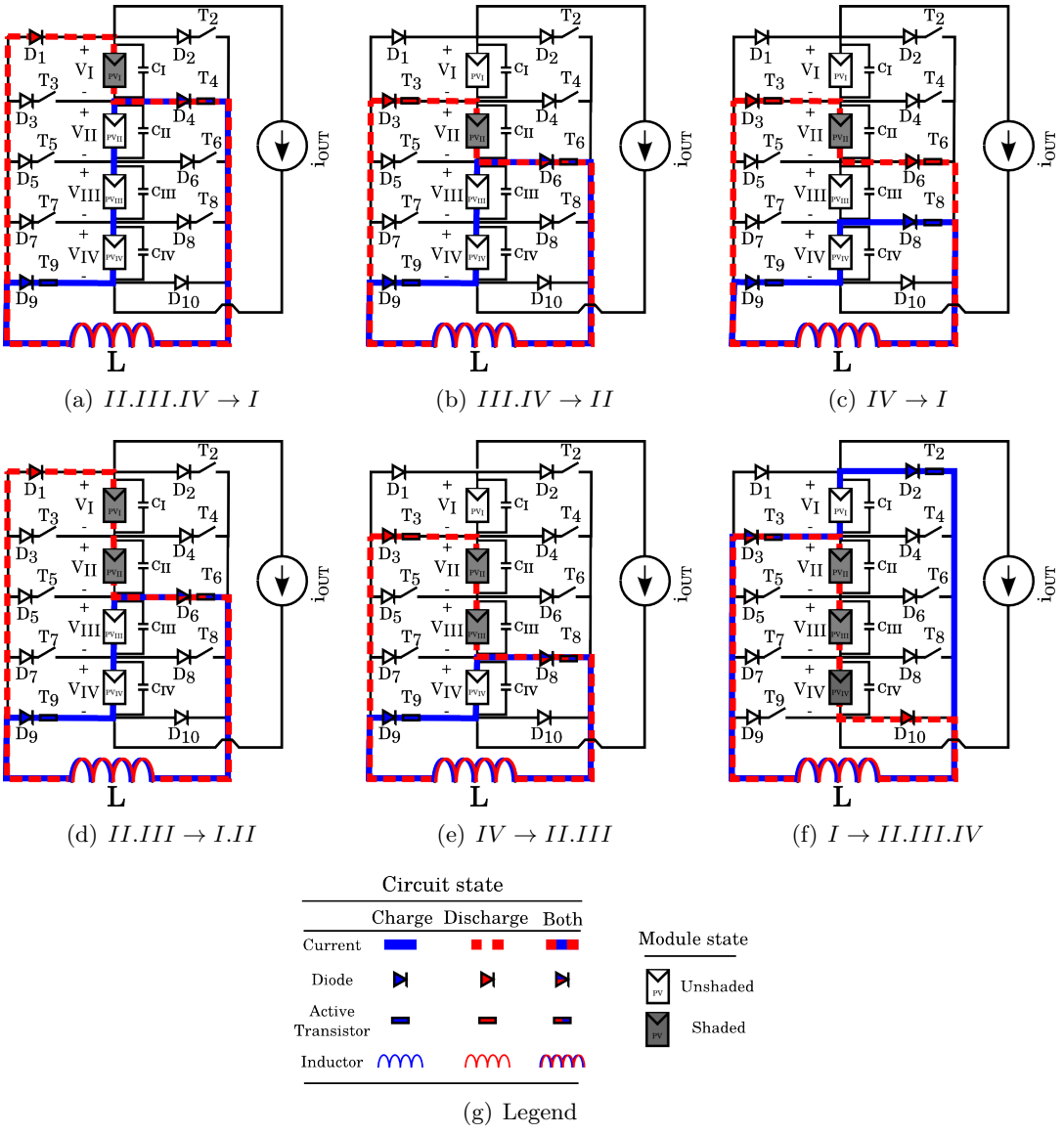

(a) $II.III.IV \rightarrow I$ (b) $III.IV \rightarrow II$ (c) $IV \rightarrow I$

(d) $II.III \rightarrow I.II$ (e) $IV \rightarrow II.III$ (f) $I \rightarrow II.III.IV$

(g) Legend

Figure 3.11: Circuit representations showing the active switches and inductor current path for each BSS example

The examples above confirm the high flexibility provided by the transistor network of the PV Equalizer. They also show that the number of cell groups charging and discharging in a BSS can vary from 2, as in figure 3.11(c), to 7 as in figure 3.13(c). Their duty cycle also changes, which will have an impact in the size of the capacitors and the inductor. Thus, each of them should be taken into consideration during the design of the prototype.

Complex Switching Strategies

The two BSS presented in figure 3.12 can be used to create a switching strategy that harvests all the surplus energy in groups PV_I, PV_{II} and PV_{IV}. It is called a **complex switching strategy or CSS**, being composed of the two BSS and represented by $I.II \rightarrow III$ and $IV \rightarrow III$. Their impact on the power production is studied into detail in chapter 4.

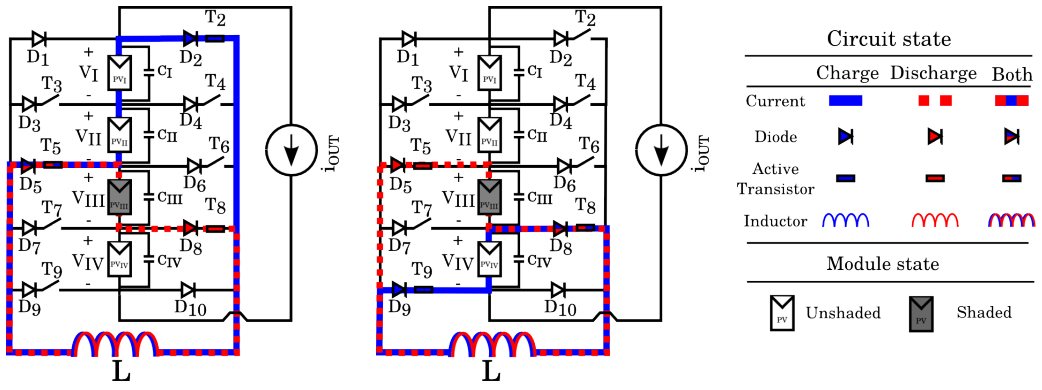

(a) $I.II \rightarrow III$ (b) $IV \rightarrow III$ (c) Legend

Figure 3.12: Circuit representation of a CSS

Universal BSS ($All \rightarrow X$)

There are strategies which use the whole PV module either during the charge or the discharge phase, called **Universal BSS**. Denoted as $All \rightarrow III$, $All \rightarrow II.III$ and $All \rightarrow I.II.III$, these strategies are investigated as a possible "Universal" substitute to the CSS. Table 3.4 shows three examples.

Table 3.4: A few examples of BSS

Cell groups charging	*Cell groups discharging*	*BSS*	Duty Cycle	*Figure*
All	III	$All \rightarrow III$	0.20	3.13(a)
All	II & III	$All \rightarrow II.III$	0.33	3.13(b)
All	I, II & III	$All \rightarrow I.II.III$	0.43	3.13(c)

Figure 3.13 shows their circuit representation.

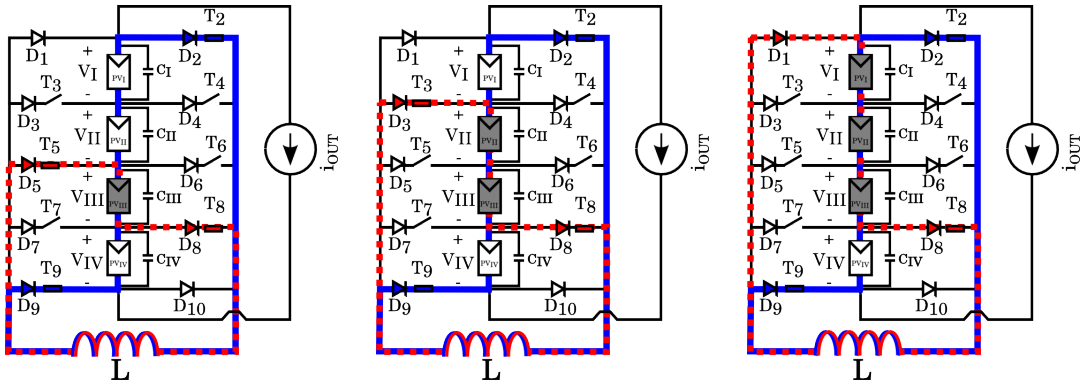

(a) *All → III* (b) *All → II.III* (c) *All → I.II.III*

Figure 3.13: Circuit representations showing the active switches and inductor current path for the Universal BSS

The equations defining the current in the inductor and the output current change in these cases. This is due to the fact that equation 3.6 is replaced by 3.35.

$$i_{OUT_{CH}} + i_{L_{CH}} = i_{IV_{CH}} + i_{CIV_{CH}} \tag{3.35}$$

Using this equation and the deduction procedures from section 3.2, leads to equations 3.36 and 3.37.

$$\overline{i_L} = \frac{SF \cdot i_{USH}}{(1-D)} \tag{3.36}$$

$$\overline{i_{OUT}} = \left(1 - SF \cdot \left(\frac{D}{1-D}\right)\right) \cdot i_{USH} \tag{3.37}$$

Equation 3.36 shows that the use of the Universal BSS implies a rise in the inductor current. It constitutes, thus, a trade-off: *higher losses against an easier response to shadows*. Its implications will be taken into account during the study of the PV Equalizer performance.

3.3.2 Bypass function

The second correction function is called bypass. As its name indicates, it allows the equalizer to short circuit any cell group, having a similar effect that of bypass diodes. It is useful for situations where the equalize function might not be effective, such as very high SF or actual defaults in the cells. Figure 3.14 shows its principle.

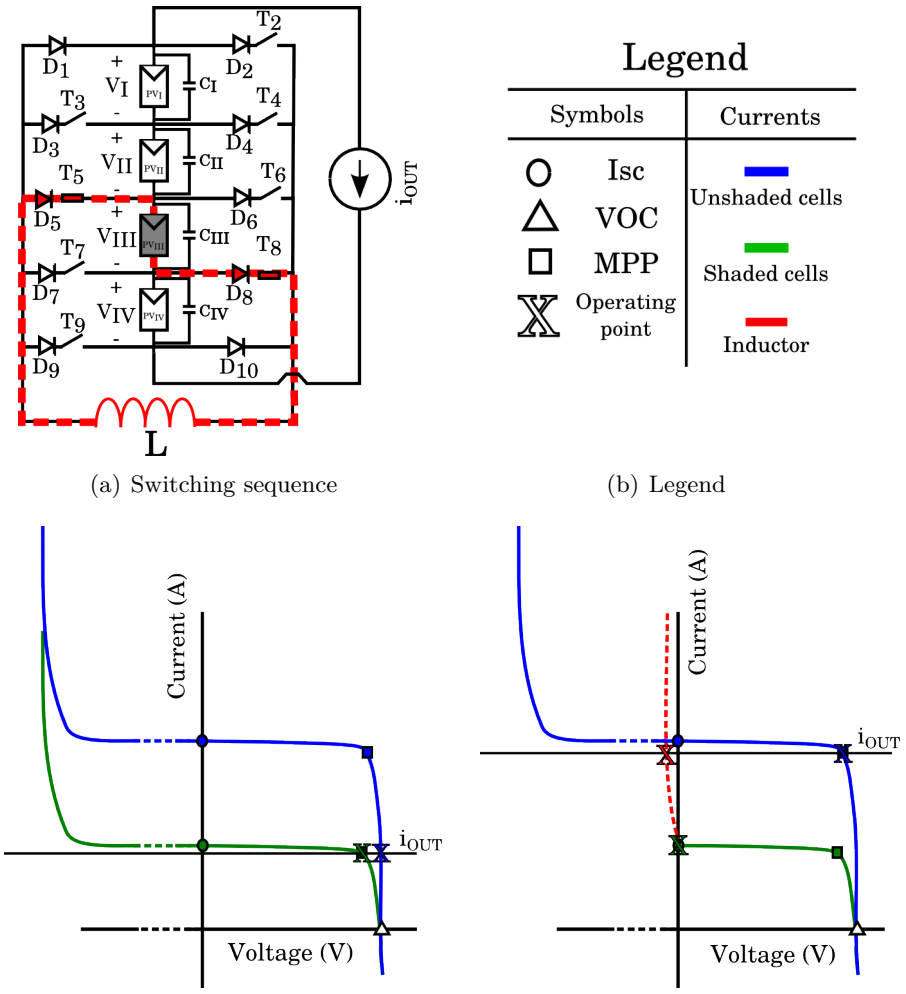

(a) Switching sequence

(b) Legend

(c) Operation point before activating the switches

(d) Operation point after activating the switches

Figure 3.14: Bypass principle

Consider that a shadow is cast over cell group PV_{III} in figure 3.14(a). Under normal conditions, the output current is limited by the shaded cell group as shown in figure 3.14(c). By activating the switches in figures 3.14(a), a new current path, shown in red, becomes available.

Under this bypass-equivalent condition, the MPPT is now free to seek another MPP *if its algorithm allows it.* As it does so, the operating point of the system changes to that in figure 3.14(d). This effect is similar to the one provided by bypass diodes, as shown in figure 2.36 on page 54.

The bypass function can also be applied to several cell groups, requiring only prior knowledge about the location of the shadow. If the different shaded cell groups have the same shading factor, the bypass principle is exactly the same as in figure 3.14. However, if these groups have two different SF or are non-contiguous, the result is slightly different. Figure 3.15 shows an example.

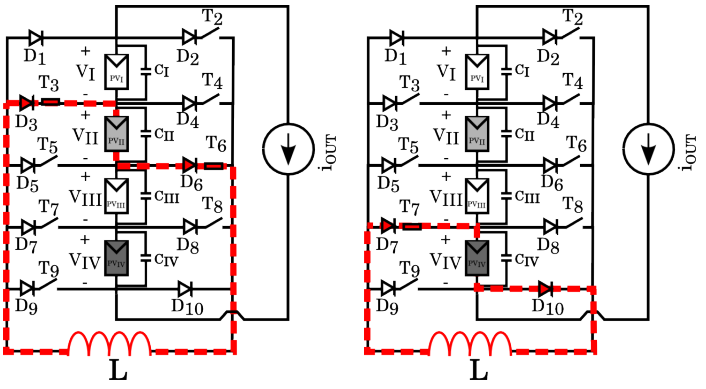

(a) Bypass PV_{IV} (b) Bypass PV_{II}

Figure 3.15: Bypass principle for non-contiguous shaded cell groups

The equations associated with this bypass technique are described in table 3.5.

Table 3.5: Transistor equations

Bypass PV_{IV}		*Bypass* PV_{II}	
$i_{OUT} - i_L = i_{IV} + i_{CIV}$	(3.38)	$i_{OUT} - i_L = i_{II} + i_{CII}$	(3.39)
$i_{OUT} = i_{II} + i_{CII}$	(3.40)	$i_{OUT} = i_{IV} + i_{CIV}$	(3.41)

The time during which the inductor is connected to group PV_{II} is represented by T_{II} and its equivalent for PV_{IV} by T_{IV}. The total bypass period is their sum, given by T. Using these when combining equations 3.38 with 3.41 and 3.40 with 3.39 allows the description of the system currents in steady state as follows.

$$\overline{i_{OUT}} = \overline{i_{IV}} + T_{IV} \cdot \overline{i_L} \tag{3.42}$$

$$\overline{i_{OUT}} = \overline{i_{II}} + T_{II} \cdot \overline{i_L} \tag{3.43}$$

If the system is considered in its MPP, its output current will be equal to that of an unshaded cell group. With the inductor current being the same for both expressions, they can be used to yield two expressions.

$$\overline{i_L} = i_{USH} \cdot (SF_{IV} + SF_{II}) \tag{3.44}$$

$$\frac{T_{II}}{T_{IV}} = \frac{SF_{IV}}{SF_{II}} \tag{3.45}$$

Equations 3.44 and 3.45 show the consequence and condition for bypassing non-contiguous cell groups. Its consequence is a steep rise in the inductor current, which becomes the sum of the current needed by both cell groups. The condition for it to work is respecting the equality in equation 3.45, where highly shaded cell groups require proportionally more bypass time.

As a result, the current flowing through the inductor may be several fold that of the unshaded cell groups, raising questions about bypassing non-contiguous cell groups at all. In the prototype devised for this work, the number of cell groups is limited to four, which reduces the possible number of non-contiguous shadow occurrences. However, this should be taken in consideration for bigger applications.

Thus, in this work, the bypass function will be restricted to contiguous shadow states. Their maximum current flowing through the inductor would occur only when the shading factor is one or that of an unshaded cell group.

3.3.3 Search function

The diagnosis functions are used to detect the presence and movement of the shadow. One of these is a direct sampling of the energy available in each cell group through the use of the search function. Its principle is to use the highly flexible transistor network of the equalizer to access each cell group individually and briefly connect it to the inductor. This will trigger a current peak, which will be used to determine the presence of the shadow.

The example shown in figure 3.16 illustrates its general idea. In it, a shadow of 0.8 SF is located at the cell group PV_I. The search function is triggered to sweep the entire PV module.

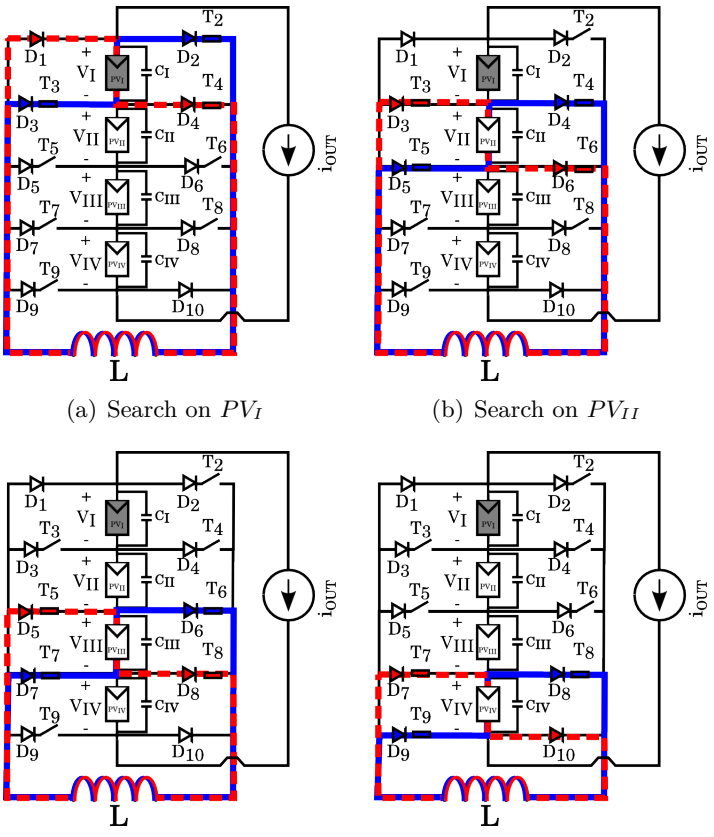

(a) Search on PV_I (b) Search on PV_{II}

(c) Search on PV_{III} (d) Search on PV_{IV}

Figure 3.16: General idea of the search function

The search samples the energy by connecting to a single cell group to promptly return it afterwards. The expected result of the search is a different reaction in the first current peak, signaling the presence of a shadow over its corresponding cell group, shown in figure 3.17.

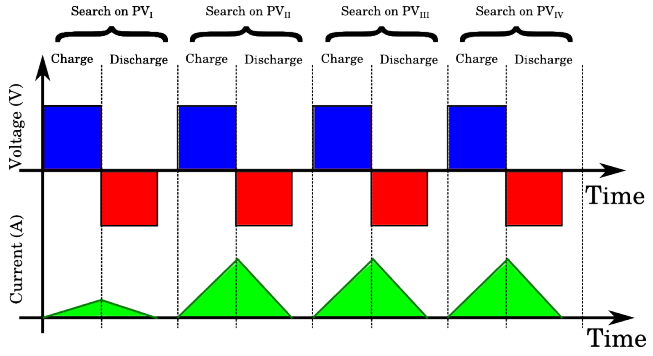

Figure 3.17: Expected search result

The search function represents an interruption in the current output. If its charge period is long enough, all the current available in the cell group being searched flows through the inductor. When the shading factor of this cell group is zero, the inductor current will reach its maximum.

Other aspects of the search function, as well as other techniques for diagnosing the shadow will be presented and studied in chapter 5.

3.3.4 Summary of the functions

The PV Equalizer can perform three functions: equalize, bypass and search. The first erases the presence of the shadow, the second short-circuits a given cell group and the third extracts peaks to deduce the shadow state. Their analysis has shown that each one imposes specific voltage and current conditions to the components of the PV Equalizer. Table 3.6 summarizes them according to each function

Table 3.6: Conditions imposed by each function

Function	*Restrictions*
Equalize	The maximum inductor current varies from 1 to X times i_{USH}. The maximum forward and reverse voltages seen by the switching leg are V_{PV}.
Bypass	If only one cell group is bypassed, the maximum inductor current is i_{USH}. If n groups are shaded, it will be $n \cdot i_{USH}$.
Search	The maximum steady-state inductor current will be i_{USH} for long searches over cell groups with a SF of 1.

These conditions provide the basis for sizing a prototype, study its performance and, utterly, determining its benefits to the PV system robustness.

3.4 Efficiency study

The previous sections have presented the PV Equalizer power electronics structure, operating principle and functions. Their gathered knowledge has provided enough elements to push the analysis further and take into account imperfections. As shown previously by the intermittency theory, these are the only obstacle in the way of a perfect robustness for parallel PRobES. Their assessment is proposed below through an efficiency study.

However, an efficiency study depends heavily on design choices and their consequences. These will be clarified first by an overview of the prototype used in this work. They will

be followed by the description and estimation of the losses. Finally, a description of the PV module power production as a function of the shadow will be presented.

The result will be an estimation of the benefits brought by the PV Equalizer to the robustness of its PV module.

3.4.1 Prototype Overview

The components chosen for the prototype used in this work are the basis to determine its losses, and, by consequence its efficiency. Its design answered to some rules that were set according to certain performance criteria.

The first performance criterion relates to the voltage and current ripple of the PV Equalizer. They are of the utmost importance, due to their direct impact over power production. If the PV Equalizer induces important current or voltage ripples on any of the I-V curves, the MPPT system is incapable of tracking the MPP. Specially when it comes to the variable used by the MPPT to control the PV module. If it is voltage-based, a special attention should be given to attenuating the voltage ripple. The same is true for current-based MPPT.

They are estimated through I-V curves, as shown in figure 3.18 were used as a reference.

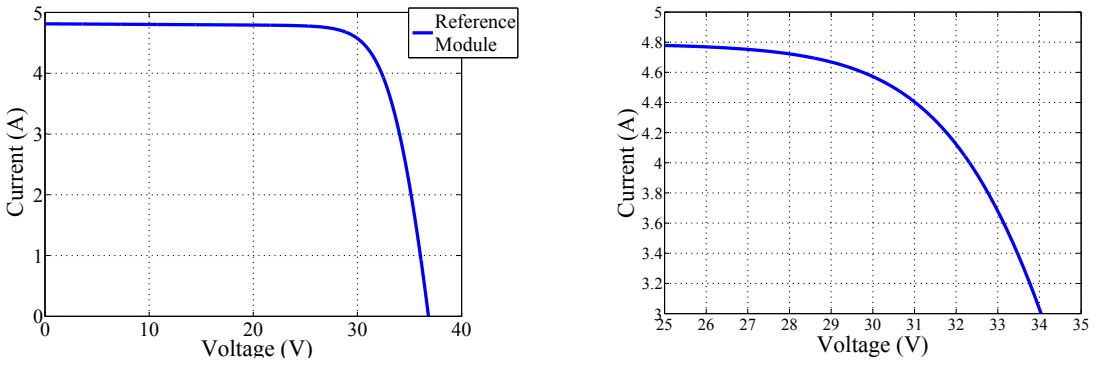

(a) Total I-V curve

(b) Zoom in on the MPP

Figure 3.18: The I-V curve of the reference PV module

Using the knees of the I-V curves as a reference, it is possible to see that small voltage variations lead to large current disturbances.

The second performance criterion was related to choosing which shading factors and functions should be used by the PV Equalizer. Considering the high current needed by non-contiguous bypass, it was ruled out for the moment. Universal BSS will also not be used, even if they will be studied in later chapters. As for shading factors, the PV Equalizer will be designed to address their full scale, from 0 to 1.

The third performance criterion is transparency from the outside. The PV Equalizer should not interfere in the normal operation of the MPPT. Thus, the switching frequency of the former must be several fold higher than of the latter.

The design rules are summarized in table 3.7.

These rules guided the choice of the transistors, diodes and capacitors of the PV Equalizer, along with the construction of its inductor. All their technical details are available in appendix B and will not be presented here. Their main characteristics, however, are summed up in table 3.8.

Table 3.7: Equalizer design rules

Design variable	**Desired value**
Maximum inductor current	$5A$
Inductor current ripple (Δi_L)	$1A$
Capacitor voltage ripple (ΔV_C)	$50mV$
Transistor reverse and direct voltage	$60V$
Working frequency (f)	$100kHz$
Operation modes availability	All but non-contiguous bypass and Universal BSS
Shading factors	All

Table 3.8: The values adopted for the components in this work

Component	*Variable*	*Value*	*Unit*
Diode	Diode threshold voltage (V_{th})	$(1 + 0.1 \cdot i_L) \cdot 0.55$	V
	Diode recovery time (t_{rr})	25	ns
	Diode recovery current (i_{rrm})	$i_F + 2$	A
P-MOS Transistor	Transistor rise time (tP_r)	55	ns
	Transistor fall time (tP_f)	41	ns
	Transistor ON resistance (RP_{dsON})	100	$m\Omega$
N-MOS Transistor	Transistor rise time (tN_r)	27	ns
	Transistor fall time (tN_f)	25	ns
	Transistor ON resistance (RN_{dsON})	110	$m\Omega$
Inductor	Inductance (L)	100	μH
	Inductor resistance (R_L)	20	$m\Omega$
Capacitor	Capacitance (C)	220	μF
	Capacitor resistance (R_C)	–	–
PV module	PV module voltage (V_{PV})	30	V
	PV cell group voltage (V_{PVg})	7.5	V
	PV unshaded current (i_{USH})	4.2	A

An important note should be given about the choice of the transistors. The PV Equalizer uses both N-MOS and P-MOS transistors to guarantee the unidirectional behavior of the inductor current. Their in-built diodes must be in opposition with their corresponding diodes in the same switching leg. Thus, odd transistors are P-MOS while even transistors are N-MOS.

The next step is to provide the equations that calculate the losses of the system.

3.4.2 Prototype Losses

The losses of a power electronics structure are composed by the sum of its conduction and switching losses. Their equations depend on how the structure switches and its current path. Figure 3.19 shows these for the PV Equalizer.

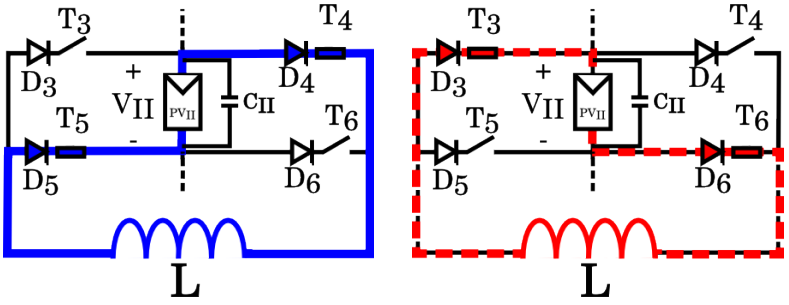

(a) Charge phase (b) Discharge phase

Figure 3.19: The charge and discharge switching and current path for the PV Equalizer

In the example shown above, two switching legs are systematically used during charge and discharge. They are activated together and must connected in series. In the worst case scenario, a total of four switch during a full period.

The estimation of the conduction and switching losses will be done separately in the sections below and added up in the end.

Using these assumptions, the losses can be estimated.

Conduction Losses

The conduction losses are estimated by adding up the contributions from the diodes, the switches and the inductor. They are detailed in equations 3.46, 3.47 and 3.48.

$$P_{COND_{diodes}} = 1.1 \cdot [(i_{L_{RMS_{CH}}} + i_{L_{RMS_{DCH}}}) + 0.1 \cdot (i^2_{L_{RMS_{CH}}} + i^2_{L_{RMS_{DCH}}})] \tag{3.46}$$

$$P_{COND_{switches}} = 2 \cdot R_{dsON} \cdot (i^2_{L_{RMS_{CH}}} + i^2_{L_{RMS_{DCH}}}) \tag{3.47}$$

$$P_{COND_L} = R_L \cdot (i^2_{L_{RMS_{CH}}} + i^2_{L_{RMS_{DCH}}}) \tag{3.48}$$

The inductor RMS current is calculated based on figure 3.20.

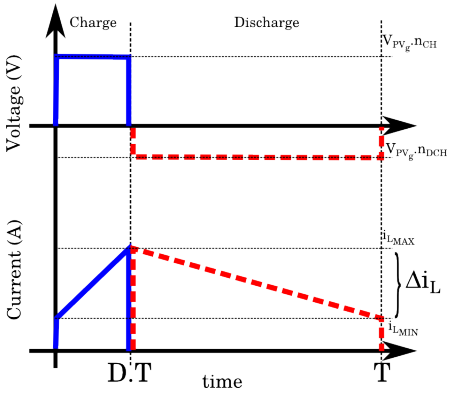

Figure 3.20: The graph used as a base to calculate the RMS current

The expression of the inductor maximum and minimum current, along with its current variation during charge and discharge are given by equation 3.49, 3.50 and 3.51, respectively.

$$i_{L_{MAX}} = \overline{i_L} + \frac{\Delta i_L}{2} \tag{3.49}$$

$$i_{L_{MIN}} = \overline{i_L} - \frac{\Delta i_L}{2} \tag{3.50}$$

$$\Delta i_L = \frac{n_{CH} \cdot V_{PVg} \cdot D \cdot T}{L} \tag{3.51}$$

Using these equations, it is possible to deduce the RMS currents of the PV Equalizer during charge and discharge. They are expressed by equations 3.52 and 3.53, respectively.

$$i_{L_{RMS_{CH}}} = \sqrt{D \cdot \left(\overline{i_L}^2 + \frac{\Delta i_L^2}{12} \right)} \tag{3.52}$$

$$i_{L_{RMS_{DCH}}} = \sqrt{(1-D) \cdot \left(\overline{i_L}^2 + \frac{\Delta i_L^2}{12} \right)} \tag{3.53}$$

The average inductor current is recalled in equation 3.54, its expression for the Universal BSS is recalled in equation 3.55.

$$\overline{i_L} = SF \cdot i_{USH} \tag{3.54}$$

$$\overline{i_{L_{Universal}}} = \frac{SF \cdot i_{USH}}{(1-D)} \tag{3.55}$$

The RMS current puts in evidence that *conduction losses depend largely on the shading factor and slightly on its shape.*

Besides the RMS current, the conduction conditions for each BSS are also needed to estimate the conduction losses. They regroup the number of cell groups participating in the charge (n_{CH}) and discharge (n_{DCH}) phases, the duty cycle (D) and the shadow state, varying with each switching strategy. They are detailed in table 3.9.

Table 3.9: The conduction conditions for different BSS

Switching Strategy	D	n_{CH}	n_{DCH}	*Shadow Shape*
$II.III.IV \rightarrow I$	0.25	3	1	[1 0 0 0]
$III.IV \rightarrow II$	0.33	2	1	[- 1 0 0]
$IV \rightarrow I$	0.50	1	1	[0 - - 1]
$II.III \rightarrow I.II$	0.50	2	2	[1 1 0 0]
$IV \rightarrow II.III$	0.66	1	2	[- 1 1 0]
$I \rightarrow II.III.IV$	0.75	1	3	[0 1 1 1]
$All \rightarrow III$	0.20	4	1	[0 0 1 0]
$All \rightarrow II.III$	0.33	4	2	[0 1 1 0]
$All \rightarrow I.II.III$	0.43	4	3	[1 1 1 0]

A few CSS will also be used in this study to assess their impact on switching losses. The first two CSS are related to some special shadow states, while the third is used to study losses for long CSS. Their conduction conditions are detailed table 3.10

Table 3.10: The conduction conditions for the CSS

Switching Strategy	D	n_{CH}	n_{DCH}	*Shadow Shape*
$II.III \rightarrow I$	0.33	2	1	[1 0 0 -]
$II.III \rightarrow IV$	0.33	2	1	[- 0 0 1]
$I \rightarrow II.III$	0.66	1	2	[0 1 1 -]
$IV \rightarrow II.III$	0.66	1	2	[- 1 1 0]
$I \rightarrow II$	0.50	1	1	[0 1 - -]
$I \rightarrow III$	0.50	1	1	[0 - 1 -]
$I \rightarrow IV$	0.50	1	1	[0 - - 1]

Finally, the same current will be considered flowing through the components during switch ON. The same is true during switch OFF.

The bypass mode is considered to have only conduction losses.

Switching Losses

The estimation of the switching losses for the PV Equalizer is complex, requiring a series of assumptions about how its components operate.

The first assumption concerns how the different time responses of the active components affect their switching losses. During switch ON, the faster transistor will close before the totality of the current is established, having less losses. However, since the faster transistor will also open first, it is the slower transistor that will finish its switching at zero current and reduce its losses during switch OFF. As for the diodes, only its switching OFF losses will be taken into account.

The second assumption concerns the distribution of voltage during switching. During switch ON, the voltage across the two transistors will be considered equal and half of the total. During switch OFF, the voltage will be considered as divided evenly across the two diodes and two transistors.

Finally, **the third assumption** is that charging and discharging losses are composed of the turning ON and OFF of a different number of transistors according to the switching strategy. Tables 3.11 shows how many N or P transistors are turned ON or OFF during each phase of the BSS. Their diodes are also listed by a Di and, when two are turned OFF, they are noted by 2Di.

Table 3.11: The switching conditions for different BSS

Switching	*Charge*		*Discharge*	
Strategy	*ON*	*OFF*	*ON*	*OFF*
$II.III.IV \rightarrow I$	P	Di	–	P
$III.IV \rightarrow II$	P	P+Di	P	P+Di
$IV \rightarrow I$	N+P	N+P+2Di	N+P	N+P+2Di
$II.III \rightarrow I.II$	P	Di	–	P
$IV \rightarrow II.III$	P	P+Di	P	P+Di
$I \rightarrow II.III.IV$	N	Di	–	N+Di
$All \rightarrow III$	N+P	N+P+2Di	N+P	N+P+2Di
$All \rightarrow II.III$	N+P	N+P+2Di	N+P	N+P+2Di
$All \rightarrow I.II.III$	N+P	N+2Di	N	N+P+2Di

The switches used during CSS are listed in table 3.12. The switching losses of all BSS composing a CSS are summed up to deduce the total switching losses.

Table 3.12: The switching conditions for the CSS

Switching	*Charge*		*Discharge*	
Strategy	*ON*	*OFF*	*ON*	*OFF*
$II.III \rightarrow I$	N	Di	–	P+Di
$II.III \rightarrow IV$	P	Di	–	N+Di
$I \rightarrow II.III$	N	N+Di	N	N+Di
$IV \rightarrow II.III$	P	P+Di	P	P+Di
$I \rightarrow II$	N+P	P+2Di	N	N+Di
$I \rightarrow III$	N	N+Di	N+P	N+P+2Di
$I \rightarrow IV$	N+P	N+P+2Di	P	N+P+2Di

Using these assumptions, the diode switching losses are estimated by equation 3.56. The total switching losses in the transistors are given by equation 3.57.

$$P_{SWITCH_{diode}} = t_{rr} \cdot [n_{DCH} \cdot (i_{L_{MIN}} + 2) + n_{CH} \cdot (i_{L_{MIN}} + 2)] \cdot V_{PVg} \cdot f \tag{3.56}$$

$$P_{SWITCH_{switches}} = SW_{CH_{ON}} + SW_{CH_{OFF}} + SW_{DCH_{ON}} + SW_{DCH_{OFF}} \tag{3.57}$$

The different contributions are given by equations 3.58 through 3.61. In them, the N and P denote the transistor used during the specific switching action their equation describe. There are a total of four, one ON and one OFF during CHARGE plus one ON and one OFF during DISCHARGE. For example, N or P transistors that are turned ON during the CHARGE phase will be used in equation 3.58.

The denominators (1+N) and (1+P) represent the reduction of losses when both transistors switch together. The (N+P+Di) denominator translates the division of voltage along all the components switching together. The diode only appears in the OFF switch. If two are used, Di is replaced by 2Di.

$$SW_{CH_{ON}} = \frac{f \cdot i_{L_{MIN}} \cdot V_{PVg}}{2 \cdot (N + P)} \cdot \left(\frac{N}{1 + P} \cdot n_{CH} \cdot t_{Nr} + P \cdot n_{CH} \cdot t_{Pr} \right) \tag{3.58}$$

$$SW_{CH_{OFF}} = \frac{f \cdot i_{L_{MIN}} \cdot V_{PVg}}{2 \cdot (N + P + Di)} \cdot \left(N \cdot n_{DCH} \cdot t_{Nr} + \frac{P}{1+N} \cdot n_{DCH} \cdot t_{Pr} \right) \tag{3.59}$$

$$SW_{DCH_{ON}} = \frac{f \cdot i_{L_{MAX}} \cdot V_{PVg}}{2 \cdot (N + P)} \cdot \left(\frac{N}{1+P} \cdot n_{DCH} \cdot t_{Nf} + P \cdot n_{DCH} \cdot t_{Pf} \right) \tag{3.60}$$

$$SW_{DCH_{OFF}} = \frac{f \cdot i_{L_{MAX}} \cdot V_{PVg}}{2 \cdot (N + P + Di)} \cdot \left(N \cdot n_{CH} \cdot t_{Nf} + \frac{P}{1+N} \cdot n_{CH} \cdot t_{Pf} \right) \tag{3.61}$$

The switching losses are influenced by both the shape of the shadow and its shading factor. However, they can be greatly reduced in certain switching strategies where certain switching legs are permanently ON.

Losses and Shadow

Both the conduction and switching losses were found to be influenced by the shading factor and the shadow shape. To verify them, the evolution of the losses with the shadow will be traced for all BSS and CSS listed in tables 3.11 and 3.12. Figure 3.21 shows the results.

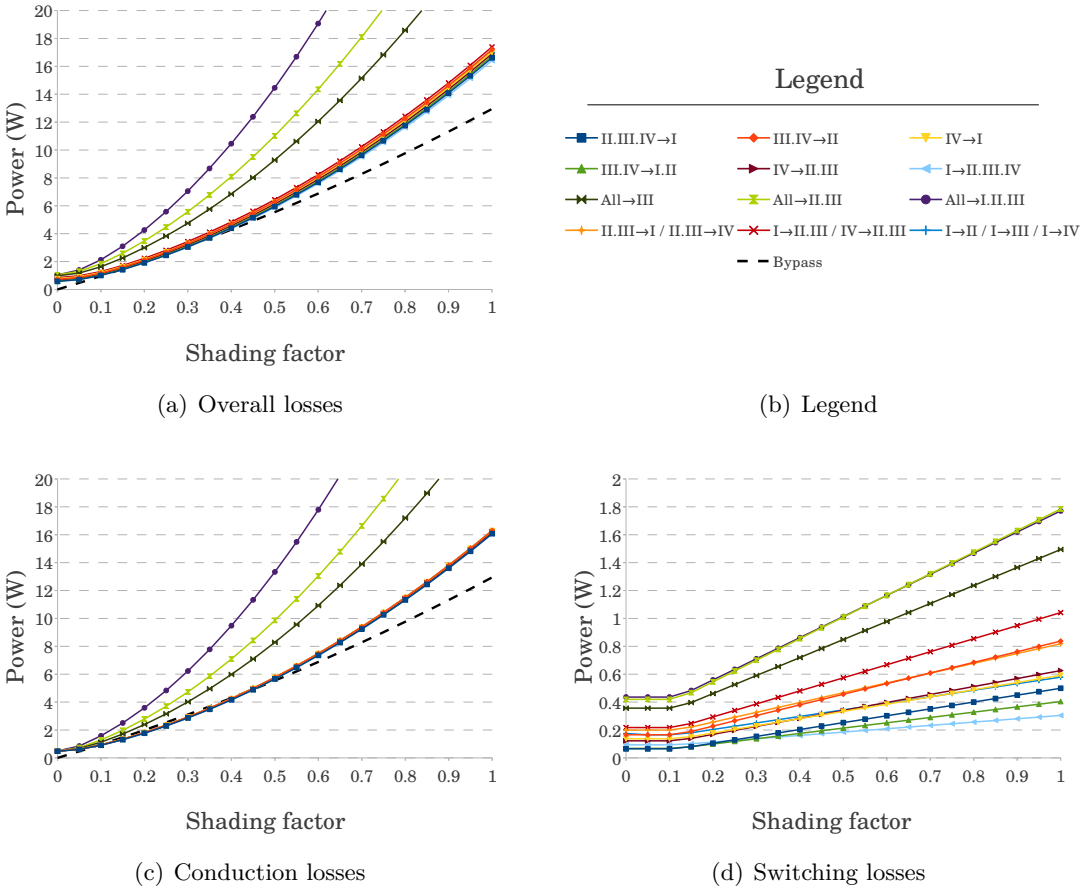

(a) Overall losses

(b) Legend

(c) Conduction losses

(d) Switching losses

Figure 3.21: Equalizer losses

Figure 3.21(a) shows that the BSS and CSS have, basically, the same losses. This is explained when comparing the conduction losses in figure 3.21(c) with the switching losses in figure 3.21(d). For SF between 0 and 0.4, the switching losses represent 30% to 10% of total losses, respectively. However, as the shading factor rises it drives the current flowing through the inductor up. Thus, for SF between 0.8 and 1, the switching losses represent less than 10% to less than 5%, depending on the switching strategy.

The Universal BSS have higher conduction losses since they force the inductor current higher than the other strategies. However, as will be shown below, they also transfer more power between unshaded and shaded cell groups. Thus, their use must still be studied further.

In the case of the PV module used in this work, each cell group produces around 40 W under 1000 $\frac{W}{m^2}$. Thus, if these are shaded beyond an SF of 0.75 or 0.80, then the equalizing is not energy efficient. As a conclusion, most of the effort during the conception of the Equalizer must be concentrated into lowering its conduction losses. This is important because **if the PV Equalizer is more efficient, it can compensate higher SF.** As a consequence, it will have a higher robustness enhancement.

3.4.3 Effects of the shadow in power production

With the description of the losses as a function of the shading factor for different shapes, the overall efficiency of the PV Equalizer can now be estimated. To do so, a series of curves will compare the evolution of power production with the shadow for equalizing, bypassing and doing nothing. Their comparison shows how much power is gained by using the PV Equalizer providing clues to how it improves the robustness of the PV module.

The results are shown in figure 3.22, according to the number of cell groups receiving energy from the Equalizer.

Figure 3.22 shows that the switching strategies which use all the cell groups at least once while minimizing the number of transistors switching have a higher power production. It also shows that different switching strategies have different SF beyond which equalizing is no longer energy efficient. It can be as high as 0.9 for $I \rightarrow II.III.IV$ or as low as 0.45 for $IV \rightarrow I$.

When compared to bypassing or doing nothing, the PV Equalizer is most effective for shadows covering half of the PV module. It can theoretically raise power output by 30 W for the $III.IV \rightarrow I.II$ at a SF of 0.55. As the shadow becomes wider, the Equalizer becomes more efficient for higher SF values, but its contribution is much smaller.

To confirm some of these results, an experimental validation of two BSS will be conducted.

Practical validation

To validate these curves, a few measurements were made using the prototype developed in this work. Due to the challenge of making photovoltaic measurements in stable conditions, the number of switching strategies was reduced.

The weather conditions and shading factor of the measurement are detailed in table 3.13. The ambient temperature is represented by TA, while the module temperature is represented by TM. The shading factor of the measurements were provided by using plastic sheets whose characteristics are detailed in Appendix B.

Their results are shown in figure 3.23, where the lines are linear expansion fitted to the measured points.

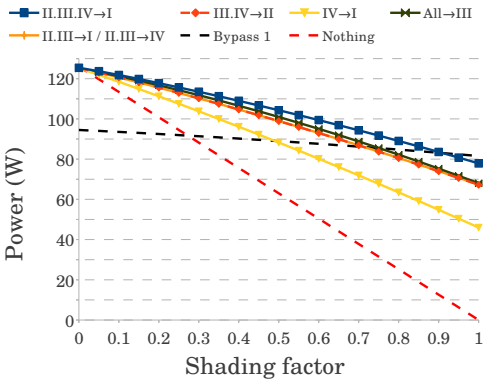

(a) One cell group shaded

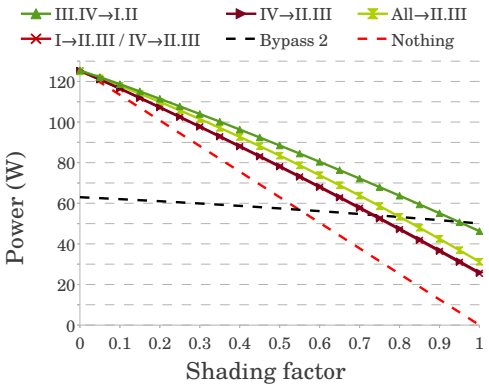

(b) Two cell groups shaded

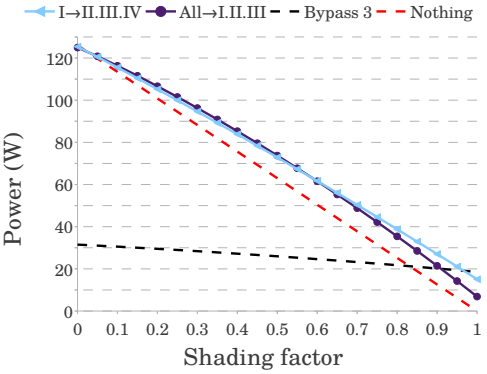

(c) Three cell groups shaded

Figure 3.22: Overall power production of the Equalizer according to its operation

Table 3.13: The measurement conditions

Switching Strategy	*Irr* ($\frac{W}{m^2}$)	T_A (℃)	T_M (℃)	SF (plastic layers) PV_I	PV_{II}	PV_{III}	PV_{IV}
$II.III.IV \rightarrow I$	798	34.2	51.4	0.21	0	0	0
	773	33.9	51.4	0.36	0	0	0
	755	33.9	51.2	0.47	0	0	0
	735	33.4	51.3	0.56	0	0	0
$III.IV \rightarrow I.II$	851	29.2	47.2	0.21	0.21	0	0
	852	29.3	47.2	0.36	0.36	0	0
	833	30.6	49.3	0.47	0.47	0	0
	834	30.8	49.1	0.56	0.56	0	0

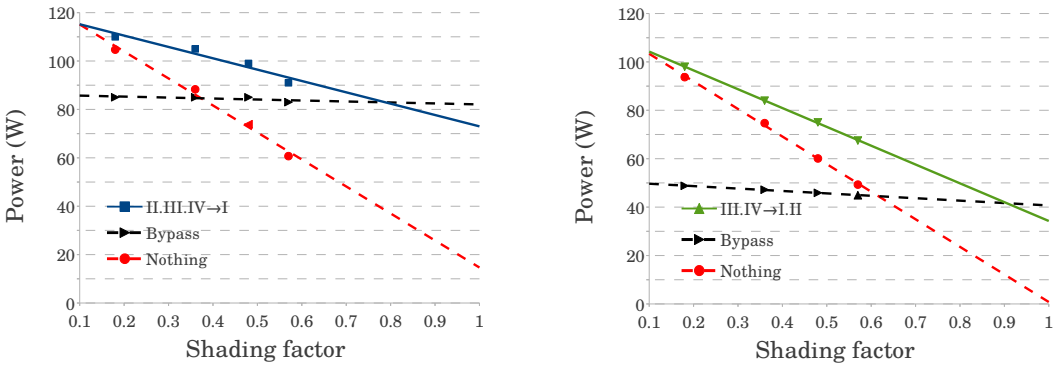

(a) $II.III.IV \rightarrow I$ (b) $III.IV \rightarrow I.II$

Figure 3.23: Validation of the influence from the shadow in power production

The measurements in 3.23(a) had a greater irradiance fluctuation, explaining the spreading of its points. The weather conditions varied less during the measurements for the BSS $III.IV \rightarrow I.II$, leading to a more accurate curve. Both results confirm the tendency of the PV Equalizer to best perform at wider shadows. The linear estimation of the results show that the SF after which the PV Equalizer is no longer efficient is located expands for wider shadows and is located at roughly 0.7 for the first BSS and 0.9 to the second.

While these results are not exhaustive they give an important first impression, confirming the potential of the PV Equalizer concept in raising the robustness of PV modules.

3.4.4 Summary of the Efficiency study

This efficiency study has estimated of the losses in the PV Equalizer and their effect in its robustness enhancement. Based on the constraints imposed by the use of its functions and the imperfections of its components, a series of equations were proposed. While the values of the components are specific for the prototype sized in this work, the method used to estimate the losses can be expanded for other applications.

The results have pointed out the potential of the PV Equalizer in mitigating the presence of the shadow. Several shadow shapes and switching strategies were used to corroborate this idea, with two of them being validated through experiments.

3.5 Conclusion

This chapter has introduced a new concept in parallel PRobES called **PV Equalizer** . Its topology, based on a battery equalizer, was presented and analyzed. Based on its switching principles, its use was generalized into four functions: equalize, bypass, search and idle. The first two mitigate the presence of the shadow, the third detects its presence and the fourth represents a stand-by between the other three.

By analyzing the topology of the PV Equalizer a few characteristics can be outlined:

- *Smaller cell groups can support larger ones.* The main advantage of doing so is to keep the output voltage from falling below a certain critical level. Since most MPPTs have a voltage threshold below which they are unable to operate this can effectively help keeping the PV system running even if on a degraded state.

- *Non-contiguous shadows can be addressed across PV plants of any size.* Any shadow can be compensated, given the right CSS. To do so, it is crucial to know where the shadow is located.
- *Most shading factors can be compensated.* Even if the entire PV plant is shaded, the equalizer can detect which parts are less shaded than others and use them to raise overall output. Depending on its shading factor, however, certain shadows are better left uncompensated. These should be bypassed instead.
- *Any shadow can be bypassed.* Contiguous shadows can be bypassed together as long as they have the same shading factor. If they do not, then a special bypass mode can be activated, granting bypass to any shadow shape. However, it comes with an important cost: a much higher current flowing through the inductor, incurring into higher losses.
- *Shadow detection depends on power production.* The search function can access any cell group and sample its energy state through a current peak. These peaks have a very specific pattern, which will be studied in detail in chapter 5 to determine the location of the shadow.
- *The sizing of passive components in the system* has a direct impact on the use of operation modes and switching strategies.

Each function imposes different current and voltage constraints over the PV Equalizer components. They were used, along with a description of the prototype components used in this work, to estimate the losses of the PV Equalizer. These losses provided the basis for describing the power benefits of the PV Equalizer in comparison with bypassing and doing nothing. Some of the results were validated through measurements, confirming an important potential of the PV Equalizer to raise the robustness of its PV module.

It is important to note, though, that all these results were acquired through the use of the PV Equalizer in controlled shadow conditions. The voltages across the cell groups were considered as fixed and the equations were deduced to work in steady state. Thus, the results from this chapter can be considered as the theoretical maximum the PV Equalizer can provide if it mitigates the shadow perfectly.

Now the challenge of this work can be split into three blocks.

First, both the equalize and bypass functions should be characterized with different shadows. An specific attention should be given to the choice of the switching strategies and duty cycles that can maximize the power production of the PV module. This should provide more insight over how the PV Equalizer finds the optimal operating conditions for maximizing the power production of the PV module. Their effects over the operating conditions of the PV Equalizer should be tested further.

Second, the diagnosis of the shadow should be studied in more detail. The search function introduced in this chapter gives a starting point as to how to find the shadow. However, it costs energy by cutting production, even if for short periods of time. Its energy cost should be compared to the quality of the information it provides, and other potential diagnosis methods should also be provided.

Finally, the potential of the PV Equalizer can only be totally fulfilled if its is capable of allying all its functions under a sturdy and reliable control algorithm. Designing, testing and validating such algorithm is an important feature to assess the true robustness enhancement. For the prototype used in this work to be largely improved, its control system

should be mature enough to provide a framework of control for any future PV Equalizer application.

Chapter 4

Mitigating Shadows: The Equalize and Bypass Functions

The previous chapter presented the PV Equalizer and described its main characteristics. Starting by its switching rules, its working principles were described as a set of function which can be used for different purposes. Two functions are responsible for mitigating the presence of the shadow, namely equalize and bypass. The first uses switching strategies to equalizer the current differences between unshaded and shaded cell groups within a PV module, effectively erasing the presence of the shadow. The second can short-circuit any cell group, contiguous or not. It was also pointed out that knowing the location and intensity of the shadow was essential for the Equalizer, since different shadow states require different switching strategies.

This chapter has the objective of characterizing the impact of the shadow over the operating conditions of the equalize and bypass functions. Both functions require the use of switching strategies and duty cycles, thus these will be the focus of this chapter. Their study will be guided by two questions:

- *What is the relation between the shadow and switching strategies?*

  This question focuses on how similar switching strategies have different effects on different shadows. It is essential to understand how the switching strategy can raise power production and what are the criteria for choosing the optimal switching strategy for a given shadow.

- *The equalizer can operate at a fixed duty cycle. Can any duty cycle guarantee a maximum power output?*

  The previous chapter has also shown that the PV Equalizer can operate at a fixed duty cycle. However, it is important to understand if it is also optimal. If not, clues must be given as to how it can be optimized.

Each of these questions will be addressed in a different section. Their answers will provide the basis for automatically answering to a shadow once it is found. This is an important feature for controlling the PV Equalizer and guaranteeing its maximal performance.

In an important note, the shadow is considered static in this chapter. This means that while a myriad of cases will be used throughout the next two sections, they will be static over time. Dynamic phenomena such as movement or changes in the shading factor will be studied into detail in the next chapter.

Contents of this chapter

4.1 Choosing an appropriate switching strategy

Both equalize and bypass functions handle the shadow through the use of *switching strategies*. Introduced in chapter 3, these are responsible for determining which cell group gives and which receives energy in the case of the equalize function. For the bypass, they determine which group will be short-circuited.

The switching strategies are the focus of this section, whose contribution will be driven by the following question:

- *What is the relation between the shadow and switching strategies?*

Considering the knowledge dispensed about the shadow in the previous sections, this question can be further detailed into the following subsidiary questions.

1. *Is there a "generic" switching strategy that can be used to compensate all the shadows?*
2. *If not, does each shadow have its own specific switching strategy to maximize the power output?*
3. *Can shadows with different shading factors but similar shapes be treated with the same switching strategy?*
4. *Is the shading factor important for choosing a switching strategy?*
5. *Is there a simple and efficient algorithm for choosing a switching strategy?*

Answering these questions requires studying a large number of shadow scenarios, all equalized using many different switching strategies. Since the possibilities are infinite, this approach cannot pretend to be exhaustive but rather *quasi-exhaustive*. The rationale is that if it covers many possibilities, its conclusions will be used as solid clues for understanding the influence of the shadow over the switching strategies.

This section will, thus, start by recalling the characteristics of the switching strategy. This will be followed by a description of the shadow scenarios, which are regrouped into blocks to compose the *quasi-exhaustive* setup. An analysis of simulation results will follow suit, split into an overview and a block-by-block part. A reduced number of measurements will be used to validate its conclusions. Finally, the questions above are answered by an algorithm designed to aid the PV Equalizer to choose the optimal switching strategy based on the shadow shape.

4.1.1 Quasi-exhaustive study setup

The most important issue of a quasi-exhaustive study is to determine how many scenarios are needed to reach plausible conclusions. In the case of switching strategies this issue is twofold, as the shadow scenarios and switching strategies must be chosen together. Limiting both of them is paramount, otherwise thousands of simulations would be necessary to reach any conclusion at all. The principles and conditions used to achieve these simplifications are proposed in this study setup.

Switching Strategies reminder: definitions and conventions

The switching strategies are divided in two: basic and complex.

The Basic switching strategies (BSS) have only one charge and discharge period. Two examples of BSS are given in figure 4.1(a) and 4.1(b).

Complex switching strategies (CSS) are those where two or more BSS are needed. The greater number of switches participating in the CSS tend to rise switching losses. As an example, the two BSS in figure 4.1 can be combined into a CSS.

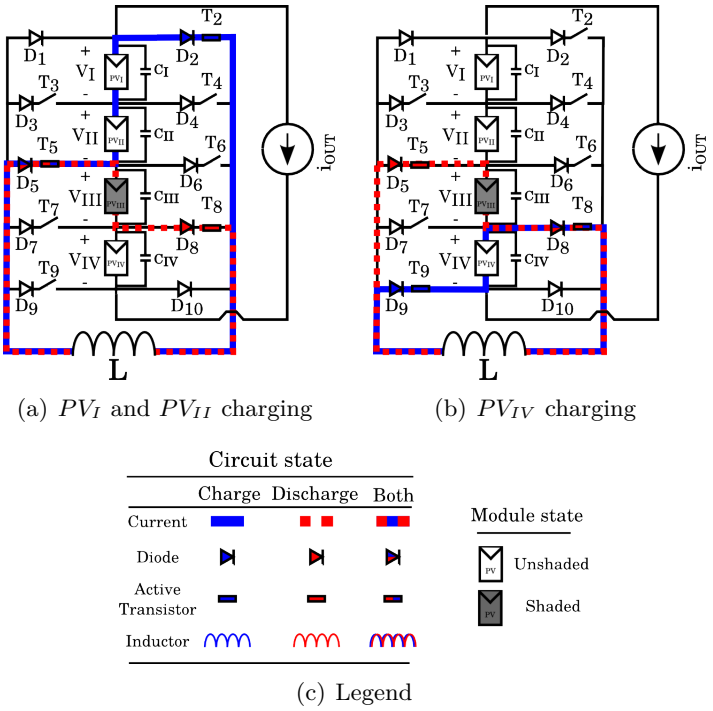

(a) PV_I and PV_{II} charging (b) PV_{IV} charging

(c) Legend

Figure 4.1: Two BSS, which can be combined into a CSS

During this section, a large number switching strategies will be handled. To avoid confusion their convention is recalled in figure 4.2.

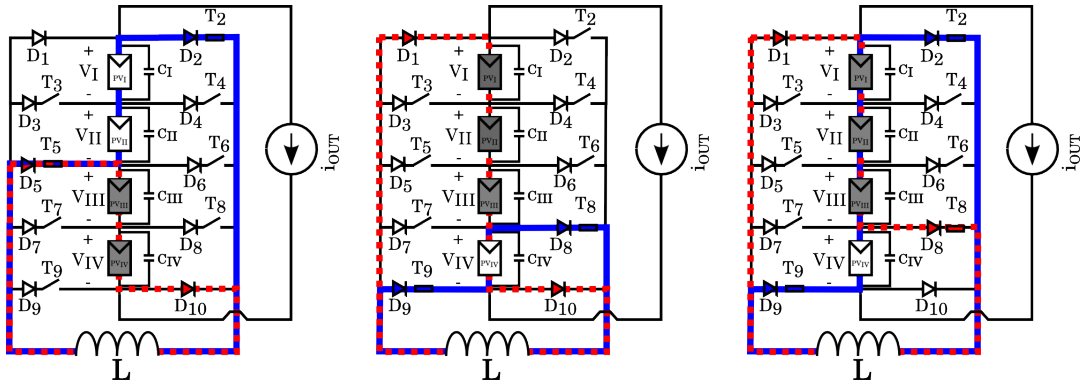

(a) $I.II \rightarrow III.IV$ (b) $IV \rightarrow All$ (c) $All \rightarrow I.II.III$

Figure 4.2: Three examples of the proposed convention

Figure 4.2(a) represents a BSS, which charges with groups PV_I and PV_{II}, while discharging over groups PV_{III} and PV_{IV}. The equalizing process is represented by an arrow,

going from the charging to the discharging cell groups. The groups are represented by roman numerals, from I to IV. When they are used together during charge or discharge their numbers are separated by a point, as in *I.II* or *III.IV*. Figure 4.2(b) represents another BSS, but with other characteristics. In it, the discharge over the entire group of cells is not represented by *I.II.III.IV* but rather by *All*. It is used for a more compact notation. Figure 4.2(c) shows another example of the use of *All*, where the three cell groups discharging are represented by *I.II.III*.

In this section, BSS or CSS will be presented as in table 4.1 to save space. It shows the result of applying this convention to figure 4.1.

Table 4.1: Example of coded table based on the example of figure 4.1

Figure	*Switching Strategies*		
	1^{st}	2^{nd}	3^{rd}
4.1(a)	$I.II \rightarrow III$	–	–
4.1(b)	$IV \rightarrow III$	–	–
4.1	$I.II \rightarrow III$	$IV \rightarrow III$	–

The CSS of figure 4.1 is represented by its two BSS, namely 1^{st} and 2^{nd}. In table 4.1, a third BSS, represented by 3^{rd}, is not used and expressed by the − symbol. This allows representing BSS and CSS in the same table and will be used later in this section.

The duty cycle of the switching strategies will be considered fixed. They will be calculated using equation 3.12 introduced in chapter 2 and recalled below. In the case of the CCS the duty cycle will also be independent. Thus, a single CSS may have up to 3 different duty cycles.

$$D(i) = \frac{n(i)_{SH}}{n(i)_{SH} + n(i)_{USH}} \tag{3.12}$$

Where n_{SH} represents the number of shaded cells and n_{USH} represents the number of unshaded ones. The (i) represent the number of the BSS to which the duty cycle is attributed.

Shadow scenarios

The shadow is a random phenomenon with random properties. It is completely dependent on the environmental conditions and objects surrounding the PV module. In this work, the presence of a shadow over a PV module constitutes a shadow case, composed of a shadow shape and shading factors for each PV cell group.

It is clearly difficult to choose which shadow cases are "representative" of the majority of occurrences. Furthermore, for each shadow scenario, a virtually infinite number of switching strategies can be applied. Thus, a special care should be taken while devising the simplifying hypothesis used to limit their number.

The first hypothesis is that not all shading factors need to be simulated, since their effect on current is considered as linear. Previous work Wang et al. [2012] support this hypothesis, which is confirmed through the characteristics of the PV module used in this work, as shown in appendix B. Thus, only four SF were chosen to study the shadow: 0.0, 0.2, 0.5 and 0.8.

The second hypothesis is that since the shadows are considered binary in occurrence. Thus, there can only be 16 possible shapes: [0 0 0 0] to [1 1 1 1].

Table 4.2: The shading factors of the shadow scenarios

Block	*Case*	*Shading factor* PV_I	PV_{II}	PV_{III}	PV_{IV}	*Description*	*Objective*
1	1	0	0	0	0.8	One cell group is shaded. Only one SF.	Determine the effectiveness of BSS or CSS against local and small shadows.
	2	0	0	0	0.5		
	3	0	0	0	0.2		
	4	0	0	0.8	0		
	5	0	0	0.2	0		
2	6	0.8	0	0.8	0.8	Two or three cell groups are shaded. Only one SF.	Study how the effectiveness of the BSS and CSS change with the shadow shape.
	7	0	0.8	0.8	0		
	8	0	0.8	0.8	0.8		
	9	0.8	0	0	0.8		
3	10	0	0	0.8	0.2	Two or three cell groups are shaded. Different SFs.	Study the effectiveness of BSS and CSS against the shadow shape and SF at the same time.
	11	0	0.2	0.5	0.8		
	12	0	0	0.2	0.5		
	13	0	0.5	0.5	0.8		
	14	0	0.2	0	0.8		
	15	0	0.2	0.5	0		
4	16	0.2	0.5	0.8	0.8	All four cell groups are shaded. Different SFs.	Study if mildly shaded cell groups can be used to equalize heavily shaded ones.
	17	0.2	0.2	0.5	0.5		
	18	0.2	0.5	0.2	0.5		
	19	0.2	0.5	0.8	0.5		
	20	0.2	0.2	0.5	0.8		

Finally, **the third hypothesis** states that certain shadow shapes are considered equivalent. Shadow cases such as [1 0 0 0] or [0 0 0 1], will, then, use similar switching strategies.

After using these hypothesis, 20 shadow cases have been chosen, as shown in table 4.2. To facilitate their study, they are regrouped into four blocks, according to their similarities and purposes.

The switching strategies will be chosen according to each shadow scenarios and their number will be limited.

Switching strategies scenarios

Choosing the switching strategies is also challenging, as each shadow scenario can be treated in many different ways. To limit their number, another set of hypothesis is proposed.

The first hypothesis is that the CSS will be composed by no more than 3 BSS. **The second hypothesis** is that the BSS will try to involve as many cell groups as possible during the equalizing. **The third and final hypothesis** is that Universal strategies must also be used during the study.

Even with these simplifications, a total of 178 cases have been chosen. Their complete list with all their results is available at the Appendix C. For the purpose of studying the effect of the shadows over the switching strategies, only the best results will be used in this chapter, as listed in table 4.3. Their results will be studied in detail in a block-by-block analysis.

It is important to note that the ranking of the best switching strategies might be done

Table 4.3: The best rating switching strategies used in the block-by-block analysis

Case	*Switching Strategies* 1^{st}	2^{nd}	3^{rd}	*Case*	*Switching Strategies* 1^{st}	2^{nd}	3^{rd}
1	$I.II.III \rightarrow IV$	–	–	*11*	$I.II.III \rightarrow III.IV$	–	–
	$All \rightarrow IV$	–	–		$I.II \rightarrow IV$	–	–
2	$I.II.III \rightarrow IV$	–	–	*12*	$I.II \rightarrow IV$	–	–
	$All \rightarrow IV$	–	–		$I.II.III \rightarrow III.IV$	–	–
3	$I.II.III \rightarrow IV$	–	–	*13*	$I \rightarrow IV$	–	–
	$All \rightarrow IV$	–	–		$I.II.III \rightarrow II.III.IV$	–	–
4	$All \rightarrow III$	–	–	*14*	$All \rightarrow IV$	–	–
	$I.II \rightarrow III$	–	–		$I.II.III \rightarrow IV$	–	–
5	$All \rightarrow III$	–	–	*15*	$I \rightarrow III$	$IV \rightarrow III$	–
	$I.II \rightarrow III$	$IV \rightarrow III$	–		$All \rightarrow III$	–	–
6	$II \rightarrow All$	–	–	*16*	$I.II \rightarrow II.III.IV$	–	–
	$II \rightarrow I$	$II \rightarrow III.IV$	–		$I \rightarrow III.IV$	–	–
7	$I \rightarrow II.III$	$IV \rightarrow II.III$	–	*17*	$I.II \rightarrow III.IV$	–	–
	$All \rightarrow II.III$	–	–		$All \rightarrow III.IV$	–	–
8	$I \rightarrow All$	–	–	*18*	$I \rightarrow II$	$III \rightarrow IV$	–
	$All \rightarrow II.III.IV$	–	–		$I \rightarrow II$	$I \rightarrow IV$	–
9	$II.III \rightarrow I$	$II.III \rightarrow IV$	–	*19*	$I \rightarrow III$	–	–
	$II.III \rightarrow All$	–	–		$All \rightarrow III$	–	–
10	$I.II \rightarrow III$	–	–	*20*	$I.II.III \rightarrow III.IV$	–	–
	$I.II.III \rightarrow III$	–	–		$I.II \rightarrow IV$	–	–

under non-optimal duty cycle conditions. The next section will address the effects of the duty cycle and an overall analysis will be proposed in the end of this chapter.

4.1.2 Simulation results

Due to the important amount of data, this quasi-exhaustive study requires a steady and structured analysis to mine all important information from the simulations. An indicator of the switching strategy efficiency, proposed by equation 4.1, is used to rank them from most to least efficient.

$$\eta = \frac{P_{Produced}}{\sum_{i=1}^{n}(SF_i \cdot P_{i_{unshaded}})} \tag{4.1}$$

In this expression, the denominator is the sum of the power available in each cell group of the PV module. The power of each cell group is considered as the product of its own shading factor with a reference power. This reference power, considered as unshaded, is the power of the cell groups at 1000 $\frac{W}{m^2}$. Thus, an η of 1 means that the switching strategy delivers all the power that the PV module can produce.

The model used during the simulations is described in detail in appendix A. The numerator is the output power calculated by using the simulation results once it reaches steady-state conditions. These simulation take losses into consideration through the imperfections of the components used in the model.

The results will be studied in five parts: a general and four per-block analyses. The conclusions will be summed up at the final part of this section and validated in the next through measurements.

General Analysis

A general analysis is proposed first. In it, the switching strategies are regrouped into five categories according to their complexity. The categories related to the BSS are shown in table 4.4, where n_{tot} represents the total number of cell groups within the PV module.

Table 4.4: The categories of the BSS

Category	*Criteria*	*Switching Strategies* 1^{st}	2^{nd}	3^{rd}
Complete	$n_{CH} + n_{DCH} = n_{tot}$	$II.III.IV \rightarrow I$	–	–
		$I.II \rightarrow III.IV$	–	–
Incompl.	$n_{CH} + n_{DCH} \neq n_{tot}$	$II.III \rightarrow I$	–	–
		$II.III.IV \rightarrow I.II$	–	–
Universal	n_{CH} or $n_{DCH} = n_{tot}$	$All \rightarrow II$	–	–
		$I \rightarrow All$	–	–

The BSS are divided into Simple, Incomplete and Universal. The Simple BSS are those that involve all of the cell groups ($I.II.III \rightarrow IV$). The Incomplete BSS are those in which either not all groups participate($I \rightarrow II$) or some groups participate more than once ($I.II.III \rightarrow III.IV$). The Universal BSS are those in which all cell groups either charge ($All \rightarrow I$) or discharge ($IV \rightarrow All$) together.

The categories related to the CSS are shown in table 4.5.

Table 4.5: The categories of the CSS

Category	*Criteria*	*Switching Strategies* 1^{st}	2^{nd}	3^{rd}
CSS2	Two BSS	$I \rightarrow II.III$	$IV \rightarrow II.III$	–
		$All \rightarrow II$	$All \rightarrow IV$	–
CSS3	Three BSS	$I.II \rightarrow II$	$I.II \rightarrow III$	$I.II \rightarrow IV$
		$I \rightarrow IV$	$I \rightarrow IV$	$I \rightarrow II.III$

The CSS are divided into CSS2 and CSS3, composed of two and three BSS respectively.

Figure 4.3 shows the mean efficiency for each category with their minimum and maximum (min/max) scatter.

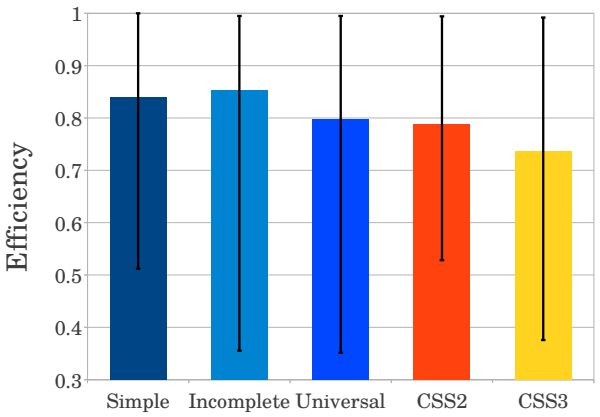

Figure 4.3: The average efficiency per category with the maximum and minimum scattering

The BSS strategies have a higher average efficiency, the majority of their occurrences being concentrated between 0.8 and 0.9. The Incomplete BSS delivers more power, and its occurrences are largely concentrated beyond 0.8. However, it has a min/max scatter ranging from 0.35 to 0.99, similar to the Universal strategies. The Simple BSS have a slightly lower average but a lower scatter.

These results show that **no single switching strategy works for all of the shadow scenarios**. Thus, shadows are best compensated by specific and well thought strategies.

The CSS2 have an overall efficiency similar to the Universal BSS, with different min/max scatters. This shows that the latter are not so "Universal" after all. It may work well in some cases, but its use should be analyzed further and compared with CSS2. The CSS3 strategies have a low average efficiency and a large min/max scatter. They work very well in some specific cases, which will be described further in detail in the block analyses.

The idea of a well thought strategy is reinforced by these results. But that does not mean complicated, as **complicated CSS have a lower probability of success**.

To confirm some of these general results, each block of shadow scenarios will be analyzed separately.

First Block - Small shadows

The first block concentrates its attention in small and simple shadows. Table 4.6 shows the two best strategies for each of its shadow scenarios.

The first three cases have their best results by using Complete BSS, while the last two have a better performance by using the Universal one. This points to an influence of the shadow shape in the efficiency of a given strategy. In cases 1, 2 and 3 the shaded and unshaded groups are contiguous, having a clear separation between them. In all of them the simple BSS is the best choice. In cases 4 and 5, the shaded cell group is located in between two unshaded blocks, thus being non-contiguous. In these cases, the universal BSS is the best choice.

Thus, **the continuity of the shadow must be taken into account when choosing the switching strategy**.

Second Block - Non-contiguous and homogeneous shadows

The second block of shadow scenarios proposes more insight about non-contiguous shadows. Table 4.7 shows its best strategies.

Table 4.6: The best results for the first block

Case	*Shading Factor*				η	*Switching Strategies*		
	PV_I	PV_{II}	PV_{III}	PV_{IV}		1^{st}	2^{nd}	3^{rd}
1	0	0	0	0.8	0.97	$I.II.III \rightarrow IV$	–	–
					0.93	$All \rightarrow IV$	–	–
2	0	0	0	0.5	0.99	$I.II.III \rightarrow IV$	–	–
					0.96	$All \rightarrow IV$	–	–
3	0	0	0	0.2	0.99	$I.II.III \rightarrow IV$	–	–
					0.97	$All \rightarrow IV$	–	–
4	0	0	0.8	0	0.91	$All \rightarrow III$	–	–
					0.90	$I.II \rightarrow III$	–	–
5	0	0	0.2	0	0.99	$All \rightarrow III$	–	–
					0.99	$I.II \rightarrow III$	$IV \rightarrow III$	–

Table 4.7: The best results for the second block

Case	*Shading Factor*				η	*Switching Strategies*		
	PV_I	PV_{II}	PV_{III}	PV_{IV}		1^{st}	2^{nd}	3^{rd}
6	0.8	0	0.8	0.8	0.82	$II \rightarrow All$	–	–
					0.77	$II \rightarrow I$	$II \rightarrow III.IV$	–
7	0	0.8	0.8	0	0.85	$I \rightarrow II.III$	$IV \rightarrow II.III$	–
					0.84	$All \rightarrow II.III$	–	–
8	0	0.8	0.8	0.8	0.82	$I \rightarrow All$	–	–
					0.76	$All \rightarrow II.III.IV$	–	–
9	0.8	0	0	0.8	0.85	$II.III \rightarrow I$	$II.III \rightarrow IV$	–
					0.84	$II.III \rightarrow All$	–	–

In all cases, the universal BSS is the best choice or very close to it. In cases 7 and 9, both CSS2 and Universal have similar efficiencies. These cases are also the first to have similar ratings to what could have been achieved by using bypass diodes.

Thus, **the universal BSS is systematically the best choice to non-contiguous shadows**.

Third Block - Non-homogeneous shadows

All of these shadow scenarios above have only one SF. This might not be the case under real conditions, making it necessary to understand the response of the system not only under non-homogeneous shadow shapes but also under different SF. The third block proposes several examples of such conditions and its best switching strategies are listed in table 4.8.

Table 4.8: The best results for the third block

Case	*Shading Factor*				η	*Switching Strategies*		
	PV_I	PV_{II}	PV_{III}	PV_{IV}		1^{st}	2^{nd}	3^{rd}
10	0	0	0.8	0.2	0.93	$I.II \rightarrow III$	–	–
					0.90	$I.II.III \rightarrow III$	–	–
11	0	0.2	0.5	0.8	0.92	$I.II.III \rightarrow III.IV$	–	–
					0.86	$I.II \rightarrow IV$	–	–
12	0	0	0.2	0.5	0.98	$I.II \rightarrow IV$	–	–
					0.97	$I.II.III \rightarrow III.IV$	–	–
13	0	0.5	0.5	0.8	0.92	$I \rightarrow IV$	–	–
					0.92	$I.II.III \rightarrow II.III.IV$	–	–
14	0	0.2	0	0.8	0.92	$All \rightarrow IV$	–	–
					0.91	$I.II.III \rightarrow IV$	–	–
15	0	0.2	0.5	0	0.95	$I \rightarrow III$	$IV \rightarrow III$	–
					0.92	$All \rightarrow III$	–	–

Cases 10, 12, 14 and 15 have two shaded cell groups. In all of them, the cell group with a SF of 0.2 does not need to participate in equalizing. The best choices are those that focus their energy of the unshaded cell groups into the highly shaded one, either through CSS2 or the Universal strategies.

Thus, **compensating a highly shaded cell group should be the priority during the equalizing process**. This can be acknowledged as evidence supporting the use of a binary shadow model.

Cases 11 and 13 have the same shape but different SF. In them cell groups with a SF of 0.5 are found to participate either during charge and discharge or not at all. In case 11, if the cell group with a SF of 0.2 does not participate in the equalizing, the efficiency of the system diminishes.

It is extremely important to properly choose which groups are considered unshaded and which are considered shaded. Failure to do so may incur in an important loss in efficiency. Thus, the more precise is the information about the shadow location, the more efficient the equalizing may be.

Fourth Block - Mild shadows

To further explore the challenge of telling the difference between shaded and unshaded cell groups, the last block proposes shadow scenarios where all cell groups are shaded. The best strategies for this block are listed in table 4.9.

Table 4.9: The best results for the fourth block

Case	*Shading Factor*				η	*Switching Strategies*		
	PV_I	PV_{II}	PV_{III}	PV_{IV}		1^{st}	2^{nd}	3^{rd}
16	0.2	0.5	0.8	0.8	0.93	$I.II \rightarrow II.III.IV$	–	–
					0.91	$I \rightarrow III.IV$	–	–
17	0.2	0.2	0.5	0.5	0.99	$I.II \rightarrow III.IV$	–	–
					0.98	$All \rightarrow III.IV$	–	–
18	0.2	0.5	0.2	0.5	0.95	$I \rightarrow II$	$III \rightarrow IV$	–
					0.93	$I \rightarrow II$	$I \rightarrow IV$	–
19	0.2	0.5	0.8	0.5	0.94	$I \rightarrow III$	–	–
					0.87	$All \rightarrow III$	–	–
20	0.2	0.2	0.5	0.8	0.95	$I.II.III \rightarrow III.IV$	–	–
					0.92	$I.II \rightarrow IV$	–	–

Cases 16, 19 and 20 confirm that cell groups with a SF of 0.5 should either charge and discharge or do nothing. They also confirm that strategies focusing on the highest shaded cell group tend to have a high efficiency.

Case 17 confirms that if the shaded and unshaded groups are contiguous then the Complete BSS is the best choice.

Finally, Case 18 shows that the **CSS2 can work if it profits from the symmetries of the shadow to minimize its switching losses**. A total of 5 transistors and 1 diode are used in the best switching strategy (T_2, T_3, T_5, T_7 and D_{10}). However, they only switch 4 times, because T_3, T_5 and T_7 are used in both BSS.

Simulation conclusions

The general conclusion from the simulations is that **no single switching strategy works for all shadow scenarios**. This implies that there is a direct relationship between the shadow and the switching strategies. The impact of the homogeneity and continuity of the shadows on the performance of the switching strategies was studied, giving place to five specific conclusions.

1. The Complete BSS is systematically the best choice to contiguous shadows
2. The Universal BSS is systematically the best choice to non-contiguous shadows
3. When equalizing non-homogeneous cell groups, those highly shaded should be the priority.
4. It is extremely important to properly choose which groups to consider unshaded or shaded.
5. The CSS works better if it profits from the symmetries of the shadow to minimize its switching losses

The experimental validation that follows seeks to validate these results and formalize them into overall criteria for choosing the switching strategies.

4.1.3 Experimental validation

The series of experiments proposed below have the objective of validating the simulations results proposed in this section.

Since measuring several switching strategies and shadow cases under the same weather conditions can be very difficult, their number has been limited. For each block, only one case is studied. For each case, the two most efficient strategies is measured and compared. Their details and weather conditions are shown in table 4.10. Where T_M represents the module temperature, T_A represents the ambient temperature and Irr represents the irradiance during the measurements.

Table 4.10: Measured scenarios and their BSS

Case	*Shading Factor*				*Switching Strategies*		*Irr*	T_A	T_M
	PV_I	PV_{II}	PV_{III}	PV_{IV}	1^{st}	2^{nd}	$(\frac{W}{m^2})$	$(℃)$	$(℃)$
2	0	0	0	0.55	$I.II.III \rightarrow IV$	–	550	32.7	45.9
					$All \rightarrow IV$	–	564	33.0	46.6
Bypass					–	–	568	33.1	47.0
7	0.76	0	0	0.76	$II.III \rightarrow I$	$II.III \rightarrow IV$	829	36.3	54.1
					$II.III \rightarrow All$	–	873	38.8	58.5
Bypass					–	–	823	36.2	54.5
12	0	0	0.21	0.55	$I.II \rightarrow IV$	–	897	32.0	54.6
					$I.II.III \rightarrow III.IV$	–	941	31.6	55.2
Bypass					–	–	935	32.6	55.8
18	0.21	0.55	0.21	0.55	$I \rightarrow II$	$III \rightarrow IV$	830	35.0	53.1
					$I \rightarrow II$	$I \rightarrow IV$	841	36.4	54.3
Bypass					–	–	856	36.0	54.7

For each case, an estimation of the maximum theoretical power was calculated. It serves as a reference power to which all measurements of its corresponding case are compared. To calculate it, the power of each cell group is estimated separately according to its SF, which requires their local current and voltage.

The current of each cell group is estimated from I-V measurements using bypass diodes, shown in figure 4.4. The values used are detailed in table 4.11.

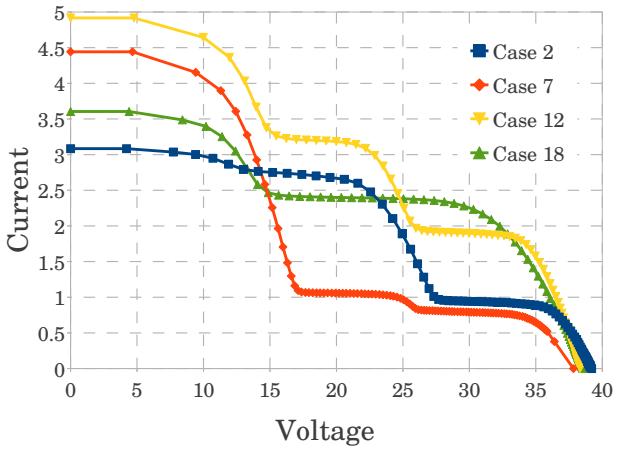

Figure 4.4: I-V curves of the bypass measurements

The voltage is more difficult to estimate since a single I-V curve was traced. The voltage of a cell group fluctuates approximately between 8.5 V and 6.5 V. This variation is essentially due to the irradiance and shading factor of the cell group. A value of 7.5 V was adopted for all groups, representing a compromise and a conservative estimation. Thus, the theoretical power is expected to be overestimated.

The theoretical power for each case is calculated in table 4.11

Table 4.11: Maximum theoretical power for each case

Cell group	*Case 2*		*Case 7*		*Case 12*		*Case 18*	
	I(A)	P(W)	I(A)	P(W)	I(A)	P(W)	I(A)	P(W)
PV_I	2.60	19.50	0.75	5.62	4.00	30.00	2.20	16.50
PV_{II}	2.60	19.50	3.61	27.10	4.00	30.00	3.35	25.13
PV_{III}	2.60	19.50	3.61	27.10	3.09	23.18	2.20	16.50
PV_{IV}	0.99	7.43	0.75	5.62	1.80	13.50	3.35	25.13
Total P_{theo} *(W)*		65.93		65.40		96.68		83.26

The measurements were conducted under different irradiation conditions, which may cause difficulties in their comparison and lead to false conclusions. To avoid these, a correction will be applied to their measured power. Since the theoretical power was calculated based on the currents produced by the bypass diodes measurements, it is logical to use the same irradiance as reference. Thus, the irradiance of the switching strategies will be corrected to that of the bypass diode for each case according to equation 4.2.

$$Irr_{corrected} = Irr_{original} + (Irr_{diode} - Irr_{original}) \tag{4.2}$$

Where the $Irr_{corrected}$ is the irradiance after correction, Irr_{diode} is the irradiance measured during the tracing of the I-V curve using bypass diodes and $Irr_{original}$ is the irradiance measured with the switching strategies. This correction is applied for each case independently.

The efficiency levels obtained by measurements, along with their measured and corrected power are shown in table 4.12.

Table 4.12: Efficiency of each measured scenario

Case	*Shading Factor*				*Switching Strategies*		*Power (W)*		*Eff.*
	PV_I	PV_{II}	PV_{III}	PV_{IV}	1^{st}	2^{nd}	*Meas.*	*Corr.*	
2	0	0	0	0.55	$I.II.III \rightarrow IV$	–	56.51	58.36	0.89
					$All \rightarrow IV$	–	53.62	54.00	0.82
Bypass					–	–	56.16	–	0.85
7	0.76	0	0	0.76	$II.III \rightarrow I$	$II.III \rightarrow IV$	49.84	49.48	0.76
					$II.III \rightarrow All$	–	50.45	47.56	0.73
Bypass					–	–	44.76	–	0.68
12	0	0	0.21	0.55	$I.II \rightarrow IV$	–	69.45	72.39	0.75
					$I.II.III \rightarrow III.IV$	–	69.37	68.93	0.71
Bypass					–	–	68.60	–	0.71
18	0.21	0.55	0.21	0.55	$I \rightarrow II$	$III \rightarrow IV$	56.03	60.41	0.72
					$I \rightarrow II$	$I \rightarrow IV$	64.47	63.34	0.76
Bypass					–	–	67.57	–	0.81

To complement the efficiency results, the P-V curves of each case are shown in figure 4.5. They are analyzed together to give a clear idea of the changes inflicted by the switching strategies on the power production of the PV module.

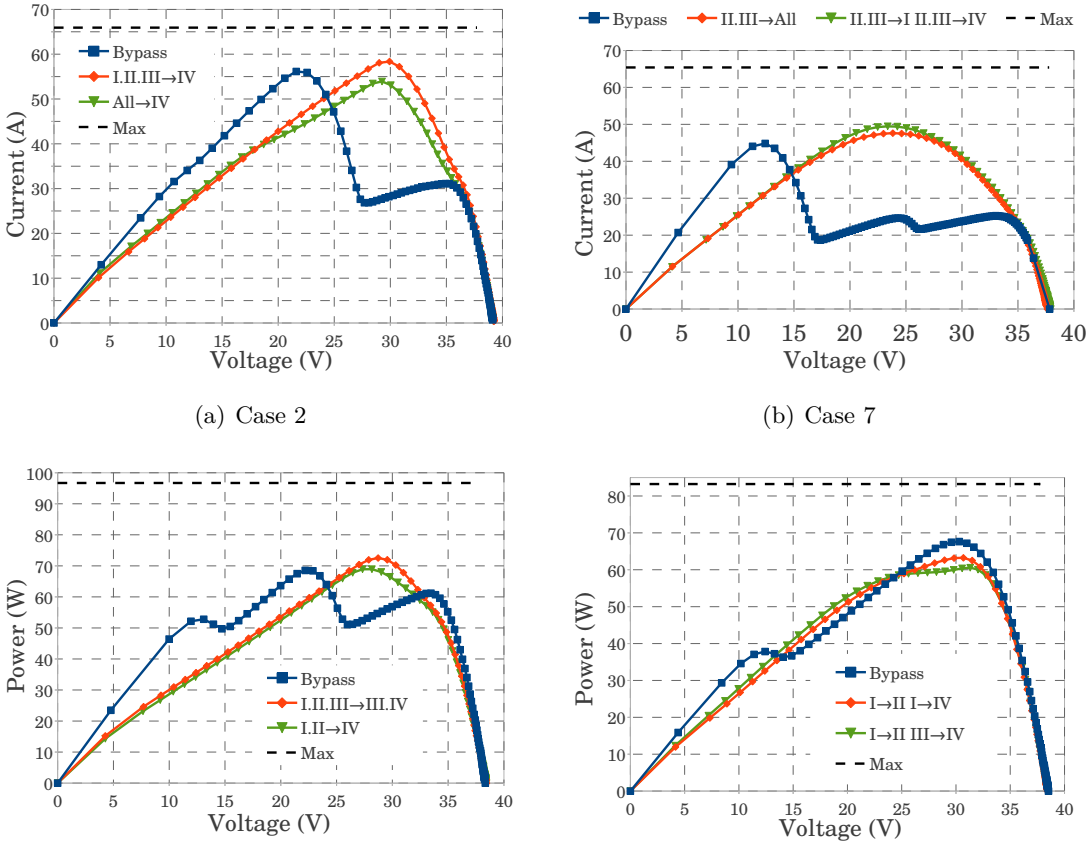

(a) Case 2

(b) Case 7

(c) Case 12

(d) Case 18

Figure 4.5: The experimental P-V curves of each case

The maximum theoretical power is represented by the Max dashed line. The results for the bypass diodes are also shown for comparison.

The switching strategies of cases 2, 7 and 12 have lower efficiencies than in the simulations, can be due to an overestimation of the maximum theoretical power. Still, their ranking is the same. Only case 18 has different results.

Case 2, shown in figure 4.5(a), confirms the Complete BSS as the most straightforward answer to the homogeneous shadows, having a better efficiency than the Universal BSS. Although their power peak is similar to the one obtained with the bypass diodes, both strategies gain nearly 8 V (20% of the module V_{OC}), sparing the MPPT of operating at lower voltages.

The strategies for case 7, shown in figure 4.5(b), show that the Universal BSS and the CSS2 may have similar results, the latter performing better when exploring the symmetries of the shadow. The Universal strategy may be used for such shadows if a quick reaction to the shadow is needed. The gain in voltage is more important in this case, nearly 12 V (30% of the module V_{OC}).

Case 12, shown in figure 4.5(c), has two strategies with very close performances. This confirms the idea that a mildly shaded cell group should either participate during charge

and discharge or not at all. Thus, properly detecting these groups can be confirmed as an important issue. Its voltage gains are less important, around 4 V.

Finally, figure 4.5(d) has a different result from the simulations. The more specific switching strategy, ($II.III \rightarrow I$ and $II.III \rightarrow IV$) which explores the symmetries of the shadow is less efficient than the other. By closely looking at the P-V curve, an indentation can be seen at peak power. This may be due to small fluctuations of irradiance which were not perceived during the measurements. The PV module performs much better without any equalizing at all, as it can be seen from the bypass curve. Thus, the Equalizer should be capable of determining if it is appropriate to compensate a shadow and stop in case power production falls.

Based on these results, the conclusions from the simulations can be considered as accurate and valid. A summary of all the results discussed in this section is proposed below.

4.1.4 Summary of the results

The results of this study are summarized in table 4.13, which elaborates the criteria for choosing the optimum switching strategy according to three shadow types: contiguous, non-contiguous and mildly shaded. Their length is described by n_{USH} and n_{SH}, which are the number of unshaded and shaded cells respectively.

Table 4.13: Optimal switching strategies

Shadow Type	*Shadow Length*	*Solution Category*	*State Example*	*Optimal Switching Strategies* 1^{st}	2^{nd}
Contiguous	$n_{USH} > n_{SH}$	Simple	[0 0 0 1]	$I.II.III \rightarrow IV$	–
	$n_{USH} < n_{SH}$		[0 1 1 1]	$I \rightarrow II.III.IV$	–
	$n_{USH} = n_{SH}$		[1 1 0 0]	$III.IV \rightarrow I.II$	–
Non Contiguous	$n_{USH} > n_{SH}$	Universal	[0 1 0 0]	$All \rightarrow II$	–
	$n_{USH} < n_{SH}$		[1 1 0 1]	$III \rightarrow All$	–
	$n_{USH} = n_{SH}$	CSS2	[0 1 0 1]	$I \rightarrow II$	$III \rightarrow IV$
Mildly	$n_{USH} > n_{SH}$	Incomplete	[0 0 0.5 1]	$I.II \rightarrow IV$	–
	$n_{USH} < n_{SH}$		[0 0.5 1 1]	$I \rightarrow III.IV$	–
	$n_{USH} = n_{SH}$		[0 0.5 1 0.5]	$I \rightarrow III$	–

Now, the subsidiary questions stated in the beginning of this section may be answered.

1. *Is there a "generic" switching strategy that can be used to compensate all the shadows?*

   No. The closest to a "generic" switching strategy is the principle used to determine the Universal BSS. But it was proven to not be Universal at all.

2. *If not, does each shadow have its own specific switching strategy to maximize the power output?*

   Each of the 16 binary shadows can be considered as having its own specific switching strategy. In cases where the distinction is not as clear (non-homogeneous shadows) it is paramount to properly define which groups will participate during equalizing and which will not.

3. *Can shadows with different shading factors but similar shapes be treated with the same switching strategy?*

   It depends on the detection and representation of the shadow. Those with the same shape but different SF might be considered as different binary shadow cases. Cases 10 and 12 are examples of similar shadow shapes with different SF being treated with different switching strategies. Conversely, cases 1 trough 5, 11 and 13 show similar shapes that might be treated with the same switching strategy.

4. *Is the shading factor important for choosing a switching strategy?*

   It depends on how many levels of representations are used in the shadow model. In the case of a binary shadow model, the priority is to clearly estimate the shadow shape. The more complex the shadow representations become, the more important it will be to precisely estimate the shading factor.

   In either case, a failure to properly estimate the shadow shape may incur in choosing a wrong strategy, ultimately leading to a poor efficiency of the equalizer. An special attention should be given to non-homogeneous and non-contiguous shadows. They were found to be much more complicated to clearly detect and compensate than others.

5. *Is there a simple and efficient algorithm for choosing a switching strategy?*

   Yes, but only if the shadow has been detected correctly. The criteria described in table 4.13 can be used to choose the appropriate strategy directly from the vector representing the shadow.

These results also provide some important elements to the detection of the shadow.

First, it should be as precise as possible to raise the chances of properly choosing which cell group is unshaded and which is shaded. In practice either the second search routine can be used, allying the search peaks with i_{OUT} measurements, or the charge time may be chosen as to give the first search routine enough precision.

Second, the binary shadow model might be expanded to ternary, quaternary or more. The middle values may be attributed to mildly shaded cell groups. Adding new levels raise the complexity of the switching strategies but grants a better power output in the case of shadow scenarios with mildly shaded cell groups.

Finally, an algorithm for choosing the optimal switching strategy for a given shadow is proposed in figure 4.6. It proposes solutions for binary or more complex shadow representations.

A final and important remark is to remember that these tests were performed for fixed duty cycles. Their impact on the power production is, as of this moment, unclear. Thus, the next sections should look back in these results to confirm them or revisit these ideas through other methods. This brings forth the two final step remaining before the development of a control algorithm for the Equalizer: how to choose its duty cycle? And, how does it change the efficiency of a given switching strategy?

4.2 Choosing the duty cycle

In order to compensate the shadow, the Equalizer must make two choices. First, it must choose the switching strategy as explained in the previous section. Then, a duty cycle must be assigned to it, according to a certain criteria. Finding this criteria is the objective of this section.

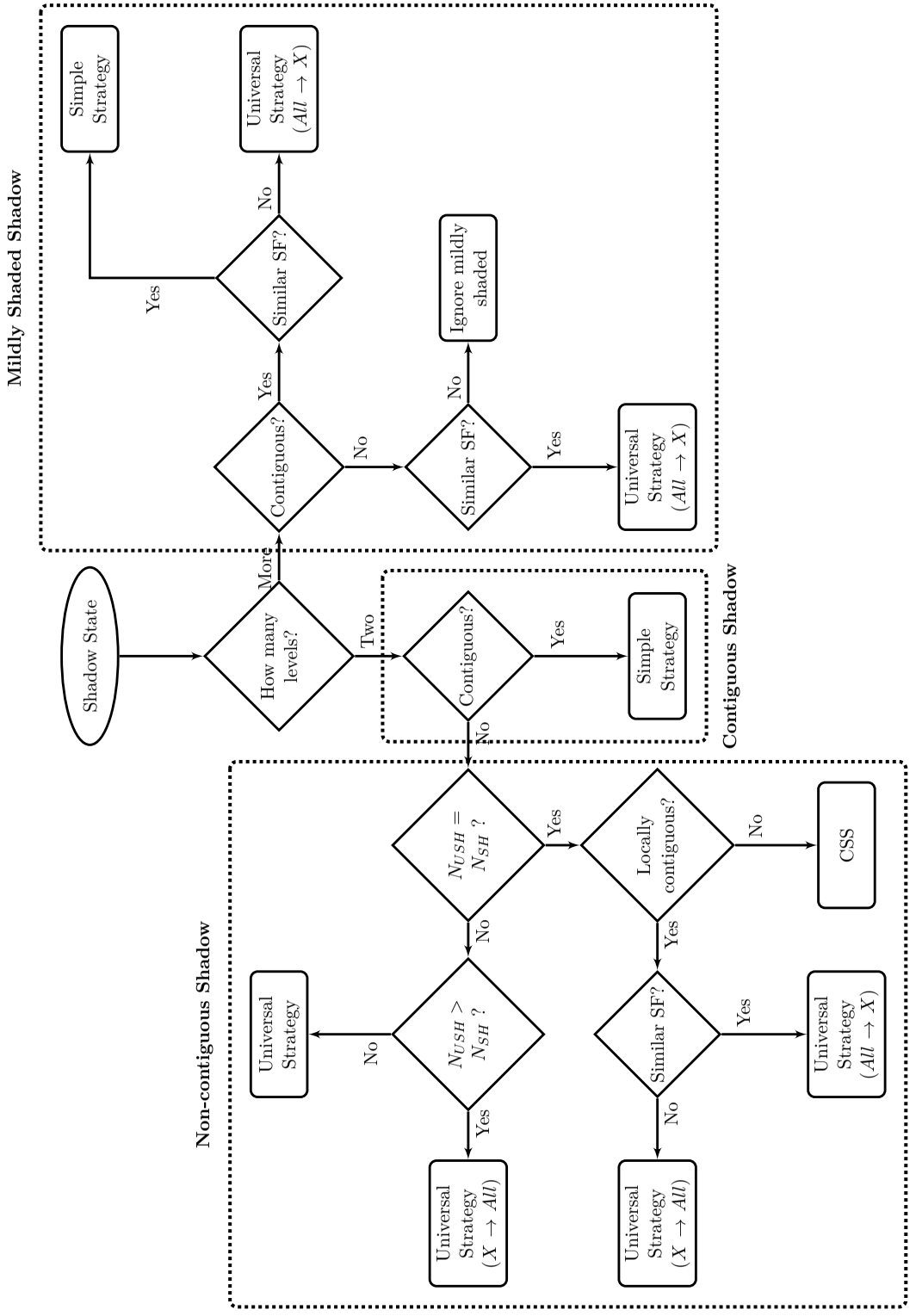

Figure 4.6: Algorithm for choosing the optimal switching strategy

This section proposes a study guided by the following question:

- *The equalizer can operate at a fixed duty cycle. Can any duty cycle guarantee a maximum power output?*

This study will be conducted in two parts. First a more detailed theoretical description of the duty cycle will be proposed. Its expression will be rewritten, taking losses and imperfections of the equalizer into consideration. Its objective is to give a global overview of the impact of the duty cycle in the equalizing. Second, a simulation and experimental study will describes its effect in the form of P-V curves. A final summary of this section details the finding and conclusions from this study.

4.2.1 Theoretical study

In chapter 3 the equalizer was shown to be able to work at fixed duty cycle. This is only possible because the PV module is a voltage controlled current source, capable of adapting itself to any operating point imposed by the MPPT. However, this does not mean any duty cycle value is appropriate for maximizing the power output of the PV Equalizer.

A simple approach to calculate the duty cycle was proposed in chapter 3, based on equation 3.12. In this equation, n represents the number of cell groups participating in the charge (CH) or discharge (DCH) phases of the BSS and the average inductor voltages is equal to zero.

$$D = \frac{n_{DCH}}{n_{CH} + n_{DCH}} \tag{3.12}$$

However, under real operating conditions the losses of the components have an influence over the voltage drop during charge and discharge of the Equalizer. Figure 4.7 proposes a simplified circuit to describe them.

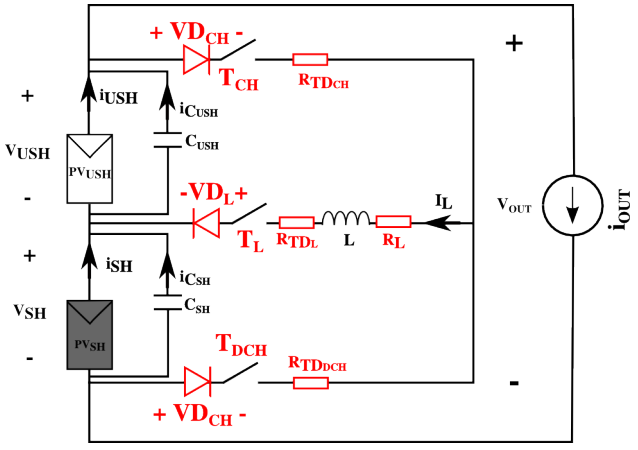

Figure 4.7: Simplified equalizer circuit with losses in red. The grey module represents the shaded cells.

By taking into consideration these imperfections, the duty cycle of the equalizer that guarantees a zero-sum voltage across the inductor for a given BSS and operating voltage can be described by equation 4.3.

$$D = \frac{V_{SH} + \mathbf{R_{DCH}} \cdot \mathbf{i_L} + \mathbf{VD_{DCH}} + \mathbf{VD_L}}{V_{USH} + V_{SH} + \delta \mathbf{V}} \tag{4.3}$$

Where R_{DCH}, R_{CH}, δV and i_L are defined by the equations 4.4 to 4.7.

$$\mathbf{R_{DCH} = RTD_{DCH} + RTD_L + R_L} \tag{4.4}$$

$$\mathbf{R_{CH} = RTD_{CH} + RTD_L + R_L} \tag{4.5}$$

$$\mathbf{\delta V = (R_{CH} - R_{DCH}) \cdot i_L + (VD_{DCH} - VD_{CH})} \tag{4.6}$$

$$\mathbf{i_L = i_{USH} - i_{SH}} \tag{4.7}$$

Equation 4.3 shows that the duty cycle is influenced by the imperfections of the Equalizer. Its value, thus, depends on the internal resistances of the transistors and voltage threshold of the diodes, shown in bold. These tend to drift under different temperatures, vary for different technologies and differ from component to component. Since there are infinite possible scenarios, the duty cycle cannot be studied with the same quasi-exhaustive approach proposed for the switching strategy study. It requires a more general approach that relates the power output and the duty cycle for any condition.

The general expression of the PV module power output is described by equation 4.8.

$$P_{OUT} = i_{OUT} \cdot V_{OUT} \tag{4.8}$$

For Simple BSS, $V_{USH} + V_{SH}$ is determined by equation 4.9, while the current output of the system is described by equation 4.10.

$$V_{OUT} = V_{USH} + V_{SH} \tag{4.9}$$

$$i_{OUT} = (1 - SF \cdot D) \cdot i_{USH} \tag{4.10}$$

Putting equations 4.10 and 4.3 together is troublesome since there is no explicit expression of V_{OUT} as a function of the duty cycle. Thus, a different approach is proposed to calculate P_{OUT}, composed of four premises.

First, the Equalizer is considered in steady-state where the voltage is considered evenly shared across all cell groups. Second, the values of V_{OUT} will vary from 0 to V_{OC}. Third, for each chosen V_{OUT} there are two average current values i_{USH} and i_{SH}, chosen according to the reference I-V curve shown in figure 4.8. Fourth, the imperfections of the equalizer are similar to those in Appendix B and recalled in table 4.14.

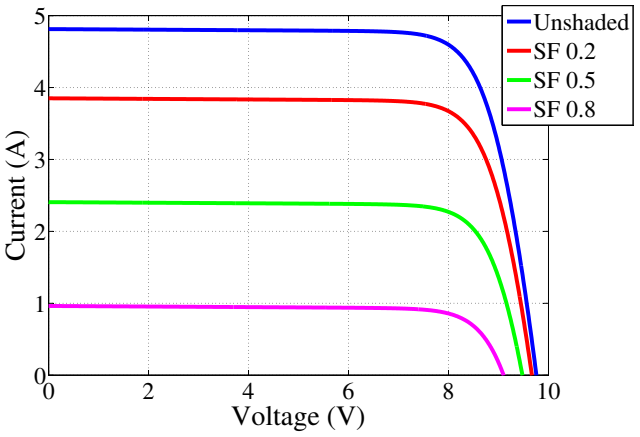

Figure 4.8: The I-V curves of each cell group

Table 4.14: The imperfections of the PV equalizer

Variable	*Value*
$V_D(V)$	1.1
$R_T(m\Omega)$	220
$R_L(m\Omega)$	20

Based on these premises, choosing the charge and discharge voltage of the system defines V_{OUT} and a pair of charge and discharge currents. For each voltage and current pair there is only one possible duty cycle value. Using it in equation 3.23 gives the output current of the system which can be used to calculate a single output power value. By calculating many of these, a tendency of how the duty cycle influences the power output can be estimated.

This method is applied to the two BSS and shadow conditions described in table 4.15.

Table 4.15: Details of the theoretical scenario

BSS	*Shading factor*			
	PV_I	PV_{II}	PV_{III}	PV_{IV}
$I.II \rightarrow III.IV$	0	0	0.5	0.5
$I.II.III \rightarrow IV$	0	0	0	0.5

The variation of power with the duty cycle is given in figure 4.9.

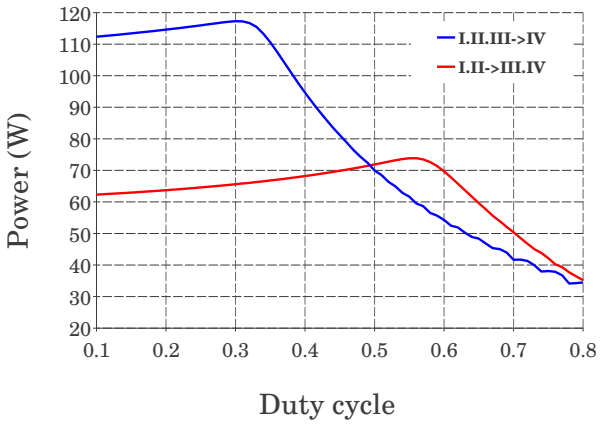

Figure 4.9: The influence of the duty cycle in the power output

For both BSS used in this example, a maximum power point is visible at a duty cycle value nearly 15% higher than the value calculated by using equation 3.12. Thus, for a given BSS there is a duty cycle that compensates the imperfections of the system and maximizes the power output.

As for the CSS, expressing equation 4.8 is much more complicated. Thus, the results from the BSS will be considered as potentially the same for the CSS. Their validation will be made directly through simulation and measurements.

4.2.2 Simulation study

The simulations proposed below have the objective of validating the existence of a single duty cycle that maximizes the power output of an equalized PV module. In it each shadow scenario will have a corresponding fixed switching strategy and a variable duty cycle. Two BSS and a single CSS are considered enough to validate the principle since it is considered inherent to the equalizing process.

The details of the simulations are described in table 4.16.

Table 4.16: Details of the duty cycle study scenario

BSS	*Shading factor*			
	PV_I	PV_{II}	PV_{III}	PV_{IV}
$I.II \rightarrow III.IV$	0	0	0.8	0.8
$I.II.III \rightarrow IV$	0	0	0	0.8
$I \rightarrow II.III$ $IV \rightarrow II.III$	0	0.8	0.8	0

The results will consist of P-V curves, one for each duty cycle value and are confronted to those of the theoretical study. They are shown in figure 4.10.

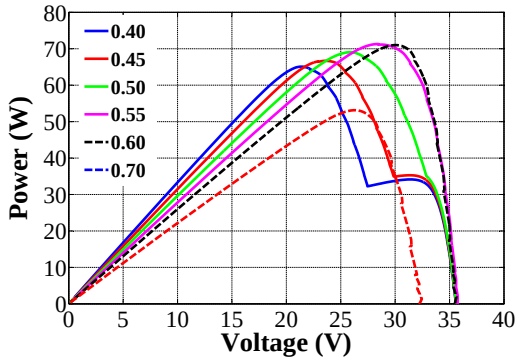

(a) $I.II \rightarrow III.IV$

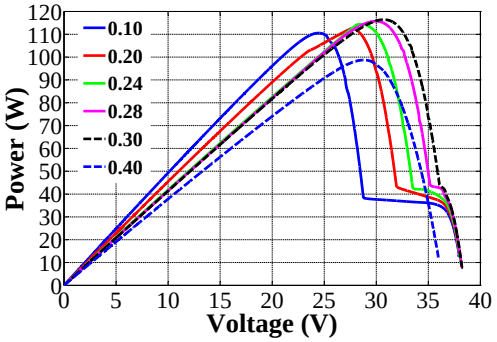

(b) $I.II.III \rightarrow IV$

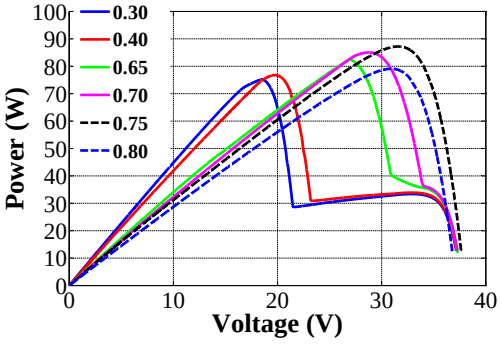

(c) $I \rightarrow II.III$ and $IV \rightarrow II.III$

Figure 4.10: Simulation P-V curves for the duty cycle study

The duty cycle has a clear impact in the presence of the several local maximum power points. If it is underestimated, the P-V curves show several MPPs as in duty cycles 0.4, 0.1 and 0.3. Since the charge phase is largely underestimated, the equalizer behavior approaches that of the bypass mode.

As the duty cycle approaches its optimum, the current from the unshaded groups is gradually transfered to the shaded ones. As their currents draws close their local MPP disappear, leaving the P-V curves with a single MPP. It rises until compensating the imperfections, thus reaching a single optimum duty cycle around 0.6, 0.3 and 0.7 for figures 4.10(a), 4.10(b) and 4.10(c) respectively.

If the duty cycle is overestimated, the current i_{OUT} cannot flow because of the equalizer diodes. Their unidirectional current sense makes the equalizer become the equivalent of an open circuit, stopping power production. This explains the voltage loss in figures 4.10(a), 4.10(b) and 4.10(c) around a duty cycle of 0.70, 0.40 and 0.8, respectively.

Thus, the choice of the duty cycle is seen to have a double influence over the output of the PV module. First, it changes the internal distribution of current among unshaded and shaded cells. Second, it imposes the same voltage across the different cell groups, confirming the premises from the theoretical study.

Figure 4.10(c) shows that the CSS may also have a duty cycle that maximizes power production. The values of the two duty cycles composing the CSS were kept the same to reduce the number of curves.

In order to compare the simulations with the theory the MPP of each duty cycle are extracted and plotted over figure 4.9, yielding figure 4.11. In it, the simulation results are plotted in dashed lines and identified by a (sim).

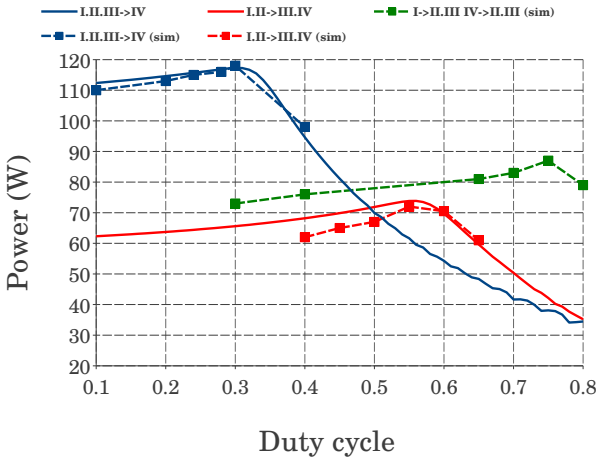

Figure 4.11: Comparison of the theoretical and simulation results

All the scenarios have a duty cycle that maximizes the power output. Their theoretical estimation is close but not exact. The CSS also follow the same tendency. To validate these effects, measurements are proposed in the next section.

4.2.3 Experimental study

The objective of this experimental study is to validate the fact that the variation of the Equalizer duty cycle has the effect of "erasing" the local MPP caused by shading on a PV module. The limited number of cases used during the duty cycle study allow for a full reproduction of the simulated results.

The shading factor used in the measurements is shown in table 4.17. For the characteristics of the plastic layers used to simulate the shadow, refer to Appendix B.

Table 4.17: Duty cycle scenarios

Case	*Switching Sequences* 1^{st}	2^{nd}	*SF*
1	$I.II.III \rightarrow IV$	–	[0 0 0 0.76]
2	$I.II \rightarrow III.IV$	–	[0 0 0.76 0.76]
3	$I \rightarrow II.III$	$IV \rightarrow II.III$	[0.76 0 0 0.76]

The irradiance and temperature changes are described in table 4.18.

Table 4.18: Weather conditions during the duty cycle measurements

Case	*Duty Cycle*	*Irr* $(\frac{W}{m^2})$	T_A ℃	T_M ℃
1	0.30	820	37.2	57.4
	0.50	820		
	0.55	780		
	0.60	778		
	0.70	818		
2	0.20	757	34.1	53.9
	0.24	752		
	0.28	751		
	0.30	748		
	0.40	745		
3	0.30	684	35.8	55.1
	0.65	681		
	0.70	676		
	0.75	675		

The results are presented in figures 4.12 and 4.13. several P-V curves per case, one for each duty cycle.

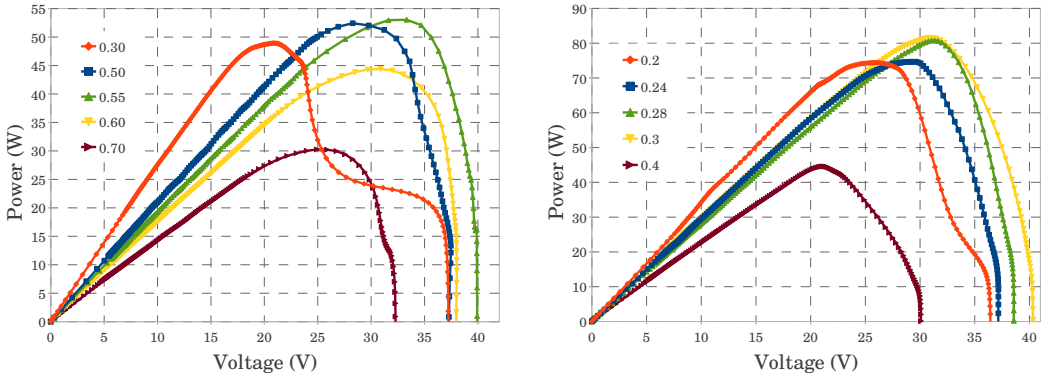

(a) Case 1 - $I.II \rightarrow III.IV$ (b) Case 2 - $I.II.III \rightarrow IV$

Figure 4.12: Experimental P-V curves for the BSS

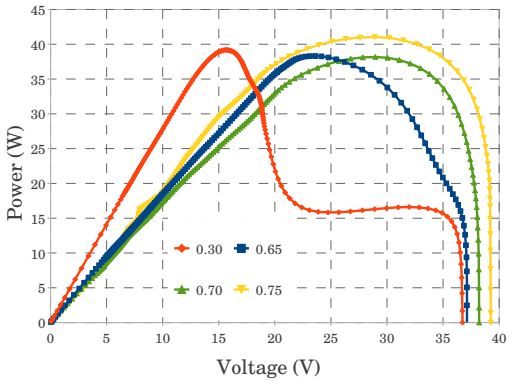

Figure 4.13: Experimental P-V curves for the CSS
Case 3 - $I \rightarrow II.III$ and $IV \rightarrow II.III$

Figure 4.12 and 4.13 validate the duty cycle choice simulation results for all the scenarios. For low duty cycles, the system behaves as if equipped with bypass diodes. There is only one duty cycle that maximizes power output, considered optimal. For a higher value of the duty cycle, its open circuit voltage starts to shrink, showing signs that the system becomes an open circuit.

The comparison between the simulation and the measurements is shown in figure 4.14. It validates the existence of an optimal duty cycle. It is important to note that these results were obtained under different irradiance condition from the simulations, which also shows that the optimal duty cycle is independent of the SF.

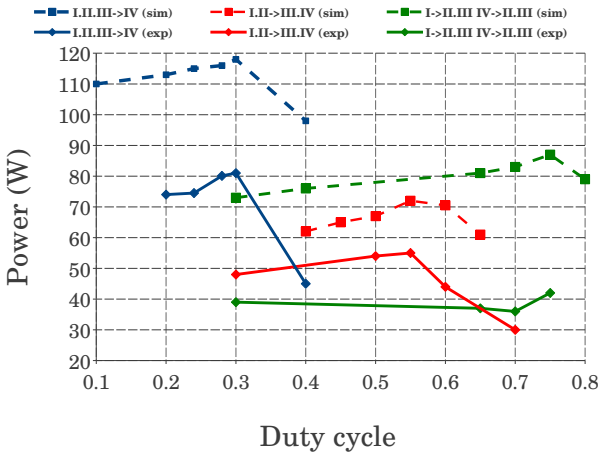

Figure 4.14: Comparison between simulation and experimental results

With all the needed data and conclusions, a summary of the duty cycle study can link these findings with the development of the Equalizer control system.

4.2.4 Summary of results

The main conclusion of the duty cycle study concerns its role during equalizing. It was found that the duty cycle controls the amount of energy being transferred from the unshaded to the shaded cell groups. To resume this effect, three values can be considered: zero, optimal and one.

When zero, the duty cycle forces the shaded PV cell group to behave as if bypassed. When optimal, the energy drawn from the unshaded cell groups offsets the losses of the Equalizer, all the rest being shared with the shaded cell groups. When equal to one, the duty cycle forces the unshaded PV cell group to behave as an open circuit.

As a consequence, only one duty cycle can maximizes the power output for a given switching sequence. It can be found by a **disturb and observe algorithm**, similar to the one used by the MPPT. This control method will be called **Optimal Duty Cycle Tracker (ODCT)** in the rest of this work. An alternative method is to apply an offset to the duty cycle, sparing the effort of controlling its duty cycle. Both solutions can be used together, the offset giving an initial estimate close to the maximum and the ODCT making small corrections around it.

The ODCT can also be applied to CSS. It is recommended, however, to control all duty cycles together to simplify the problem.

As for its possible influence in the ranking of the switching strategies, there are a few reasons to believe that it is not the case. First, it is important to note that the adjustment of the duty cycle starting from the value calculated by equation 3.12 leads to small gains of power. It could break a tie between two good strategies but it cannot allow a poorly chosen strategy to have a much better performance. Second, the measurements shown in figure 4.5 do not display important deformations in their P-V curves. This would show a too low duty cycle. Finally, all the duty cycles used during the switching strategy study were slightly underestimated. This has applied a similar handicap to all the strategies.

As all the aspects of the equalizing process studied and known, all that is left is to put them together to design a control algorithm for the Equalizer.

4.3 Conclusion

This chapter has characterized the impact of the shadow over the equalize and bypass functions provided by the PV Equalizer. Their study was guided by two questions, one focusing on the switching strategies and the other on the duty cycle. Their results can are summed up in their answers below.

- *What is the relation between the shadow and switching strategies?*

  The switching strategy depends on the shadow state and none is capable of addressing all possible shadows. An algorithm for choosing the optimal switching strategy according to the shadow state was proposed in figure 4.6, page 116. It is the result of a quasi-exhaustive study involving 20 shadow cases and 178 different switching strategies.

- *The equalizer can operate at a fixed duty cycle. Can any duty cycle guarantee a maximum power output?*

  No. For a given switching sequence, there is only one duty cycle that maximizes the power output of the PV module. Two techniques were proposed to find it.

  The first is **disturb and observe algorithm**, similar to the one used by the MPPT. It should, however, be designed to avoid interfering with i_{OUT}. Thus, the control of the duty cycle must be designed to be slower than that of the MPPT, giving it plenty of time to reach the steady-state before applying a new disturbance. This control method is called **Optimal Duty Cycle Tracker (ODCT)**.

  The other method is a simple offset. It could be given to the duty cycle, sparing the effort of controlling it. This offset should be between 10% to 15% of the duty

cycle theoretical value, but it may be calibrated with time through a trial and error algorithm.

Ideally, both solutions can be used together. The offset would give the ODCT an initial estimate close to the maximum, reducing the time needed to find the optimal duty cycle.

A CSS can also have its duty cycles controlled, but controlling them independently adds another degree of freedom to the ODCT. A simple, albeit not optimal, solution to this potential problem is to control all the duty cycles of a given CSS simultaneously.

Both answers must be taken into consideration when devising the control system for the PV Equalizer.

Now that any shadow state can be mitigated the next step is to find it, for accurate detection is the prerequisite of optimal mitigation.

Chapter 5

Finding Shadows: Search Function and Other Diagnose Methods

The previous chapter has characterized the influence of the shadow over the current compensation functions of the PV Equalizer. They were shown to be highly dependent on a correct diagnosis of the shadow. A wrong estimation of the shadow shape may lead to the choice of an incorrect switching strategy, ultimately leading to a lower power output.

This works presents three diagnose methods going from highly intrusive to highly predictive. They are called: direct, semi-direct and indirect diagnosis. This chapter will describe and study them in detail through the following set of questions.

- *How can the search function be used to find the shadow?*

  The search function provides current peaks that used to find the shadow. By studying how these peaks vary under different conditions, a useful pattern can be deduced for later use.

- *How are the electric variables of the PV module affected by changes in the shadow?*

  If certain electric variables are found to be dependent on the shadow, they can be observed and their behavior used for control purposes.

- *Is there any general rule to the shadow behavior? If so, how can the Equalizer predict it?*

  Recurrent behavior can be memorized and predicted. The development of a predictive model can be of interest for long-term operation of the PV Equalizer.

This chapter is composed of a total of three section, each addressing a different method and its question. Their results are summed up in the end of each section and the conclusion of this chapter will use all its evidence to provide clues to the development of a control algorithm.

Contents of this chapter

5.1 Direct shadow diagnosis: search function

The numeric shadow model introduced in chapter 2 allows the Equalizer to express the SF and the shadow shape as a data vector. Its binary equivalent is determined based on the application of a threshold to the components of the data vector. A method for acquiring the information on the shadow and building this data vector, called **the search function**, was already introduced in chapter 3. It is based on the successive acquisition of current peaks, one per cell group connected to the PV Equalizer. The purpose of this section is to study these current peaks in detail and link them to the numeric shadow model and estimate how they impact the PV module power production by answering the following question:

- *How can the search function be used to find the shadow?*

Figure 5.1 recalls the principle of the search function. It considers the cell group PV_I to be shaded by a SF of 0.5.

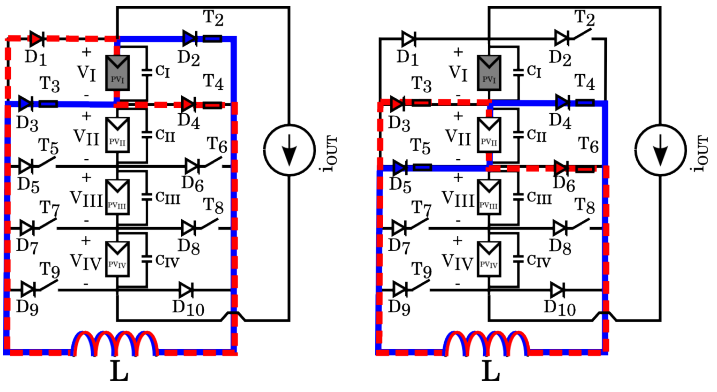

(a) Search on PV_I (b) Search on PV_{II}

(c) Search on PV_{III} (d) Search on PV_{IV}

Figure 5.1: The principle of the search function

To search for a shadow over a PV cell group, the PV Equalizer connects the inductor to it for a certain period of time. The inductor current value is acquired and the energy is immediately returned to the concerned cell group through a discharge. Their expected result is shown in figure 5.2. The dead time between peaks guarantees a total discharge of the inductor before the acquisition of a new peak.

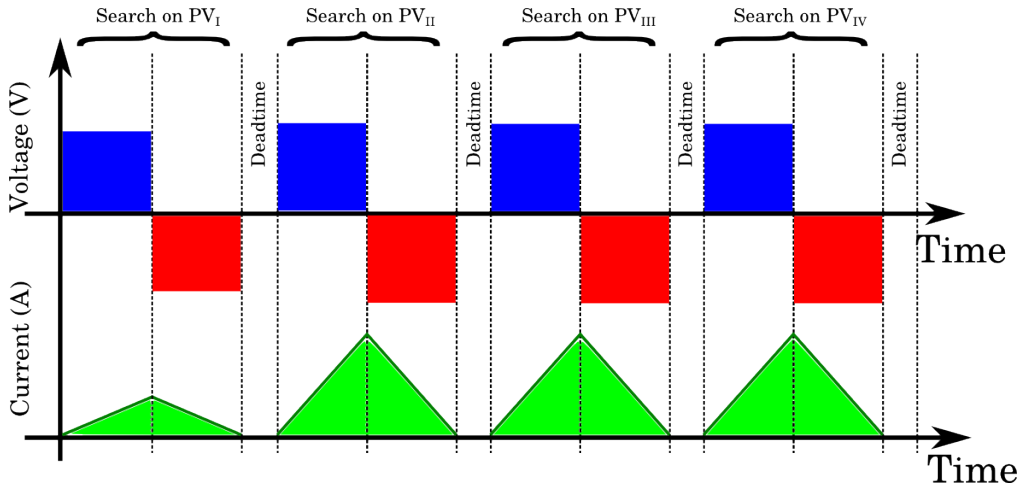

Figure 5.2: Expected result of the search function

A careful analysis of both figures 5.1 and 5.2 indicates that four variables may influence the current peaks during the search: the duration of the charge, the output current, the shadow shape and the shading factor. To properly detect the shadow, it is important to tell the difference between the first and last two. Consequently, the first question of this section must be decomposed into a new series of questions which take these four variables into consideration.

1. *What is the effect of the duration of the charge over the current peaks?*
2. *How do the shading factor and the shadow shape influence the current peaks? Can their effects be easily discerned?*
3. *How does the output current influence the current peaks?*
4. *How does the equalize function influence the current peaks?*

Their answers are proposed through theoretical and simulation studies which will be in turn validated through measurements.

5.1.1 Theoretical study

The theoretical study seeks to understand the influence of several variables over the search through a simplified circuit analysis. The search will be studied for a single cell group and only during the charge phase as shown in figure 5.3.

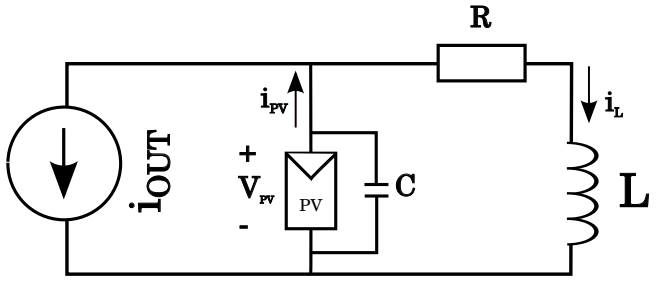

Figure 5.3: PV system equivalent circuit

In figure 5.3, the current source i_{OUT} represents the chopper connected in series with the PV module. The resistance in the circuit represents the sum of the resistances in the active and passive components. The influence of the diodes is not taken into consideration in this simplified circuit.

In this second order circuit, the capacitor voltage and inductor current of the system are described by equations 5.1 and 5.2.

$$\frac{\delta i_L}{\delta t} + \frac{R \cdot i_L}{L} - \frac{V_{PV}}{L} = 0 \tag{5.1}$$

$$\frac{\delta V_{PV}}{\delta t} - \frac{(i_{OUT} - i_{PV})}{C} - \frac{i_L}{C} = 0 \tag{5.2}$$

Equations 5.1 and 5.2 can be combined to yield equation 5.3.

$$\frac{\delta^2 i_L}{\delta^2 t} + \frac{\delta i_L}{\delta t} \cdot \frac{R}{L} + \frac{i_L}{L \cdot C} = -\frac{(i_{OUT} - i_{PV})}{L \cdot C} \tag{5.3}$$

To find the solution to this equation, the attenuation of the system must be estimated. This can be done by using the attenuation factor (α) and natural frequency (ω_0) of equation 5.3, which are described as follows.

$$\omega_0^2 = \frac{1}{L \cdot C} \tag{5.4}$$

$$\alpha = \frac{R}{2 \cdot L} \tag{5.5}$$

Typical values for the elements of the equivalent circuit are given in table 5.1.

Table 5.1: The variables of the PV model

Variable	*Value*
Resistance - R	$400m\Omega$
Inductance - L	$100\mu H$
Capacitance - C	$220\mu F$

Using the values from table 5.1, the circuit can be considered as underdamped, since α is 1000 and ω_0 is 6742. In this case, the solution for this second order differential equation is proposed by equation 5.6.

$$i_L(t) = V_{PV} \cdot A(t) + (i_{OUT} - i_{PV}) \cdot B(t) \tag{5.6}$$

Where V_{PV} and i_{PV} are the voltage and current in the cell group, respectively.
The constants A and B are given by equations 5.7 and 5.8.

$$A(t) = \left[\frac{e^{-\alpha \cdot t} \cdot sin(\omega d \cdot t)}{L \cdot \omega d}\right] \tag{5.7}$$

$$B(t) = \left[1 - e^{-\alpha \cdot t} \cdot cos(\omega d \cdot t) - \frac{\alpha}{\omega d} \cdot e^{-\alpha \cdot t} \cdot sin(\omega d \cdot t)\right] \tag{5.8}$$

The ωd is defined as follows:

$$\omega d = \sqrt{(\alpha)^2 - (\omega_0)^2} \tag{5.9}$$

Equation 5.6 can only be calculated by adopting a certain set for V_{PV}, i_{PV} and i_{OUT}. The first two are linked to the shading factor, while the third is independent. They are studied in two theoretical scenarios.

In the first scenario, the shading factor varies. This is expressed by a variation in the V_{PV} and i_{PV}. Their values are extracted from the I-V curves of the PV module to which the Equalizer prototype was designed. Its characteristics are detailed in Appendix B.

In the second scenario, it is i_{OUT} that varies. Both scenarios are detailed table 5.2, the bold variables are those allowed to vary.

Table 5.2: The two theoretical scenarios

Scenario	*Variable*	*Values*					
1	**SF**	1.0	0.8	0.6	0.4	0.2	0.0
	$\boldsymbol{V_{PV}(V)}$	5.43	7.28	7.44	7.53	7.59	7.65
	$\boldsymbol{i_{PV}(A)}$	0.03	0.88	1.8	2.72	3.61	4.53
	$i_{OUT}(A)$	fixed - 0.5					
2	SF	fixed - 0.4					
	$V_{PV}(V)$	fixed - 7.53					
	$i_{PV}(A)$	fixed - 2.72					
	$\boldsymbol{i_{OUT}(A)}$	0.5	1	1.5	2	2.5	3.0

In both scenarios, the search will be calculated for a “short” and “long” time. The objective is to determine which is the most convenient for finding the shadow. This initial estimation of the charge time will be used as a basis for further studies.

The time needed by the system to converge to 5% of its final current value is nearly 3 ms. Thus, the “short” charge time is considered to be 400 μs, while the “long” one is 5 ms. The first does not allow the circuit enough time to start its own damping. The second gives enough time for the damping of the system to pass.

The results for first scenario are shown in figure 5.4.

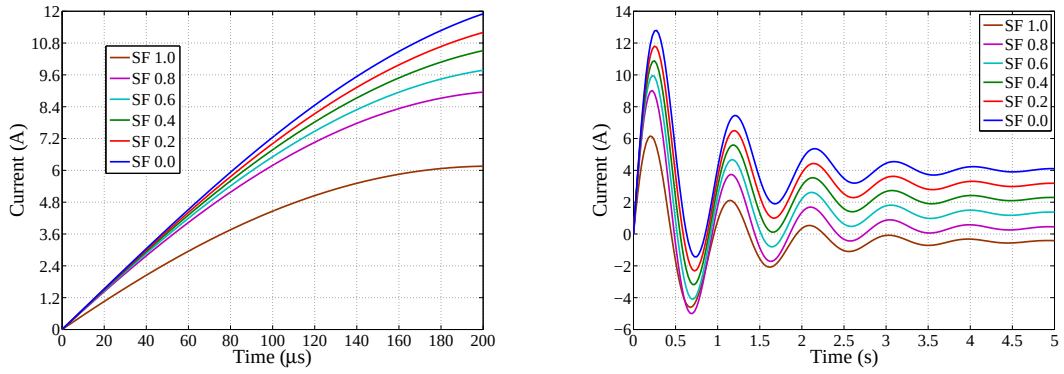

(a) Short search (b) Long search

Figure 5.4: The influence of SF in the circuit response

In figure 5.4(a) as the difference between i_{OUT} and i_{PV} approach zero, the peaks become lower. However, the difference between the responses for a SF of 0.8 and 0.0 is 3 A at 200μs, falling for faster search times. As a consequence, detecting the shading factor is easier for long searches.

The results in steady state are shown in figure 5.4(b). The inductor current at 5 ms rises by regular steps for different SF. They converge to roughly i_{PV} minus i_{OUT}, as expected from equation 5.6. Thus, longer searches may provide a direct estimation of the shading factor, *provided that* i_{OUT} *remains stable.*

The results for the second scenario are shown in figure 5.5. The inductor current follows the pattern of the precedent scenario. As the i_{OUT} raises and approaches i_{PV} the system becomes less excited and its steady state current value is lower.

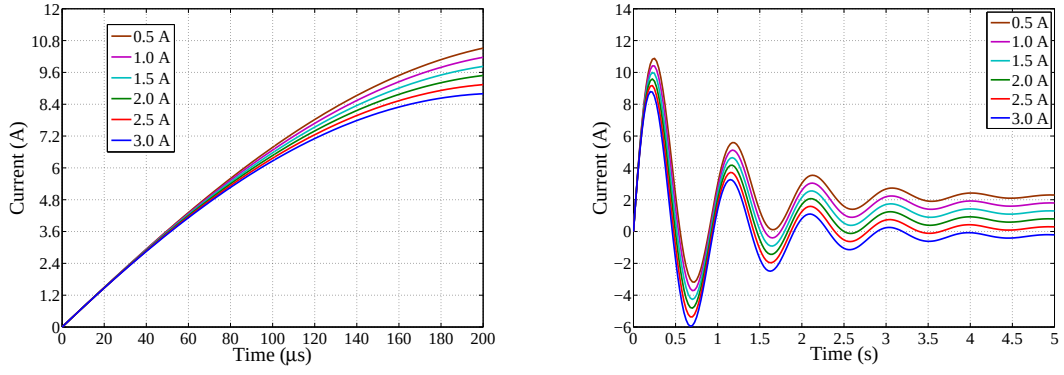

(a) Short search (b) Long search

Figure 5.5: The influence of i_{OUT} in the circuit response

Based on these results, an important fact about the influence of the charge time on the search can be deduced. Faster searches are largely influenced by the voltage. In the case of longer searches, they are influenced by the currents of the PV system.

The search time should be chosen taking into consideration its impact on the prototype sizing. A longer charge time will require less precision but greater ranges, while shorter ones

will restrain the range but require greater precision. Longer searches will put enormous constraints in the sizing of capacitors, forcing them to reduce sizes for faster performances. However, smaller capacitors imply in higher voltage and current ripples during equalizing. The current overshoot during the search will also impose a certain stress over the inductor and influence its sizing. The implications of these facts in the sizing of the prototype discourage longer searches, as described in appendix B.

Another interesting insight, this time concerning the deduction of the shading factor, can be drawn from these results. There are, basically, two possible ways to determine the shading factor from the current peaks. The first is to perform a search on each cell group as quickly as possible in order to have a similar i_{OUT}. Once the readings are compared, the highest peaks will be considered as unshaded while the lowest peaks will be considered as shaded. However, since this technique gives an estimation of the shaded voltage, it is not precise in terms of shading factor. Its results are best suited for determining the shadow shape.

The second is to know the unshaded short circuit current of the PV module, perform a long search and read i_L . Using these three, the information concerning the SF can be estimated directly. The advantage of this technique is that it gives a direct indication of the shading factor. However, it requires a priori knowledge, a second reading and no changes in i_{OUT}. All of these conditions make this method unfeasible in practice. Thus, due to its simplicity, the first method will be studied into further detail through the simulations and measurements.

Due to the limitations of the circuit model used in this theoretical study, the next steps will be given using the simulation model developed in this work. Its details are given in appendix A.

5.1.2 Simulation study

The theoretical study has reached two important conclusions. First, shorter searches are preferable but its current peaks are less precise in terms of shading factor. Second, the method for deducing the location of the shadow is to cross-compare these peaks. The objective of this simulation study is to further understand the influence of the shadow over the voltage of the PV cell groups and their current peaks.

Four variables were found to influence the current peaks: the charging time, the shading factor, i_{OUT} and the shadow shape. Each will be allowed to vary in a separate simulation scenario. Their details are shown in table 5.3, where the bold variables are those allowed to vary in each scenario.

The first scenario verifies the influence of the charge time. Two SF are used, 0.2 and 0.8, the first being more difficult to detect than the second. The i_{OUT} is chosen to allow both SF to work under the same conditions. The charge times assumes three values: 10 μs, 40 μs and 200 μs. They are chosen to determine their precision and range, which will later be the basis for sizing the sensor of the prototype. The shadow shape remains the same.

In **the second scenario**, the influence of the SF will be verified. Four different SF will be used to limit the number of simulations. The value of i_{OUT} was chosen to be lower than all the i_{PV}. This was done to allow all SF to react to the search, since the diodes on the switching legs of the Equalizer would block if i_{OUT} was higher than i_{PV}. The charge time of 40 μs was chosen for being an intermediate speed value, representing a compromise between speed and precision easier to reproduce later, during the measurements. The shape of [0 0 0 1] was chosen because all cell groups being identical, only the study of a

Table 5.3: The four simulation scenarios

Scenario	*Variable*	*Values*
	***ChargeTime*(μs)**	**10,40 and 200**
	SF	fixed - 0.2 and 0.8
1	$I_{OUT}(A)$	fixed - 1.0
	Shape	fixed - 0 0 0 1
	Function	fixed - OFF
	$ChargeTime(\mu s)$	fixed - 40
	SF	**0.2, 0.4, 0.6 and 0.8**
2	$I_{OUT}(A)$	fixed - 0.5
	Shape	fixed - 0 0 0 1
	Function	fixed - OFF
	$ChargeTime(\mu s)$	fixed - 40
	SF	fixed - 0.4
3	$\boldsymbol{I_{OUT}(A)}$	**0.5, 1.0, 1.5, 2.0, 2.5 and 3.0**
	Shape	fixed - 0 0 0 1
	Function	fixed - OFF
	$ChargeTime(\mu s)$	fixed - 40
	SF	fixed - 0.4
4	$I_{OUT}(A)$	fixed - 2.5
	Shape	**0010, 0101, 1011 and 0110**
	Function	fixed - OFF
	$ChargeTime(\mu s)$	fixed - 40
	SF	fixed - 0.4
5	$I_{OUT}(A)$	variable
	Shape	**0011, 0001, 0000, 1011, 1001, 1000, 1111, 1101 and 1100**
	Function	fixed - Equalize

single peak is necessary.

The purpose of **the third scenario** is to validate the influence of the i_{OUT}. An SF of 0.4 was chosen because its i_{PV} is near to 2.5, which reduces the number of i_{OUT} values. They evolve in steps of 0.5 A from 3.0 A to 0.5 A. The charge time and shadow shape remain the same as in the second scenario, for the same reasons.

The fourth scenario studies the influence of the shape. The SF of 0.4 is used together with an i_{OUT} of 2.5 A, so that the PV module is considered to be operating exactly on its MPP. The charge time used is the intermediate speed of 40 μs. The first and second shadow shapes, [0 0 1 0] and [0 1 1 0], represents an isolated shadows. The second and third shapes, [0 1 0 1] and [1 0 1 1], represent non-contiguous shadows. All the cell groups are shaded at least once.

The fifth and final scenario studies the influence of the equalize function over the current peaks. The SF of 0.4 is used together with an i_{OUT} slightly superior to it of 3.3 A, so that the now Equalized PV module is considered to be operating close to its MPP. The charge time used is the intermediate speed of 40 μs. The shadow shape used will be [0 0 1 1], associated with a fixed BSS. The equalizer function will require certain changes to the shadow in order to study the effect of wrong detections.

Scenario 1 - Variable charge time

The influence of the charge time for different SF is shown in figure 5.6. In each figure, the results for an SF of 0.2 are traced in a solid line, while those for an SF of 0.8 are traced in a dashed one. An overall observation of these curves shows a similar effect of the search in all of them. The difference in the fourth peak is barely perceptible for a low SF and is clearly distinguishable for a high SF.

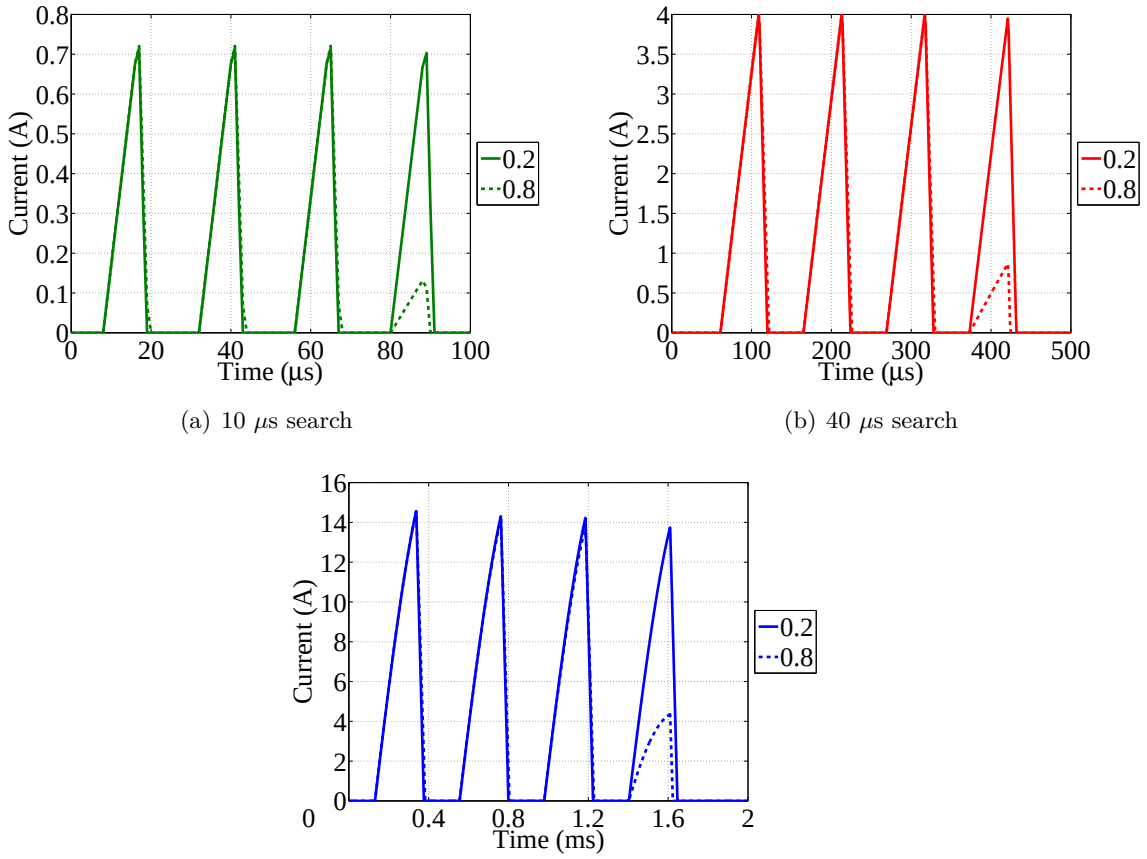

(a) 10 μs search

(b) 40 μs search

(c) 200 μs search

Figure 5.6: Simulation results for the variable charge time

The similar response of all the three simulated charge times confirm the clear dominance of the voltage in the short search. This can be validated by a closer analysis of the I-V curves used in the simulations, shown in figure 5.7. With the i_{OUT} at 1 A, the voltage difference between the cell group with a SF of 0.2 and those unshaded is below 100 mV. When the SF raises to 0.8, this difference grows up to 7 V. Thus, any of the search times used above are bound to have their results driven by the voltage of the cell group or, more indirectly, by i_{OUT}.

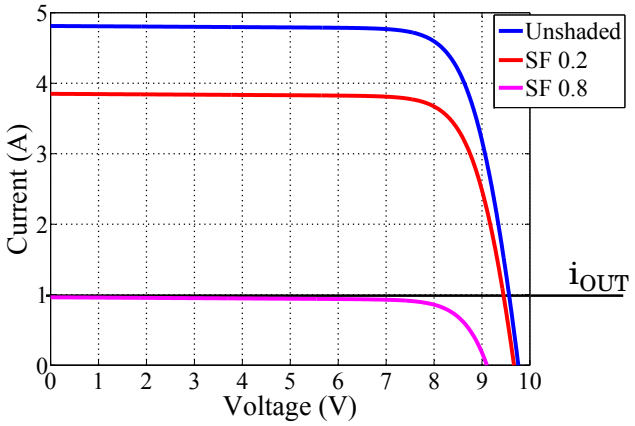

Figure 5.7: Detail of the I-V curves used in the simulation

In terms of precision, choosing a charge time has an important impact over design of the sensor monitoring the inductor current. In figures 5.6(a), 5.6(b) and 5.6(c) the current variation is of 200 mA, 3 A and 10 A, respectively. The necessary range and precision to detect them are easily available in commercial sensors. For shortest search noise might be an important issue, which needs to me confirmed during the measurements.

Another criteria that can be used is the current for which the inductor was sized. The prototype used in this work was designed for operating at 5 A or nearly the short circuit current of the PV module at 1000 $\frac{W}{m^2}$. Stressing the inductor with an overshoot of current such as the one provided by the long search might heat it up, raise losses or simply saturate its core.

Finally, the criteria that will decide between the two shortest searches will be their resistance to noise, which will be provided during the experimental validation.

Scenario 2 - Variable SF

Figure 5.8 shows the results for the impact on the search of variations in the shading factor. The peak on the right in figure 5.8(a) corresponds to the shaded cell group, which reacts as the SF rises. Its detail in figure 5.8(b) shows that the peak is sensitive to the SF closer to the fixed i_{OUT}, with very small variations for the other SF. Zooming in further in figure 5.8(c) confirms this reaction.

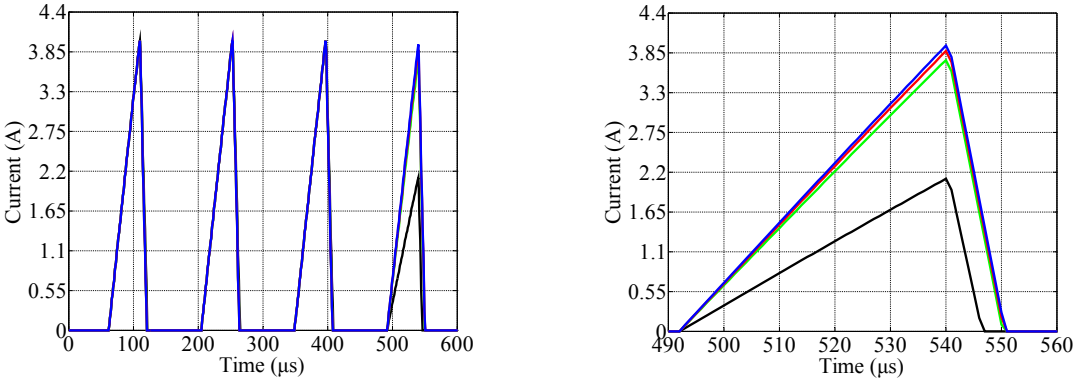

(a) Overall results

(b) The shaded cell group peak

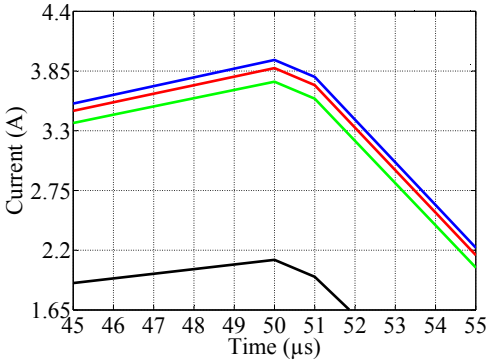

(c) Detail of the shaded cell group peak

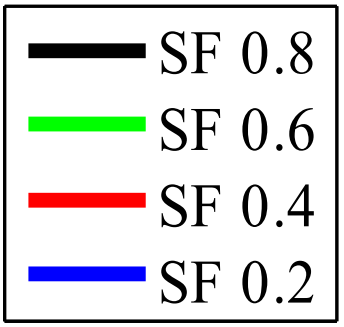

(d) Legend

Figure 5.8: Simulation results for the variable SF

The direct interpretation of these results is that the search is more precise as i_{OUT} draws closer to i_{PV}. As a consequence, the search should not be conducted while the MPPT is in transitory state and seeking a new MPP. Somehow, the Equalizer is required to "know" the state of the MPPT, either by communicating directly with it or by monitoring i_{OUT}.

These results confirm that the closer i_{OUT} is from the i_{PV} of the shaded cell group, the easier the detection becomes. This effect is linked to the excitation of the RLC circuit composed by the capacitor, inductor and the sum of resistances. This can be better explained by recalling the expression inductor current, but considering it for a fixed time.

$$i_L(40\mu s) = V_{PV} \cdot A(40\mu s) + (i_{OUT} - i_{PV}) \cdot B(40\mu s) \tag{5.10}$$

Both A and B can now be seen as fixed values, both depending only on the circuit constants. Thus, what will determine the height of the current peak is the cell group voltage and the proximity between i_{OUT} and i_{PV}. Figure 5.9 shows how the voltage changes with the shading factor for the fixed i_{OUT}, corresponding to the current peaks. The operating point of the shaded cell group is much closer to its local MPP for a SF of 0.8.

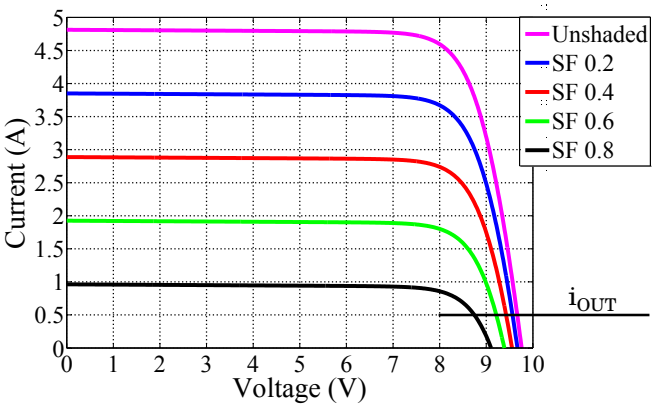

Figure 5.9: The reaction for different SF I-V curves

A similar phenomenon occurs when i_{OUT} varies for a fixed shading factor.

Scenario 3 - Variable i_{OUT}

The influence of i_{OUT} is further explored in figure 5.10. The shaded current peak shape is on the right of figure, 5.10(a). For a better visibility, figure 5.10(b) shows only the peak corresponding to the shaded cell group. Its variation is very subtle from 0.5 A to 2.5 A and it suddenly goes to zero at 3.0 A. Figure 5.10(c) provides a closer zoom.

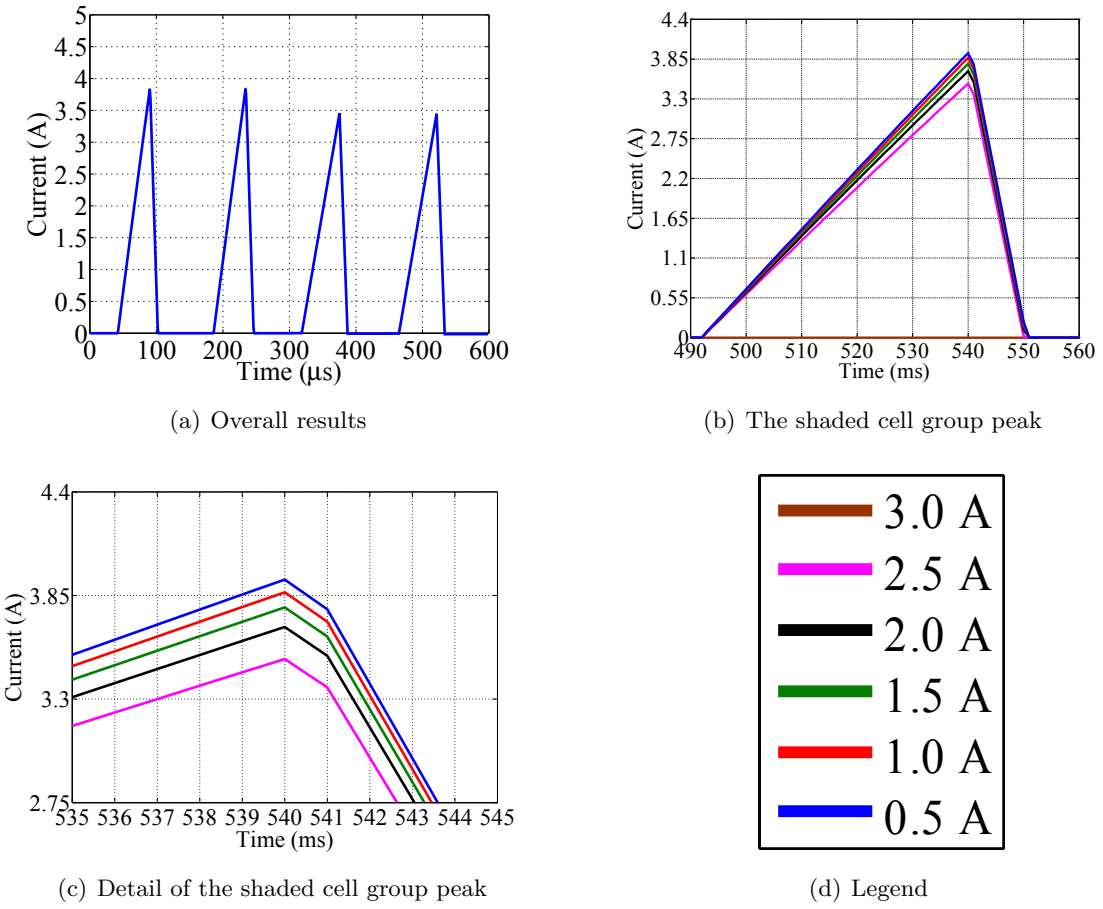

(a) Overall results

(b) The shaded cell group peak

(c) Detail of the shaded cell group peak

(d) Legend

Figure 5.10: Simulation results for the variable i_{OUT}

To explain this behavior, figure 5.11 shows how the voltage of the shaded cell group varies as i_{OUT} raises. Its voltage is roughly 9.5 V for and i_{OUT} of 0.5 and 8.5 V for 2.5 A, explaining the slight variation in the peaks. When i_{OUT} becomes 3 A, the shaded cell group becomes unable to react for its voltage is negative.

These results confirm that the current peak reacts to i_{OUT} as it approaches the i_{MPPT} of the shaded cell group. Another way of putting it is that the peaks carry more information about the shadow as the system draws closer to its local MPP. This reinforces the fact that the search should be conducted only when the system is in steady-state.

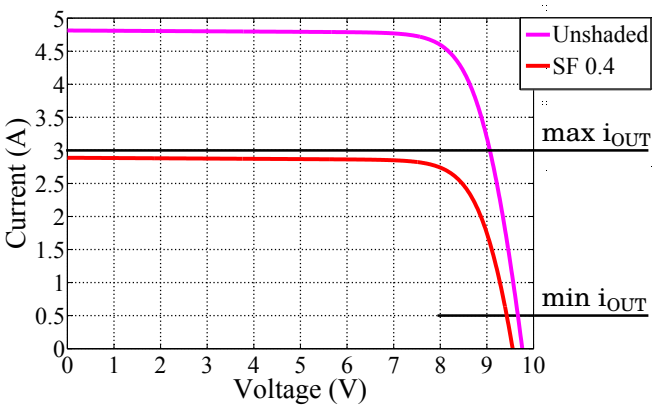

Figure 5.11: The reaction for different i_{OUT}

Scenario 4 - Variable shadow shape

The shadow shape of the system is linked to the binary representation proposed in this chapter. By validating its capacity to represent the shadow, the correlation between the search function and the shadow model can be completely achieved. From all the 16 possible binary cases, only 4 will be shown in this study to simplify the analysis, figure 5.12 shows the results.

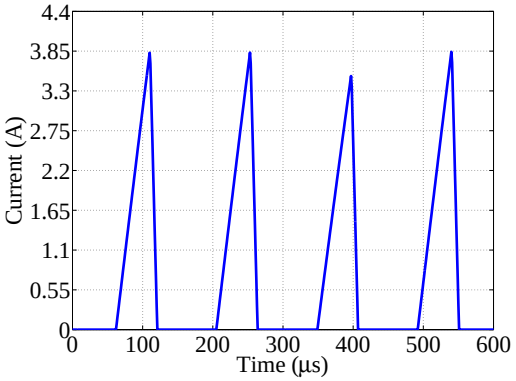

(a) State 0 0 1 0

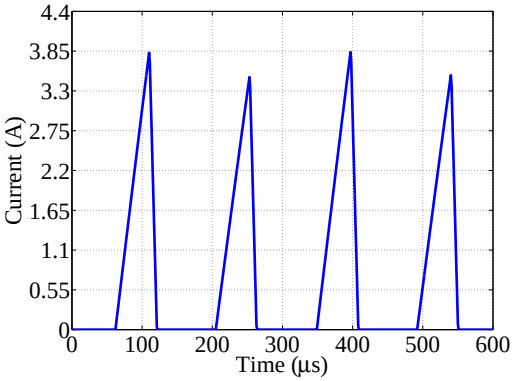

(b) State 0 1 0 1

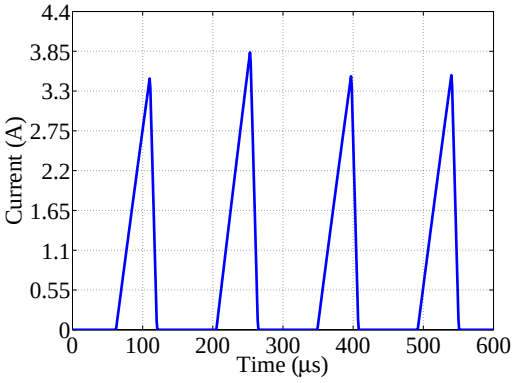

(c) State 1 0 1 1

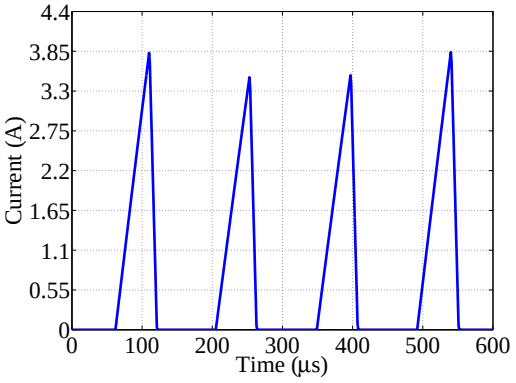

(d) State 0 1 1 0

Figure 5.12: Simulation results for the variable shapes

The shadow shapes are clearly identifiable. All peaks react to the shadow and correspond to their binary representation, validating its use in the detection when the PV Equalizer is idle. It is also important to validate this behaviour during equalizing to know how the system should react in the case of a change in the shadow.

Scenario 5 - The influence of the equalizing function

Another important element of the detection is to identify the effects of the equalizing function in the current peaks. Any differences or similarities with the previous results could lead to new criteria for detection the shadow shape or SF. In addition, they should also be studied for clues to when to stop equalizing.

The equalize function was shown, in chapter 3, to induce changes the operating conditions of the cell groups. In steady-state conditions, the cell groups were found to operate at a local current, different from i_{OUT} and close to the local MPP. They will create a slight difference in equation 5.11, as shown below.

$$i_{L_k}(40\mu s) = V_{PV_k} \cdot A(40\mu s) + (i_{local_k} - i_{PV_k}) \cdot B(40\mu s) \tag{5.11}$$

Where k is the cell group over which the search is taking place. This makes the peaks no longer comparable among themselves as they represent how much energy is available, at that discharge rate, locally. However, they still bear information that can be helpful during Equalizing. Specially if the shadow was wrongly estimated.

To show how they can be used to correct the initial shadow estimation, all possible errors must be simulated and studied. The example that will be used is shown in figure 5.13(a), where cell groups PV_{III} and PV_{IV} are shaded and receiving energy from groups PV_I and PV_{II}. The other cases shown in figure 5.13 are eight possible error cases. All of the cases are equalized by a fixed BSS of $I.II \rightarrow III.IV$, represented by the arrow above the figures.

The cases are organized according to the number of shaded cell groups charging and discharging the inductor. On the first line, the reference case and errors 1 and 2 show two unshaded cell groups supporting either none, one or both shaded, respectively. The second line shows the same discharge pattern, but for a combination of one shaded and one unshaded cell group charging. Finally, the third line uses two shaded cell groups to charge the inductor, discharging over the same as before. The results will show the search peaks of each case and their interpretation using I-V curves.

The reference case in figure 5.14 show that the shadow was correctly estimated, the lower peaks corresponding to the shaded cell groups. The I-V curve shown in figure 5.14(b) illustrates how the distribution of current within the cell groups influence their local voltage. With equalizing taking place, the local current rises to its local optimum while their voltage falters. In this case, the peaks draw close together making their cross-comparison different from previous cases.

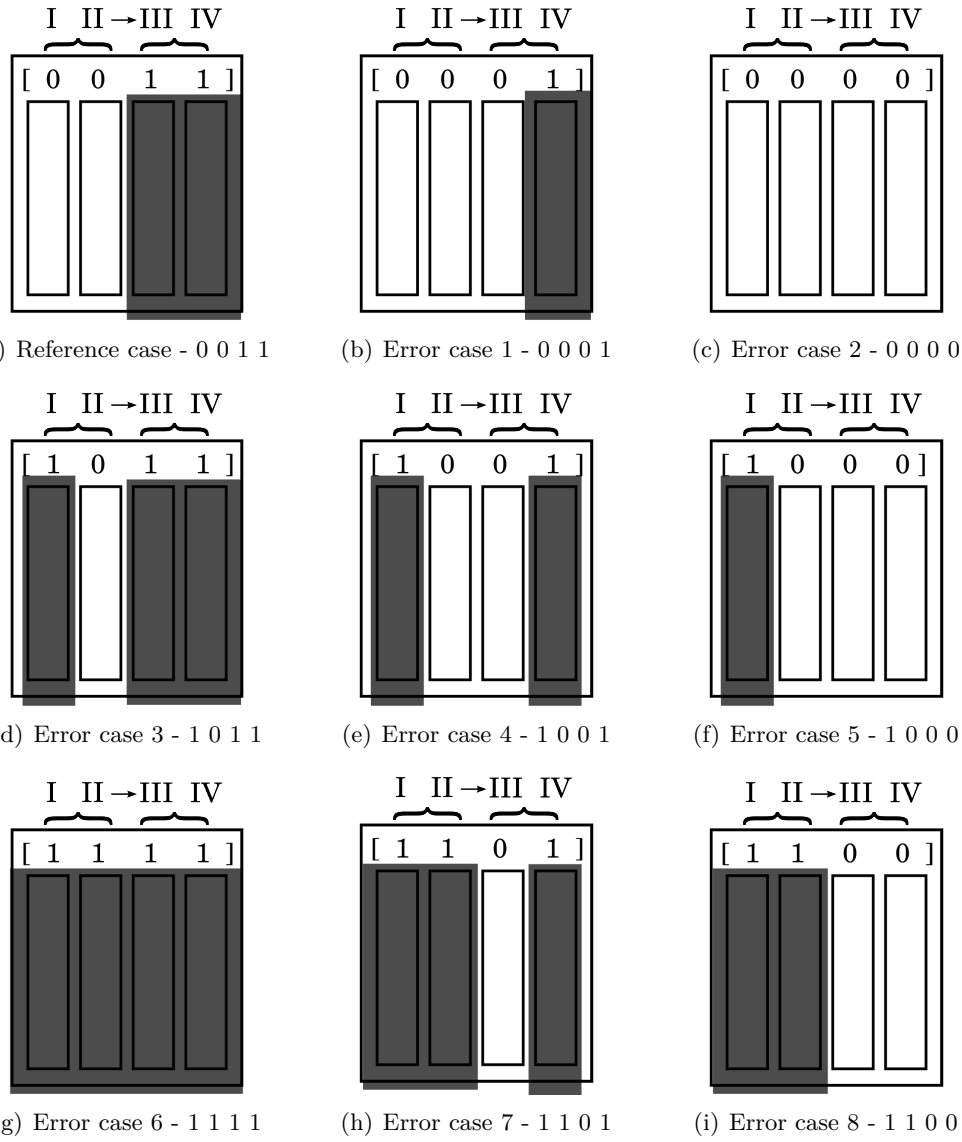

(a) Reference case - 0 0 1 1 (b) Error case 1 - 0 0 0 1 (c) Error case 2 - 0 0 0 0

(d) Error case 3 - 1 0 1 1 (e) Error case 4 - 1 0 0 1 (f) Error case 5 - 1 0 0 0

(g) Error case 6 - 1 1 1 1 (h) Error case 7 - 1 1 0 1 (i) Error case 8 - 1 1 0 0

Figure 5.13: The eight error cases

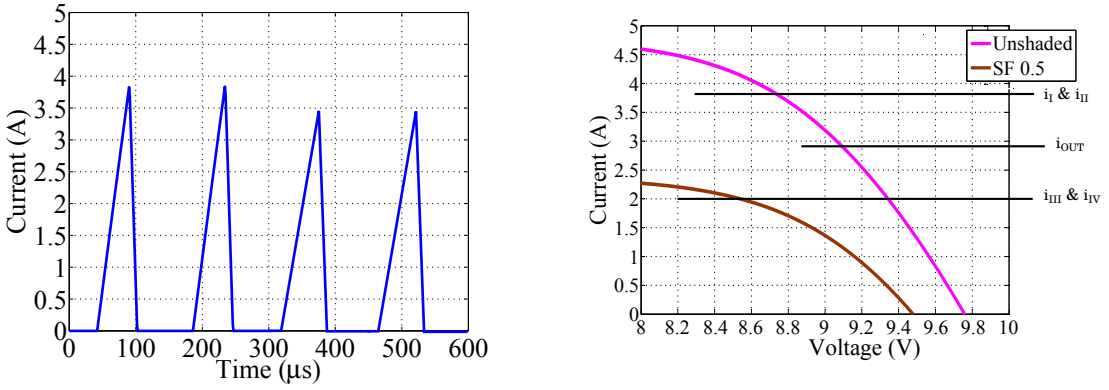

(a) Current peaks (b) Operating conditions

Figure 5.14: The results for the reference case - [0 0 1 1]

When the shadow moves away from cell group PV_{IV}, its peak becomes higher than the other three, as shown in figure 5.15(a). This is explained by the fact that its local voltage rises as the cell group is forced to operate together with cell group PV_{III}, which is shaded, due to equalizing. Thus, if a peak considered shaded becomes much higher than the others, it can be interpreted as unshaded and its state should be changed from one to zero.

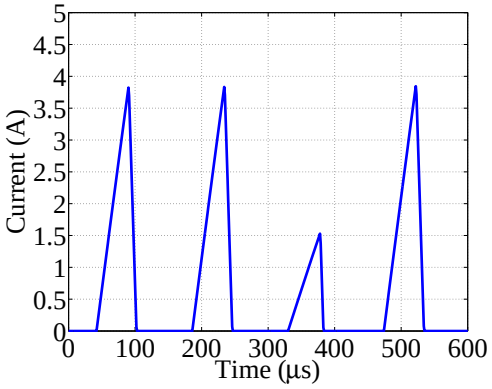

(a) Current peaks

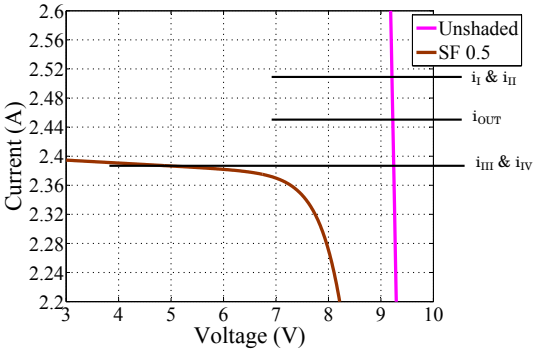

(b) Operating conditions

Figure 5.15: The results for cases 1 - [0 0 1 0]

Once the shadow is completely gone, the PV Equalizer should be able to realize it is unshaded and stop. In this case, the current peaks of the cell groups considered unshaded is slightly higher than those considered shaded, as shown in figure 5.16(a). This behavior is due to the fact that the equalizing forces their current to be different as shown in figure 5.16(b). This situation is delicate because it can also be achieved during equalizing as the duty cycle approaches its optimum. A special care should be taken when interpreting this result.

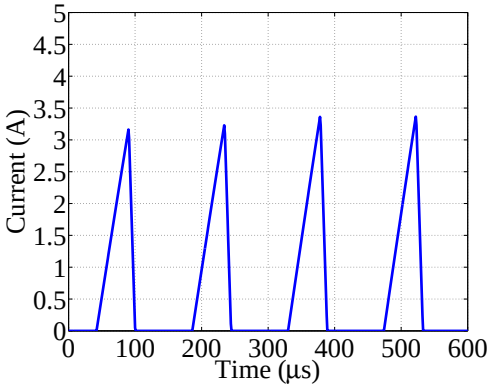

(a) Current peaks

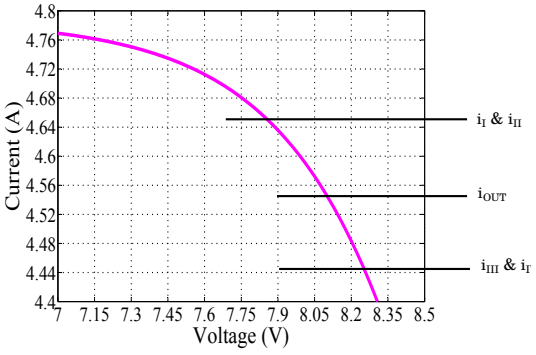

(b) Operating conditions

Figure 5.16: The results for cases 2 - [0 0 0 0]

When the shadow moves over the cell groups considered unshaded, all the peaks will react as shown in figure 5.17(a). With cell group PV_I shaded, the MPPT will track its current. As a consequence all the other peaks rise, each for different reasons. Group PV_{II}

is still unshaded and has a much higher voltage, leading to a higher peak. The i_{SH} of groups PV_{III} and PV_{IV} is forced below their MPP, leading to higher voltages and higher peaks.

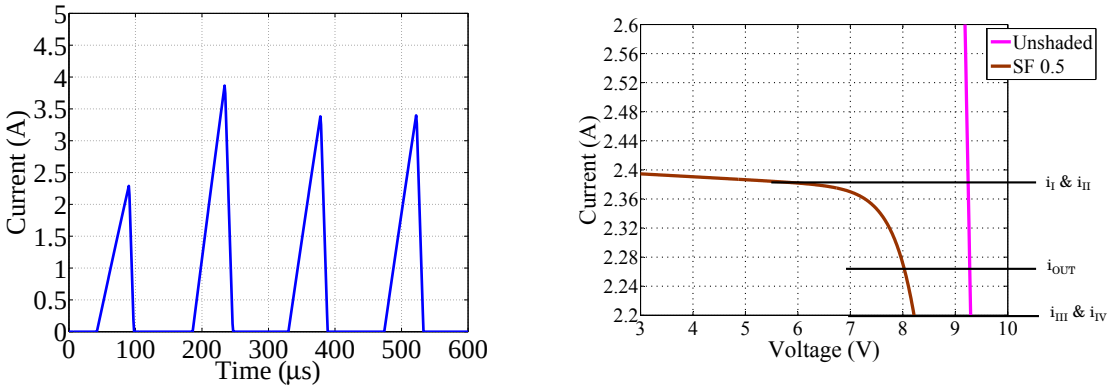

(a) Current peaks

(b) Operating conditions

Figure 5.17: The results for case 3 - [1 0 1 1]

In case 4, the shadow moves away from group PV_{IV} leading it to have more voltage and a higher peak, as shown in figure 5.18.

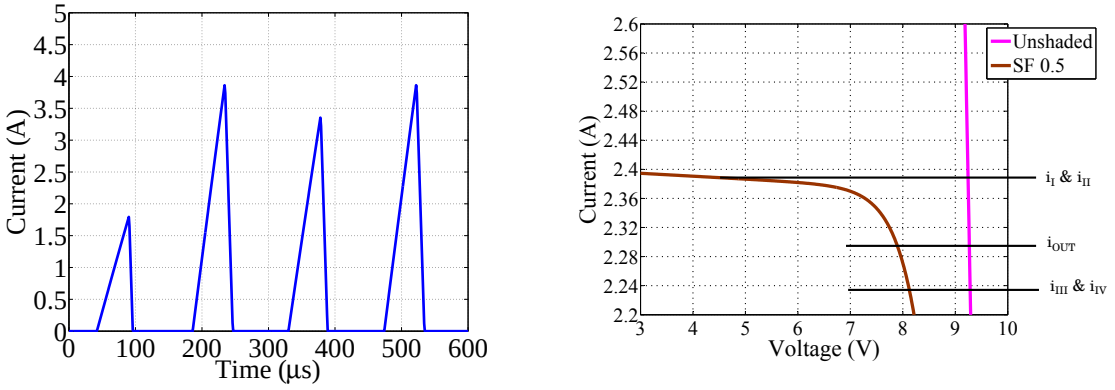

(a) Current peaks

(b) Operating conditions

Figure 5.18: The results for case 4 - [1 0 1 0]

When the shadow has moved away from both groups PV_{III} and PV_{IV}, their peaks match that of group PV_{II} for their voltage difference is below 100 mV. Cell group PV_I is still holding the i_{OUT} down and displaying a low peak due to its low voltage.

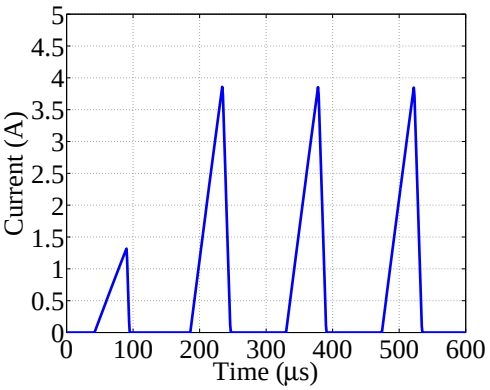

(a) Current peaks

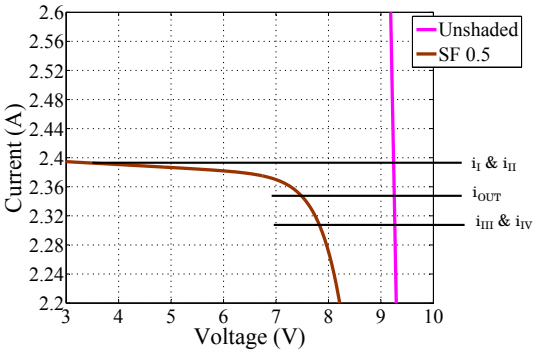

(b) Operating conditions

Figure 5.19: The results for case 5 - [1 0 0 0]

If the shadow eventually covers the totality of the PV module, equalizing becomes pointless and should also stop. Its peaks, shown in figure 5.20(a) resemble those in figure 5.14(a). In both cases, their voltages are drawn very close, making the interpretation of the peaks difficult. If equalizing is halted when the PV module is actually shaded, i_{OUT} would track again the current of the shaded cell groups and power production would fall. Thus, interpreting peaks very close to each other is tricky and should be done carefully.

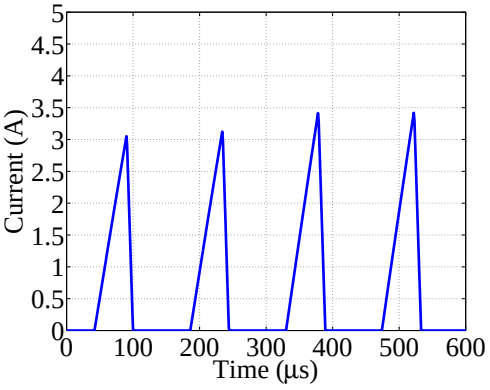

(a) Current peaks

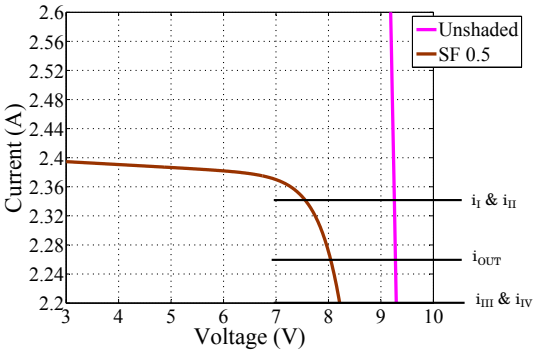

(b) Operating conditions

Figure 5.20: The results for case 6 - [1 1 1 1]

With the shadow gone from group PV_{IV}, both its voltage and current peak rise, as shown in figure 5.21. This confirms that cell groups receiving energy with peaks higher than those giving can be taken as a sign of a change in the shadow.

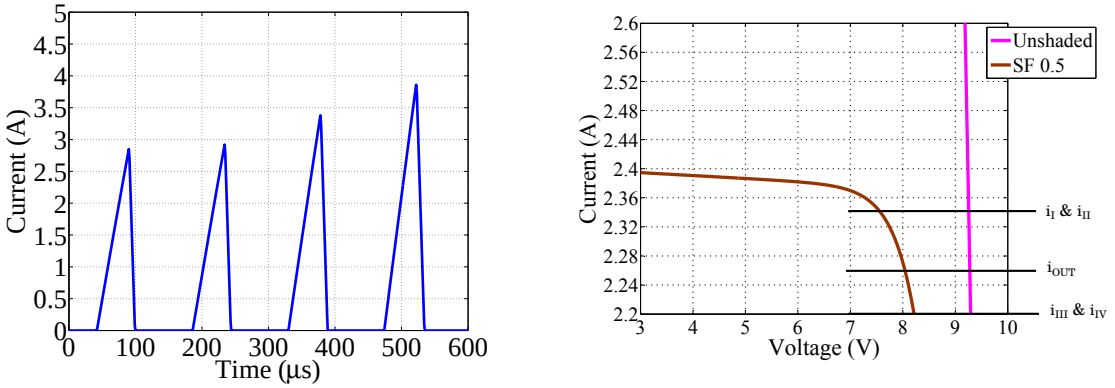

(a) Current peaks

(b) Operating conditions

Figure 5.21: The results for case 7 - [1 1 1 0]

Finally, figure 5.22 shows when the situation is totally reversed. In it, shaded cell groups find themselves supporting unshaded ones with an important consequence to their peaks. Such a high difference among them is a clear sign that the cell groups considered as zero should be switched to one and vice-versa.

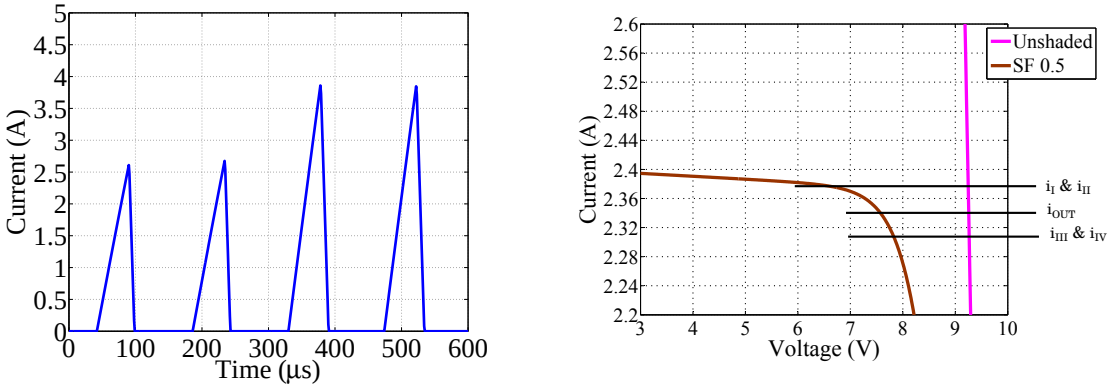

(a) Current peaks

(b) Operating conditions

Figure 5.22: The results for case 8 - [1 1 0 0]

With the interpretation of the peaks done for many different scenarios, all their results can now be summarized into a method for interpreting the current peaks.

Summary of the simulation study

The main conclusion of this study is that there is a clear difference between the interpretation of the peaks before and after equalizing.

While the PV Equalizer is idle, the current peaks give a direct estimation of the shadow shape. To do so requires a threshold to be calculated based on their value. An average between the highest and lowest peak can be used, as the example shows in figure 5.23.

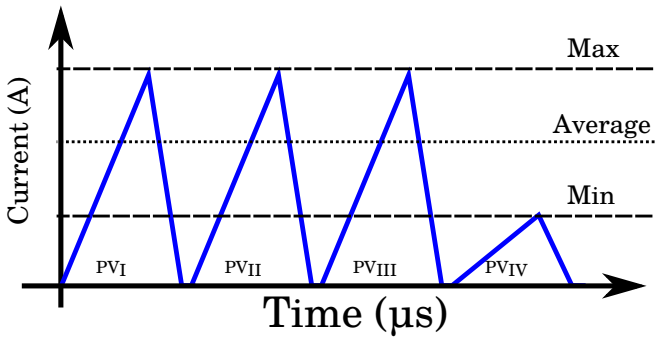

Figure 5.23: Interpretation while idle

Every peak higher than the threshold is consider unshaded, while all those below are shaded. The height of the shaded peaks can be used as a criteria to chose between Equalize and Bypass mode. Under average peaks use the first, much lower ones use the second.

If equalizing is taking place, then the interpretation of the peaks change. Their local shadow state must be taken into account and their verification is done in four steps. As an example, figure 5.24 shows peaks in the case of a switching strategy of $I.II \rightarrow III.IV$ is being used.

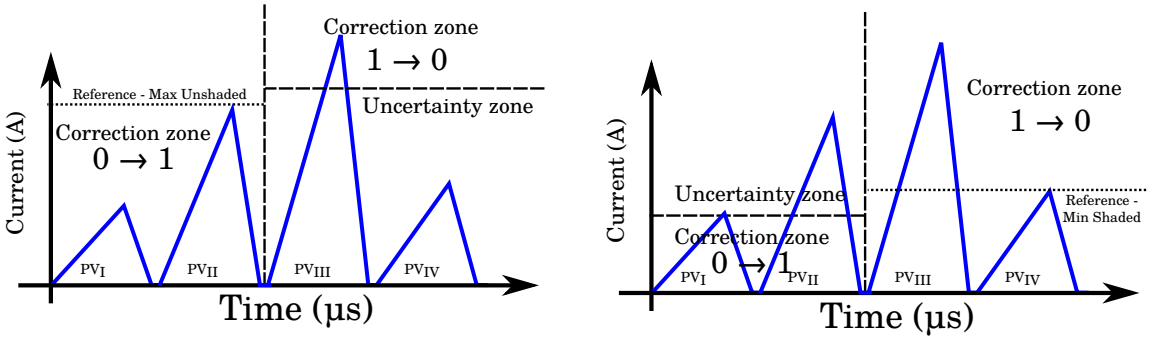

(a) Using the unshaded cells as reference

(b) Using the shaded cells as reference

Figure 5.24: Interpretation while equalizing

The first and second verifications are represented in figure 5.24(a). They are done using the highest peak value of the unshaded cell groups as a reference. The first verification is to check the peaks of the other unshaded cell groups and determine if they were wrongly estimated. In the example, cell group PV_I is much lower than the reference peak, meaning it is actually shaded. This correction is effectuated in the red correction zone, bringing the local state from zero to one. The second verification checks the peaks from the shaded cell groups. If their value is too high, they are considered as unshaded and corrected from one to zero. This is represented by the green correction zone.

The third and fourth verification steps use the lowest peak of the shaded cell groups as a reference, as shown in figure 5.24(a). They first check if any shaded cell groups are much higher than the reference, potentially indicating a zero wrongly estimated as one. This is represented by the green correction zone in figure 5.24(b). The final step is to determine

if any unshaded cell group is much lower than those shaded. This means that the local state is actually zero, and should be corrected as shown by the red zone in figure 5.24(b).

In both cases, there is a grey zone of uncertainty within which it is impossible to tell if the system is correctly equalized or wrongly shaded. If the peaks are within this zone, no action correction should be performed.

This criteria must be validated through measurements.

5.1.3 Experimental validation

The simulation study found two different criteria for interpreting the results from the current peaks. It has also determined that further studies are still necessary to determine which "short" time is better suited for the search. Thus, the objective of this experimental study is two-fold: confirm the simulations results through reproduction and determine which time is best suited for detection.

These experiments will try to reproduce as closely as possible the simulation setups and parameters. Their experimental equivalents are detailed in table 5.4. All measurements were performed under similar irradiance and temperature conditions of 600 $\frac{W}{m^2}$ and 28 ℃, respectively.

Plastic layers are used during the experiments to simulate the shadow. Their equivalent SF are characterized in detailed in Appendix B.

The first scenario reproduces the impact of the charge time in the search. The times are slightly different for the sake of simplicity of implementation, and their conclusions are considered as equivalent. The second scenario has a shading factor similar to its simulation equivalent. However, the currents are slightly different due to the irradiance available during the measurements. The third scenario has very similar conditions to the simulation. The fourth and last scenario seeks to reproduce the same shapes as in the simulations.

Scenario 1 - Variable time

The first scenario studies the impact of the charge time in the search. Unlike the simulation results, the graphs issued from the two shading factors will not be traced together, essentially due to the noise from the switching of the transistors. The results are shown in figures 5.25, 5.26 and 5.27.

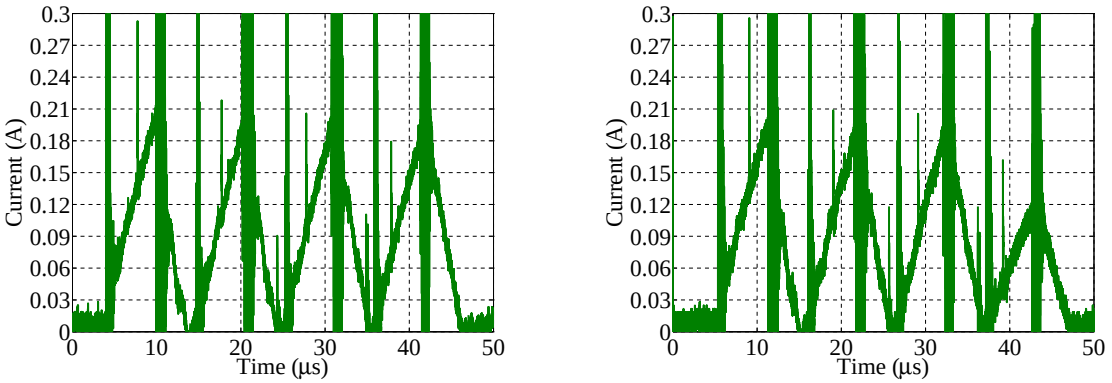

(a) 4 μs search - 0.35 SF

(b) 4 μs search - 0.56 SF

Figure 5.25: Experimental results for the variable time

Table 5.4: The four experimental scenarios

Scenario	*Variable*	*Values*
1	$ChargeTime(\mu s)$	**4, 40 and 400**
	SF	fixed - 0.56 and 0.35
	$I_{OUT}(A)$	fixed - 1.5
	Shape	fixed - 0 0 0 1
	Function	fixed - OFF
2	$ChargeTime(\mu s)$	fixed - 40
	SF	**0.78, 0.69, 0.56 and 0.35**
	$I_{OUT}(A)$	fixed - 0.5
	Shape	fixed - 0 0 0 1
	Function	fixed - OFF
3	$ChargeTime(\mu s)$	fixed - 40
	SF	fixed - 0.35
	$I_{OUT}(A)$	**0.5, 1.0, 1.5, 2.0, 2.2 and 2.3**
	Shape	fixed - 0 0 0 1
	Function	fixed - OFF
4	$ChargeTime(\mu s)$	fixed - 40
	SF	fixed - 0.56
	$I_{OUT}(A)$	fixed - 1.0
	Shape	**0010, 0101, 1011 and 0110**
	Function	fixed - OFF
5	$ChargeTime(\mu s)$	fixed - 40
	SF	fixed - 0.56
	$I_{OUT}(A)$	variable
	Shape	**0011, 0001, 0000, 1011, 1001, 1000, 1111, 1101 and 1100**
	Function	fixed - Equalize

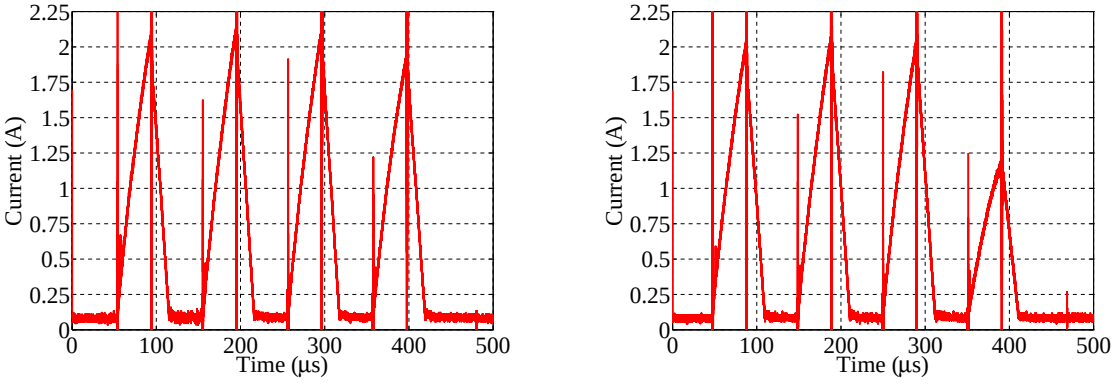

(a) 40 μs search - 0.35 SF

(b) 40 μs search - 0.56 SF

Figure 5.26: Experimental results for the variable time

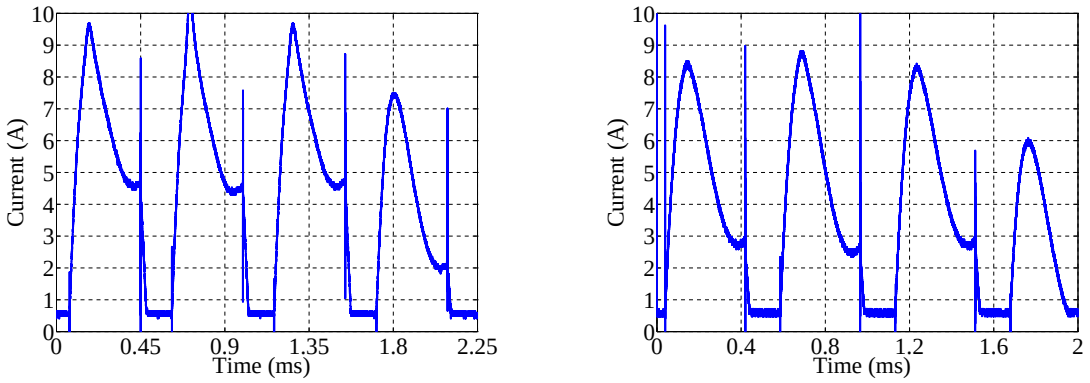

(a) 400 μs search - 0.35 SF

(b) 400 μs search - 0.56 SF

Figure 5.27: Experimental results for the variable time

In an overall analysis, the same SF has a proportionally similar impact in all the charge times, showing that the voltage has a major impact on the peaks. It is also clear that the higher SF is easier to detect than the lower one.

These figures also provide the final criterion to choose the charge time for the search function. The noise due to the switching of the transistors has an important impact over the fastest search, as shown in figure 5.25(a). This is mitigated for 40 μs search, as shown in 5.25(b). Combining a reduced impact over the voltage, a range within the scope of the short circuit current of the PV module (5 A) and a higher resistance to noise, the 40 μs search is the natural choice for the search.

Another important aspect brought forth by the noise is the moment when the reading should take place. To avoid the switching noise, the reading should happen slightly before or right after it.

Scenario 2 - Variable SF

The second scenario reproduces impact of SF variations over the current peaks. Its results are shown in figure 5.28.

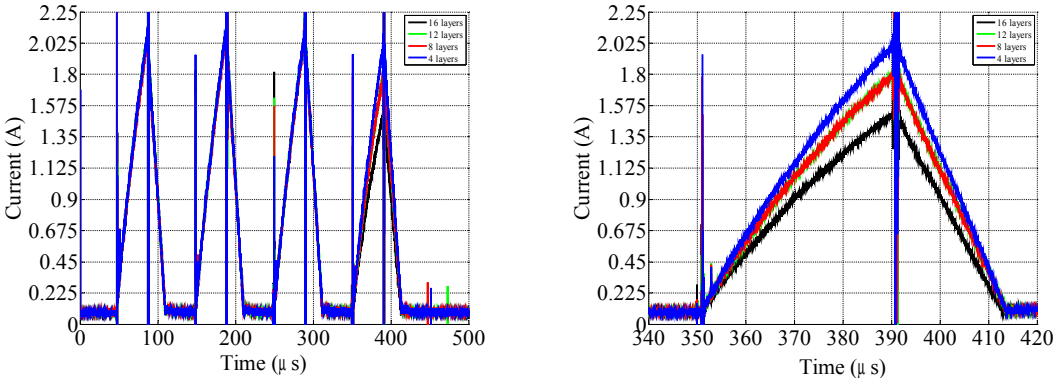

(a) Overall results

(b) The shaded cell group

Figure 5.28: Experimental results for the variable SF

The current peaks of all cell group are shown in figure 5.28(a), the shaded one being located on the right. Its details are shown in figure 5.28(b).The intermediate SF are all

bundled together while the lowest and highest ones are well separated, making any precise estimation of the SF very difficult. These results confirm that the closer i_{OUT} is from the i_{PV} of the shaded cell group, the easier the detection becomes.

Scenario 3 - Variable i_{OUT}

The study of the influence of i_{OUT} in the variations of the search current peaks is shown in figure 5.29.

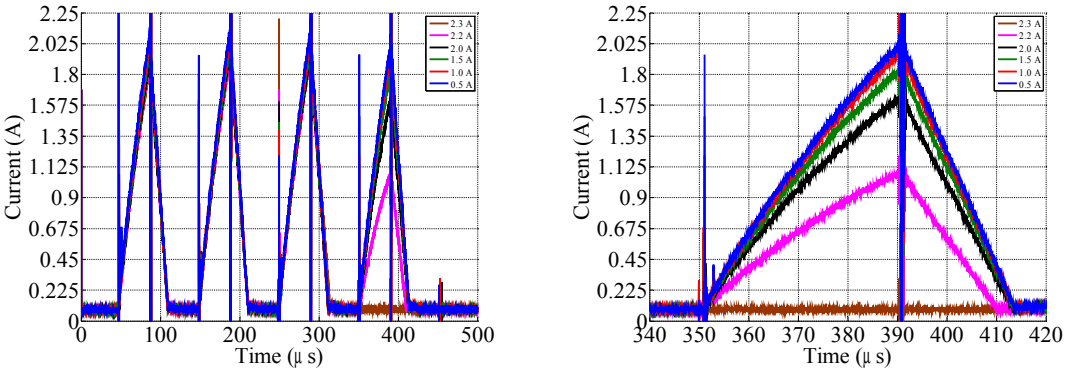

(a) Overall results

(b) The shaded peak

Figure 5.29: Experimental results for the variable i_{OUT}

The four peaks are shown in figure 5.29(a), and detailed further in figures5.29(b).As i_{OUT} draws closer to the i_{PV} of the shaded cell group, its peak lowers, suddenly disappearing between currents 2.2 A and 2.3 A. These results confirm the simulations.

Scenario 4 - Variable shape

The same 4 shadows shapes are used to validate the simulation results, as shown in figure 5.30.

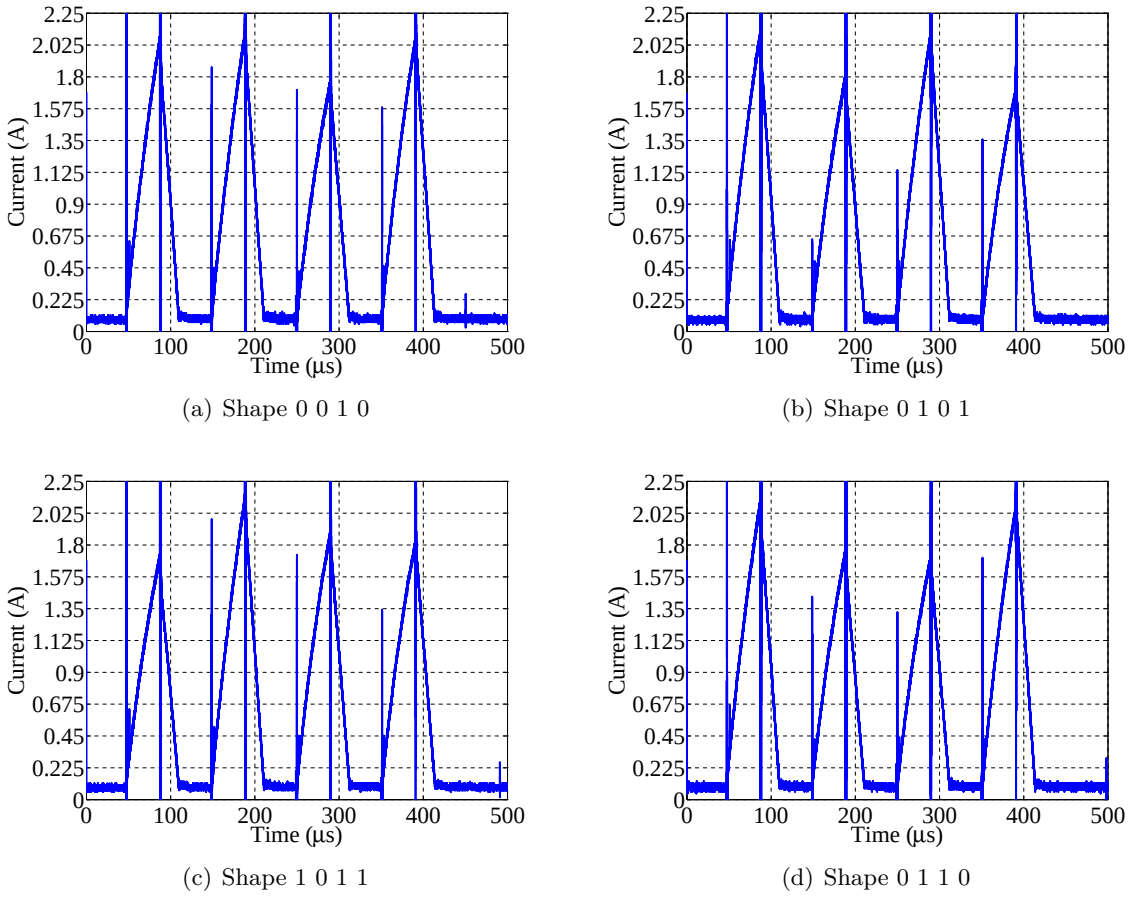

(a) Shape 0 0 1 0

(b) Shape 0 1 0 1

(c) Shape 1 0 1 1

(d) Shape 0 1 1 0

Figure 5.30: Experimental results for the variable shapes

All the shadow shapes can be clearly detected by a margin of nearly 300 mA. This validates the use of the binary model in the representation of the shadow.

Scenario 5 - Equalize function

The experimental results for the influence of the equalize function on the current peaks are shown in figure 5.31. The reference case is the same, where cell groups PV_I and PV_{II} are giving energy to cell groups PV_{III} and PV_{IV}. The BSS used is fixed at $I.II \rightarrow III.IV$.

The same patterns are shown in all cases, confirming the interpretation of the peaks deduced from the simulation results. However, the current peak from cell group PV_I is shown to be systematically lower than its counterparts, indicating a potentially smaller capacitor. Such imperfections must be taken into account when designing the control system of the PV Equalizer.

Finally, all the conclusions from the simulations and theoretical studies are considered as confirmed, which allows to proceed to a general summary of this section.

5.1.4 Summary of the results

The search study was conducted to understand how four different variables can impact the search technique. The inductor charge time, the shading factor, the shadow shape and the output current. They have been studied in a series of theoretical, simulation

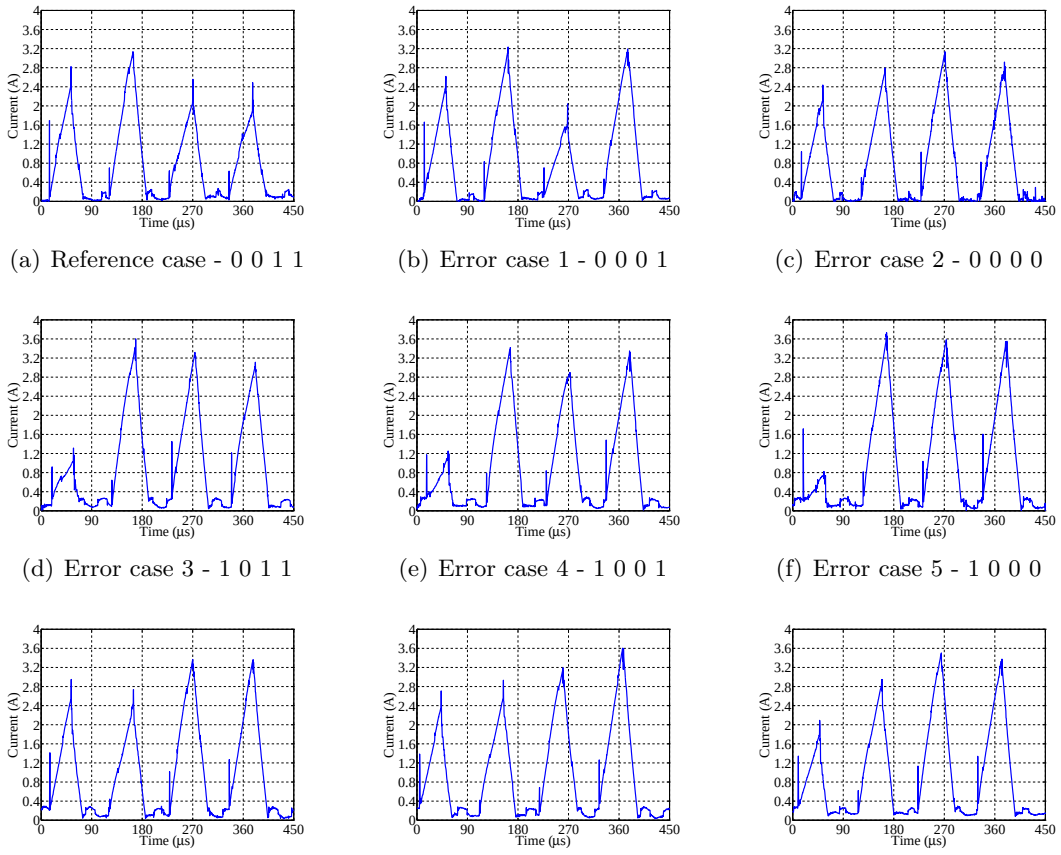

(a) Reference case - 0 0 1 1 (b) Error case 1 - 0 0 0 1 (c) Error case 2 - 0 0 0 0

(d) Error case 3 - 1 0 1 1 (e) Error case 4 - 1 0 0 1 (f) Error case 5 - 1 0 0 0

(g) Error case 6 - 1 1 1 1 (h) Error case 7 - 1 1 0 1 (i) Error case 8 - 1 1 0 0

Figure 5.31: The experimental validation of the eight error cases

and experimental studies. Taking their conclusions into account, the questions from the beginning of this section can now be answered.

- *What is the effect of the duration of the charge over the current peaks?*

  The charge time has an important impact in the components of the PV Equalizer and the power production of the PV module. Longer searches bring the voltage of the cell group close to zero and require a total discharge of the capacitors. It may lead to an important current overshoot in the inductor, stressing it in terms of current. Shorter searches can be used to avoid this current overshoot, but allow only the detection of the shadow shape. Finally, the choice of the search time will have an impact in both the design of the PV Equalizer and its control system. .

- *How do the shading factor and the shadow shape influence the current peaks? Can their effects be easily discerned?*

  The current peaks were found to be dependent, at the same time, from the SF and the i_{OUT}. Similar peaks were read for different SFs, making its direct estimation difficult. By comparing i_{OUT} and the PV module short circuit current at the moment the peaks react the most may give a rough estimation of the SF. The shape can be found by cross-comparison between the current peaks, making it much easier to detect than the shading factor.

- *How does the output current influence the current peaks?*

  At MPP, i_{OUT} is considered very close to i_{MPP} and the current peak corresponding to the shaded cell group will be smaller compared to the others. Thus, detection of the shadow shape is guaranteed. If the MPPT is in a transitory state away from its MPP, then the search might be completely ineffective. The Equalizer must wait for a steady state before conducting a search.

- *How does the equalize function influence the current peaks?*

  The method for interpreting the current peaks changes when the equalize function is active. This is largely due to the fact that the currents of the shaded and unshaded cell groups will be different and close to their local i_{MPP}. Furthermore, if the shadow changes during equalizing the peaks can be used, to a certain degree of precision, to detect these changes and change the switching strategy accordingly. Figure 5.24 in page 147 explains the method for interpreting them in detail.

Other less intrusive methods are also proposed in this work.

5.2 Semi-Direct shadow diagnosis: observing variables

The direct shadow diagnosis was shown to be an intrusive but precise method for assessing the existence of shadows in the PV module. It has, however, an uncertainty zone within which no conclusion can be drawn about the shadow. This could lead to situations where the PV Equalizer would be unable to determine if it should turn itself back to idle, potentially wasting energy in the process. Moreover, the recurrent use of the search function may lead to delays between the manifestation of the shadow and the reaction of the PV Equalizer. In order to solve these issues, another diagnosis method is proposed in this section.

The semi-direct diagnosis is based on the observation of electric variables to deduce changes in the shadow state and studied through the following question:

- *How are the electric variables of the PV module affected by changes in the shadow?*

  Considering the shadow as a phenomenon spanning several minutes, observing electric variables linked to it may avoid useless searches. However, it is important to determine which variables can be observed and what does their behavior correspond to in terms of shadow movement.

A theoretical study will be conducted to determine which variables should be observed, followed by an experimental validation.

5.2.1 Theoretical study

The shadow movement is a succession of changes in the shadow state. To go from one state to another implies a change either in the shading factor or in the width of the shadow. Sometimes even both. This makes any electric variable directly affected by them is a potential candidate for observation.

Observing variables brings forth the important issue of time span and their relation. Shadow movement can be considered as dependent on the Sun, spanning several dozen of seconds or minutes. Voltages and currents are several orders of magnitude faster, changing in a matter of micro or miliseconds. Thus, it is the evolution of the *average and steady-state values* of the electric variables that must be observed.

To assess which variable is better suited for being used, the electric variables of the PV Equalizer are listed and evaluated in table 5.5. Where $\overline{V_{out}}$ and $\overline{i_{OUT}}$ stand for the average output voltage and current. Those in the shaded cell groups are represented by $\overline{V_{SH}}$ and $\overline{i_{SH}}$ and their unshaded counterparts are represented by $\overline{V_{USH}}$ and $\overline{i_{USH}}$. The duty cycle is represented by D, while the shading factor is represented by SF. The losses during charge and discharge are represented by $V_{losses_{CH}}$ and $V_{losses_{DCH}}$.

Table 5.5: The electric variables of the Equalizer

Electric Variable (ref.)		*Information*
$\frac{\overline{V_{USH}} + V_{losses_{CH}}}{\overline{V_{SH}} + V_{losses_{DCH}}} = \frac{(1-D)}{D}$	(5.12)	The voltage distribution among the cell groups depends on the duty cycle.
$\overline{V_{out}} = \frac{\overline{V_{USH}}}{(1-D)}$	(5.13)	The output voltage depends on the voltage of the unshaded cell group and the duty cycle.
$\overline{i_L} = SF \cdot \overline{i_{USH}}$	(5.14)	The current in the inductor is directly dependent on the shading factor and the current in the unshaded cell group.
$\overline{i_{OUT}} = (1 - SF \cdot D) \cdot \overline{i_{USH}}$	(5.15)	The output power is dependent, at the same time, on the shading factor, the duty cycle and the current in the unshaded cell group.

All voltages present no direct information about either the SF or the shadow width. They are rather dependent on the value of the output current and the duty cycle, requiring their knowledge for comparison.

The inductor and output currents are directly linked to the shading factor, making them good candidates for observation. However, neither seem to have a direct relation to the shadow width. To find out which variable carries indirect information about it, an example is proposed in figure 5.32.

The shadow is at first confined to cell groups PV_{III} and PV_{IV} in figure 5.32. It then moves over cell group PV_{II} in figure 5.32(b). The PV Equalizer is active and equalizing by using a fixed switching strategy of $I.II \rightarrow III.IV$.

When the shadow expands, its width is considered to rise over time having a positive time variation. Its new state now covers cell group PV_{II} which is being used to charge the inductor, denoted by a red "X" over it. With the expansion of the shadow width, a cell group which was previously considered unshaded becomes shaded. This can be translated, in terms of electric variables, as a reduction of $\overline{i_{USH}}$. Thus, observing the evolution of $\overline{i_{USH}}$ over time is an indirect way of observing the evolution of the shadow width.

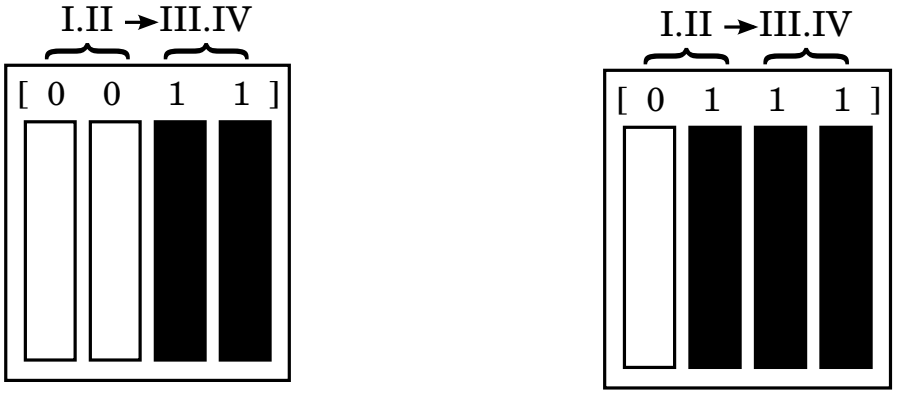

(a) Initial shadow state

(b) Shadow state after expansion

Figure 5.32: Example of a variation in the shadow width

Both the mean inductor and output currents are affected, at the same time, by the shading factor and the current of the unshaded cell group. This makes it necessary to observe both together and cross comparing their results to deduce if its is the SF or the shadow width that changes. Their dynamic behavior is be expressed by equations 5.16 and 5.17.

$$\Delta\overline{i_L} = \Delta SF \cdot \overline{i_{USH}} + SF \cdot \Delta\overline{i_{USH}} \tag{5.16}$$

$$\Delta\overline{i_{OUT}} = (1 - SF \cdot D) \cdot \Delta\overline{i_{USH}} - D \cdot \overline{i_{USH}} \cdot \Delta SF \tag{5.17}$$

Once again is important to remember that *both equations denote variations in average currents* and that their behavior is considered as *changing slowly* over time. Variations in the duty cycle will be considered as too fast and ignored in this analysis.

The minus sign in equation 5.17 shows that the influence of the shadow over the currents is not the same. It can be expected, then, that they will have a complementary behavior which can be used to clearly distinguish changes in the shadow width from those in the shading factor. Their cross analysis will be conducted by systematically considering a part of their equation as fixed and allow the others to vary. As a first approach, variations in the shading factor, or ΔSF, will be considered zero, giving equations 5.18 and 5.19.

$$\Delta\overline{i_L} = SF \cdot \Delta\overline{i_{USH}} \tag{5.18}$$

$$\Delta\overline{i_{OUT}} = (1 - SF \cdot D) \cdot \Delta\overline{i_{USH}} \tag{5.19}$$

In this case, both $\overline{i_{OUT}}$ and i_L will rise or fall together with $\overline{i_{USH}}$ since SF is fixed. If both current rise, the shadow width is shrinking. For example, going from [0011] to [0001]. On the contrary, when both current fall the shadow width is expanding, as from [0011] to [0111].

If the variations in the current of the unshaded cell group, or $\Delta\overline{i_{USH}}$, are considered zero, the equations 5.16 and 5.17 become:

$$\Delta\overline{i_L} = \Delta SF \cdot \overline{i_{USH}} \tag{5.20}$$

$$\Delta\overline{i_{OUT}} = -D \cdot \overline{i_{USH}}\Delta SF \tag{5.21}$$

Now, the $\overline{i_{OUT}}$ and $\overline{i_L}$ will have complementary behaviors, depending on the variation of the shading factor. If $\overline{i_{OUT}}$ rises and $\overline{i_L}$ falls, the shading factor is diminishing. On the contrary, when $\overline{i_{OUT}}$ falls and $\overline{i_L}$ rises, the shading factor is rising. In both cases, the shadow width remains constant.

If either only $\Delta\overline{i_{OUT}}$ or only $\Delta\overline{i_L}$ is zero, then the dynamic behavior of the system is physically inconsistent during equalizing. While idle, however, there is no current in the inductor and only the output current mean value can be observed. Its expression is different, given by equation 5.22.

$$\Delta\overline{i_{OUT}} = \Delta\overline{i_{USH}} \tag{5.22}$$

In this case, the MPPT is considering all cell groups unshaded. Thus, if the output current falls suddenly, it means a shadow has appeared.

Summary of the theoretical analysis

To summarize this analysis, table 5.6 resumes the conditions in which the currents vary over time during equalizing.

Table 5.6: Correlation between the shadow and the currents durring equalizing

	$\Delta\overline{i_L} > 0$	$\Delta\overline{i_L} < 0$
$\Delta\overline{i_{OUT}} > 0$	$\Delta\overline{i_{USH}} > 0$ $\Delta SF = 0$	$\Delta\overline{i_{USH}} = 0$ $\Delta SF < 0$
$\Delta\overline{i_{OUT}} < 0$	$\Delta\overline{i_{USH}} = 0$ $\Delta SF > 0$	$\Delta\overline{i_{USH}} < 0$ $\Delta SF = 0$

Its interpretation in terms of movement is detailed in table 5.7.

Table 5.7: Shadow movements based on current changes during equalizing

	$\Delta\overline{i_L} > 0$	$\Delta\overline{i_L} < 0$
$\Delta\overline{i_{OUT}} > 0$	The shadow width is shrinking and its SF is constant.	The shadow width is stopped and its SF falling.
$\Delta\overline{i_{OUT}} < 0$	The shadow width is stopped and its SF is rising.	The shadow width is expanding and its SF is constant.

When the shadow width is expanding or shrinking, a search could be triggered to check its the new state. If only the shading factor is changing, corrections in the duty cycle during equalizing should suffice to handle it.

In order to validate these tables, an experiment will be conducted.

5.2.2 Experimental study

This experimental study has the objective of confirming the correlations between the variations in the shadow, the output current and the inductor current. To do so a particular shadow setup will be used and its results will consist of a trace over time of the output and inductor currents.

Shadow setup

The experiment will use a fixed BSS of $I.II \rightarrow III.IV$. The shadow described in figure 5.33 is composed of four parts. The first and last are dedicated to changes in the shading factor, while the second and third are to changes in the shadow width. The decomposition of the shadow over time is shown in figure 5.33 and its corresponding time trace in figure 5.33(c).

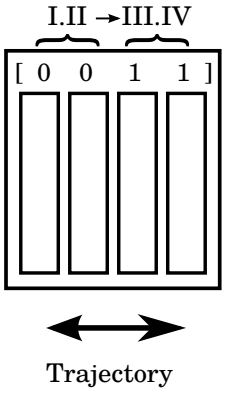

(a) Overview of the shadow state studied

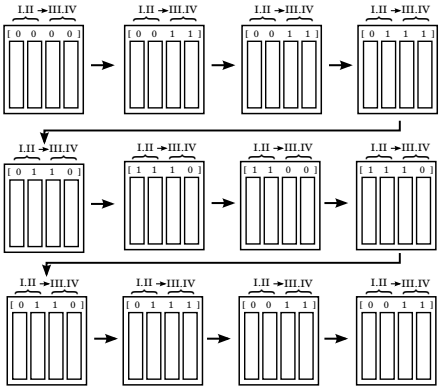

(b) Decomposition of the shadow

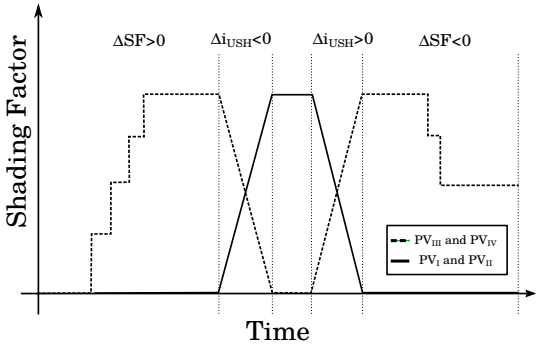

(c) Shading factor variation over time

Figure 5.33: The shadow movement studied

The temperature of the module was 51.3 ℃ and the ambient temperature was 32.5 ℃. The irradiance received was 813 $\frac{W}{m^2}$ and the SF varied from 0.21 to 0.56.

Experimental results

The results are shown in figure 5.34.

At first, the MPPT takes its time to find the MPP with no shadow, as shown between 0 and roughly 30 seconds. Once the MPP is found, only a small current is flowing through the inductor.

The first part of the curve, between 60 and 120 seconds, shows the appearance of the shadow and its shading factor rising over time. During this part, the average inductor current rises while the average output current falls, as expected.

The second and third parts, between 120 and 168 seconds, show both currents falling and rising together. In this part, the shadow was moved back and forth, from cell groups PV_I and PV_{II} to groups PV_{III} and PV_{IV}.

Finally, in the fourth part from 168 to 220 seconds, the shadow was removed and the MPPT found the original MPP again.

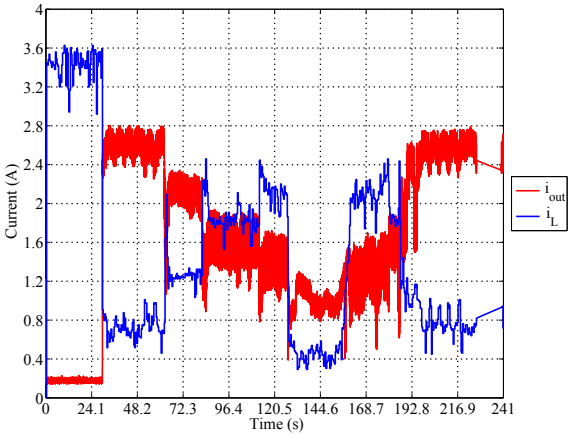

Figure 5.34: The experimental results

These results confirm the use of the average inductor and output currents to observe changes in the shadow over long spans of time. They should be used during the conception of the control algorithm as an alternative to the direct diagnosis mode.

5.2.3 Summary of the semi-direct detection

The semi-direct diagnosis is a less intrusive method for detecting the presence of the shadow. It is based on the observation of the average values of the inductor and output currents, allowing the PV Equalizer to monitor the evolution of the shadow in real-time with little energy cost.

Two variables were found to carry information about the shadow: the inductor and output currents. Both are affected by the shading factor and the shadow width at the same time. However, their cross-comparison can be used to clearly distinguish which change in the shadow is taking place. The correlation is clearly shown in table 5.7 in page 157.

Still, this method uses the search to determine the changes in the shadow width. Could these changes be anticipated with a certain precision, no search would be required at all. This possibility is explored further in the next section.

5.3 Indirect shadow diagnosis: deducing changes

The direct and semi-direct diagnosis methods rely on the sampling of the energy state within the cell groups to estimate the presence of the shadow. While the first does so recurrently, the second observes the mean inductor and output currents in order to determine when is the best moment to trigger a search. Neither approach considers any prior knowledge of the shadow. Furthermore, both direct and semi-direct methods consider, implicitly, that all shadow states are equally likely to occur anytime.

But with shadows being guided by the Sun and objects around the PV module considered fixed, there is a likelihood that their behavior is not totally random. This section

seeks to study the shadow and its propagation over the PV module to determine how closely linked the shadow states are. Its studies are guided by the following question:

- *Is there any general rule to the shadow behavior? If so, how can the Equalizer predict it?*

  By describing a general rule for the shadow behavior, the PV Equalizer could anticipate expansions or contraction in the shadow width and automatically change its switching strategy. It could mean, eventually, dispensing the use of searches to ambiguous cases.

To answer this question, a theoretical study of the shadow movement with the shadow model will determine correlations among the 16 binary states of the PV module used in this work. It will be followed by the observation of a natural shadow and its impact on the MPP of the PV module to validate its premises.

5.3.1 Theoretical study

This theoretical study seeks to determine, through the evaluation of movement scenarios involving different shadow shapes, the correlation between the 16 binary shadow states. The shadow shapes were chosen to reflect the possible widths of the shadow and its eventual discontinuities and are shown in figure 5.35.

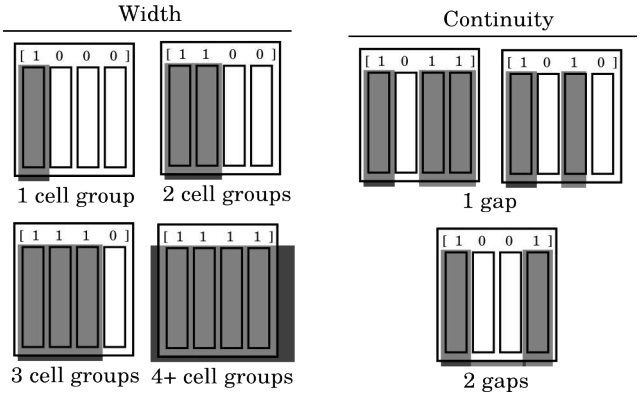

Figure 5.35: The shadows used in this theoretical study

In terms of movement, two types were studied: translation and rotation. The first refers to fast shadows, such as clouds, passing over the PV module, while the second are related to static shadows. Two examples are described in figure 5.36.

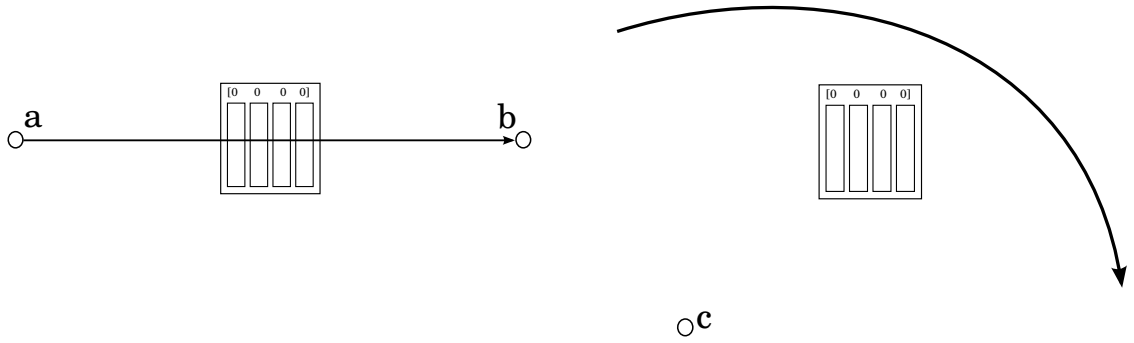

(a) Translation movement (b) Rotation movement

Figure 5.36: The two types of movement

Translation movement requires a path, in figure 5.36(a) represented by the arrow going from point a to b. Rotation requires a pivot point, which is represented by point c in figure 5.36(b). The states that compose their movement are given in figure 5.37.

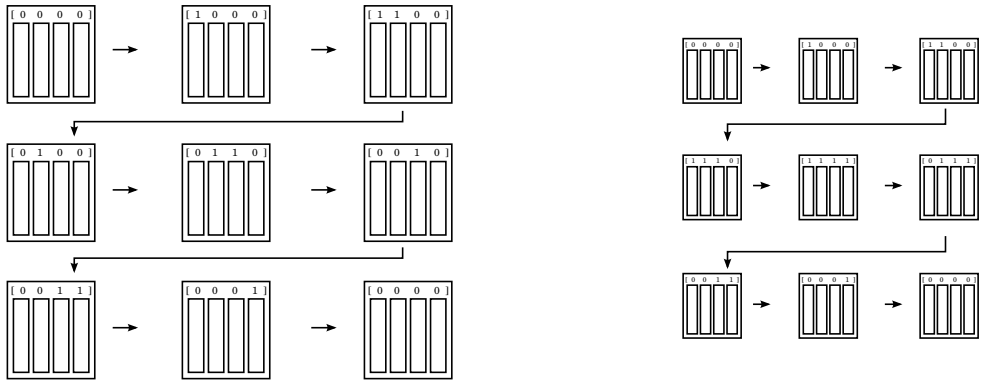

(a) Decomposition of the translation movement (b) Decomposition of the rotation movement

Figure 5.37: The decomposition of the shadow movement

To simplify the representation of the states, a more compact representation method is shown in figure 5.38. The shadow states are shown within circles and disposed in a way that non-contiguous shadows are either within or outside of the circle formed in figure 5.38(b).

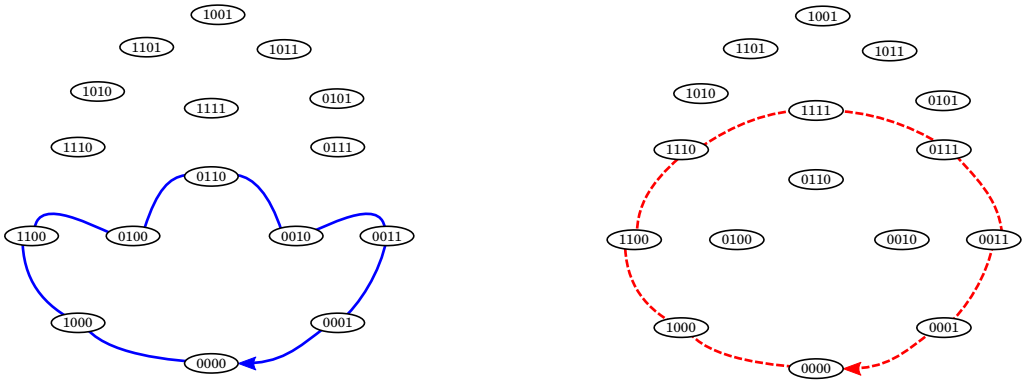

(a) The translation movement in compact notation (b) The rotation movement in compact notation

Figure 5.38: Compact shadow state representation

All the seven types of shadows were studied, their results are shown in figure 5.39 according to the type of movement.

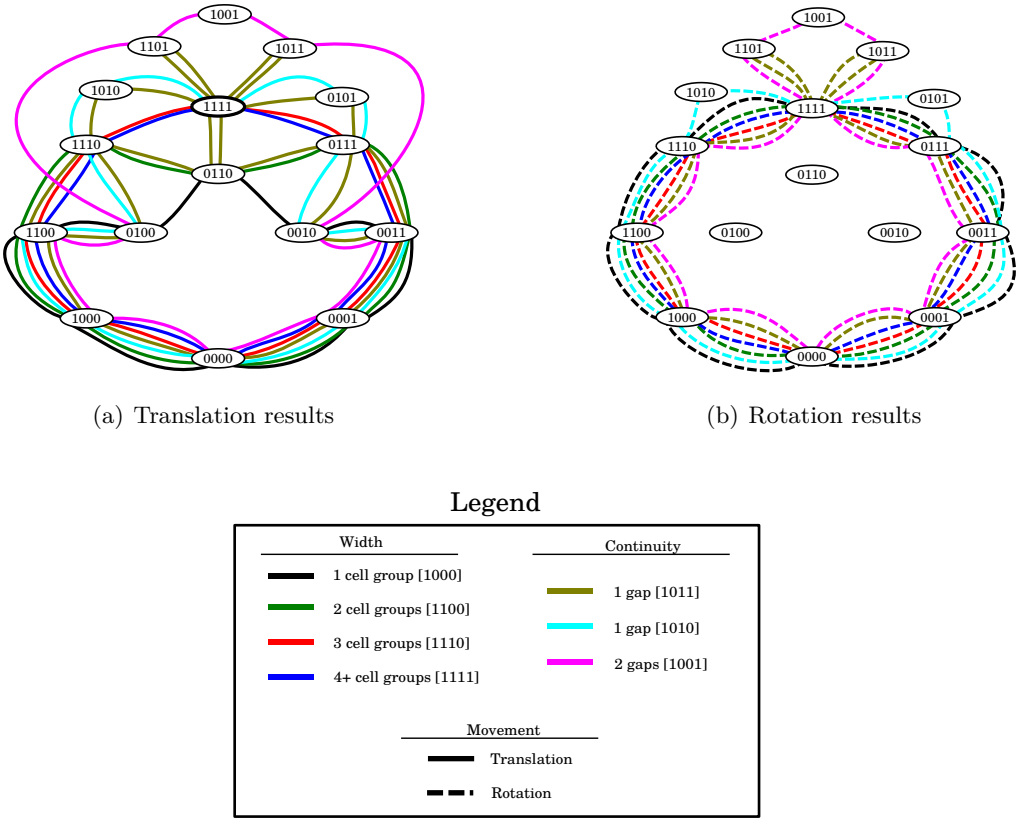

(a) Translation results (b) Rotation results

(c) Color legend of the figures

Figure 5.39: The theoretical results of shadow movement

It is possible to see that both the translation and rotation are characterized by a full turn of the circle composed by the contiguous states. Non-contiguous shadows states are

more used by the translation than by the rotation. These results show that there are a certain number of base states which are used by all the shadows studied while others are rarely used, if not at all. Using these cases as a base to estimate the probability of transition between states yields the Markov chain model shown in figure 5.40. The red lines compose what can be considered as the most probable path of the majority of shadow scenarios. The blue lines are other less likely but still probable scenarios. The green lines represent rare transitions, that are very specific to certain locations and objects projecting the shadow.

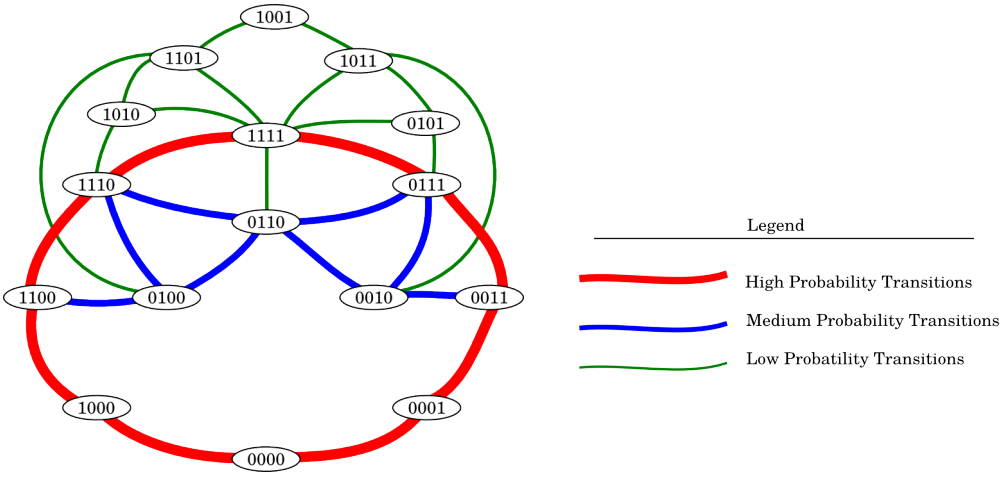

(a) The final result (b) Color legend

Figure 5.40: The assembled results from the shadow study

Using this model as a reference, the movement of a natural shadow will be studied in the next section. Its objective is to ascertain the basic principles of shadow movement upon which the model was built.

5.3.2 Experimental validation: Natural shadow observations

Observing natural shadows is a challenging feat that requires observing the right PV system, at the right time with the right equipment. With these conditions in mind, the observation of the reference PV module are conducted in two parts.

The first part is to find the right time to observe the shadow. In this phase consist of constantly tracing the I-V curves of the PV module during a bright and cloudless day during regular intervals of several minutes. The only disturbances will be due to the presence of static shadows giving a good indication of what is the best time window to observe their movement into more detail.

The second part is to observe the shorter time window in detail. Based on the results of the first part, I-V curves will be traced in intervals of 10 seconds during a shorter time window. Its analysis will give a clear evolution of the shadow shape over time and help determine if it follows a similar path given by its Markov Chain.

During this experiment, the PV module will be equipped with bypass diodes. Their use allows a clear view of the shadow width through I-V traces.

The PV module used in this results for the first part are given in figure 5.41. It traces the MPP current and voltage for each I-V curve measured during the day. There are two clear reductions before 11:00 and around noon.

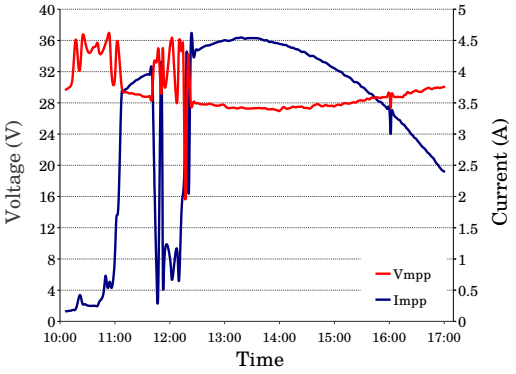

Figure 5.41: The MPP variation during the day

The results from the second part are concentrated between 10:30 and 13:00. Again I-V curves are traced, but this time every 10 seconds to extract the evolution of the MPP with the shadow. The results are shown in figure 5.42.

Three periods can be distinguished from the evolution of the MPP. Before 11:30, when the shadow is covering the totality of the module with small oscillations in power production. Between 11:30 and 11:50 when the shadow is clearly moving away from the PV module. After 11:50 when the shadow is present but does not seem to activate the bypass diodes. The second period is studied further to observe the transitions in the shadow.

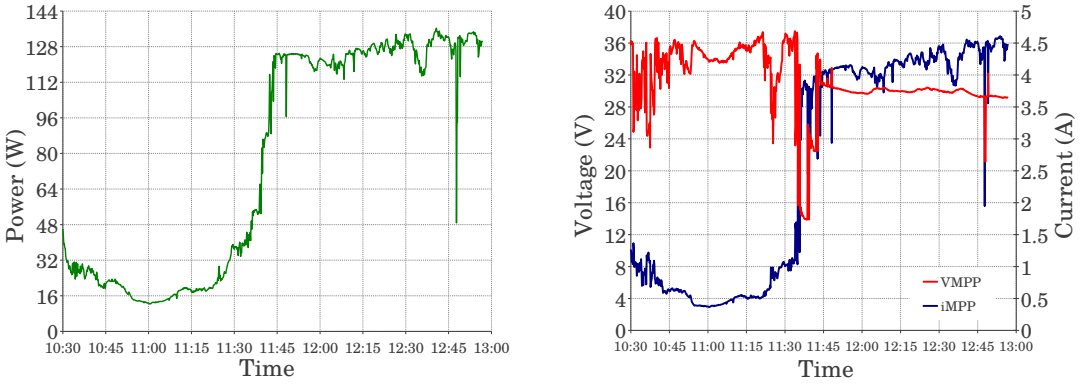

(a) MPP variation

(b) MPP current and voltage variation

Figure 5.42: The MPP variation during a shorter window of time

Figure 5.43 zooms in between 11:30 and 11:45. It puts into evidence, through colored circles, clear voltage steps that show transitions in the shadow. It employs certain colored circles which will be described further below.

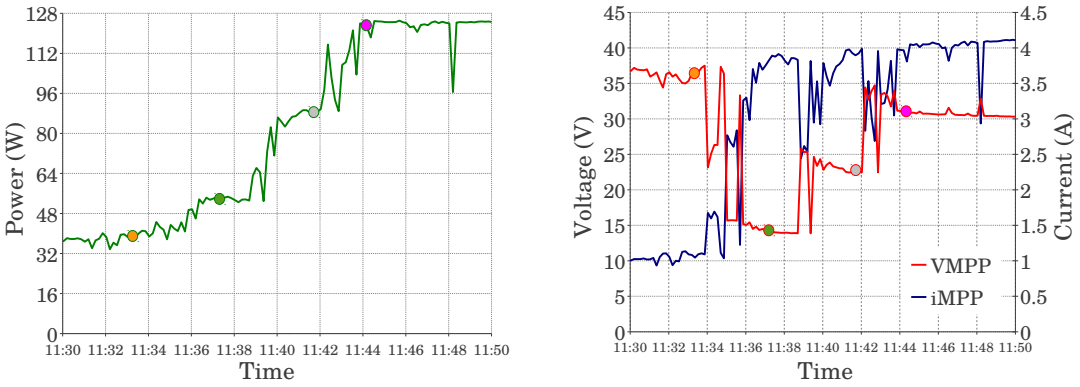

(a) MPP variation

(b) MPP current and voltage variation

Figure 5.43: The MPP variation during shadow transition

The steady rise in power production is characterized by steps, as can be seen in its voltage curve. Some specific time windows can be picked as examples. For instance, 11:36 to 11:38, 11:40 to 11:42 and 11:44 to 11:50. Among these steps are oscillating transitions, as can be seen in the time windows 11:34 to 11:36, 11:38 to 11:40 and 11:42 to 11:44. These were caused by the wind that shook the tree during the measurements. Four colored circles highlight moments which the system can be considered stable between oscillations. Their I-V curves serve to study the steady-state evolution of the shadow. The result, matching the colors used in the circles, are shown in figure 5.44.

The evolutions of the I-V curves show the shadow disappearing over time, going steadily from [0111] to [0000]. They give an important evidence of the veracity of the Markov Chain. Further studies should be conducted, however, to validate other state transitions. These are not in the scope of this work.

5.3.3 Summary of the indirect detection

This section has proposed a study of the correlation among shadow states in order to deduce a general model of shadow movement. By analyzing several different shadow shapes and movement scenarios, a Markov Chain was built putting into evidence that transition between contiguous shadow states are more likely than those between those non-contiguous. A natural shadow was observed and the transition between states [0111], [0011], [0001] and [0000] were confirmed through their respective I-V curves.

The Markov chain proposed in this section gives the PV module the possibility of guessing the next state without using the search function. Another potential use is for the PV Equalizer to gradually migrate from the direct diagnosis to its indirect equivalent by calibrating its own Markov Chain. This could bring a long time adaptation of the system to its local and potentially recurrent shadow.

However, more data should be acquired to test other transitions of the table, with especial attention to non-contiguous shadows.

5.4 Conclusion

This chapter has proposed and studied three diagnosis methods for the PV Equalizer: direct, semi-direct and indirect. Each was studied by a different section and their results can be summed up in the answer to the questions below.

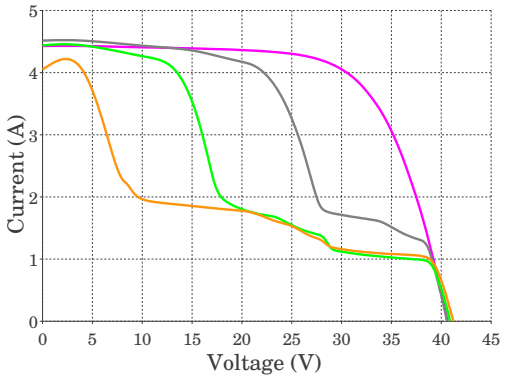

(a) The I-V curves showing the evolution of the shadow

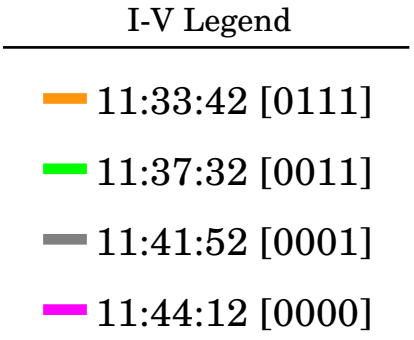

(b) Legend of the I-V curves

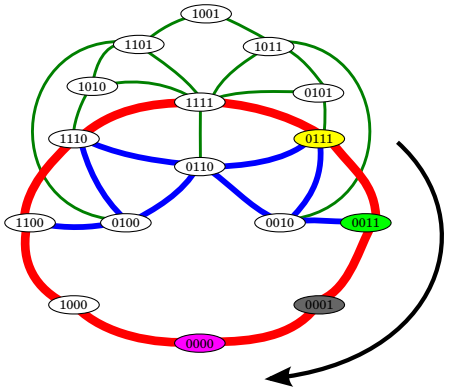

(c) The evolution of the shadow over the Markov chain

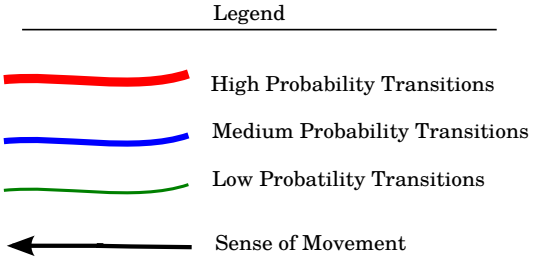

(d) Legend of the Markov Chain

Figure 5.44: The shadow variation over a long period of time

The semi-direct method observes the mean inductor and output currents in order to determine changes in the shadow shape prior to the use of the search function, triggering it less often.

The indirect method uses a Markov Chain model to automatically switch after a shadow transition without the use of the search function.

Finally, the original questions of this section may be answered.

- *How can the search function be used to find the shadow?*

  The search function is the basis of the direct diagnosis method. Through its recurrent use, current peaks can be acquired and analyzed to determine the shadow shape. Their interpretation, however, was found to change according to the function being performed by the PV Equalizer.

  While idle, the peaks can be used to calculate an average for cross-comparison. During equalizing, their local shadow state must be taken into account to determine if the shadow has moved or not. In the case of bypassing, the output current forces the shaded cell group in reverse bias and they have no peaks.

  By using these criteria, the PV Equalizer can track movements on the shadow and adapt itself to changes in the shadow state. However, if the peaks are too close to one

another their information about the shadow is inconclusive. The "proximity" above which their information can be considered as useful should be taken into account when using the direct search for controlling the PV Equalizer.

- *How are the electric variables of the PV module affected by changes in the shadow?*

  Only two variables were found to carry information about the shadow: the inductor and output currents. Both are affected by the shading factor and the shadow width at the same time, which characterize changes in the shadow. However, their cross-comparison can be used to clearly distinguish which change in the shadow is taking place. The correlation is clearly shown in table 5.7 in page 157. It is important to note that due to the long time spans involved, variations are better observed through the mean values of the currents.

  The observation of these currents can be used to trigger searches only when the shadow width changes. This allows changes in the switching strategy to better mitigate the new shadow. Changes in the shading factor can be tackled by changes in the duty cycle, which are already controlled by the optimal duty cycle tracker.

  Is there any general rule to the shadow behavior? If so, how can the Equalizer predict it?

  Yes. The study of different shadow shapes and movement scenarios has shown that there is a clear correlation between certain shadow states. Their transitions have been described in terms of a Markov Chain in figure 5.40 in page 163. A natural shadow was observed to verify some of the transitions given, showing an interesting potential for the model developed. However, a more extensive study of the shadow should be conducted to verify other transitions, specially for non-contiguous shadows.

  This Markov Chain can be used to predict the next state of the shadow according to its movement. It can also be calibrated by the PV Equalizer itself over time to eventually stop using the search function.

Using the conclusions from this chapter and chapter 4, the shadow state can be estimated, its corresponding switching strategy chosen and an appropriate duty cycle sought. Now all the elements are in place to design a control system for the PV Equalizer.

Chapter 6

Control Algorithm

Previous chapters have characterized the PV Equalizer in relation to the shadow. Based on their findings, any shadow cast over the PV module can be found by means of one of three diagnosis methods and mitigated either through equalizing or bypassing.

The objective of this chapter is to put their knowledge together in order to propose a control algorithm capable of finding the shadow and reacting to its movement.

Contents of this chapter

6.1 Algorithm Overview

The control algorithm proposed in this chapter is shown in figure 6.1. It has four basic blocks: Initialize System, Wait, Detect and Execute. Each one bears a contribution from the results of one or more previous sections of this chapter.

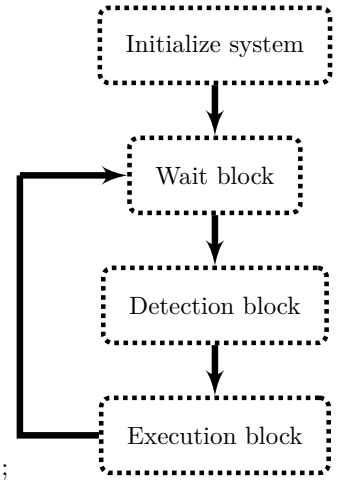

Figure 6.1: Control algorithm overview

The *Initialize System* block depends on the technology on which the Equalizer is implemented. It sets up all the initial configurations needed to perform its tasks, such as timers and analog-to-digital converters. It also handles the initial calibration of the search function.

The *Wait* block waits for a predetermined length of time, handles the tracking of the optimal duty cycle and observes the evolution of the average inductor and output currents.

The *Detection* block regroups all intelligent functions of the algorithm. For the direct and semi-direct diagnosis methods, it acquires the current peaks by triggering the search, calculates the threshold based on the current peaks and estimates the binary shadow vector. It also chooses between the equalize, bypass and OFF modes or corrects the shadow. For the indirect diagnosis method, it seeks out data from the Markov Chain and decides which transition has taken place.

The *Execution* block turns the equalizing ON and OFF, chooses its switching strategy and duty cycle based on the shadow binary vector. Their choice is conditioned by the function chosen to be used by the Detection block.

These blocks and their respective algorithms will be described in detail in the sections below.

6.2 Initialize System Block

The algorithm of the Initialize block is shown in figure 6.2.

The Initialize System block starts by turning the whole Equalizer system ON and setting up the operating conditions of its embedded digital microcontroller. Most of it is specific to the technology used, and further information can be found in the prototype described in appendix B. However, there is one aspect that should be taken into consideration and applies to any version of the Equalizer: the calibration of the search peaks.

Current peaks bear differences among themselves even in the absence of shadow. This can be due to many different elements, such as noise from the chopper controlling the PV

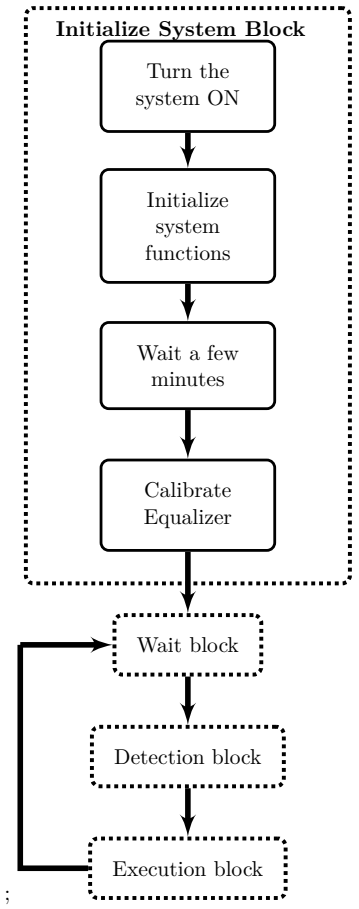

Figure 6.2: Algorithm of the Initialize System block

module, thermal drift in the component of the Equalizer or even differences in the characteristics of the PV cells composing the different cell groups, called **internal mismatch**. Thus, it should be expected that the peaks will never be equal and the procedure described below must be taken in order to mitigate this problem.

After the initial setup, the algorithm waits for a few minutes. During this time, the MPPT is expected to converge to a steady state. Once the power production is stable, the calibration begins. This procedure is important, because it is imperative that the Equalizer does not turn on accidentally, for it would deliberately reduce the overall power production of the PV system.

As an example, consider the current peak measurements shown in figure 6.3. These were done over a time period of nearly 5 minutes, under a constant irradiance of 900 $\frac{W}{m^2}$, module temperature of 60 ℃ and no shadow.

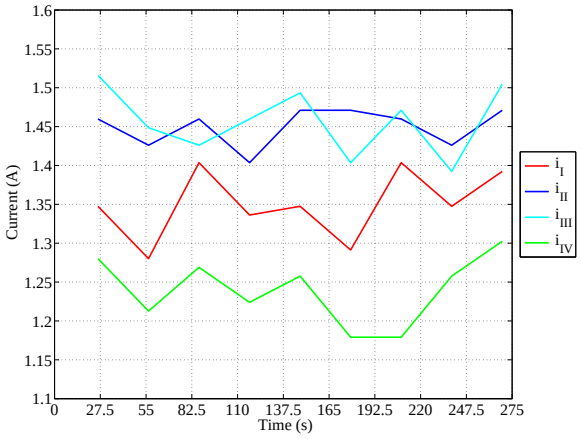

Figure 6.3: The search results of the prototype with no shadow

Both groups PV_I and PV_{IV} are lower than the others. Thus, an initial calibration of the Equalizer must be done to guarantee a certain proximity of the peaks. This is done by acquiring the peaks for a certain period, calculating their average, choosing the higher as reference peak and adding the different to the others. In the example above, the average of the readings is shown in table 6.1.

Table 6.1: The average offset in the readings

Cell group	*Peak average (A)*
PV_I	1.34
PV_{II}	1.42
PV_{III}	1.43
PV_{IV}	1.23

The results of the search after calibration are shown in 6.4.

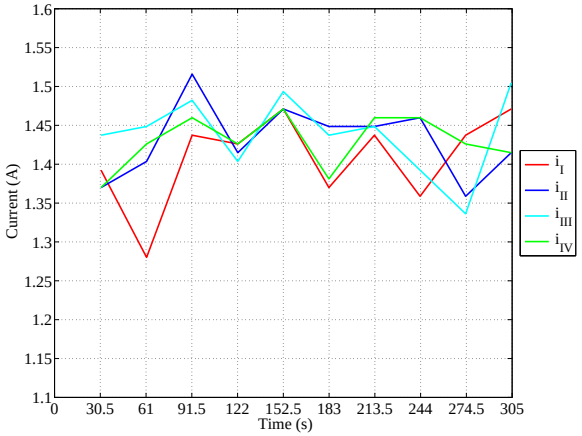

Figure 6.4: The search results after calibration

While the averages are much closer, there are still differences among the readings. To solve this problem, an idle zone can be implemented around 10% of the maximum peak value. If all the current peaks fall into it, the Equalizer will use the idle function, thus avoiding inconsistent shadow detections.

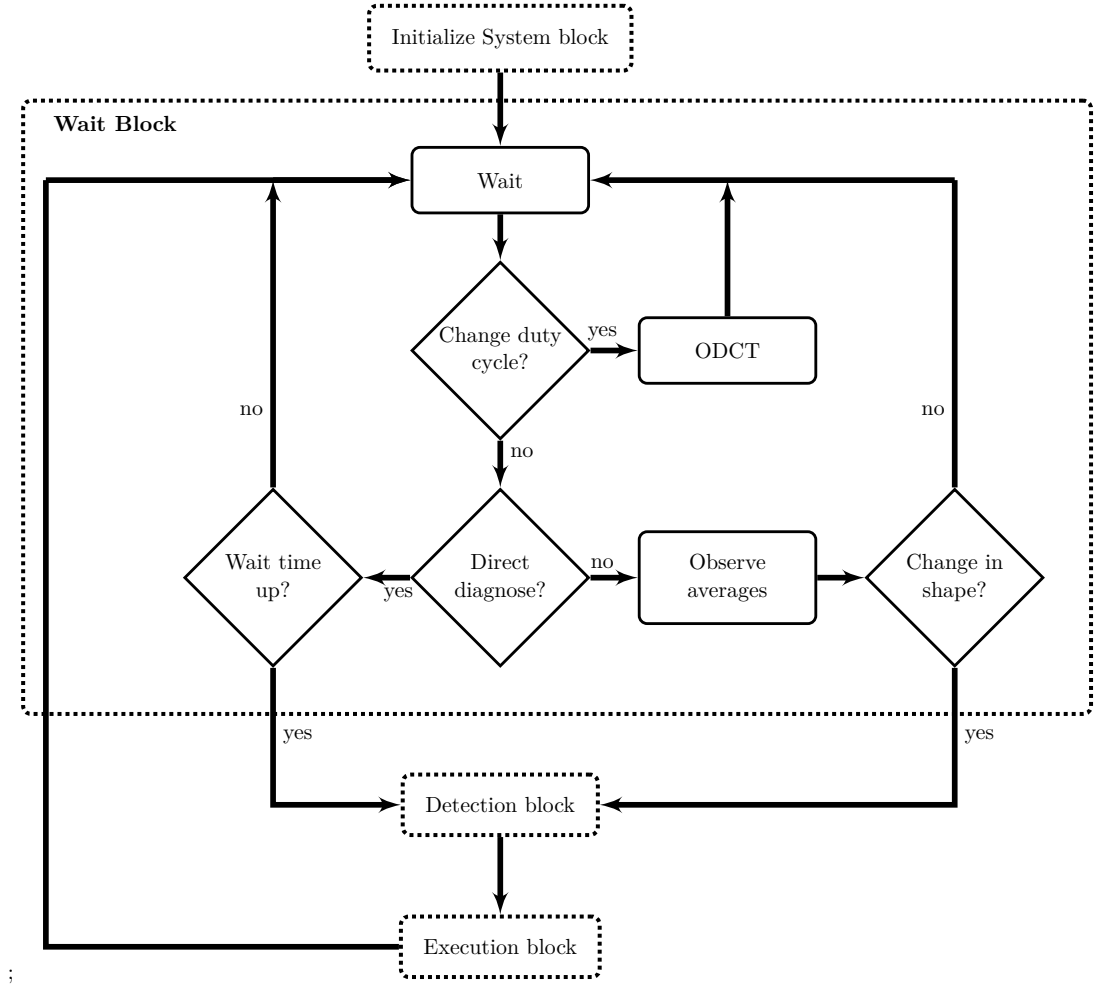

Figure 6.5: The algorithm of the wait block

Another benefit from the idle zone is avoiding low SF shadows. Chapter 3 has shown that, due to its losses, the Equalizer is not effective against them. By using both the initial calibration and the idle zone, the chances of prematurely activating the Equalizer become nil, as will be shown in the experimental section.

Once the Equalizer is calibrated, the algorithm can proceed to the detection block.

6.3 Wait block

As its name indicates, the most important function of this block is to wait. However, waiting does not necessarily imply in being idle. The wait block performs two other functions in the meanwhile: tracking the optimal duty cycle and monitoring the PV module. The algorithm of this block is detailed in figure 6.5.

This section describes these two functions and determine how long the wait function should last depending on their time needs.

6.3.1 Monitoring function

Monitoring depends on the type of diagnosis that is being used by the PV Equalizer.

If the *direct diagnosis* is being used, two aspects should be taken into consideration to determine the time between searches: the response of the MPPT and the propagation of the shadow. The response of the MPPT determines when a new steady state is found.

This is an important variable, considering the dependence of the current peaks on a stable output current shown in section 5.1.

To determine how long this represents, the MPPT was characterized under an irradiance of 954 $\frac{W}{m^2}$. A shadow was installed over the cell group PV_{IV}, first with an SF of 0.36 at 45 seconds and then 0.60 at 75 seconds. The shadow was removed at 120 seconds. The results are shown in figure 6.6.

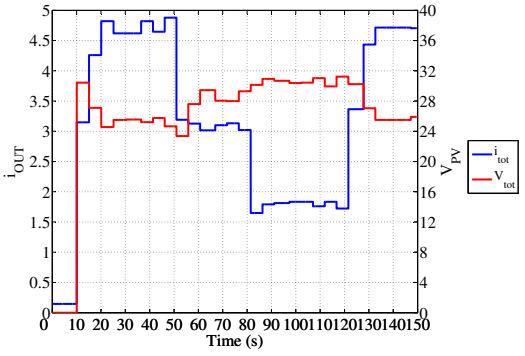

(a) The variation of voltage and current

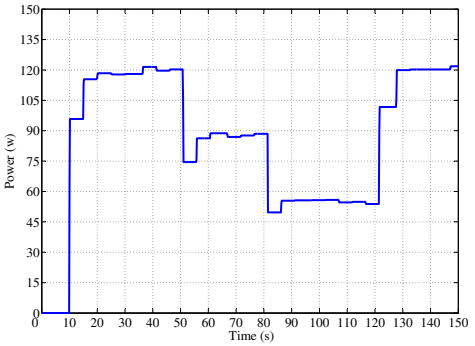

(b) The variation in power

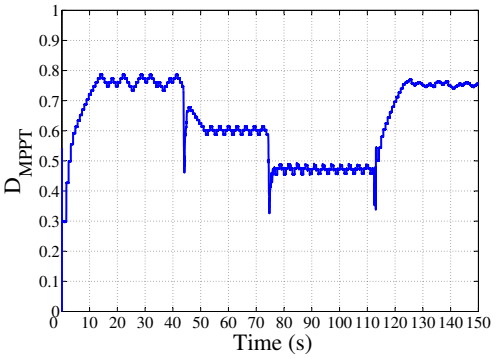

(c) The variation of the duty cycle

Figure 6.6: Characterization of the time response of the MPPT

Figure 6.6(c) shows the evolution of the MPPT duty cycle. It takes nearly 12 seconds to converge to the MPP from zero. When the shadow is cast over the PV module, the MPPT takes nearly 10 seconds to converge to a new reference. If the SF is reinforced the answer is even faster: nearly 5 seconds. After removing of the shadow, the MPPT takes again nearly 12 seconds to converge.

The propagation of the shadow determines how fast the peaks should be acquired to reproduce its movement. To have an idea of the how much time this represents, the movement of a natural shadow studied in section 5.3 will be used as a reference. Its result, recalled in figure 6.7, shows the evolution of the shadow through the changes in the I-V curves of the PV module. The time between changes is roughly 2 minutes.

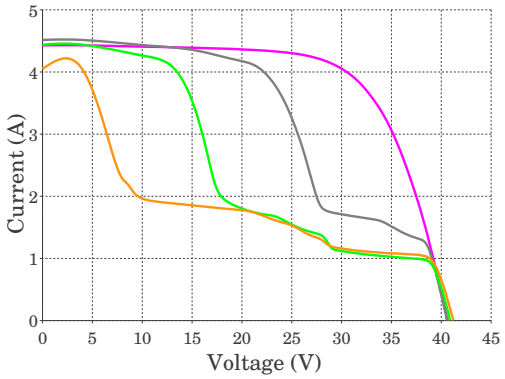

(a) The evolution of the I-V curves over time

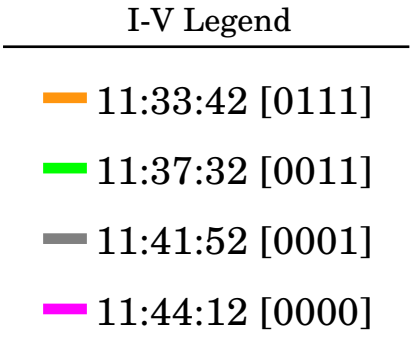

(b) Legend

Figure 6.7: The time response of a shadow

Thus, direct diagnosis monitoring should be slower than the time constant of the MPPT but faster than the shadow.

For both the semi-direct and indirect diagnosis, waiting is performed differently. They constantly observe the average inductor and output currents to determine movements of the shadow. Its principle is recalled in table 6.2, which was first defined in section 5.2. Where $\Delta\overline{i_{OUT}}$ and $\Delta\overline{i_L}$ represents the variation in the average output current and inductor current, respectively.

Table 6.2: The correlation between the inductor, output current and movement

	$\Delta\overline{i_L} > 0$	$\Delta\overline{i_L} < 0$
$\Delta\overline{i_{OUT}} > 0$	The shadow width is shrinking and its SF is constant.	The shadow width is stopped and its SF falling.
$\Delta\overline{i_{OUT}} < 0$	The shadow width is stopped and its SF is rising.	The shadow width is expanding and its SF is constant.

Both $\overline{i_{OUT}}$ and $\overline{i_L}$ are calculated from the average of several measurements. Noise or MPPT oscillations can be a problem since both create variations in both curves. To avoid detecting inconsistent shadow movement, a certain variation threshold will be used. So, the current must not only vary, but vary more than this threshold to be considered as shadow movement.

If the shadow is expanding or contracting, the algorithm goes to the detection block. In the cases where only the shading factor changes the algorithm remains in the wait block and the optimal duty cycle tracker (ODCT) is considered to be enough to mitigate its effects.

6.3.2 ODCT function

After the shadow is found and the equalize function activated, power production can be optimized by using the **Optimal Duty Cycle Tracker (ODCT)**. Its principle, similar to the MPPT, resided on the influence the duty cycle has over the power output of the PV module. Unveiled, in section 4.2, its main idea is recalled in figure 6.8.

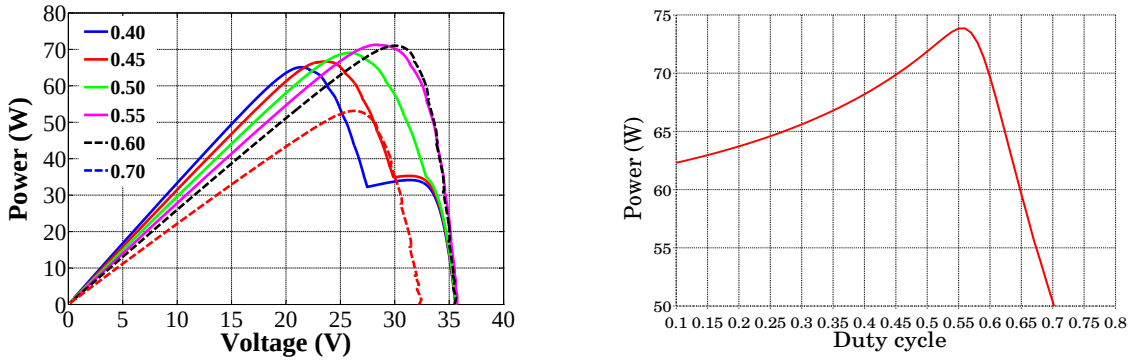

(a) Changes on the P-V curve

(b) The evolution of the MPP with the duty cycle

Figure 6.8: Simulation results showing the influence of the duty cycle over the P-V curve of the reference PV module

The influence of the duty cycle in the presence of the local MPP is shown in figure 6.8(a). When the duty cycle is underestimated (0.40), the PV module behaves as if bypassed. As the duty cycle rises (0.45 and 0.50), the two local MPP begin to disappear. Once the system approaches the optimal duty cycle (0.55 and 0.60), the transfer of energy from unshaded to the shaded cell groups approaches its maximum. If the duty cycle continues to rise (0.70), the diodes in the switching legs of the Equalizer begin to choke i_{OUT} and reduce the power output. This principle is resumed by plotting the power output as a function of the duty cycle, as in figure 6.8(b). Its global maximum is the **optimal duty cycle (ODC)**.

Finding the ODC can be achieved by applying small disturbances in the duty cycle and observing the reaction of the power output. If power raises, then the disturbance is leading the system into the good direction and should be reinforced. On the contrary, if power falters, then the disturbance should be inversed.

Tracking the optimal duty cycle also depends on the MPPT. At each disturbance, it must be given enough time to converge to the new MPP. Since the MPPT takes about 12 seconds to converge to a new MPP during steady-state, the duty cycle might only be changed a few times before the next measurement routine. This could be extended over longer periods of time if the shadow does not change.

6.3.3 Choice of the wait period

The choice of the time window will depend on which diagnosis function is being used.

For the direct diagnosis, the PV Equalizer should wait the time of the MPPT to converge to a new MPP and for the ODCT to get closer to the optimal duty cycle. However, the time should be no more than a minute, otherwise the reaction to the changes of the shadow risks being too slow, wasting power. Thus, a compromise time of 24 seconds was adopted for this method.

For the semi-direct and indirect diagnosis, the waiting time does not need to be that long. They can be constantly monitoring the evolution of the mean inductor and output currents every few seconds allowing a faster reaction to the appearance of the shadow. Thus, their waiting period will be 2 seconds. However, once movement has been detected, the semi-direct diagnosis should give the MPPT enough time to converge to a new MPP

before triggering a search. This time was chosen to be 12 seconds being of the slowest answer of the MPPT.

6.4 Detection block

The entry to this block depends on which diagnosis method is being used. The direct method goes directly to the search and calculate peaks function. The semi-direct method will wait a few seconds, giving the MPPT enough time to converge, before triggering the search. The indirect method will access its Markov Chain and determine the next shadow state.

This creates two separate branches within the detection block, one based on the analysis of the current peaks and the other based on the Markov chain. The first branch interprets the peaks according to the function currently being used. The second simply analyzes a table whose values correspond to the transition probabilities between shadow states. The highest value is used to choose the next state. These two branches will be explained in detail in this section.

The algorithm of the detection block is shown in figure 6.9.

Once the shadow is detected, a binary vector is sent to the execution block for further processing.

6.4.1 Current analysis branch

Either the direct or the semi-direct diagnosis method base their decision on the use of current peaks. These are acquired in a burst of measurements giving a vector of values which will be used to determine the location of the shadow. However, their interpretation changes according to the function that is currently being used by the PV Equalizer.

There are a total of three functions: equalize, bypass or idle. Each one has its own path, as explained below.

Equalize path

This path is taken if the system is equalizing. As shown in chapter 5, equalizing changes the currents within each cell group, also having an effect on their peaks. This is recalled by the example in figure 6.10, where cell groups PV_I and PV_{II} are giving energy to cell groups PV_{III} and PV_{IV} through the switching strategy $I.II \rightarrow III.IV$.

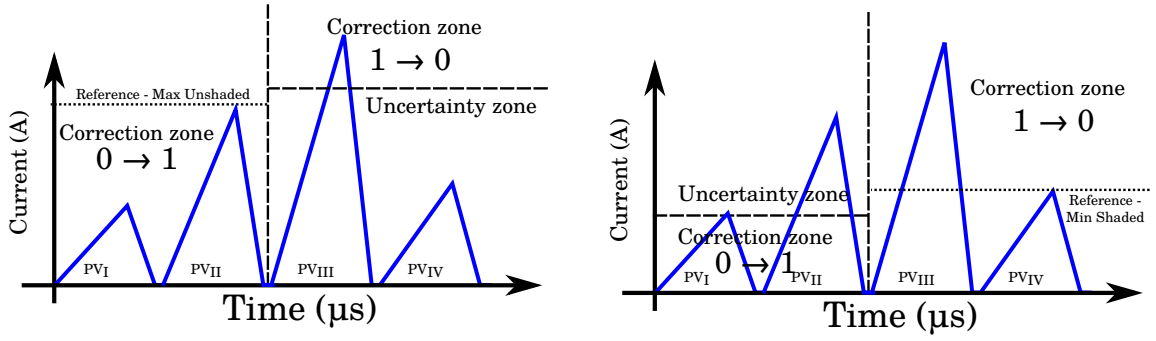

(a) Using the unshaded cells as reference

(b) Using the shaded cells as reference

Figure 6.10: Interpretation of the peaks during equalizing

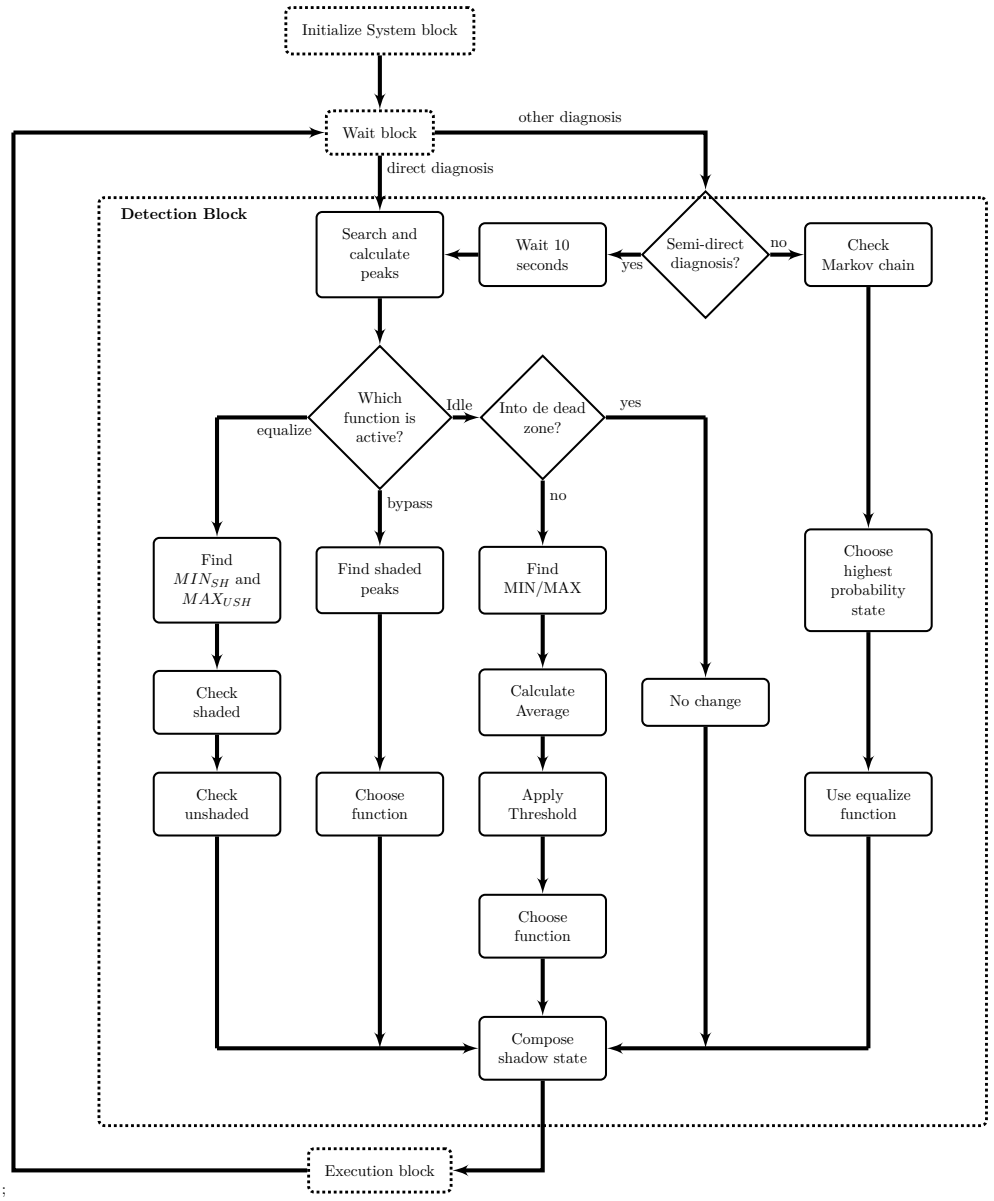

Figure 6.9: Detection algorithm

In figure 6.10(a), the peak in cell group PV_{II} is used as a high reference to analyze the other three peaks. Unshaded cell groups (0) whose peaks are lower than the high reference are switched to shaded (1), as shown in the red correction zone. Shaded cell groups (1) whose peaks are higher than the high reference are switched to unshaded (0), as shown in the green correction zone.

In figure 6.10(b), the peak from cell group PV_{IV} is used as a low reference to analyze the other three peaks. Shaded cell groups whose peaks are higher than the low reference are switched to unshaded (0), as shown by the green correction zone. Unshaded cell groups (0) whose peaks are lower than the low reference are switched shaded (1), as shown by the red correction zone.

In both correction cases, there is a grey uncertainty zone which refers to the fact that no conclusion can be drawn by peaks which are too close to each other.

This correction is shown in the algorithm as finding the minimum shaded peak (MIN_{SH}), the maximum unshaded peak (MAX_{USH}), checking the shaded cell groups and then those unshaded. As the algorithm checks, it also corrects the peaks accordingly. The new state

is then sent to the compose shadow state function.

Bypass path

If the bypass function is operating, there are no current peaks over the shaded cell groups because these have slightly negative voltages. However, if a peak does appear, it means that the shading factor of the cell group is no longer high enough to justify bypassing it. In this case, the system stops bypassing and the equalize function is activated.

Idle path

The idle branch is responsible for finding the shadow and choosing the function to be used to mitigate it. First the function is chosen, according to the differences between the peaks. Thus, there are three possible cases, as shown in figure 6.11.

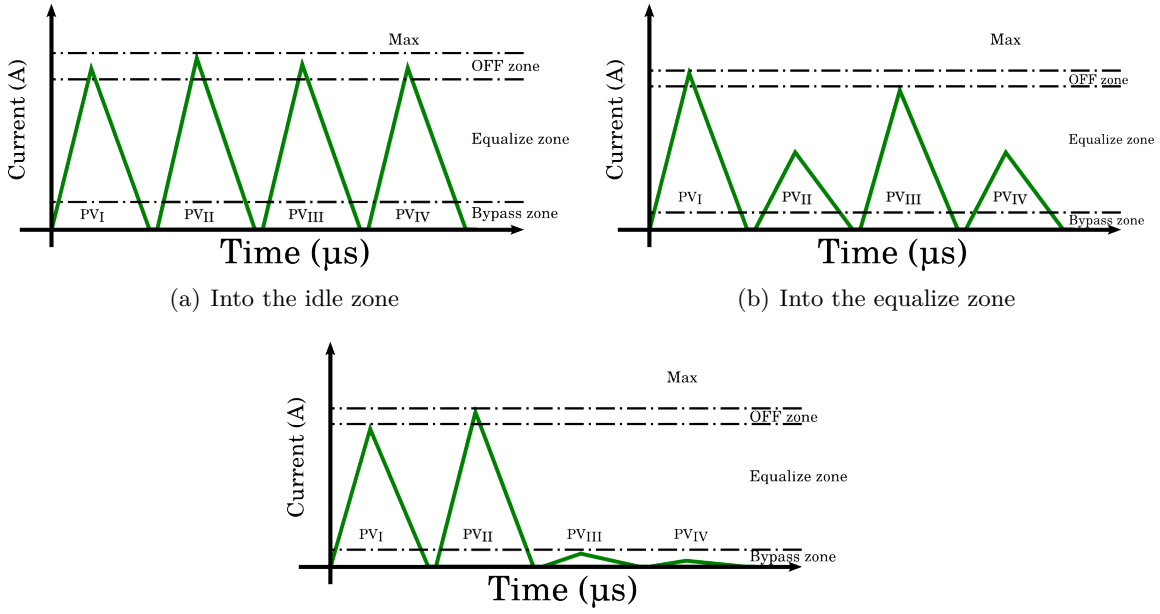

(a) Into the idle zone

(b) Into the equalize zone

(c) Into the bypass zone

Figure 6.11: The three mode zones around the current peaks

In figure 6.11(a), the peaks are too close together, falling all into the idle zone. In this case there is no shadow, and the PV Equalizer remains idle.

In figure 6.11(b), the peaks fall within the equalize zone. This means that there is a shadow and equalizing it is the best solution. In this case, the shadow is detected through the use of a threshold, calculated from the average between the highest and lowest peak. All peaks below the threshold are considered shaded and all those above are considered unshaded. In the example, cell groups PV_{II} and PV_{IV} would be considered shaded.

In figure 6.11(c), the shaded peaks are too low, falling into the bypass zone. Although the shadow is present, equalizing it is not the best solution. The detection is also done through the use of a threshold.

With the shadow and the function chosen, the information is sent to the function that composes the binary shadow state vector.

6.4.2 Markov chain branch

This branch uses the Markov Chain model proposed in chapter 5 to determine the next state of the system. It is translated, in practice, by a table whose values determines the probabilities of transition between two different states.

The diagonal of the table is the correlation of the state with itself and has no meaning. If the shadow is expanding, the values sought are located above the diagonal. If the shadow is contracting, the values are located below it. The highest transition value is chosen and the branch sends the information to the function that composes the shadow state.

The Markov chain branch will be considered to always use the equalize function in this work for simplicity.

6.5 Execution block

The Execution block translates the choices of the Detection block into real control commands to the Equalizer transistors. Based on the shadow state and the operation mode, this block makes two choices: the switching strategy and its duty cycle. They are then translated into commands that are sent to the transistors themselves. Its algorithm is shown in figure 6.12.

6.5.1 Switching strategy choice

The shadow state received from the Detection block carries all the information needed to choose the best strategy. This choice can be made through two different approaches.

The first is to implement the algorithm issued from the conclusions of section 4.1. In it, the shape of the shadow is opposed to its representation, leading to an algorithm than can be adapted to any Equalizer application. It is recalled in in figure 4.6 in page 116.

The second is to pre-code the results in a fixed table, whose size will vary according to the number of cell groups and was chosen for simplicity. The correspondence between the switching strategies and the 16 binary shadow states is shown in table 6.3.

Table 6.3: Pre-coded switching strategies for the 2-level detection

Shadow State	*Switching Strategies* 1^{st}	2^{nd}	*Shadow Case*	*Switching Strategies* 1^{st}	2^{nd}
[0000]	–	–	[1000]	$II.III.IV \rightarrow I$	–
[0001]	$I.II.III \rightarrow IV$	–	[1001]	$II.III \rightarrow I$	$II.III \rightarrow IV$
[0010]	$All \rightarrow III$	–	[1010]	$II \rightarrow I$	$III \rightarrow IV$
[0011]	$I.II \rightarrow III.IV$	–	[1011]	$II \rightarrow All$	–
[0100]	$All \rightarrow II$	–	[1100]	$III.IV \rightarrow I.II$	–
[0101]	$I \rightarrow II$	$III \rightarrow IV$	[1101]	$III \rightarrow All$	–
[0110]	$I \rightarrow II.III$	$IV \rightarrow II.III$	[1110]	$IV \rightarrow I.II.III$	–
[0111]	$I \rightarrow II.III.IV$	–	[1111]	–	–

From the eight non-contiguous shadow states, half use the Universal strategy while the rest use the CSS. From the eight remaining cases, [0000] and [1111] were considered as non-equalizable, instantaneously triggering the idle function. The rest use BSS strategies.

The choice of the switching strategy is followed by the estimation of the duty cycle, according to the function used.

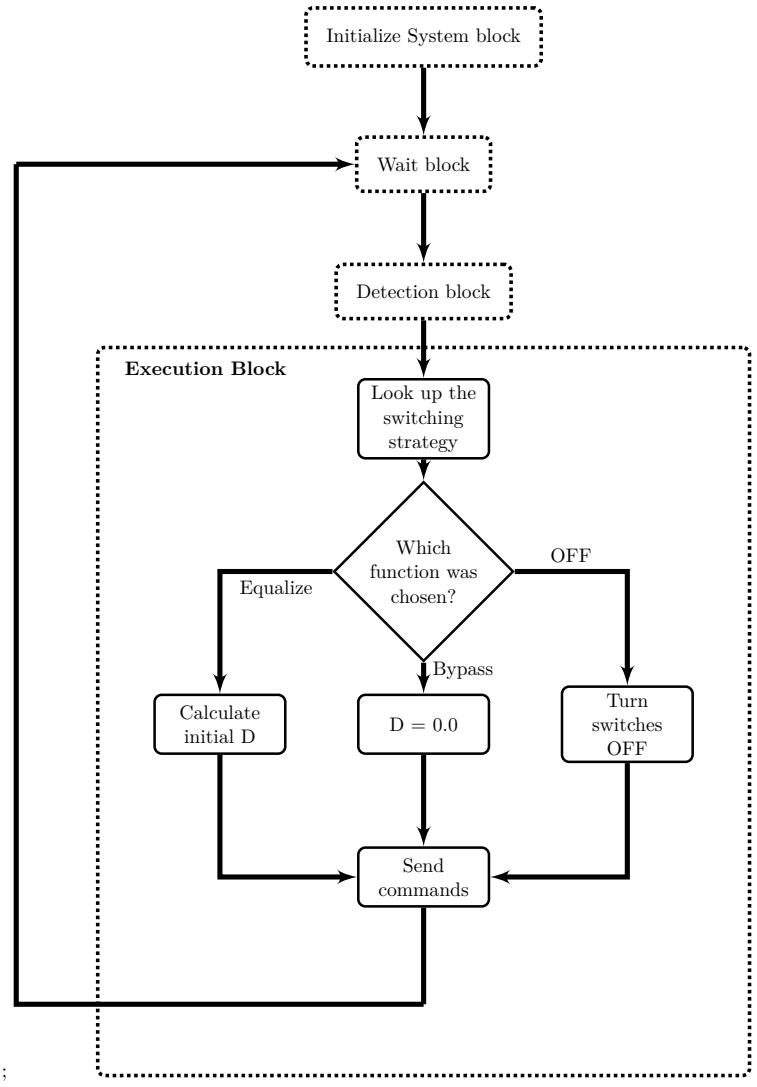

Figure 6.12: Execution algorithm

6.5.2 Duty cycle choice

The choice of the duty cycle is mainly influenced by the function chosen by the Detection block.

The *idle function* commands all switches to be turned off. There is no switching and the system simply remains idle at it heads back into the Wait block.

The *equalize function* calculates the initial duty cycle in two steps. First, equation 6.1 is used to calculate the theoretical duty cycle(s). In this equation, n_{CH} represents the number of cells charging, n_{DCH} represents the number of those discharging and (i) represents the number of the BSS to which the duty cycle is attributed in the case of the CSS. It will be used by BSS, CSS and Universal strategies.

$$D(i) = \frac{n(i)_{DCH}}{n(i)_{CH} + n(i)_{DCH}} \tag{6.1}$$

As was shown in section 4.2, the theoretical duty cycle is not enough to assure the full transfer of current between shaded and unshaded cell groups. To attain it and maximize the power production, the optimal duty cycle tracker (ODCT) is used by the Wait block. As the ODCT requires time to converge, the initial estimation of the duty cycle may help making it faster.

This initial estimation was also studied in section 4.2. It was found that adding 10% to 15% of the theoretical duty cycle may suffice to get the ODCT an starting point a few disturbances closer to the optimum duty cycle.

For the *bypass function*, the duty cycle is set to zero. The PV Equalizer considers, in this case, that the MPPT is capable of tracking the highest power peak of the PV module and simply waits for the moment when the shadow is gone.

6.5.3 Send commands function

With the switching strategy chosen and the initial duty cycle estimated, the control system is now ready to send the signals to the transistors. Two pairs of transistors are needed during the equalizing, one during charge and the other during discharge. The PV Equalizer has 8 transistors indexed going from 2 to 9.

To illustrate the relation between the transistor indexes and shadow, an example is provided in figure 6.13. In it, the number of shaded cell groups is represented by n_{SH} and their initial position is called pos_{SH}. The position is numbered from 1 to 4, representing cell groups PV_I to PV_{IV}, respectively. The same logic applies to the number of unshaded cell groups, called n_{USH}, and their initial position, called pos_{USH}.

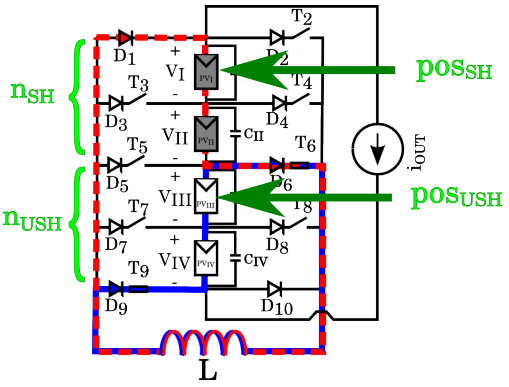

Figure 6.13: Example used to illustrate the definition of the shadow position

In figure 6.13, groups PV_{III} and PV_{IV} are unshaded, making n_{USH} equals to 2. They start in cell group PV_{III}, making their pos_{USH} equals to 3. The indexes of the transistors used during charge are T_6 and T_9. A similar analysis can be made for the shaded part, having n_{SH} equals to 2 and pos_{SH} equals to 1. The indexes of the active components used during discharge are D_1 and T_6.

Using n_{SH}, n_{USH}, pos_{SH} and pos_{USH} to deduce the indexes of the transistors pairs gives the equations in table 6.4. These equations use $T1_{CH}$ and $T2_{CH}$ as the transistor pair used during the charge phase, while $T1_{DCH}$ and $T2_{DCH}$ represent the transistor pair used during the discharge phase.

Table 6.4: Transistor equations

Charge Phase		*Discharge Phase*	
$T1_{CH} = (2 \cdot pos_{USH})$	(6.2)	$T1_{DCH} = (2 \cdot pos_{SH}) - 1$	(6.3)
$T2_{CH} = 2 \cdot (pos_{USH} + n_{USH}) - 1$	(6.4)	$T2_{DCH} = 2 \cdot (pos_{SH} + n_{SH})$	(6.5)

Once the commands are calculated, the system upon which they are implemented is programmed to repeat them until further notice. The duty cycle is converted from its 0 to 1 format into a number best handled by the microcontroller in the embedded Equalizer.

The algorithm cycle is now complete and the system moves back into the Wait block. Now the control algorithm will be tested on the prototype and under real shading conditions for validation.

6.6 Experimental validation

Due to time constraints, the experimental validation of the control algorithm will be limited to the direct and semi-direct methods. The shadow setup used during the experiments will be presented first, followed by the weather conditions. The results will be shown in terms of power production, shadow detection and the influence of the PV Equalizer over the MPPT.

6.6.1 The shadow setup

This test consists of letting the whole system operate with no shadow, suddenly shade cell group PV_{IV} for a given time and then swiftly remove the shadow. The PV Equalizer is expected to find the shadow, compensate it, detect its absence and switch back into idle. The expected output of this test is shown in figure 6.14 and described below.

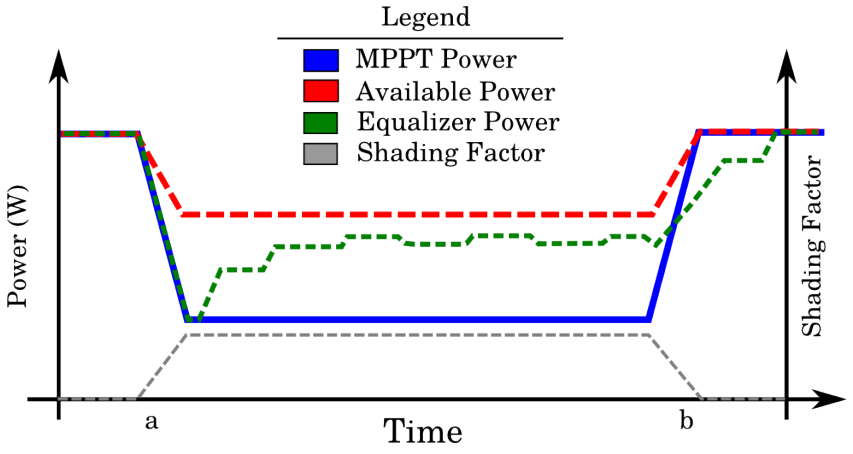

Figure 6.14: The shadow setup used in this experiment

The shadow is cast over the PV module at point a and disappears at point b. Its shading factor, shown in gray, has a slight ascending curve that represents the time it takes for setting up the shadow. In experimental conditions this may represent several seconds, being the reason for using a slope instead of a step.

The line in blue shows the power output of the system without the use of the Equalizer. Its recess from point a to b represents the impact of the shadow in power production.

The dashed line in red shows the power available by adding the local power productions of each cell group. It represents the maximum theoretical power available. The gap between the blue and red in this area represents the power that can actually be gained by using the Equalizer. An efficient Equalizer is expected to get the most out it, being as close as possible to the red line.

The green line shows a hypothetical power production yielded by the use of the PV Equalizer. It is expected to not turn on before the shadow, represented by the matching of the green and blue lines before point a. Once the shadow appears, some time is expected to pass before detection, as represented by the gap between green and red right after point a. While on, the Equalizer will seek the optimal duty cycle, represented by the oscillation

of the green curve between points a and b. Finally, it is expected to turn back into idle function once the shadow is gone, with a certain loss of power in the process.

6.6.2 Experimental setup

There is a total of four separate measurement sets. The first is done without the PV Equalizer to assess the power loss imposed by the shadow. The second is conducted with a switching strategy considered to be "near optimal", it is used as a reference to the power that can be potentially harvested. The third and fourth are done using the direct and semi-direct diagnosis methods, respectively. The indirect diagnosis, better suited for moving shadows, was not tested in these conditions.

The measurements details for each of the five sets are described in table 6.5.

Table 6.5: The time variables used during the experiments

Condition	Experimental set			
	No Equalizer	*Optimal*	*Direct*	*Semi-direct*
Duration	5'06"	5'07"	6'07"	5'32"
Shadow in	0'48"	0'53"	0'47"	0'43"
Shadow out	4'25"	4'30"	4'40"	4'38"
SF	8 layers (0.52)	8 layers (0.52)	8 layers (0.52)	8 layers (0.52)
Shadow state	[0001]	[0001]	[0001]	[0001]

The weather conditions for each measurement are described in table 6.6.

Table 6.6: The weather conditions during the experiments

Measurement	*Weather conditions*		
	Irradiance ($\frac{W}{m^2}$)	T_A (℃)	T_M (℃)
No equalizing	951	38	58
Fixed equalizing	943	39	58
Direct diagnosis	939	38	57
Semi-Direct diagnosis	950	35	59

6.6.3 Experimental results

The first experimental results, shown in figure 6.15 is composed by the reference measurements. It shows, in blue, the effect of the shadow over the power production of the PV module. The power yield by using the PV Equalizer with its corresponding optimal switching strategy is shown in red.

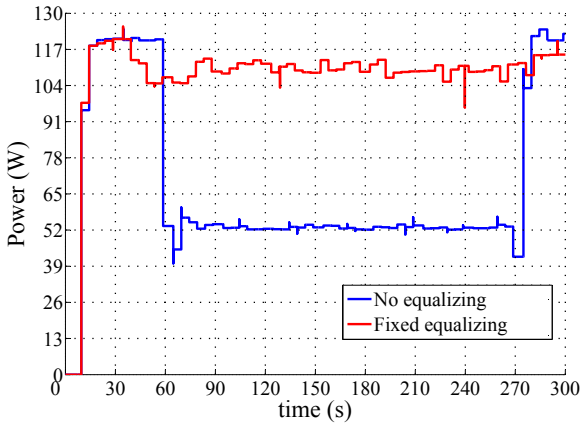

Figure 6.15: Reference power curve

There is a clear power gain between roughly 60 and 270 seconds. This power gain is the reference and the control algorithm should be capable of attaining it.

The results obtained using the direct diagnosis method are shown in figure 6.16.

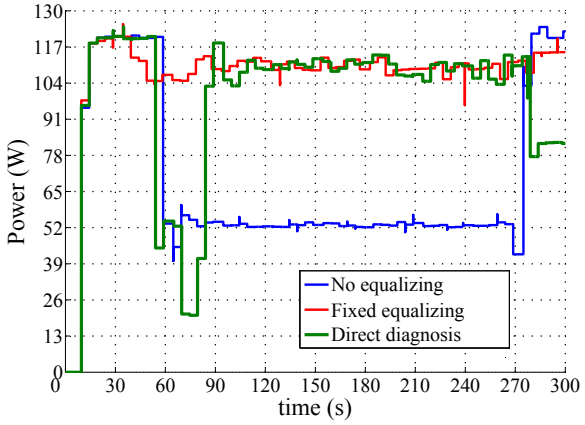

Figure 6.16: Power yield using the direct diagnosis method

The shadow is set at around 60 seconds, driving the power production down. The control system takes about 30 seconds to identify the presence of the shadow, with the power shooting up to the reference at nearly 90 seconds. When the shadow is removed, however, power production falls down to nearly 78 W.

To better understand these results, figure 6.17 provides further information about the duty cycle of both PV Equalizer and MPPT. It shows that the shadow is actually found at 30 seconds, but the equalizing saturates the MPPT control. Since the voltage distribution among the cells change abruptly, the MPPT looses its reference.

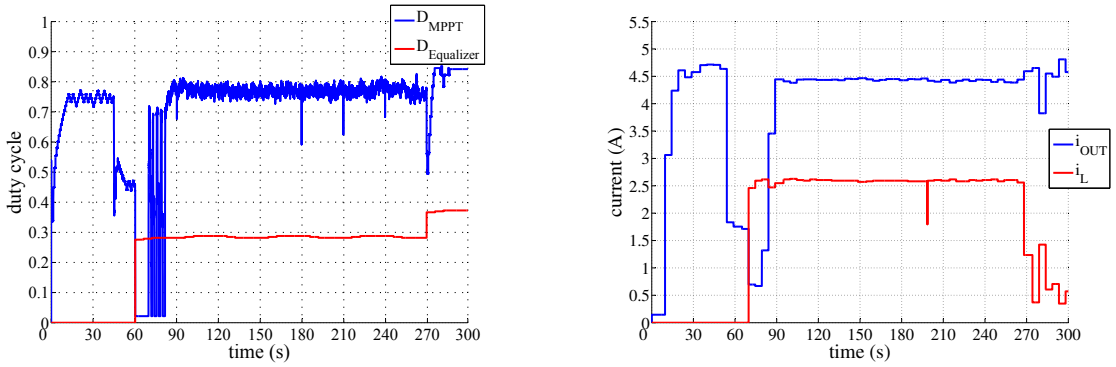

(a) PV Equalizer and MPPT duty cycles

(b) i_L and i_{OUT}

Figure 6.17: Evolution of other variables during the direct diagnosis experiment

The power results for the semi-direct diagnosis method are shown in figure 6.18.

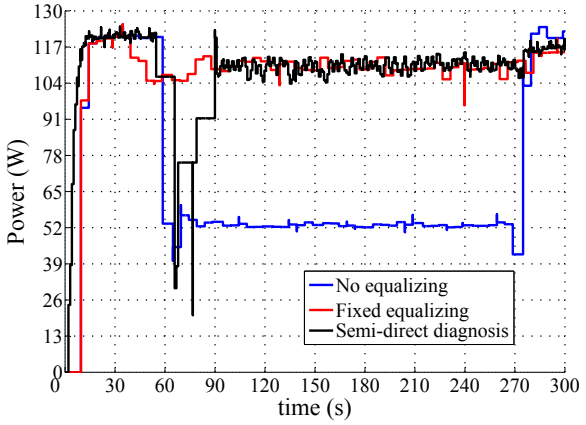

Figure 6.18: Power yield using the semi-direct diagnosis method

The response of the system is very similar to the direct method. There is a flat power variation between roughly 60 and 90 seconds, due to the 12 seconds the algorithm waits. Thus, the system detects variations in both the inductor and output currents three times during this period. More details of the evolution of the system during the experiment are shown in figure 6.19

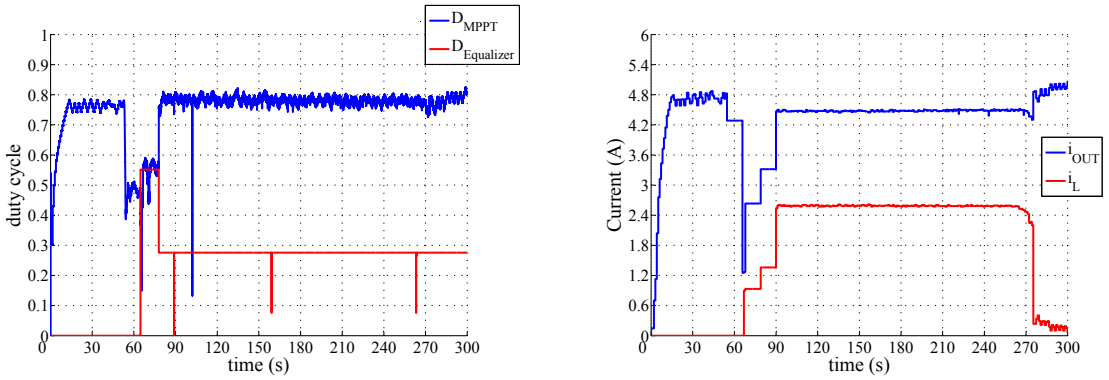

(a) PV Equalizer and MPPT duty cycles

(b) i_L and i_{OUT}

Figure 6.19: Evolution of other variables during the semi-direct diagnosis experiment

The steps showing the transition between 60 and 90 seconds show that the system detects a shadow, calls for a search and waits for 12 seconds. During this period, no readings take place which is shown by the flat lines in both curves. As both $\Delta\overline{i_{OUT}}$ and $\Delta\overline{i_L}$ rise, the system triggers new searches, causing more flat periods. Finally the system stabilizes and no new searches are called.

At nearly 270 seconds, the shadow is removed, causing the inductor current to fall. No search is called at this moment because the variation in the output current falls within the current threshold limit. Since $\Delta\overline{i_L}$ with zero $\Delta\overline{i_{OUT}}$ are considered as physically inconsistent, the system does nothing in these cases.

Comparing the results from both diagnosis methods yields figure 6.20.

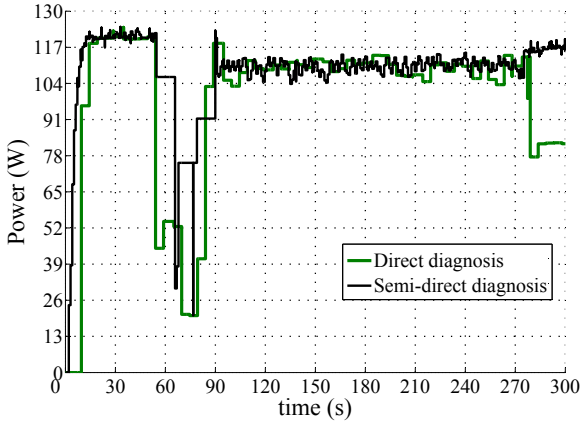

Figure 6.20: Comparison of the direct and semi-direct diagnosis method

The two diagnosis method take a similar time to react to the presence of the shadow. This confirms that the recurrent use of the search might be avoided by the observation of the average inductor and output currents.

Neither method is capable of detecting of stopping the PV Equalizer once it is on. It is an important feature that should be developed in further research.

6.7 Conclusion

This chapter has proposed a control algorithm for the PV Equalizer based on the techniques and methods developed in chapters 4 and 5. This algorithm is structured in four blocks, namely: initialize, wait, detect and execute. Each block is built based on some data or fact shown in previous chapters.

The initialize block starts up the control system upon which the PV Equalizer is coded. The wait block handles the monitoring of the system and the optimal duty cycle tracker. The detection block applies the different diagnosis methods to the data acquired by the PV Equalizer, determines the shadow state and the mitigating function to be applied. The execution block uses the shadow state to determine the switching strategy and duty cycle.

Their experimental validation was conducted only with the direct and semi-direct methods. Its results have shown that both methods were capable of finding and mitigating the presence of the shadow. Neither was able, however, to stop the PV Equalizer after the shadow was removed.

Time constraints have not yet allowed experiments using the indirect diagnosis method and moving shadows. These remain as perspective for comparing the three diagnosis methods under dynamic shadow conditions.

With the control system developed and validated, a final comparison of the PV Equalizer with other PRobES can now take place.

Chapter 7

Conclusion and Future Work

This thesis had the objective of proposing a new solution to the problem of intermittency in photovoltaic plants. Its approach was to change the topology of parallel PRobES from Cùk or Flyback based converters to a PV Equalizer inspired from a Buck-Boost. The several upgrades brought forth by this topology were offset by its major difficulty: control. In order to operate properly, the PV Equalizer needs to choose a switching strategy and duty cycle adapted to the shadow cast upon it. Thus, its control challenge was two-fold, finding the shadow and then determining the strategy best suited to mitigate it.

Several techniques were investigated throughout this work and their results were used to set up a control system capable of finding the shadow, detecting its movement and choosing the optimal strategy to mitigate it. With their results, this work comes full-circle and it is time to compare the gains brought by the PV Equalizer to other applications in the literature. In extension of this analysis, it is also time to determine the next steps to be taken, either in improving the current prototype and control system or in more broader and bolder research perspectives.

Contents of this chapter

7.1 Conclusions on the PV Equalizer

The conclusions concerning the potentials of the PV Equalizer are proposed in this section through two parts. First, its overall evaluation is conducted following the method used in chapter 2 that was applied to the other PRobES available in the current literature. Second, a comparison shows the improvements granted by the PV Equalizer and pave the way for future work.

7.1.1 Overall evaluation of the PV Equalizer

The criteria used in this overall evaluation are based on the method proposed in chapter 2. There are a total of seven criteria: Granularity, Passive Components, Efficiency, Power Gain, Reliability, Integration Potential and Control Simplicity. Each will be analyzed separately first, and then put together to compare the benefits of the PV Equalizer with those of other PRobES.

Granularity

The PV Equalizer is based on a highly granular topology. By adding new switching legs to its main concept, designers can go all the way down to a few cells. It is limited, however, to a certain number of cells because the discharge voltage must be higher than a two-diode forward-bias voltage. This can be improved, however, by certain changes in the topology which will be suggested in the next section.

Another element that grants it a high granularity is its diagnosis methods. By using current peaks, the PV Equalizer can control any number of cell groups with a single current sensor. Adding an extra sensor, to the output current, may provide even less losses on the long run by using the semi-direct diagnosis method.

Passive components

The passive components of the PV Equalizer are one of its greatest forces and weaknesses.

Using a single inductor is clearly an important improvement brought by this application to the current literature. Although it cannot be integrated, it is now no longer an obstacle to the integration of the system.

The capacitors, however, are still a great challenge. So far in this work, chemical and ceramic capacitors were tested. Both were destroyed in several occasions. Their short life-span and fragility are an important obstacle to this or any parallel PRobES. Further improvements to this issue are also described in the next section.

Efficiency

The efficiency of the PV Equalizer was found, in chapter 3, to vary according to the shading factor and width of the shadow. The technology used greatly contributed to cripple the performance of the prototype developed in this work. Improvements, such as changing transistors and diodes or integrating the structure could provide an important upgrade to its ratings.

Power Gain

While the prototype proposed in this work is by no means efficient, it did raise the power output of a PV plant by almost 40% is certain measurements, as shown in figures 3.23(a)

and 3.23(b) in page 95.

But its power gain can really be put in perspective when compared to other PRobES under equivalent shadow and equalizing conditions. Some of the results from data published in the literature can be picked as a means of comparison. Table 7.1 shows six PRobES, along with their equivalent shading conditions and switching strategies. It is important to clearly state that from all of these, only the works of Shimizu et al. [2001, 2003] have results issued from measurements. The others are all simulations and do not take into consideration the system losses.

Table 7.1: Equivalent shading conditions

PRobES	*SF*	*Equivalent BSS*
DMPPT 1 [Ramos-Paja et al., 2010]	0.36	$I.II.III \rightarrow IV$
DMPPT 2 [Giral et al., 2011]	0.57	$I.II \rightarrow III.IV$
DMPPT 3 [Nguyen and Low, 2010]	0.48	$I.II.III \rightarrow IV$
GCC 1 [Shimizu et al., 2003]	0.37	$I.II.III \rightarrow IV$
GCC 2 [Shimizu et al., 2001]	0.60	$I.II \rightarrow III.IV$
REA 1 [Nimni and Shmilovitz, 2010]	0.50	$I.II \rightarrow III.IV$

Their power gain comparison yields figure 7.1.

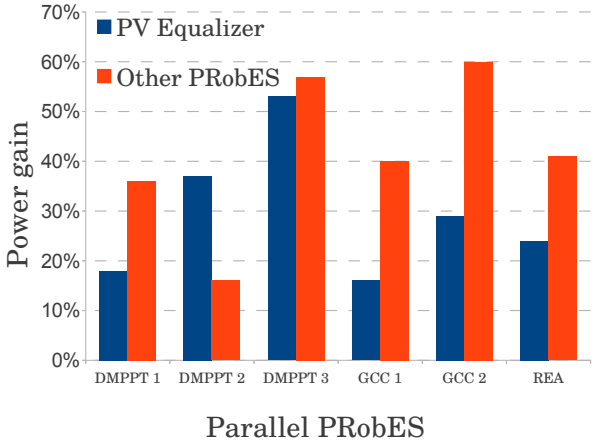

Figure 7.1: Relative power gain comparison among PRobES

There are three cases where the Equalizer had a performance lower than the other PRobES. For the DMPPT 1 the shading factor is very low and the simulation does not take losses into consideration. For the two GCC, their structure has only two transistors and one inductor. However, when compared in terms of real power gain, the PV Equalizer has similar ratings, as shown in figure 7.2.

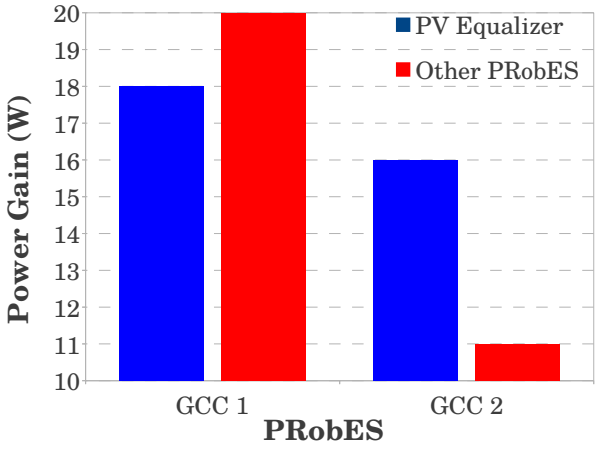

Figure 7.2: Absolute power gain comparison between the PV Equalizer and the GCC

Reliability

The reliability of the PV Equalizer depends on how its components behave over time. This work did not study their operation over long periods, but the experience acquired with the prototype has shown that its most fragile components are the capacitors. Transistors, diodes and the inductor are rather robust and did not posed problem during this work. Other less important elements are the sensors and the microcontroller, both upon with the operation of the system relies completely. The important number of components in the PV Equalizer make it even more important the perspective of integrating it monolithically.

However, considering the active components, the loss of one of them may still allow the PV Equalizer to operate in a degraded condition. This can be provided by adding special features to its control algorithm which would enable it to auto-diagnose faults in itself. Possible actions would be to trigger signals that would eventually bring in maintenance intervention.

Integration potential

Previous work has shown that the same switching leg used by the PV Equalizer has an interesting integration potential [**?**]. This interesting feature gives it an important advantage over other parallel PRobES currently available in the literature and should be explored in further work.

Control Simplicity

Finally, this feature was one of the contributions sought out by this thesis. The control algorithm proposed in this work has shown an important potential for enabling the PV Equalizer to control itself with very few sensors. The three diagnosis methods can also acquire information over time and learn from the recurrence of the local shadows with the potential of reducing control cost over time.

Comparison with other PRobES

Using the overall evaluation of the PV Equalizer and the other PRobES, a final cross-comparison is proposed in figure 7.3.

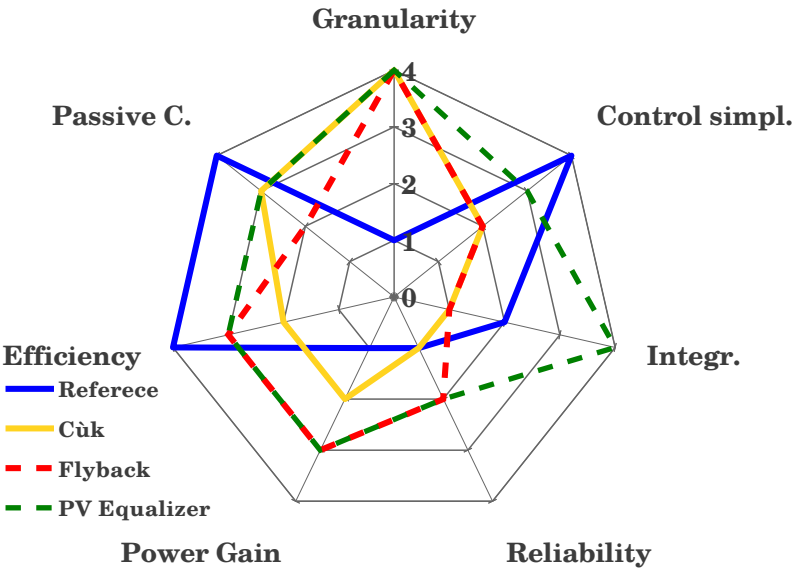

Figure 7.3: The final comparison among parallel PRobES

This final comparison shows that the PV Equalizer represents a mix from the best qualities of the other parallel PRobES, while providing an important control contribution and displaying an interesting integration potential.

There is still improvements to be made in all of the issues shown in figure 7.3. The next section list several ideas to seek them.

7.2 Research Perspectives

One of the main objectives of this thesis was to provide evidence that the breakthrough in the topological concept of parallel PRobES provided by the PV Equalizer is actually feasible. This has lead to several ideas and possibilities to make its use a reality in field applications. Their list, provided in this section is by no means exhaustive, but are considered are the most important blocking points and ideas that once sought would definately provide great ground for improvement.

Improvements in Power Electronics

There are three important power electronics improvements that could definitely change the ratings of the PV Equalizer. The first is the use of Schottky diodes in the switching legs. The second is to not use diodes at all.

As shown in chapter 2, losses are widely driven by the diode. Thus the first improvement would be to upgrade the switching leg of the system by replacing the diode with another transistor, the losses of the system are expected to be greatly reduced.

Another important improvement would be to totally integrate the structure into a single monolithic block. Certain authors such as have already proposed similar studies on the field.

These two improvements would greatly improve losses and reliability, actually pushing the Equalizer into a more satisfying performance.

The third issue is the capacitors. Electrolitic and ceramic capacitors were used in this work, but both were destroyed on several occasions. The eventual use of two electrolitic

capacitors in series with their negative part interconnected might be a solution for this problem. Once they are interconnected, their voltage polarity is no longer an issue. Their use should be investigated in further research.

The use of bidirectional chemical capacitors could provide a

Interactions with the MPPT

Throughout this study, interactions between the MPPT and the Equalizer were not taken into account. However, they happen in many levels and influence the overall system more than first expected.

In the *hardware level*, the capacitors of the Equalizer could be helpful during the sizing of the MPPT chopper. Their presence stabilizes the PV module voltage, which in turn requires a smaller inductor to be controlled. By cross analyzing both structures, an optimal system could be dimensioned where the losses of both the Equalizer and the system chopper can be reduced.

In the *software level*, the lack of communication between them was sometimes a barrier, especially during the detection of the shadow. If they could communicate, the Equalizer could effectively search at a constant output current, leading to a faster search of the shadow. The MPPT could also signal directly to the Equalizer when a change in its switching strategy becomes harmful to power production.

Mixed control algorithms

This work has focused its attention to the proposition and validation of three detection methods: direct, semi-direct and indirect. The first two were validated by the control algorithm separately, yielding different and interesting results. However, it would be interesting to improve the control algorithm in order to use them together. Cross comparing their results could be a way of rendering the control algorithm less prone to false detections and wrong diagnosis.

Validate the system with moving shadows

While moving shadows was an important issue during this work, getting the PV Equalizer prototype to work under moving shadow conditions revealed itself to be a difficult challenge. Experiments were performed but found inconclusive, specially due to the difficulty of moving shadows over the PV module. Validating the use of all the diagnosis functions under moving shadow conditions would give further information concerning the best way to use them together.

Multi-Agent Systems in PV plants

By reshaping the PV plant, new questions concerning its control system would inevitable rise. The plant could be seen as a multi-agent system, composed of different layers of reaction. The chopper could have different control strategies, based on the seasons or the architecture of the plant. The Equalizer could learn the recurrence of the local shadows over time and tune its Markov model to maximize the efficiency of the guesses as different parts of the same PV central could be shaded differently.

Finally, the data from the PV plant could be retrieved and more efficient Markov models could be recalculated off-line.

New Architectures for PV plants

By considering the PV plant a whole system, composed by Equalizers, Choppers and PV modules a new paradigm of plant can be conceived. The maximum robustness can be the center of a PV plant architecture. A single PV module can be considered to produce more, thus reducing the sizes of the PV plants for the same load.

Further research should include these new architectures along with the redefinition of the PV module. Smaller modules with a dedicated connectivity could replace bigger ones and allow an extended connectivity to the Equalizer system.

Validation of the Shadow Model

The Markov model itself could be the object of a further experimental research. There is not enough gathered field measurement data with the purpose of studying and understanding the shadow stochastic behavior from the PV module point of view. Observations should be focused on urban environments, where the occurrence of shadow is more likely.

7.3 Final Remarks

This work has addressed the problems of intermittency in PV plants. While a broad range of data and work is available on the field, an all-comprehensive theory capable of understanding this wealth of contributions. Thus, this thesis started by a bibliographic review of the shadow phenomenon in PV systems. From this review, a complete shadow model intertwining geometric elements of the shadow and electric connections of the PV module was proposed. The shadow model was used as a basis to create a theory on the intermittency of PV systems.

The theory proposed in this work states that the intermittency in PV systems is a two-fold issue: optical and electric. The optical intermittency can only be offset by elements external to the PV plant. The electric intermittency can only be addressed within the PV plant itself.

Among the existing methods in the literature, the Photovoltaic Robustness Enhancement Systems (PRobES) were those studied in this work. Two families of PRobES were identified, namely series and parallel. Each have their own advantages and inconveniences, which were studied in detail through a new comparison method. The parallel PRobES were found to be in a more disadvantaging position, requiring a total change in paradigm. Thus, we have chosen to focus our contribution into these by proposing the PV Equalizer.

The PV Equalizer is based on its battery equivalent and uses a singe inductor to equalize the uneven current distribution among the cell groups caused by the presence of the shadow. The modular concept use allows the PV Equalizer to be expanded from a few PV cells, to a module or an entire plant. It can also be easily integrated monolithically, paving the way for possible industrial applications.

The many advantages of the PV Equalizer were offset by a single problem: its control complexity. To solve this issue, its switching was studied and the equations of the system composed by the PV module and PV Equalizer were described. This description led to the definition of two functions types: mitigation and detection. Mitigation functions compensate the presence the shadow, while detection functions determine its location.

Mitigation functions were defined as composed by a switching strategy and a duty cycle. The switching strategies were linked to the shape of the shadow and an algorithm was proposed to properly choose them. The duty cycle was found to have a global optimum which can be reached by a disturb and observe algorithm.

Three types of detection methods were proposed and studied: direct, semi-direct and indirect.

The direct detection method consists of briefly connecting the PV Equalizer inductor to each cell group and acquire current peaks. The location of the shadow can, then, be deduced by the analysis of these peaks. Theoretical, simulation and experimental studies were thoroughly conducted to deduce the best way of using the information from these peaks. However, this method requires the recurrent acquisition of the peaks, leading to an energy cost.

The second method, called semi-direct, sought to avoid unnecessary acquisitions. It is based on the observation of the average inductor and output currents. Their behavior is such that their mutual rise or fall can be interpreted as shadow movement, which is used to trigger the acquisition of peaks. Measurements using a PV module and artificial shadows were performed to confirm their behavior.

The first two detection methods do not use any prior knowledge of the shadow. Moreover, they consider that all shadow cases have the same probability of happening. In the indirect method, these premises are reviewed and the shadow is studied based on its geometric passage over the reference PV module. The result is a Markov chain model capable of taking into consideration the probabilities of transition between different shadow scenarios. The observation of natural shadows has partially confirmed this model, which should be studied further for bigger PV centrals.

The mitigation and detection functions were used to design the control algorithm of the PV Equalizer. The general flowchart of the algorithm was presented and its aspects described. Its experimental validation was conducted using only the direct and semi-direct detection methods. The algorithm was capable of finding the shadow, choosing the correct switching strategy and optimizing the duty cycle. However, it couldn't stop the PV Equalizer after the shadow was removed. Further studies and validations of the algorithm should be sought by future work.

While this work has shown what the PV Equalizer is capable of doing, its has also shown what it should not do. It is clear that this solution is best adapted for environments with a highly concentration of shadows, such as urban areas. These areas represent a great potential for using PV systems currently unexplored. Since urban PV plants find themselves closer to the load, they represent less losses and infrastructure for the use of PV systems.

This author firmly believes that the gains associated to the use of the PV Equalizer are not limited to the energy. Its deployment on an experimental level would allow a better mapping of the shadows over cities. It could also generally change the way of designing PV plants by introducing new degrees of freedom.

If combined with a general review in the current paradigms used in the conception of PV plant, the PV Equalizer could actually be an important part of the answer to the problems of partial shading. A change which this work hopes to have introduced the basis to happen.

Appendix A

The Simulation Model

This appendix gives the details on the simulation model developed during this work. It was coded in Matlab/Simulink using the PLECs toolbox. Figure A.1 gives an overview of the system.

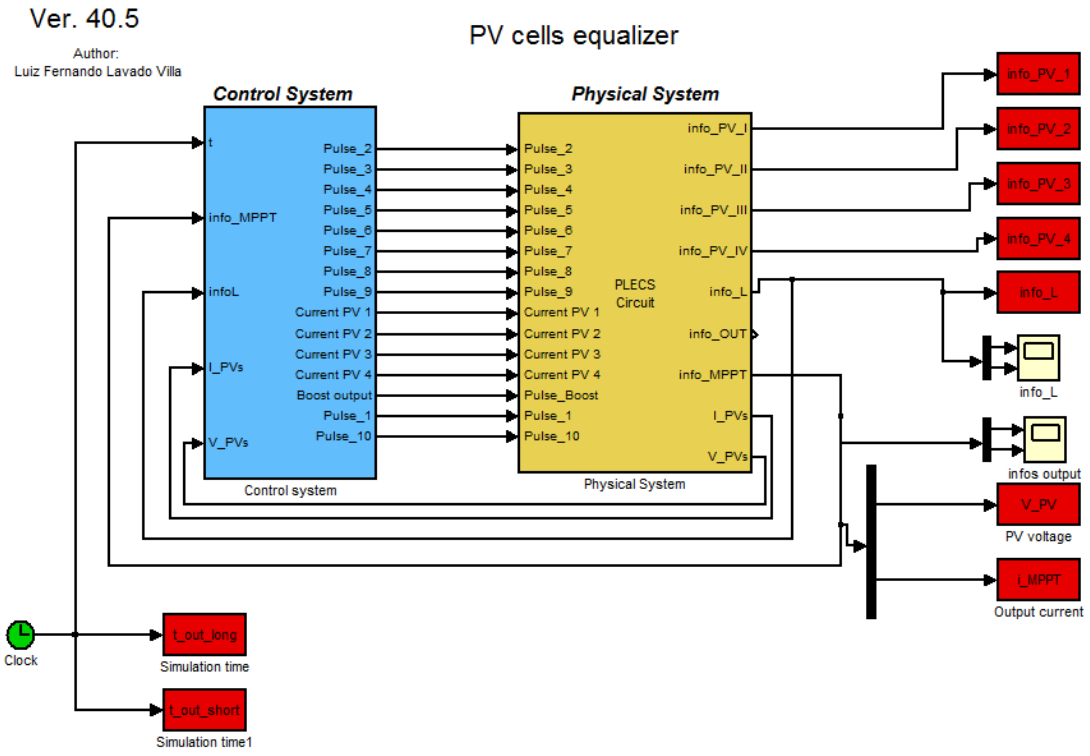

Figure A.1: The overview diagram of the simulation model

The simulation system is divided in two blocks: Physical and Control. The Physical block holds the circuit of the PV Equalizer drawn using the PLECS tool. It sends the output voltage and current along with the inductor voltage and current to the control block, while the readings from the cell groups are sent to the workspace. The Control control the PV Equalizer, the MPPT chopper and calculates the currents within the PV modules.

Throughout this appendix, simulink systems will be shown to explain how the model works. They follow a color code: data sinks are red, data sources are green, systems are cyan, switches are purple and PLECS related blocks are light yellow.

A.1 Physical System

The physical system is composed by the PV module, the PV Equalizer circuit and the MPPT chopper. They are shown in figure A.2 in parallel with a PV Equalizer figure for comparison.

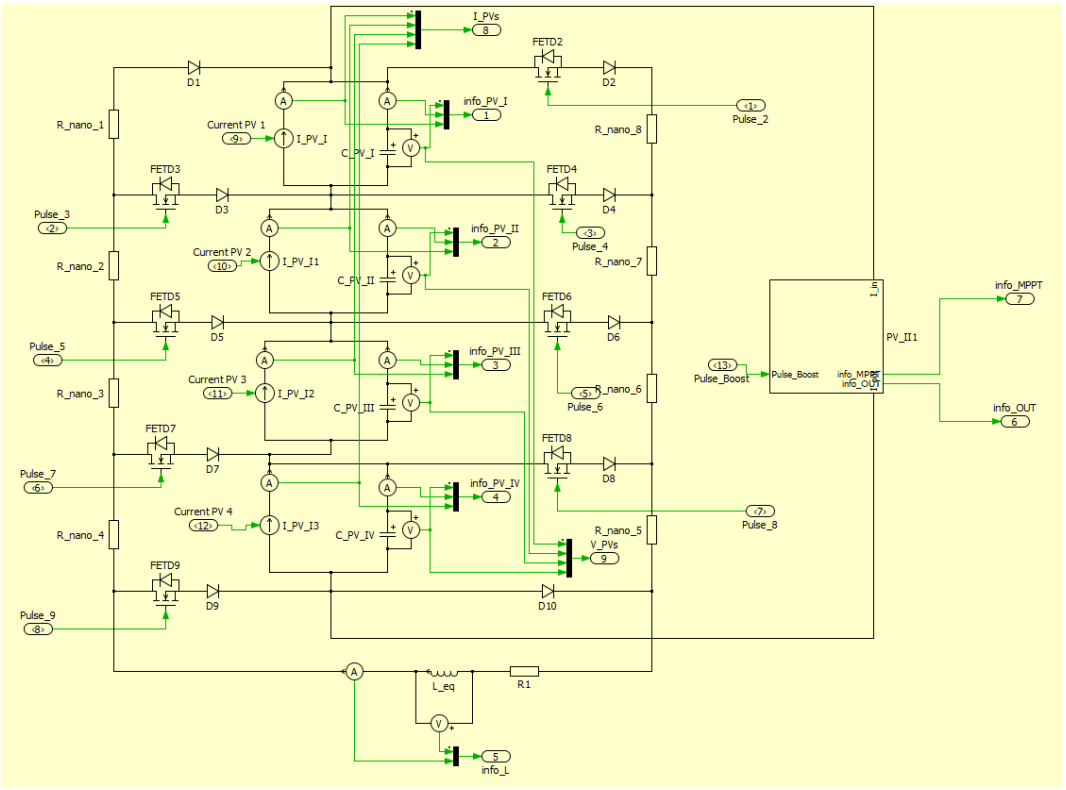

(a) The circuit model

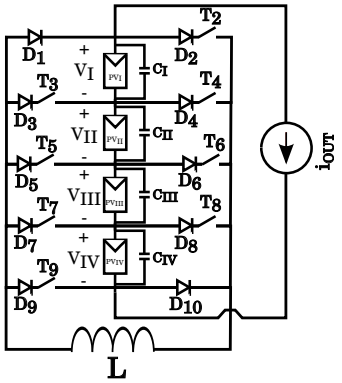

(b) The PV Equalizer circuit

Figure A.2: A comparison between the circuit model and the theoretical circuit

Each cell group, in figure A.2(a) is composed by a current source which receives the current value from the Control System. This was chosen so for speed during the simulations.

Three are acquired from each cell group and sent to the workspace: the current over the cell group itself, the current in the capacitors and their voltage. These can be used to

study what happens to each cell group individually after the simulation is finished. Figure A.3 shows I-V curves of a cell group and how they vary with irradiance.

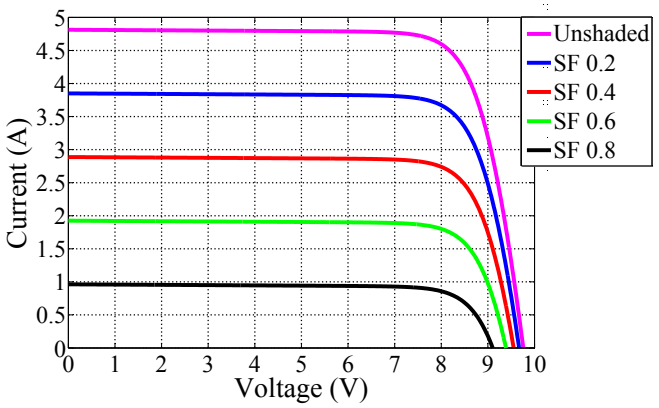

Figure A.3: The circuit of the MPPT chopper

The currents are calculated through a Lambert-W function which was developed by Damien Picaul [Picault, 2010].

The switching legs are composed by generic MOSFETs and diodes, with impulses coming from the Control System. The model allows the resistance of the MOSFETs and the forward voltage of the diodes to be set in order to estimate conduction losses. It cannot, however, be used to estimate losses due to switching.

The inductor is represented by a perfect inductance and a resistance that simulates its losses. Its voltage and current are acquired and sent to the Control System.

The MPPT is composed by the boost chopper shown in figure A.4.

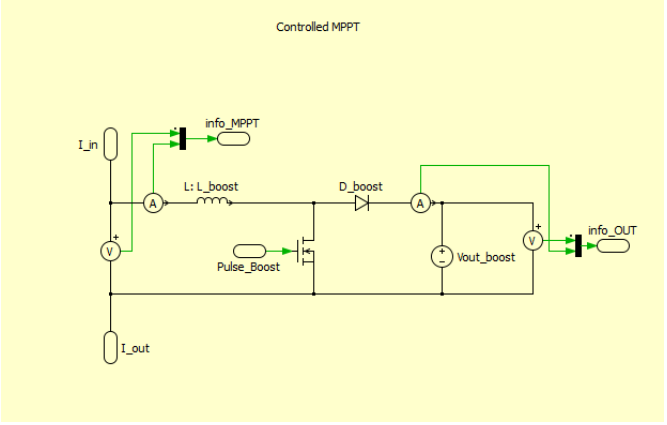

Figure A.4: The circuit of the MPPT chopper

It is controlled by a Disturb and Observe algorithm in the Control block. Its input is connected to the PV modules and its output to a fixed voltage source, simulating the DC bus. Both the input and output data are acquired and sent to the workspace for later study.

A.2 Control System

The control system of the model is composed of three parts, as shown in figure A.5

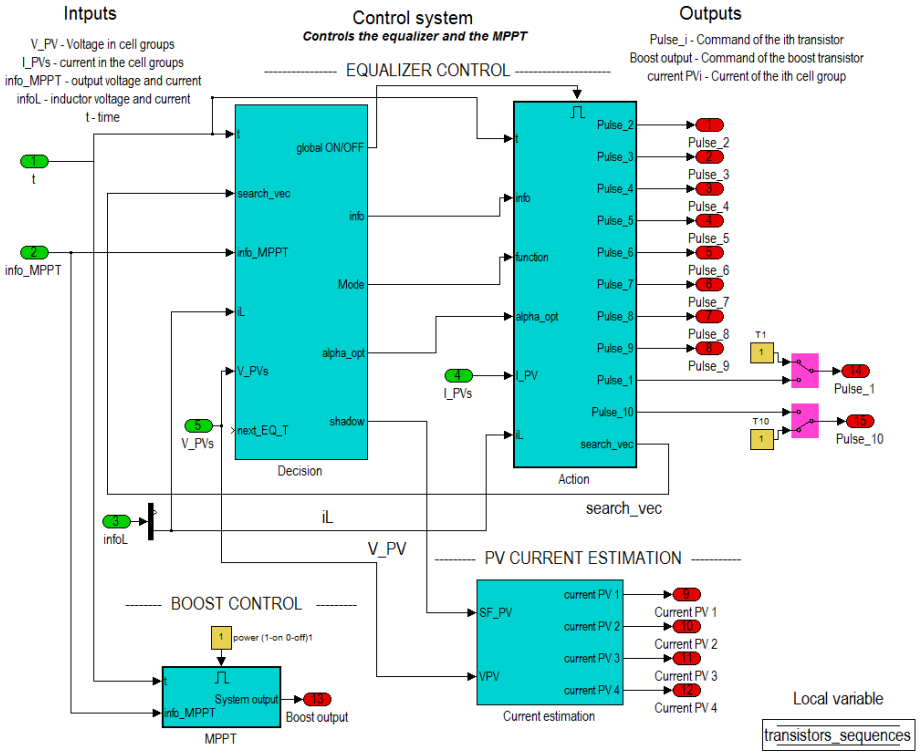

Figure A.5: The overview diagram of the control system

First, on the upper part, is the PV Equalizer control with its two sub-blocks: Decision and Action. Second, on the lower right part, is the PV Current Estimation sub-block. Finally, on the lower left part, is the Boost Control sub-block.

A.2.1 PV Equalizer control

The control system of the PV Equalizer is based on the idea that the decision sub-block configures the action sub-block. Once it is configured, the decision sub-block waits for the next moment to reconfigure it.

The decision sub-block determines if the action sub-block should be turned on, which function it will perform, the switching strategy and duty cycle. It receives the output and inductor current as well as the current peaks to control the PV Equalizer.

The action sub-block receives this information and translates them in commands that are sent to the transistors in the Physical block. This principle is shown in figure A.6.

The far command translates the information of this block into a vector of duty cycles with signs indicating if the inductors are charging or discharging. The previous period and the time are used to keep track of the moment when the impulses must change.

The close command translates the information it receives in zeros or ones, which are sent to the transistors.

A.2.2 PV current estimation

The current uses voltage from each cell group and their shading factor to calculate their current. The data is then sent to the Physical System.

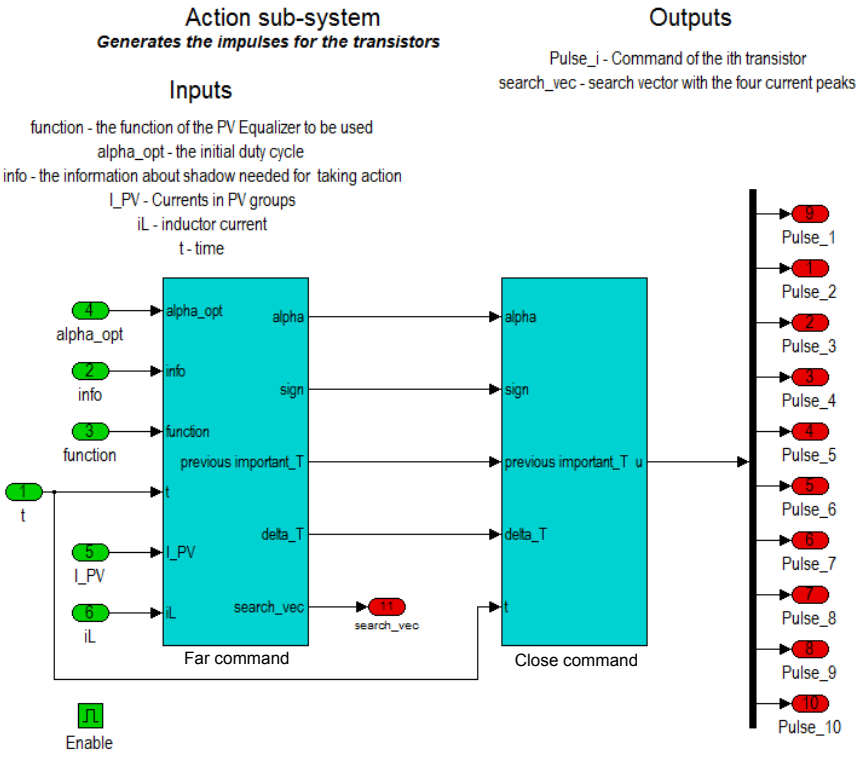

Figure A.6: The action sub-block

A.2.3 Boost control

The control system of the MPPT chopper can either follow a fixed current or track the MPP of the PV module through a disturb and observe algorithm. It is regulated by a PID controller whose parameters are set prior to the simulation.

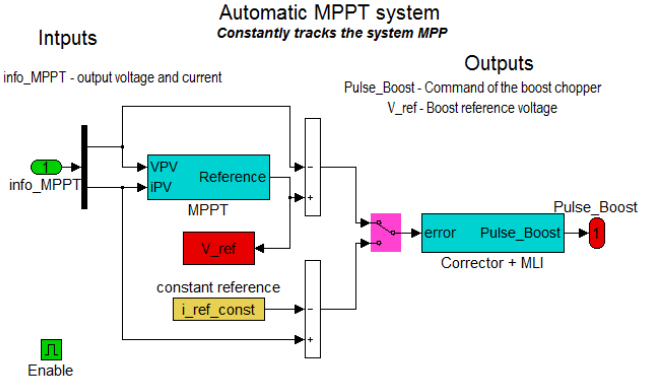

Figure A.7: The overview diagram of the control system

Appendix B

The Experimental Prototype

This appendix describes the prototype developed in this work and its elements. Its overview is proposed in figure B.1, showing three parts: Auxiliary Elements, PV Equalizer and Test Bench. Each will be described in detail below.

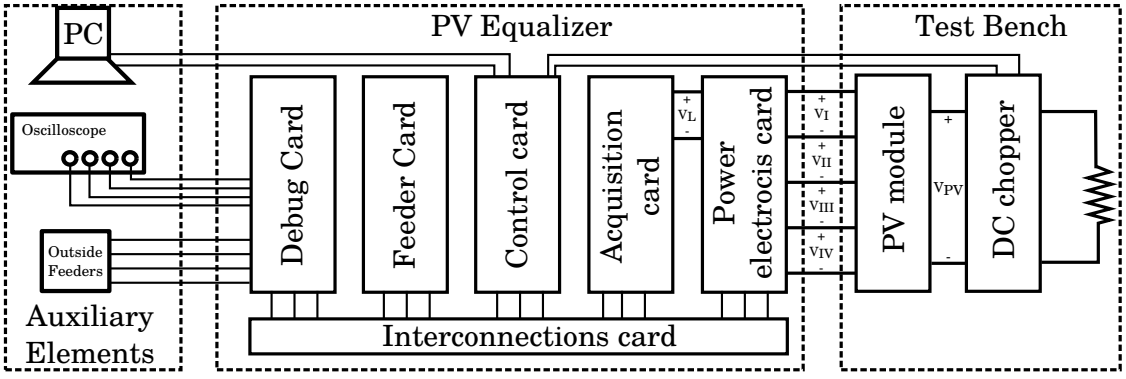

Figure B.1: Prototype overview

B.1 Auxiliary elements

Composed by a PC, an oscilloscope and an outside feeder, this part of the prototype mainly provides data acquisition and feeding support. The PC used has a C++ algorithm capable of communicating with the control card of the PV Equalizer and acquiring data. The Outside Feeder is eventually used in place of the Feeder Card for low irradiance experiments.

B.2 Test Bench

Before sizing the equalizer, its bench characteristics must be defined. The bench can be seen as everything surrounding the equalizer, thus the PV module, its MPPT and the shadows.

The PV module is a Photowatt PW1650, shown in figure B.2. It has 72 cells, organized in columns 8 of 9 cells.

Figure B.2: The reference PV module

The I-V traces of the module and its cell groups are shown in figure B.3. The irradiance under which these measurements was done is detailed in table B.1.

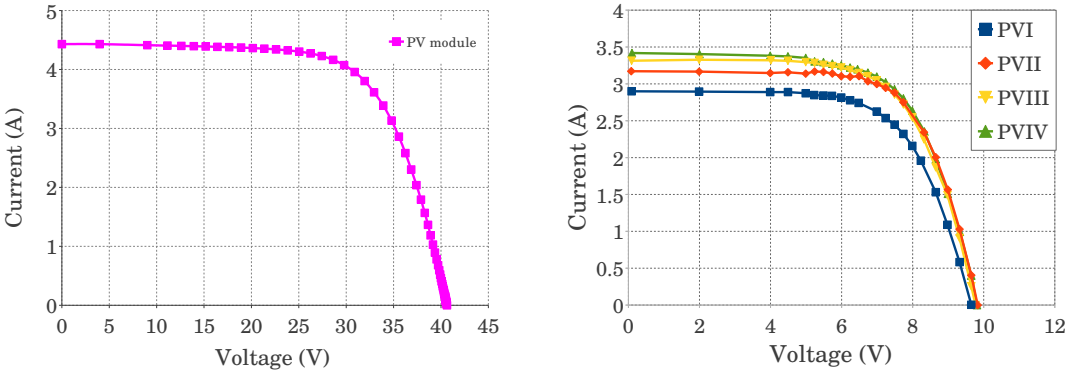

(a) The whole module

(b) Each cell group

Figure B.3: The I-V traces of the reference PV module

Table B.1: Irradiance during I-V tracing

Group measured	**Irradiance** ($\frac{W}{m^2}$)
All	930
PV_I	510
PV_{II}	570
PV_{III}	600
PV_{IV}	610

Some I-V curves were made by using the PVPM1000C40 I-V tracer. Its reference cell, shown in figure B.4, was used to measure the irradiance.

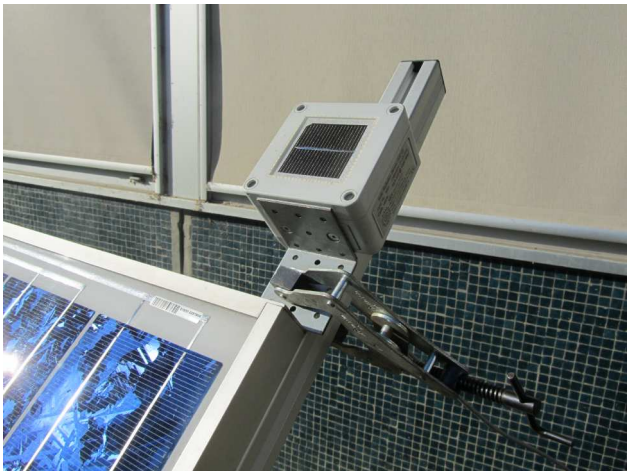

Figure B.4: The reference cell

The PV module came from the factory with four bypass diodes welded into its junction box, as shown in figure B.5. This diode disposition allows access to four cell groups, each containing 18 PV cells. The two halves of the PV module can be connected in series or parallel, allowing the PV module to have different ratings according to the needs of the designer. During this work, all groups will be connected in series and their diodes removed. The junction box was equipped with cables, connecting each cell group directly to the PV Equalizer.

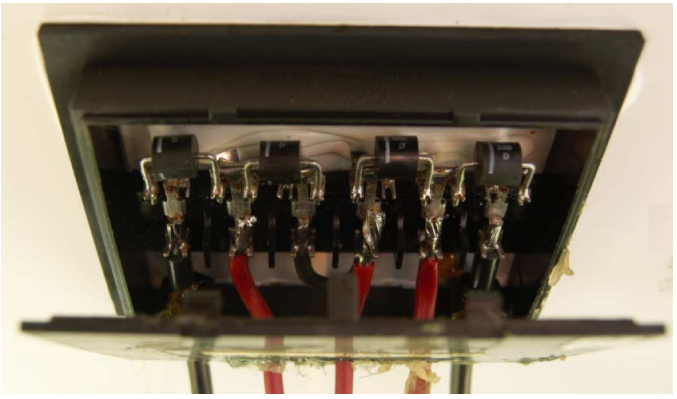

Figure B.5: The junction box with the bypass diodes

There are two types of shadow: natural or artificial. Natural shading is random and its shading factor is not controllable. Whenever it is used, a careful diagnosis procedure will estimate its characteristics as well as possible. Artificial shadow, however, can be controlled in shape and shading factor. During this work, plastic sheets have been used to craft shadows that can fit one cell group. They can then be put parallel to each other to simulate longer shadows. Figure B.6 illustrates them along with a graph characterizing their shading factor.

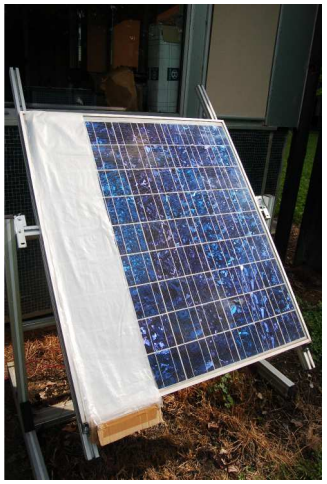

(a) The plastic sheets

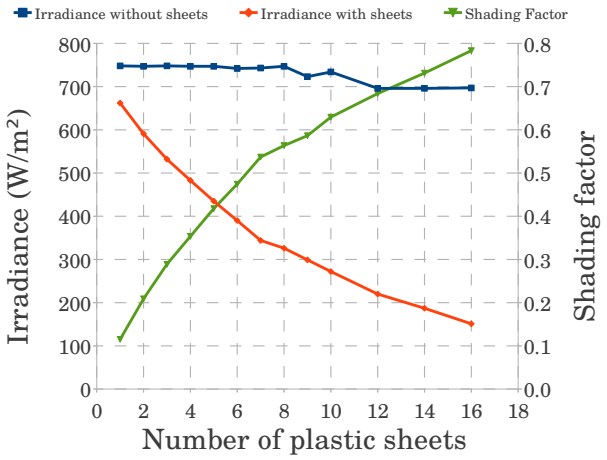

(b) Characterization of the SF

Figure B.6: Artificial shadow used in the experimental bench

The DC chopper used in this work is a reversible Buck-Boost, shown in figure B.7. It can act as a Buck when its source is connected on the high voltage side to its right, or as a Boost when connected to the low voltage side to its left. It uses two Bipolar transistors, its inductor is not fixed and it has filtering capacitors on both the low voltage and high voltage sides. The drivers and measurements are concentrated on the lower left corner, and the control impulses arrive from the PV Equalizer through a dedicated connector.

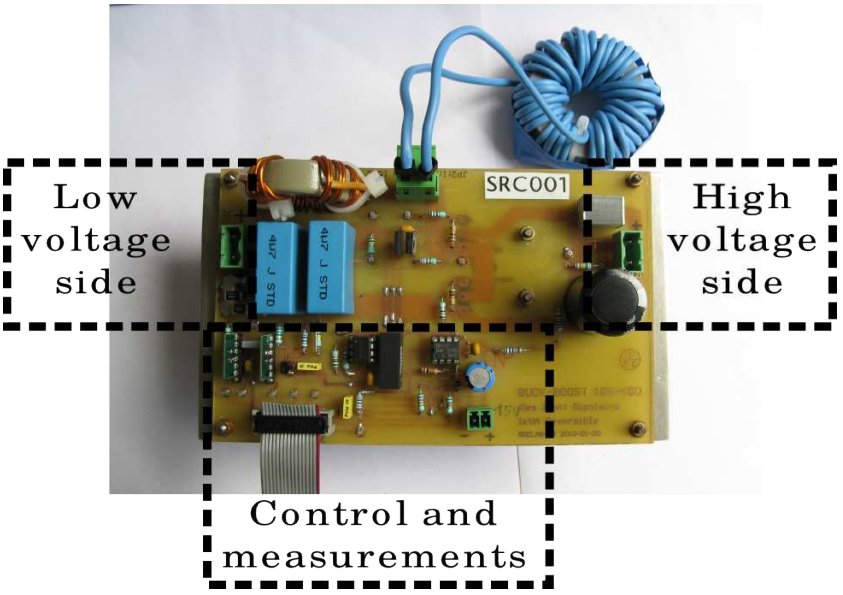

Figure B.7: The DC Chopper

The load connected to the DC chopper is a Eco 2 tubes variable resistance of 23.4 Ω and a maximum current capacity of 7.5 A.

B.3 PV Equalizer

The PV Equalizer is composed of six different cards, namely: Debug, Feeder, Control, Acquisition, Power Electronics and Interconnection. This modular approach was chosen

to ease eventual maintenance. Due to their specific design constraints, each card will be presented separately.

B.3.1 Debug Card

The debug card, shown in figure B.8, allows access to all variables related to the PV Equalizer. It is used by the oscilloscope to easily acquire, through its pins, the measurements from the acquisition card. The voltage at each cell group, the current and voltage in the inductor, the output current or the transistor impulses are available as identified in figure B.8. This card can also be used to easily feed the system from outside sources or measure the voltages from the feeder card. The pins dedicated to these are shown in the Feeder voltage square.

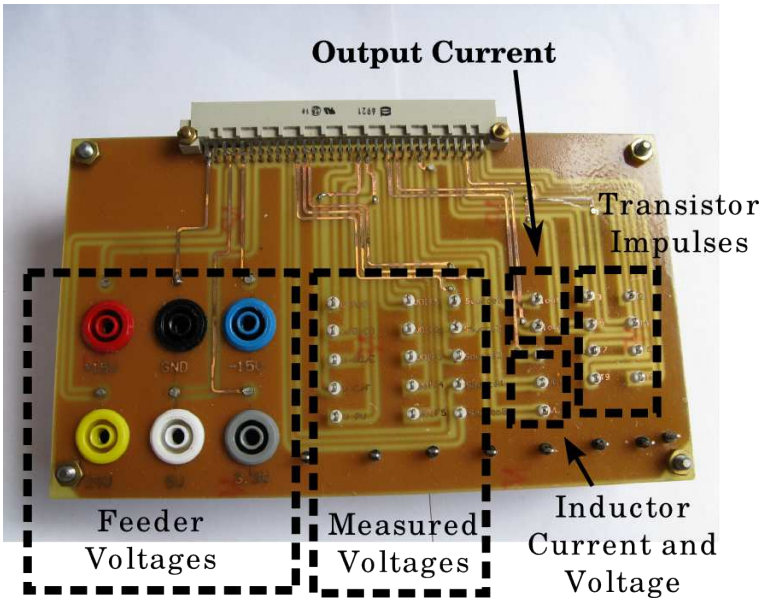

Figure B.8: The debug card

B.3.2 Feeder Card

The feeder card has a two stage DC-DC converter which uses the energy from the PV module to generate the voltages needed by the system to function. The first stage is a buck-boost which can operate between roughly 5 V and 50 V. It is connected directly to the output voltage of the PV module and its output is a stable 24 V. The second stage is connected to the output of the first stage. It generates +/- 15 V, which is used by the acquisition card and 5 V which is used by the control card.

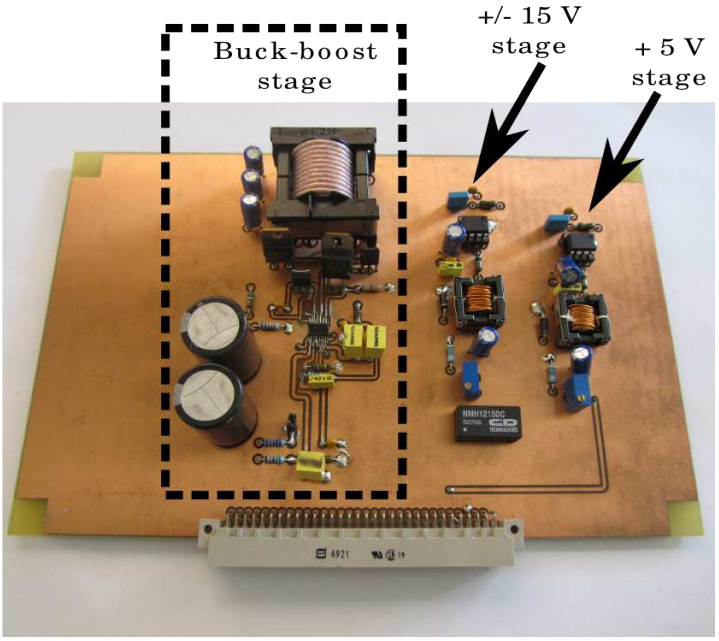

Figure B.9: The feeder card

Due to a late technical development the feeder has not yet been tested.

B.3.3 Control Card

The control card is responsible for communicating with a computer, controlling the MPPT and the PV Equalizer. It is shown in figure B.10 with each of its parts highlighted. Its interface with the outside is done through a PIC24FJ16GA002, which sends data either through the USB or to a SD card. The control system itself is composed by a PIC33FJ16GS610 mounted on a special board. The interface with the MPPT is done through a connector which sends the control impulses to the DC chopper.

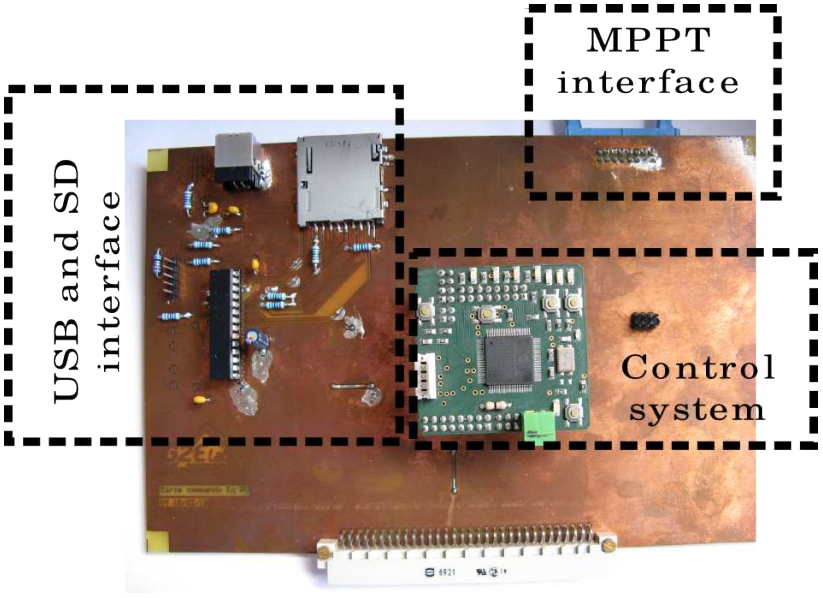

Figure B.10: The control card

B.3.4 Acquisition Card

The acquisition card is responsible for measuring several electrical variables of the PV Equalizer. It measures the voltages in each cell group and the total voltage of the PV module. The inductor current is measured through a LEM and its voltage is also available. The output current is measured in either forward or reverse, both through a shunt.

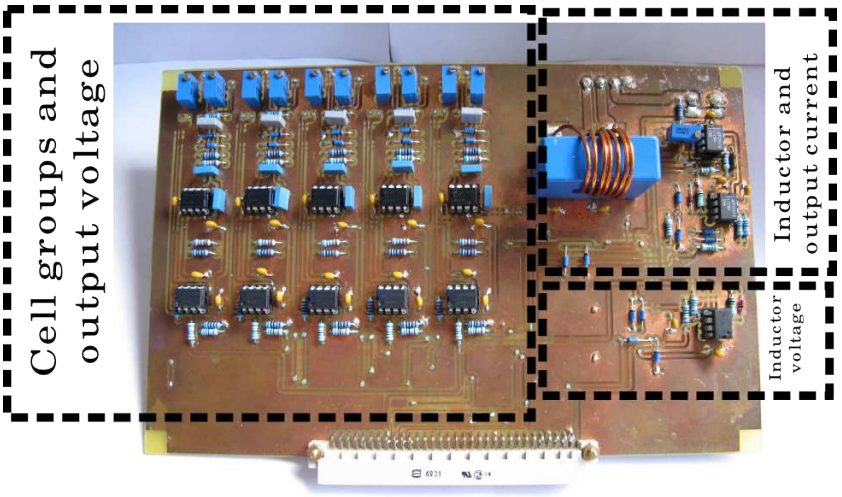

Figure B.11: The acquisition card

Their ratings were measured and are shown in figures B.12 and B.13.

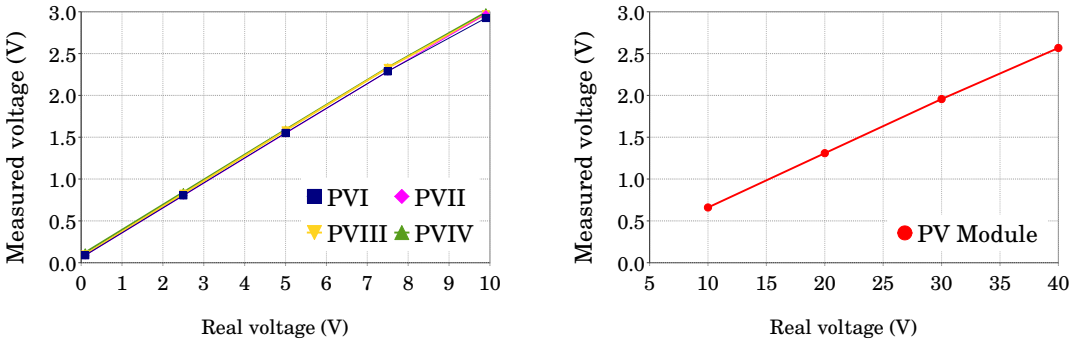

(a) Cell groups voltage

(b) Total voltage

Figure B.12: Ratings for the different voltages

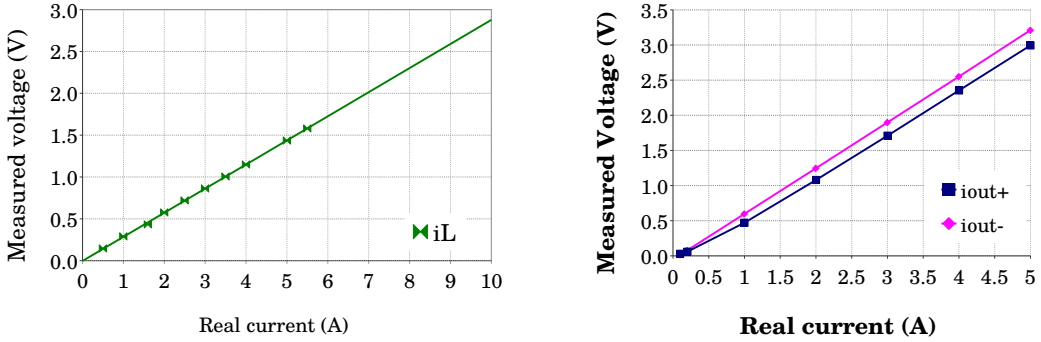

(a) Inductor current

(b) Total current

Figure B.13: Ratings for the different currents

All measurements are put into a 3.0 V scale because the maximum acceptable by the microcontroller is 3.3 V. The inductor current was not measured up to 10 A for a lack of current sources. The green line in figure B.13(a) is a linear trend line based on the measurements. The voltage in the inductor was not characterized for it was finally not used during this work.

B.3.5 Power Electronics Card

The Power Electronics card holds all the active switches, their current drivers, the capacitors and the inductor. They are highlighted in figure figure B.14.

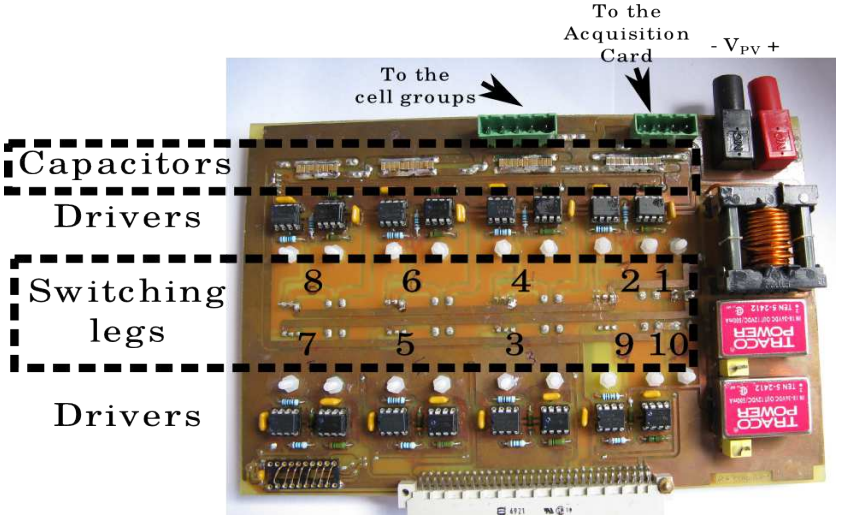

Figure B.14: The power electronics card

The information issued from the analysis performed in chapter 3 were used to design this card. Its design rules are defined using the characteristics from the test bench. They are summed up in table B.2.

The passive components of the equalizer power electronics circuit can be sized based on these design rules, equations 3.31 and 3.33 in page 77. Their values depend on the switching strategy. To calculate them, the BSS presented in chapter 3 will be used as a reference, giving table B.3.

Table B.2: Equalizer design rules

Design variable	**Desired value**	**Explanation**
Inductor current ripple (Δi_L)	$1A$	It has a low impact in power production, making this value acceptable
Capacitor voltage ripple (ΔV_C)	$50mV$	It has a hight impact in power production, making a strict control of its value necessary
Working frequency (f)	$100kHz$	Compatible with current commercial micro-controllers
Functions available	All	The equalizer must be capable of using any of its function, switching sequences and duty cycles
Shading factors	All	The equalizer must be capable of addressing any shading factor

Table B.3: Value of the components for the equalizer mode

	Switching Sequence	$L(\mu H)$	*Max* i_L	$C(\mu F)$
BSS	$II.III.IV \rightarrow I$	65.60	5.00	187.50
	$III.IV \rightarrow II$	58.30	5.00	222.20
	$IV \rightarrow I$	43.75	5.00	250.00
	$II.III \rightarrow I.II$	87.50	5.00	250.00
	$IV \rightarrow II.III$	58.30	5.00	222.20
	$I \rightarrow II.III.IV$	65.60	5.00	187.50
Universal	$All \rightarrow III$	70.00	6.25	800.00
	$All \rightarrow II.III$	116.70	7.50	666.60
	$All \rightarrow I.II.III$	150.00	8.70	571.40
CSS	$II.III \rightarrow I$ $II.III \rightarrow IV$	60.00	5.00	250.00
	$I \rightarrow II.III$ $IV \rightarrow II.III$	60.00	5.00	250.00
	$I \rightarrow II$ $I \rightarrow III$ $I \rightarrow IV$	60.00	5.00	250.00

The active components must be able to withstand, during certain BSS, to the voltage of all four PV groups together or $\pm V_{OC}$. Their current is the same that flows through the inductor. Thus, the values used to choose the components are described in table B.4. They represent a compromise between the volume of the components and the equalizer performance during BSS and CSS.

Table B.4: Chosen values for the components

Variable	**Chosen value**
Inductance	$100\mu H$
Max i_L, i_{MOSFET} and i_{diode}	$5A$
Capacitance	$220\mu F$
Active component voltage	$\pm 60V$

Table B.6: The values of the active components imperfections

Component	*Variable*	*Value*	*Unit*
Diode	Diode threshold voltage (V_{th})	$(1 + 0.1 \cdot i_L) \cdot 0.55$	V
	Diode recovery time (t_{rr})	25	ns
	Diode recovery current (i_{rrm})	$i_F + 2$	A
P-MOS Transistor	Transistor rise time (tP_r)	55	ns
	Transistor fall time (tP_f)	41	ns
	Transistor ON resistance (RP_{dsON})	100	$m\Omega$
N-MOS Transistor	Transistor rise time (tN_r)	27	ns
	Transistor fall time (tN_f)	25	ns
	Transistor ON resistance (RN_{dsON})	110	$m\Omega$

The inductor was built using the ferrite core ETD29-3C90 and single copper wire with a width of 1.25 mm^2. Its series resistance (R_S) is low due to the combination of a reduced number of turns and a large wire section. The final result are a 20 turns and a 0.18 mm air gap. Its characteristics were measured with an Aglient 4294A Precision Impedance Analyzer and are given in table B.5.

Table B.5: Inductor characteristics

Inductance (L)	**Resistance (R_L)**
$100\mu H$	$20m\Omega$

The ceramic capacitors with a rated capacitance of $22\mu F$ each were combined to reach the needed capacitance. Their performance for higher frequencies is poor and a total of 20 capacitors were needed.

The active components chosen were the fast diodes BYW29F, the P-MOS IRF9Z34N and the N-MOS IRFI530N. The two types of mosfet were used due to the position of the diodes. Two switching legs with their specific transistors and diodes are shown in figure B.15.

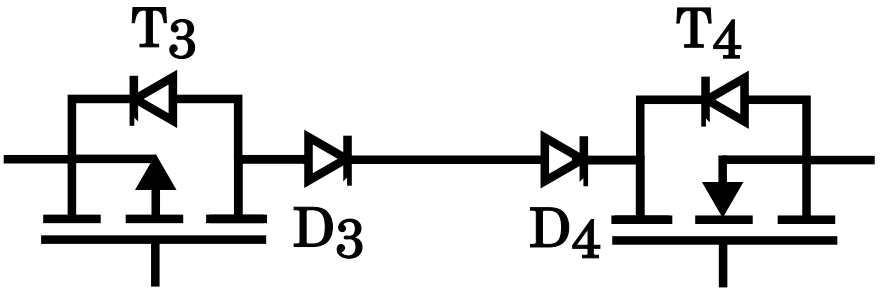

Figure B.15: The real switching leg

Their ratings are given in table B.6.

The expression for the diode losses were derived from its datasheet.

B.3.6 Interconnection Card

This card, shown in figure B.16, allows all the others to communicate among themselves. It is composed of a total of 6 64-pin connectors with all their pins connected in parallel. Thus, the other cards can be connected in any order.

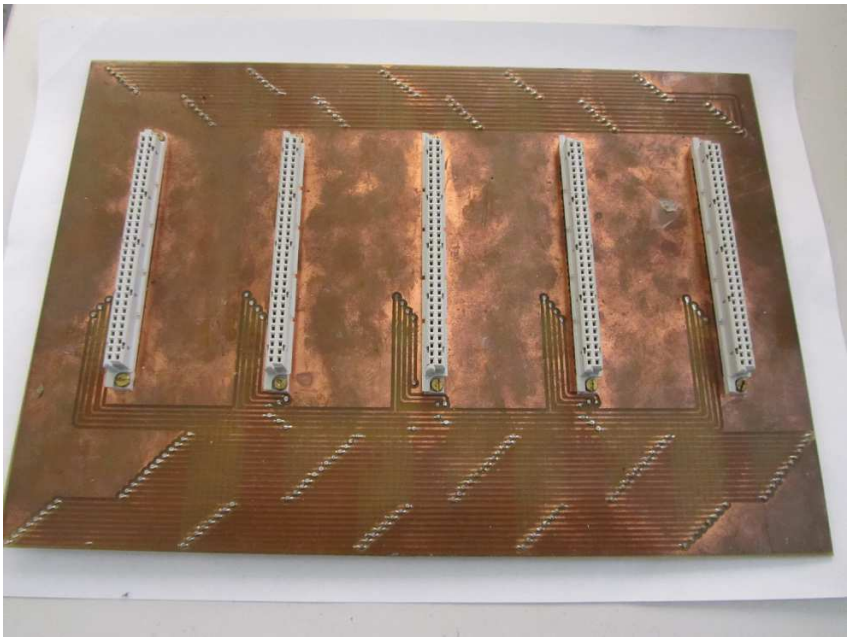

Figure B.16: The interconnection card

Figure B.17 shows all cards plugged into the the interconnection card.

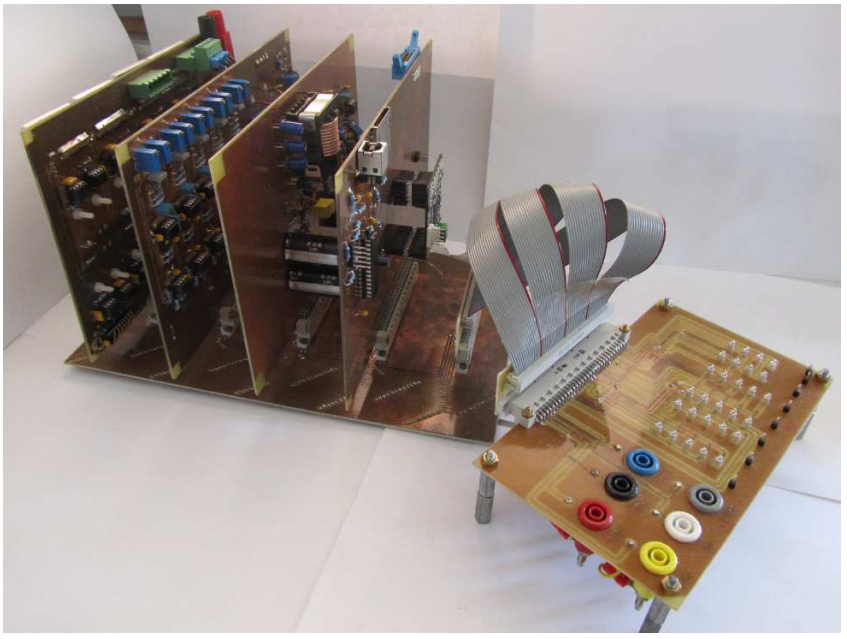

Figure B.17: All cards connected to the interconnection card

The total system, once all the elements are connected among themselves is shown in figure B.18.

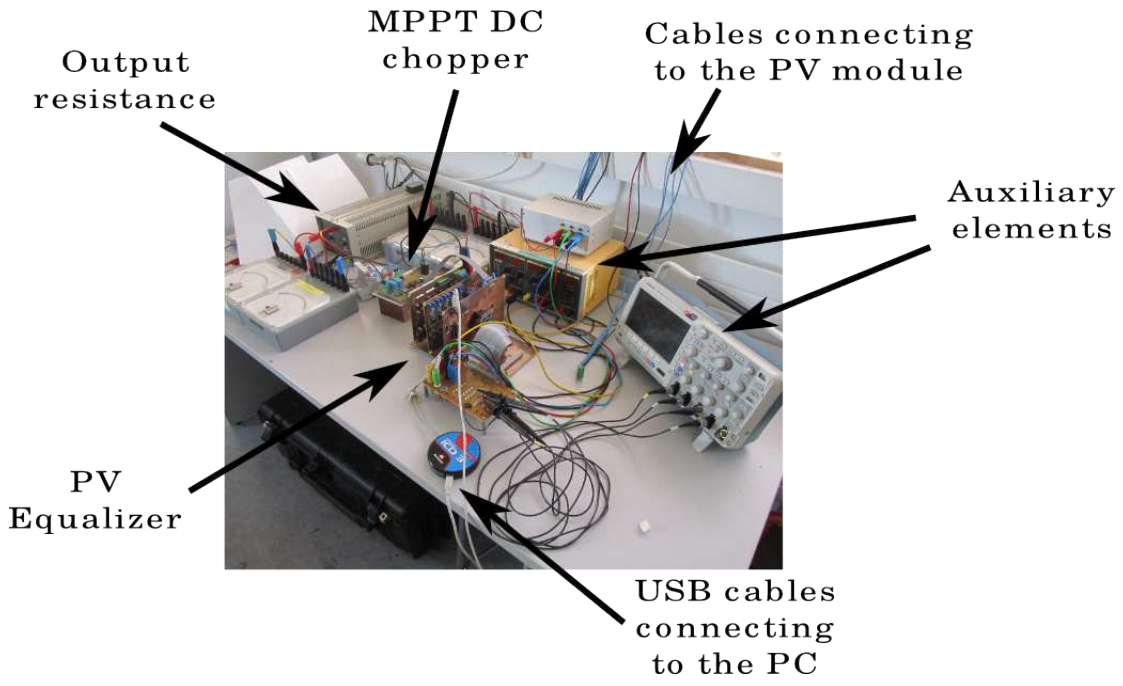

Figure B.18: The PV prototype

Appendix C

Quasi-exhaustive simulation results

This appendix details the results of the quasi-exhaustive simulation conducted in chapter 4. It shows all the switching strategies studied for each shadow case, their efficiency and output power. The shadow scenarios are recalled in table C.1.

The efficiency of each switching strategy is calculated according to equation C.1.

$$\eta = \frac{P_{Produced}}{\sum_{i=1}^{n}(SF_i \cdot P_{i_{unshaded}})} \tag{C.1}$$

Table C.1: The shading factors of the shadow scenarios

Block	*Case*	*Shading factor* PV_I	PV_{II}	PV_{III}	PV_{IV}	*Description*	*Objective*
1	1	0	0	0	0.8	One cell group is shaded. Only one SF.	Determine the effectiveness of BSS or CSS against local and small shadows.
	2	0	0	0	0.5		
	3	0	0	0	0.2		
	4	0	0	0.8	0		
	5	0	0	0.2	0		
2	6	0.8	0	0.8	0.8	Two or three cell groups are shaded. Only one SF.	Study how the effectiveness of the BSS and CSS change with the shadow shape.
	7	0	0.8	0.8	0		
	8	0	0.8	0.8	0.8		
	9	0.8	0	0	0.8		
3	10	0	0	0.8	0.2	Two or three cell groups are shaded. Different SFs.	Study the effectiveness of BSS and CSS against the shadow shape and SF at the same time.
	11	0	0.2	0.5	0.8		
	12	0	0	0.2	0.5		
	13	0	0.5	0.5	0.8		
	14	0	0.2	0	0.8		
	15	0	0.2	0.5	0		
4	16	0.2	0.5	0.8	0.8	All four cell groups are shaded. Different SFs.	Study if mildly shaded cell groups can be used to equalize heavily shaded ones.
	17	0.2	0.2	0.5	0.5		
	18	0.2	0.5	0.2	0.5		
	19	0.2	0.5	0.8	0.5		
	20	0.2	0.2	0.5	0.8		

To estimate the sum in the denominator, four reference simulations were made where all the cell groups were shaded with the same SF. Their results, shown in table C.2, will be used as the reference power for this study.

Table C.2: The reference ratings of the PV module

SF	$P_{group}(W)$	$i_{group}(A)$	$V_{group}(V)$
0.0	34.25	4.48	7.64
0.2	27.35	3.58	7.64
0.5	16.8	2.2	7.64
0.8	6.36	0.89	7.15

The switching strategies are shown per scenario, as some were studied into more detail than others. Their power

C.1 First Block

Table C.3: The switching sequences used in the shadow case 1

Case	*Shading Factor*	P_{theo}	P_{prod}	η	*Switching Strategies* 1^{st}	2^{nd}	3^{rd}
1	[0 0 0 0.8]	109.3	106.3	0.99	$I.II.III \rightarrow IV$	–	–
		109.3	101.7	0.98	$All \rightarrow IV$	–	–
		109.3	89.2	0.82	$I.II.III \rightarrow All$	–	–

Table C.4: The switching sequences used in the shadow case 2

Case	*Shading Factor*	P_{theo}	P_{prod}	η	*Switching Strategies* 1^{st}	2^{nd}	3^{rd}
2	[0 0 0 0.5]	0.99	0.97	0.99	$I.II.III \rightarrow IV$	–	–
		0.96	0.97	0.99	$All \rightarrow IV$	–	–

Table C.5: The switching sequences used in the shadow case 3

Case	*Shading Factor*	P_{theo}	P_{prod}	η	*Switching Strategies* 1^{st}	2^{nd}	3^{rd}
3	[0 0 0 0.2]	0.99	0.97	0.99	$I.II.III \rightarrow IV$	–	–
		0.97	0.97	0.99	$All \rightarrow IV$	–	–

Table C.6: The switching sequences used in the shadow case 4

Case	*Shading Factor*	P_{theo}	P_{prod}	η	*Switching Strategies* 1^{st}	2^{nd}	3^{rd}
		109.31	98.93	0.91	$All \rightarrow III$	–	–
		109.31	98.67	0.90	$I.II \rightarrow III$	–	–
		109.31	97.82	0.89	$I.II \rightarrow III$	$IV \rightarrow III$	–
		109.31	94.06	0.86	$I.II \rightarrow III$	$IV \rightarrow III$	$IV \rightarrow III$
4	[0 0 0.8 0]	109.31	93.68	0.86	$I.II.III \rightarrow III$	–	–
		109.31	93.13	0.85	$I \rightarrow III$	$II \rightarrow III$	$IV \rightarrow III$
		109.31	83.00	0.76	$I \rightarrow III$	–	–
		109.31	77.25	0.71	$I.II \rightarrow III.IV$	–	–
		109.31	64.74	0.64	$All \rightarrow All$	–	–

Table C.7: The switching sequences used in the shadow case 5

Case	*Shading Factor*	P_{theo}	P_{prod}	η	*Switching Strategies* 1^{st}	2^{nd}	3^{rd}
		130.27	129.6	0.99	$All \rightarrow III$	–	–
		130.27	129.5	0.99	$I.II \rightarrow III$	$IV \rightarrow III$	–
		130.27	129.3	0.99	$I.II \rightarrow III$	–	–
		130.27	129.2	0.99	$I \rightarrow III$	$II \rightarrow III$	$I \rightarrow III$
5	[0 0 0.2 0]	130.27	129	0.99	$I.II \rightarrow III$	$IV \rightarrow III$	$IV \rightarrow III$
		130.27	129.2	0.99	$I.II.III \rightarrow III$	–	–
		130.27	127.3	0.98	$I \rightarrow III$	–	–
		130.27	125.7	0.96	$I.II \rightarrow III.IV$	–	–
		130.27	117	0.90	$All \rightarrow All$	–	–

C.2 Second Block

Table C.8: The switching sequences used in the shadow case 6

Case	*Shading Factor*	P_{theo}	P_{prod}	η	*Switching Strategies* 1^{st}	2^{nd}	3^{rd}
		53.57	43.82	0.82	$II \rightarrow All$	–	–
		53.57	41.41	0.77	$II \rightarrow I$	$II \rightarrow III.IV$	–
6	[0.8 0 0.8 0.8]	53.57	40.44	0.75	$II \rightarrow I$	$II \rightarrow III$	$II \rightarrow IV$
		53.57	27.17	0.51	$All \rightarrow All$	–	–

Table C.9: The switching sequences used in the shadow case 7

Case	*Shading Factor*	P_{theo}	P_{prod}	η	*Switching Strategies* 1^{st}	2^{nd}	3^{rd}
7	[0 0.8 0.8 0]	81.44	65.16	0.80	$I \rightarrow II.III$	$IV \rightarrow II.III$	–
		81.44	65.13	0.80	$All \rightarrow II.III$	–	–
		81.44	59.36	0.73	$I \rightarrow II.III$	–	–
		81.44	55.26	0.68	$I.II \rightarrow II.III$	$III.IV \rightarrow II.III$	–
		81.44	55.21	0.68	$I \rightarrow II$	$IV \rightarrow III$	–
		81.44	48.04	0.59	$All \rightarrow II$	$All \rightarrow III$	–
		81.44	47.87	0.59	$I.II.III \rightarrow II.III$	$II.III.IV \rightarrow II.III$	–
		81.44	43.15	0.53	$I.II \rightarrow II$	$III.IV \rightarrow III$	–
		81.44	43.03	0.53	$I.II \rightarrow III$	$III.IV \rightarrow II$	–
		81.44	28.94	0.36	$I \rightarrow II$	$II \rightarrow III$	–

Table C.10: The switching sequences used in the shadow case 8

Case	*Shading Factor*	P_{theo}	P_{prod}	η	*Switching Strategies* 1^{st}	2^{nd}	3^{rd}
8	[0 0.8 0.8 0.8]	53.57	44.00	0.82	$I \rightarrow All$	–	–
		53.57	40.81	0.76	$All \rightarrow II.III.IV$	–	–
		53.57	40.44	0.75	$I \rightarrow II.III.IV$	–	–
		53.57	40.08	0.75	$I \rightarrow II$	$I \rightarrow III$	$I \rightarrow IV$
		53.57	30.33	0.57	$All \rightarrow II$	$All \rightarrow III$	$All \rightarrow IV$
		53.57	27.29	0.51	$All \rightarrow All$	–	–

Table C.11: The switching sequences used in the shadow case 9

Case	*Shading Factor*	P_{theo}	P_{prod}	η	*Switching Strategies* 1^{st}	2^{nd}	3^{rd}
9	[0 0.8 0.8 0]	81.44	68.9	0.85	$II.III \rightarrow I$	$II.III \rightarrow IV$	–
		81.44	68.64	0.84	$II.III \rightarrow All$	–	–
		81.44	66.46	0.82	$I.II.III \rightarrow I$	$II.III.IV \rightarrow IV$	–
		81.44	62.16	0.76	$II \rightarrow I$	$III \rightarrow IV$	$II.III \rightarrow All$
		81.44	58.39	0.72	$II \rightarrow I$	$III \rightarrow IV$	–
		81.44	52.74	0.65	$All \rightarrow I$	$All \rightarrow IV$	–
		81.44	46.72	0.57	$II \rightarrow I$	$III \rightarrow IV$	$All \rightarrow All$
		81.44	28.63	0.35	$All \rightarrow All$	–	–

C.3 Third Block

Table C.12: The switching sequences used in the shadow case 10

Case	*Shading Factor*	P_{theo}	P_{prod}	η	*Switching Strategies* 1^{st}	2^{nd}	3^{rd}
		102.4	95.48	0.93	$I.II \rightarrow III$	–	–
		102.4	91.96	0.90	$I.II.III \rightarrow III$	–	–
		102.4	90.55	0.88	$All \rightarrow III$	–	–
		102.4	80.93	0.79	$I.II \rightarrow III$	$I.II \rightarrow IV$	$I.II \rightarrow IV$
		102.4	71.24	0.70	$IV \rightarrow III$	–	–
10	[0 0 0.8 0.2]	102.4	69.82	0.68	$I \rightarrow III$	$II \rightarrow III$	$I \rightarrow IV$
		102.4	69.81	0.68	$I \rightarrow III$	$II \rightarrow III$	$II \rightarrow IV$
		102.4	68.98	0.67	$All \rightarrow III.IV$	–	–
		102.4	67.39	0.66	$I.II \rightarrow III$	$I.II \rightarrow IV$	–
		102.4	57.09	0.56	$I \rightarrow III$	$II \rightarrow IV$	–
		102.4	45.36	0.44	$I.II.III \rightarrow III.IV$	–	–

Table C.13: The switching sequences used in the shadow case 11

Case	*Shading Factor*	P_{theo}	P_{prod}	η	*Switching Strategies* 1^{st}	2^{nd}	3^{rd}
		84.99	78.35	0.92	$I.II.III \rightarrow III.IV$	–	–
		84.99	72.72	0.86	$I.II \rightarrow IV$	–	–
		84.99	71.88	0.85	$I \rightarrow IV$	–	–
		84.99	71.86	0.85	$I.II.III \rightarrow II.III.IV$	–	–
		84.99	69.48	0.82	$I.II \rightarrow III.IV$	–	–
		84.99	67.51	0.79	$I.II \rightarrow II.III.IV$	–	–
		84.99	64.24	0.76	$All \rightarrow III.IV$	–	–
		84.99	63.11	0.74	$I.II.III \rightarrow II$	$I.II.III \rightarrow III$	$I.II.III \rightarrow IV$
11	[0 0.2 0.5 0.8]	84.99	61.56	0.72	$All \rightarrow IV$	–	–
		84.99	61.47	0.72	$I \rightarrow IV$	$II \rightarrow IV$	$III \rightarrow IV$
		84.99	60.28	0.71	$I \rightarrow III.IV$	–	–
		84.99	59.84	0.70	$I.II.III \rightarrow IV$	–	–
		84.99	54.80	0.64	$I \rightarrow IV$	$II \rightarrow III$	–
		84.99	51.30	0.60	$I.II \rightarrow II$	$I.II \rightarrow III$	$I.II \rightarrow IV$
		84.99	43.50	0.51	$I \rightarrow II.III.IV$	–	–
		84.99	42.70	0.50	$All \rightarrow II.III.IV$	–	–
		84.99	41.89	0.49	$I \rightarrow II$	$I \rightarrow III$	$I \rightarrow IV$
		84.99	31.94	0.38	$All \rightarrow II$	$All \rightarrow III$	$All \rightarrow IV$

Table C.14: The switching sequences used in the shadow case 12

Case	*Shading Factor*	P_{theo}	P_{prod}	η	*Switching Strategies* 1^{st}	2^{nd}	3^{rd}
12	[0 0 0.2 0.5]	112.85	110.6	0.98	$I.II \rightarrow IV$	–	–
		112.85	109.2	0.97	$I.II.III \rightarrow III.IV$	–	–
		112.85	104.6	0.93	$I \rightarrow IV$	–	–
		112.85	104.4	0.93	$All \rightarrow IV$	–	–
		112.85	102.9	0.91	$I.II.III \rightarrow IV$	–	–
		112.85	102	0.90	$I.II \rightarrow III.IV$	–	–
		112.85	98.21	0.87	$All \rightarrow III.IV$	–	–
		112.85	97.44	0.86	$I.II \rightarrow III$	$I.II \rightarrow IV$	–
		112.85	87.61	0.78	$All \rightarrow III$	$All \rightarrow IV$	–
		112.85	91.8	0.81	$I \rightarrow IV$	$II \rightarrow III$	–

Table C.15: The switching sequences used in the shadow case 13

Case	*Shading Factor*	P_{theo}	P_{prod}	η	*Switching Strategies* 1^{st}	2^{nd}	3^{rd}
13	[0 0.5 0.5 0.8]	74.47	68.26	0.92	$I \rightarrow IV$	–	–
		74.47	68.24	0.92	$I.II.III \rightarrow II.III.IV$	–	–
		74.47	64.64	0.87	$I.II.III \rightarrow II.III$	$I.II.III \rightarrow IV$	–
		74.47	61.52	0.83	$I \rightarrow IV$	$I \rightarrow IV$	$II \rightarrow III$
		74.47	59.72	0.80	$All \rightarrow IV$	–	–
		74.47	58.86	0.79	$I.II.III \rightarrow IV$	–	–
		74.47	56.09	0.75	$II.III \rightarrow IV$	–	–
		74.47	52.38	0.70	$I.II \rightarrow II.III$	$I \rightarrow IV$	–
		74.47	51.84	0.70	$I \rightarrow II.III$	–	$I \rightarrow IV$
		74.47	51.77	0.70	$I \rightarrow IV$	$I \rightarrow II.III$	–
		74.47	50.42	0.68	$I.II \rightarrow III.IV$	–	–
		74.47	43.47	0.58	$I \rightarrow II.III.IV$	–	–
		74.47	42.22	0.57	$All \rightarrow II.III.IV$	–	–
		74.47	40.52	0.54	$All \rightarrow II.III$	$All \rightarrow IV$	–

Table C.16: The switching sequences used in the shadow case 14

Case	*Shading Factor*	P_{theo}	P_{prod}	η	*Switching Strategies* 1^{st}	2^{nd}	3^{rd}
14	[0 0.2 0 0.8]	112.85	104.3	0.92	$All \rightarrow IV$	–	–
		112.85	103.1	0.91	$I.II.III \rightarrow IV$	–	–
		112.85	102.7	0.91	$I.II.III \rightarrow IV$	–	–
		112.85	100.2	0.89	$I.II.III \rightarrow II$	$III \rightarrow IV$	$I \rightarrow IV$
		112.85	99.57	0.88	$I \rightarrow II$	$III \rightarrow IV$	$III \rightarrow IV$
		112.85	99.3	0.88	$I \rightarrow II$	$III \rightarrow IV$	–
		112.85	92.02	0.82	$I \rightarrow II$	–	–
		112.85	87.93	0.78	$All \rightarrow II$	$All \rightarrow IV$	–
		112.85	83.16	0.74	$All \rightarrow II.III.IV$	–	–

Table C.17: The switching sequences used in the shadow case 15

Case	*Shading Factor*	P_{theo}	P_{prod}	η	*Switching Strategies* 1^{st}	2^{nd}	3^{rd}
		112.85	107.5	0.95	$I \rightarrow III$	$IV \rightarrow III$	–
		112.85	104.2	0.92	$All \rightarrow III$	–	–
		112.85	103.6	0.92	$I.II \rightarrow II.III$	$IV \rightarrow II.III$	–
15	[0 0.2 0.5 0]	112.85	103	0.91	$I \rightarrow III$	$I.II \rightarrow III.IV$	$IV \rightarrow III$
		112.85	101.1	0.90	$I.II \rightarrow III$	–	–
		112.85	96.62	0.86	$All \rightarrow II.III$	–	–
		112.85	86.79	0.77	$All \rightarrow III$	$All \rightarrow II$	–

C.4 Fourth Block

Table C.18: The switching sequences used in the shadow case 16

Case	*Shading Factor*	P_{theo}	P_{prod}	η	*Switching Strategies* 1^{st}	2^{nd}	3^{rd}
		57.12	53.38	0.93	$I.II \rightarrow II.III.IV$	–	–
		57.12	51.77	0.91	$I \rightarrow III.IV$	–	–
		57.12	51.16	0.90	$I.II \rightarrow II$	$I.II \rightarrow III.IV$	$I.II \rightarrow III.IV$
		57.12	48.57	0.85	$I.II \rightarrow III.IV$	–	–
		57.12	48.4	0.85	$All \rightarrow III.IV$	–	–
		57.12	48.21	0.84	$I.II \rightarrow III$	$I.II \rightarrow IV$	–
		57.12	47.76	0.84	$I \rightarrow III$	$I \rightarrow IV$	–
16	[0 0.5 0.8 0.8]	57.12	45.6	0.80	$I.II \rightarrow II$	$I.II \rightarrow III$	$I.II \rightarrow IV$
		57.12	43.43	0.76	$I \rightarrow II$	$I \rightarrow III.IV$	$I \rightarrow III.IV$
		57.12	42.98	0.75	$All \rightarrow III$	$All \rightarrow IV$	–
		57.12	40.41	0.71	$All \rightarrow II.III.IV$	–	–
		57.12	39.52	0.69	$I \rightarrow II.III.IV$	–	–
		57.12	39.12	0.68	$I \rightarrow II$	$I \rightarrow III$	$I \rightarrow IV$
		57.12	39.07	0.68	$All \rightarrow III$	$All \rightarrow III.IV$	$All \rightarrow III.IV$
		57.12	31.09	0.54	$All \rightarrow II$	$All \rightarrow III$	$All \rightarrow IV$

Table C.19: The switching sequences used in the shadow case 17

Case	*Shading Factor*	P_{theo}	P_{prod}	η	*Switching Strategies* 1^{st}	2^{nd}	3^{rd}
		88.53	88.07	0.99	$I.II \rightarrow III.IV$	–	–
		88.53	86.79	0.98	$All \rightarrow III.IV$	–	–
		88.53	86.55	0.98	$I.II \rightarrow III$	$I.II \rightarrow IV$	–
		88.53	86.47	0.98	$I \rightarrow III$	$II \rightarrow IV$	$I.II \rightarrow III.IV$
		88.53	86.25	0.97	$I \rightarrow III.IV$	$II \rightarrow III.IV$	–
		88.53	84.30	0.95	$I \rightarrow III$	$II \rightarrow IV$	–
17	[0.2 0.2 0.5 0.5]	88.53	83.46	0.94	$I \rightarrow III.IV$	–	–
		88.53	82.29	0.93	$I \rightarrow III$	$I \rightarrow IV$	–
		88.53	82.22	0.93	$All \rightarrow III$	$All \rightarrow IV$	–
		88.53	81.22	0.92	$II.III.IV \rightarrow III.IV$	–	–
		88.53	80.98	0.91	$I.II.III \rightarrow III.IV$	–	–
		88.53	73.06	0.83	$I.II \rightarrow III$	–	–
		88.53	73.05	0.83	$I.II.III \rightarrow III$	–	–

Table C.20: The switching sequences used in the shadow case 18

Case	*Shading Factor*	P_{theo}	P_{prod}	η	*Switching Strategies* 1^{st}	2^{nd}	3^{rd}
18	[0.2 0.5 0.2 0.5]	88.53	84.30	0.95	$I \rightarrow II$	$III \rightarrow IV$	–
		88.53	82.29	0.93	$I \rightarrow II$	$I \rightarrow IV$	–
		88.53	82.23	0.93	$All \rightarrow II$	$All \rightarrow IV$	–
		88.53	80.37	0.91	$I.II.III \rightarrow IV$	$I.II.III \rightarrow IV$	–
		88.53	80.19	0.91	$I.II \rightarrow II$	$III.IV \rightarrow IV$	–
		88.53	80.19	0.91	$I.II \rightarrow IV$	$III.IV \rightarrow II$	–
		88.53	69.45	0.78	$I.II.III \rightarrow IV$	–	–

Table C.21: The switching sequences used in the shadow case 19

Case	*Shading Factor*	P_{theo}	P_{prod}	η	*Switching Strategies* 1^{st}	2^{nd}	3^{rd}
19	[0.2 0.5 0.8 0.5]	67.57	63.80	0.94	$I \rightarrow III$	–	–
		67.57	58.98	0.87	$All \rightarrow III$	–	–
		67.57	57.89	0.86	$I.II \rightarrow III$	$IV \rightarrow III$	–
		67.57	57.41	0.85	$I.II \rightarrow III$	–	–
		67.57	55.98	0.83	$I.II.III \rightarrow III$	–	–
		67.57	50.14	0.74	$I.II \rightarrow III.IV$	–	–
		67.57	40.99	0.61	$All \rightarrow II.III.IV$	–	–
		67.57	40.40	0.60	$I \rightarrow II.III.IV$	–	–
		67.57	40.01	0.59	$I \rightarrow II$	$I \rightarrow III$	$I \rightarrow IV$
		67.57	30.46	0.45	$All \rightarrow II$	$All \rightarrow III$	$All \rightarrow IV$

Table C.22: The switching sequences used in the shadow case 20

Case	*Shading Factor*	P_{theo}	P_{prod}	η	*Switching Strategies* 1^{st}	2^{nd}	3^{rd}
20	[0.2 0.2 0.5 0.8]	78.08	74.49	0.95	$I.II.III \rightarrow III.IV$	–	–
		78.08	72.13	0.92	$I.II \rightarrow IV$	–	–
		78.08	67.69	0.87	$I \rightarrow IV$	–	–
		78.08	65.92	0.84	$I.II \rightarrow III.IV$	–	–
		78.08	61.47	0.79	$All \rightarrow IV$	–	–
		78.08	60.99	0.78	$All \rightarrow III.IV$	–	–
		78.08	60.04	0.77	$I.II \rightarrow III$	$I.II \rightarrow IV$	–
		78.08	59.80	0.77	$I.II.III \rightarrow IV$	–	–
		78.08	52.84	0.68	$I \rightarrow IV$	$II \rightarrow III$	–
		78.08	47.53	0.61	$All \rightarrow III$	$All \rightarrow IV$	–

Appendix D

Details of the robustness surface calculation

This appendix gives the details for the calculation of the robustness shown in chapter 2. It is based on the sum of the power lost by all the shaded cell groups and its comparison with the maximum robustness.

First, the power lost will be estimated through the use of figure D.1. It shows the power as a function of the number of shaded cells or cell groups. The objective is to describe an expression for the red triangle. The variable P means power, n_{gSH} means the number of groups actually shaded, n_{cpg} means the number of cells per group, h means the height, b means the bas.

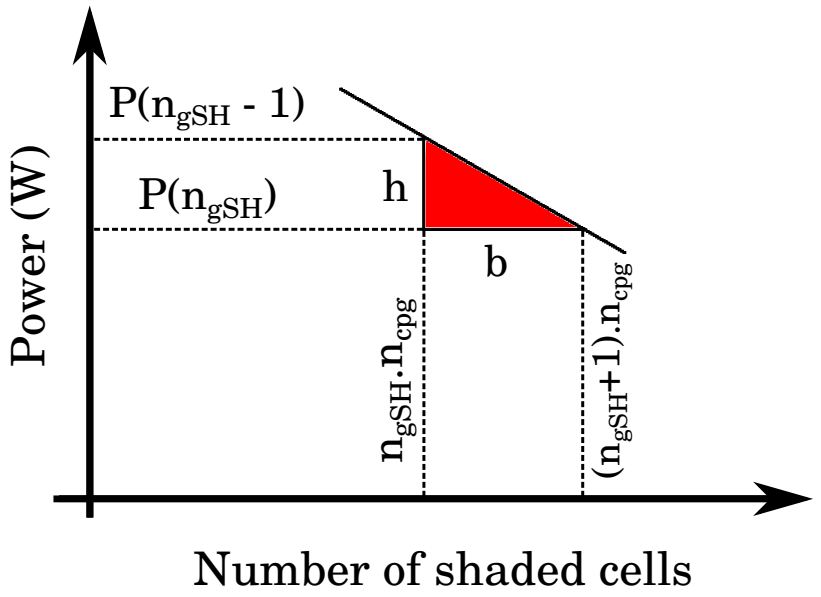

Figure D.1: The power lost due to one group

The surface determined by the red triangle is given by equation D.1. It represents the robustness lost due to the shading of a single cell group, being called Rob_{lostg}.

$$Rob_{lostg} = \frac{b \cdot h}{2} \tag{D.1}$$

The expression of the base and the height are given by equations D.2 and D.3.

$$b = (n_{gSH} + 1) \cdot n_{cpg} - n_{gSH} \cdot n_{cpg} \tag{D.2}$$

$$h = P(n_{gSH} - 1) - P(n_{gSH}) \tag{D.3}$$

By replacing the two equations above into equation D.1 gives:

$$Rob_{lostg} = \frac{n_{cpg} \cdot (P(n_{gSH} - 1) - P(n_{gSH}))}{2} \tag{D.4}$$

The expression of the power as a function of the number of shaded cell groups was given in 2 and is recalled below.

$$P(n_{gSH}) = n_{cpg} \cdot (n_{gtot} \cdot P_{USH} + n_{gSH} \cdot (P_{SH} - P_{USH})) \tag{D.5}$$

By replacing equation D.5 into equation D.4 and rearranging gives:

$$Rob_{lostg} = \frac{n_{cpg}^2 \cdot (P_{USH} - P_{SH})}{2} \tag{D.6}$$

Equation D.6 gives the power lost by one cell group. It can be used to calculate the total robustness of a PV plant only if this power is multiplied by the number of cell groups.

The maximum robustness was defined in chapter 2 and its expression is recalled in equation D.7.

$$Rob_{MAX} = n_{tot}^2 \cdot \frac{(P_{USH} + P_{SH})}{2} \tag{D.7}$$

To determine the robustness of the PV plant, the robustness lost by its cell groups must be subtracted from the maximum robustness, giving equation D.8.

$$Rob = Rob_{MAX} - Rob_{lost} \tag{D.8}$$

The total robustness lost is the sum of all the contributions from each cell group, yielding equation D.9. In it, n_{gtot} represents the total number of cell groups in the PV plant.

$$Rob = Rob_{MAX} - \sum_{1}^{n_{gtot}} Rob_{lostg} \tag{D.9}$$

Since the expression of the robustness lost by one group does not depend on the total number of cell groups, equation D.9 is equivalent to:

$$Rob = Rob_{MAX} - n_{gtot} \cdot Rob_{lostg} \tag{D.10}$$

By replacing equation D.6 into equation D.10 gives:

$$Rob = Rob_{MAX} - \frac{n_{gtot} \cdot n_{cpg}^2 \cdot (P_{USH} - P_{SH})}{2} \tag{D.11}$$

Dividing both sides of equation D.11 by Rob_{MAX} and gives:

$$\frac{Rob}{Rob_{MAX}} = 1 - \frac{n_{gtot} \cdot n_{cpg}^2 \cdot (P_{USH} - P_{SH})}{Rob_{MAX} \cdot 2} \tag{D.12}$$

Using the definition of the maximum robustness into equation D.12 gives:

$$\frac{Rob}{Rob_{MAX}} = 1 - \frac{n_{gtot} \cdot n_{cpg}^2 \cdot (P_{USH} - P_{SH}) \cdot 2}{n_{tot}^2 \cdot (P_{USH} + P_{SH}) \cdot 2} \tag{D.13}$$

Considering that the relation between n_{tot}, n_{gtot} and n_{cpg} is given by equation D.14.

$$n_{tot} = n_{gtot} \cdot n_{cpg} \tag{D.14}$$

Equation D.13 can be simplified to:

$$\frac{Rob}{Rob_{MAX}} = 1 - \left(\frac{n_{cpg} \cdot (P_{USH} - P_{SH})}{n_{tot} \cdot (P_{USH} + P_{SH})} \right) \tag{D.15}$$

This results is the definition of the robustness for PV systems.

References

I. Abdalla, J. Corda, and L. Zhang. Multilevel dc-link inverter and control algorithm to overcome the pv partial shading. *Power Electronics, IEEE Transactions on*, 28(1):14 –18, Jan 2013.

G. Acciari, D. Graci, and A. La Scala. Higher pv module efficiency by a novel cbs bypass. *Power Electronics, IEEE Transactions on*, 26(5):1333 –1336, may 2011. ISSN 0885-8993. doi: 10.1109/TPEL.2010.2095469.

M.C. Alonso-Garcia, J.M. Ruiz, and F. Chenlo. Experimental study of mismatch and shading effects in the i-v characteristic of a photovoltaic module. *Solar Energy Materials and Solar Cells*, 90(3):329–340, 2006. ISSN 0927-0248. doi: DOI:10.1016/j.solmat.2005.04.022.

J. Appelbaum, A. Chait, and D. A. Thompson. A method for screening solar cells. *Solid-State Electronics*, 38(1):246–248, 1995. ISSN 0038-1101. doi: DOI:10.1016/0038-1101(94)00139-7.

Gonzales-C.C. Arnett, J.C. Photovoltaic module hot spot durability design and test methods. page 1099âĂŞ1105. Proceedings of the 15th IEEE Photovoltaic Specialists Conference, 1981.

A. Bidram, A. Davoudi, and R. S. Balog. Control and circuit techniques to mitigate partial shading effects in photovoltaic arrays. *Photovoltaics, IEEE Journal of*, PP(99):1 –15, 2012. ISSN 2156-3381. doi: 10.1109/JPHOTOV.2012.2202879.

Long Bun. *Faults Detection and Isolation in a PV System*. Phd thesis, Institut National Polytechnique de Grenoble - INPG, December 2012.

M. Cacciato, A. Consoli, R. Attanasio, and F. Gennaro. Soft-switching converter with hf transformer for grid-connected photovoltaic systems. *Industrial Electronics, IEEE Transactions on*, 57(5):1678 –1686, may 2010. ISSN 0278-0046. doi: 10.1109/TIE.2009.2032201.

Charles E. Chamberlin, Peter Lehman, James Zoellick, and Gian Pauletto. Effects of mismatch losses in photovoltaic arrays. *Solar Energy*, 54(3):165–171, 1995. ISSN 0038-092X. doi: DOI:10.1016/0038-092X(94)00120-3.

M. Sidrach de Cardona and Ll. Mora LÃşpez. Evaluation of a grid-connected photovoltaic system in southern spain. *Renewable Energy*, 15(1-4):527 – 530, 1998. ISSN 0960-1481. doi: DOI:10.1016/S0960-1481(98)00218-3. Renewable Energy Energy Efficiency, Policy and the Environment.

C. Deline. Partially shaded operation of a grid-tied pv system. In *Photovoltaic Specialists Conference (PVSC), 2009 34th IEEE*, pages 001268 –001273, june 2009.

M. Drif, P.J. PÃĺrez, J. Aguilera, and J.D. Aguilar. A new estimation method of irradiance on a partially shaded pv generator in grid-connected photovoltaic systems. *Renewable Energy*, 33(9):2048 – 2056, 2008. ISSN 0960-1481. doi: DOI:10.1016/j.renene.2007.12.010.

Mohamed A. Eltawil and Zhengming Zhao. Grid-connected photovoltaic power systems: Technical and potential problems–a review. *Renewable and Sustainable Energy Reviews*, 14(1):112 – 129, 2010. ISSN 1364-0321. doi: DOI:10.1016/j.rser.2009.07.015.

Felix A. Farret and M. Godoy SimÃţes. *Integration of Alternatives Sources of Energy*. Wiley-Interscience, 1st edition, 2006.

Toru Fujisawa and Susumu Ohya. Study on shadow loss of crystalline si pv module affected by scattering rate of solar irradiance. pages 1975–1976. 3rd World Conference on Photovoltaic Energy Conversion, 2003.

R. Giral, C.E. Carrejo, M. Vermeersh, A.J. Saavedra-Montes, and C.A. Ramos-Paja. Pv field distributed maximum power point tracking by means of an active bypass converter. In *Clean Electrical Power (ICCEP), 2011 International Conference on*, pages 94 –98, june 2011. doi: 10.1109/ICCEP.2011.6036360.

H.; Pettersson S.; Escobar G.; Canales F. Ho, C. N.-M.; Breuninger. A comparative performance study of an interleaved boost converter using commercial si and sic diodes for pv applications. *Power Electronics, IEEE Transactions on*, 28(1):289 –299, Jan 2013.

Kyoko Ichida, Shunichi Fukushige, Akihiko Nakajima, Takashi Minemoto, and Hideyuki Takakura. Impact of environment factors on solar cell parameters of a-si[short parallel][mu]c-si photovoltaic modules. *Solar Energy Materials and Solar Cells*, 93(6-7): 879 – 883, 2009. ISSN 0927-0248. doi: DOI:10.1016/j.solmat.2008.10.011. 17th International Photovoltaic Science and Engineering Conference.

T. Ikegami, T. Maezono, F. Nakanishi, Y. Yamagata, and K. Ebihara. Estimation of equivalent circuit parameters of pv module and its application to optimal operation of pv system. *Solar Energy Materials and Solar Cells*, 67(1-4):389 – 395, 2001. ISSN 0927-0248. doi: DOI:10.1016/S0927-0248(00)00307-X.

Z.; Amjad M.; Mekhilef S. Ishaque, K.; Salam. An improved particle swarm optimization (pso)âĂŞbased mppt for pv with reduced steady-state oscillation. *Power Electronics, IEEE Transactions on*, 27(8):3627 – 3638, Aug. 2012.

L.L. Bucciarelli Junior. Power loss in photovoltaic arrays due to mismatch in cell characteristics. *Solar Energy*, 23:277–288, 1979.

R. Kadri, J. Gaubert, and G. Champenois. New converter topology to improve performance of photovoltaic power generation system under shading conditions. In *Power Engineering, Energy and Electrical Drives (POWERENG), 2011 International Conference on*, pages 1 –7, may 2011. doi: 10.1109/PowerEng.2011.6036483.

S. Kaplanis and E. Kaplani. Energy performance and degradation over 20 performance years of bp c-si pv modules. *Simulation Modelling Practice and Theory*, 19(4):1201 – 1211, 2011.

Engin Karatepe, Mutlu Boztepe, and Metin Çolak. Development of a suitable model for characterizing photovoltaic arrays with shaded solar cells. *Solar Energy*, 81(8):977–992, 2007. ISSN 0038-092X. doi: DOI:10.1016/j.solener.2006.12.001.

N.D. Kaushika and Anil K. Rai. An investigation of mismatch losses in solar photovoltaic cell networks. *Energy*, 32(5):755–759, 2007. ISSN 0360-5442. doi: DOI:10.1016/j.energy.2006.06.017.

Hajime Kawamura, Kazuhito Naka, Norihiro Yonekura, Sanshiro Yamanaka, Hideaki Kawamura, Hideyuki Ohno, and Katsuhiko Naito. Simulation of i-v characteristics of a pv module with shaded pv cells. *Solar Energy Materials and Solar Cells*, 75(3-4):613–621, 2003. ISSN 0927-0248. doi: DOI:10.1016/S0927-0248(02)00134-4.

A. Kovach and J. Schmid. Determination of energy output losses due to shading of building-integrated photovoltaic arrays using a raytracing technique. *Solar Energy*, 57 (2):117 – 124, 1996. ISSN 0038-092X. doi: DOI:10.1016/S0038-092X(96)00066-7.

Z.T. Kuznicki, J. Thibault, F. Chautain-Mathys, L. Wu, S. SidibÃĭ, S. de Unamuno, J.T. Bonarski, Z. Swiatek, and R. Ciach. Modification of a post-implantation defect activity for photovoltaic conversion. *Nuclear Instruments and Methods in Physics Research Section B: Beam Interactions with Materials and Atoms*, 147(1âĂŞ4):136 – 141, 1999.

Xue Lin, Yanzhi Wang, Siyu Yue, Donghwa Shin, Naehyuck Chang, and M. Pedram. Near-optimal, dynamic module reconfiguration in a photovoltaic system to combat partial shading effects. In *Design Automation Conference (DAC), 2012 49th ACM/EDAC/IEEE*, pages 516 –521, june 2012.

Tat Luat Nguyen and Kay-Soon Low. A global maximum power point tracking scheme employing direct search algorithm for photovoltaic systems. *Industrial Electronics, IEEE Transactions on*, 57(10):3456 –3467, oct. 2010. ISSN 0278-0046. doi: 10.1109/TIE.2009.2039450.

Y. Nimni and D. Shmilovitz. A returned energy architecture for improved photovoltaic systems efficiency. In *Circuits and Systems (ISCAS), Proceedings of 2010 IEEE International Symposium on*, pages 2191 –2194, 30 2010-june 2 2010. doi: 10.1109/ISCAS.2010.5537199.

C. Olalla, M. Rodriguez, D. Clement, Jian Wang, and D. Maksimovic. Architecture and control of pv modules with submodule integrated converters. In *Control and Modeling for Power Electronics (COMPEL), 2012 IEEE 13th Workshop on*, pages 1 –6, june 2012. doi: 10.1109/COMPEL.2012.6251785.

Sang-Hyun Park, Tae-Sung Kim, Jin-Sik Park, Gun-Woo Moon, and Myung-Joong Yoon. A new buck-boost type battery equalizer. In *Applied Power Electronics Conference and Exposition, 2009. APEC 2009. Twenty-Fourth Annual IEEE*, pages 1246 –1250, feb. 2009. doi: 10.1109/APEC.2009.4802823.

B. Patnaik, P. Sharma, E. Trimurthulu, S.P. Duttagupta, and V. Agarwal. Reconfiguration strategy for optimization of solar photovoltaic array under non-uniform illumination conditions. In *Photovoltaic Specialists Conference (PVSC), 2011 37th IEEE*, pages 001859 –001864, june 2011. doi: 10.1109/PVSC.2011.6186314.

D. Picault, B. Raison, S. Bacha, J. de la Casa, and J. Aguilera. Changing photovoltaic array interconnections to reduce mismatch losses: a case study. page 37. 9th International Conference on Environment and Electrical Engineering (EEEIC), 2010a.

D. Picault, B. Raison, S. Bacha, J. de la Casa, and J. Aguilera. Forecasting photovoltaic array power production subject to mismatch losses. *Solar Energy*, 84(7):1301 – 1309, 2010b. ISSN 0038-092X. doi: DOI:10.1016/j.solener.2010.04.009.

Damien Picault. *Reduction of mismatch losses in grid-connected photovoltaic systems using alternative topologies*. Phd thesis, Institut National Polytechnique de Grenoble - INPG, October 2010.

M.Z. Ramli and Z. Salam. A retrofit circuit to increase output power of pv system during partial shading condition. In *Innovative Smart Grid Technologies - Middle East (ISGT Middle East), 2011 IEEE PES Conference on*, pages 1 –6, dec. 2011. doi: 10.1109/ISGT-MidEast.2011.6220795.

C.A. Ramos-Paja, G. Spagnuolo, G. Petrone, M. Vitelli, and J.D. Bastidas. A multivariable mppt algorithm for granular control of photovoltaic systems. In *Industrial Electronics (ISIE), 2010 IEEE International Symposium on*, pages 3433 –3437, july 2010. doi: 10.1109/ISIE.2010.5637998.

A. Safari and S. Mekhilef. Simulation and hardware implementation of incremental conductance mppt with direct control method using cuk converter. *Industrial Electronics, IEEE Transactions on*, 58(4):1154 –1161, april 2011. ISSN 0278-0046. doi: 10.1109/TIE.2010.2048834.

T. Shimizu, M. Hirakata, T. Kamezawa, and H. Watanabe. Generation control circuit for photovoltaic modules. *Power Electronics, IEEE Transactions on*, 16(3):293 –300, may 2001. ISSN 0885-8993. doi: 10.1109/63.923760.

T. Shimizu, O. Hashimoto, and G. Kimura. A novel high-performance utility-interactive photovoltaic inverter system. *Power Electronics, IEEE Transactions on*, 18(2):704 – 711, mar 2003. ISSN 0885-8993. doi: 10.1109/TPEL.2003.809375.

L.L. Sun and H.X. Yang. Impacts of the shadingtype building-integrated photovoltaic claddings on electricity generation and cooling load component through shaded windows. *Energy and Buildings*, 42(4):455 – 460, 2010. ISSN 0378-7788. doi: DOI:10.1016/j.enbuild.2009.10.014.

V. Tyagi, N. Rahim, N. Rahim, and J. Selvaraj. Progress in solar pv technology: Research and achievement. *Renewable and Sustainable Energy Reviews*, 20(0):443 – 461, 2013.

A. Ubisse and A. Sebitosi. A new topology to mitigate the effect of shading for small photovoltaic installations in rural sub-saharan africa. *Energy Conversion and Management*, 50(7):1797 – 1801, 2009. ISSN 0196-8904. doi: DOI:10.1016/j.enconman.2009.03.016.

E.L. van Dyk and E.E. Meyer. Assessing the reliability and degradation of photovoltaic module performance parameters. *IEEE Transactions on reliability*, 53(1):83–92, March 2004. ISSN 0018-9529. doi: 10.1109/TR.2004.824831.

L.F.L. Villa, D. Picault, S. Bacha, A. Labonne, and B. Raison. Maximizing the power output of partially shaded photovoltaic plants through optimization of the interconnections among its modules. *Photovoltaics, IEEE Journal of*, 2(2):154 – 163, april 2012.

L.F.L. Villa, T.P. Ho, J.C. Crebier, and B. Raison. A power electronics equalizer application for partially shaded photovoltaic modules. *Industrial Electronics, IEEE Transactions on*, 60(3):1179 –1190, march 2013.

G.R. Walker, J. Xue, and P. Sernia. Pv string per-module maximum power point enabling converters. In *The Australasian Universities Power Engineering Conference*, pages 112 –117, september 2003. ISBN 0-473-09867-9.

Yanzhi Wang, Xue Lin, Younghyun Kim, Naehyuck Chang, and M. Pedram. Enhancing efficiency and robustness of a photovoltaic power system under partial shading. In *Quality Electronic Design (ISQED), 2012 13th International Symposium on*, pages 592 –600, march 2012. doi: 10.1109/ISQED.2012.6187554.

Yaw-Juen Wang and Po-Chun Hsu. Analysis of partially shaded pv modules using piecewise linear parallel branches model. *World Academy of Science, Engineering and Technology*, (60), 2009.

Achim Woyte, Johan Nijs, and Ronnie Belmans. Partial shadowing of photovoltaic arrays with different system configurations: literature review and field test results. *Solar Energy*, 74(3):217–233, 2003. ISSN 0038-092X. doi: DOI:10.1016/S0038-092X(03)00155-5.

Jia-Ying Ye, Kun Ding, Thomas Reindl, and Armin G. Aberle. Outdoor pv module performance under fluctuating irradiance conditions in tropical climates. *Energy Procedia*, 33(0):238 – 247, 2013.